

Mechanism of localized lignin deposition in explosive fruit

Inaugural-Dissertation

zur

Erlangung des Doktorgrades

der Mathematisch-Naturwissenschaftlichen Fakultät

der Universität zu Köln

vorgelegt von

Miguel Pérez Antón

aus Burgos, Spanien

Köln, 2020

Berichterstatter: (Gutachter): Prof. Dr. Angela Hay

Prof. Dr. Ute Höcker

Tag der Prüfung: 2.Dezember 2020

Die vorliegende Arbeit wurde am Max-Planck-Institut für Pflanzenzüchtungsforschung in Köln
in der Abteilung für Vergleichende Entwicklungsgenetik (Direktor Prof. Dr. Miltos Tsiantis)
angefertigt.

Abstract

Adaptations for dispersal are ubiquitous in nature. Plants have evolved many and varied ways to disperse their seeds, from the parachute of plumed dandelion seeds, to the exploding fruit of *Cardamine hirsuta*. A major goal in biology is to identify the molecular basis of such complex trait innovations. In *C. hirsuta*, the asymmetric deposition and lignification of secondary cell walls (SCWs) in endocarp *b* cells of the fruit valve was found to be a key morphomechanical innovation underpinning explosive seed dispersal. To gain insights into the mechanisms controlling this lignin patterning in *C. hirsuta*, we identified *less lignin (lig)* mutants that showed reduced lignification of the fruit valve. The *lig1* mutant is deficient in lignin deposition in endocarp *b* cells, resulting in a reduced seed dispersal range. By positional cloning, transgenic complementation, and the isolation of additional alleles, I demonstrate that an ortholog of the transcription factor *SPL7*, a central regulator of copper homeostasis, is the causal locus for the phenotype. Using ICP-MS to measure the concentration of copper, I show that *SPL7* is both necessary and sufficient to regulate the concentration of copper in fruit. I find that *SPL7* is expressed in endocarp *b* cells and lignified cells of the dehiscence zone, suggesting a local role in lignification. Three members of the lignin-polymerizing laccases, which are Cu-requiring enzymes, are expressed in endocarp *b* cells, where I show they precisely co-localize with lignin in the asymmetric SCWs. Using CRISPR/Cas9, I generated knock-out alleles of these three laccases. Plants with 5 mutant laccase alleles have less lignin in SCWs of endocarp *b* cells, suggesting that laccases are required for endocarp *b* lignification. I propose that copper deficiency in the *lig1* fruit, due to loss of *SPL7* function, reduces laccase activity in endocarp *b* cells, resulting in reduced lignification. Therefore, explosive seed dispersal depends on the *SPL7* pathway to provide sufficient copper to the fruit for localized lignin deposition, likely mediated by precise localization of Cu-requiring laccases.

Zusammenfassung

Anpassungen der Ausbreitung sind allgegenwärtig in der Natur. Pflanzen haben viele und vielfältige Möglichkeiten zur Verbreitung ihrer Samen entwickelt, vom Fallschirm der gefiederten Löwenzahnsamen bis zu den explodierenden Früchten von *Cardamine hirsuta*. Ein Hauptziel in der Biologie ist es, die molekulare Basis solcher komplexen phänotypischen Innovationen zu identifizieren. Bei *C. hirsuta* erwies sich die asymmetrische Ablagerung und Lignifizierung der sekundären Zellwände in den Endokarp-b-Zellen der Fruchtklappe als eine wichtige morphomechanische Innovation, die der explosiven Samenausbreitung zugrunde liegt. Um Einblicke in die Mechanismen zu gewinnen, die dieses Lignifizierungsmuster in *C. hirsuta* steuern, identifizierten wir „weniger Lignin“ (*lig*) Mutanten, die eine verminderte Lignifizierung der Fruchtklappe aufwiesen. Die *lig1*-Mutante weist einen Mangel an Lignineinlagerung in den Endokarp-b-Zellen auf, was zu einer verringerten Samenausbreitung führt. Durch Positionsklonierung, transgene Komplementierung und die Isolierung zusätzlicher Allele zeige ich, dass ein Ortholog des Transkriptionsfaktors *SPL7*, ein zentraler Regulator der Kupferhomöostase, der kausale Genlocus für diesen Phänotyp ist. Mit Hilfe von ICP-MS zur Messung der Kupferkonzentration zeige ich, dass *SPL7* sowohl notwendig als auch ausreichend ist, um die Kupferkonzentration in den Früchten zu regulieren. Ich finde heraus, dass *SPL7* in den Endokarp-b-Zellen und verholzten Zellen der Dehiszenzzone exprimiert wird, was auf eine lokale Rolle bei der Verholzung hindeutet. Drei Lignin-polymerisierenden Laccasen (*LAC4*, *LAC11* and *LAC17*), welche Cu-benötigende Enzyme sind, werden in Endokarp-b-Zellen exprimiert, bei denen ich zeige, dass sie mit Lignin in den asymmetrischen sekundären Zellwänden ko-lokalisieren. Mit Hilfe von CRISPR/Cas9 habe ich Knock-out-Allele dieser drei Laccasen erzeugt. Pflanzen mit 5 mutierten Laccase-Allelen haben weniger Lignin in den sekundären Zellwänden der Endokarp-b-Zellen, was darauf hindeutet, dass Laccasen für die Lignifizierung des Endokarp *b* erforderlich sind. Ich schlage vor, dass ein Kupfermangel in der *lig1*-Frucht aufgrund des Verlusts der *SPL7*-Funktion die Laccase-Aktivität in den Endokarp-b-

Zellen reduziert, was zu einer verminderten Ligninbildung führt. Demnach hängt die explosive Samenausbreitung von der Wirkung des SPL7-Wegs ab ausreichend Kupfer für eine lokalisierte Ligninablagerung in der Frucht zur Verfügung zu stellen, die durch eine präzise Lokalisierung der Cu-bedürftigen Laccasen vermittelt wird.

Table of Contents

Chapter 1: Introduction	1
1. Seed dispersal.....	2
2. Seed dispersal in the Angiosperms	3
3. Fruit development in Brassicaceae: a morphological template for explosive seed dispersal.....	4
4. Explosive seed dispersal in <i>C. hirsuta</i>	6
4.1 Mechanics of <i>C. hirsuta</i> fruit valve coiling.....	6
4.2 Elastic potential energy is built in the exocarp and stored for explosive release	8
4.3 The endocarp <i>b</i> layer is required for explosive seed dispersal.....	8
4.4 The geometry of the lignified SCWs in endocarp <i>b</i> cells allows explosive energy release.....	9
5. Plant cell walls	11
Chapter 2: Characterization and cloning of the <i>less lignin1</i> mutant	15
Introduction.....	16
Results.....	19
1. Endocarp <i>b</i> secondary cell walls are less lignified in the <i>less lignin 1 (lig1)</i> mutant.....	19
2. <i>lig1</i> has reduced seed dispersal range	22
3. Mapping the <i>lig1</i> mutation	24
4. A mutation in <i>SQUAMOSA PROMOTER BINDING PROTEIN-LIKE 7 (SPL7)</i> causes the <i>lig1</i> phenotype	28
5. <i>SPL7</i> complements the <i>lig1</i> mutant phenotype.....	30
6. Characterization of the <i>lig1</i> mutation in <i>SPL7</i>	33
7. <i>SPL7</i> CRISPR/Cas9 allele phenocopies <i>lig1</i>	37
Discussion	40
Chapter 3: Role of <i>SPL7</i> in lignin deposition of endocarp <i>b</i> cells	45
Introduction.....	46
Results.....	50
1. <i>SPL7</i> is expressed constitutively in <i>C. hirsuta</i> throughout development with higher expression in roots	50
2. <i>SPL7</i> is expressed in lignifying cell types of <i>C. hirsuta</i> fruits	51
3. <i>SPL7</i> is necessary for copper homeostasis in <i>C. hirsuta</i> fruit.....	54

4. SPL7 is sufficient to increase Cu concentration in <i>C. hirsuta</i> fruit	56
5. Cu supplementation to soil rescues endocarp <i>b</i> lignification in <i>spl7</i>	60
6. Reduced growth of <i>spl7-1</i> plants in Cu-limiting conditions.....	62
7. Lignification is not reduced in roots and stems of <i>spl7-1</i> plants under Cu-limiting conditions	66
8. Endocarp <i>b</i> secondary cell walls are less lignified in the <i>A. thaliana spl7</i> mutant.....	69
9. Components of SPL7 pathway are conserved in <i>C. hirsuta</i>	70
10. Transcriptomic profiling of wild-type and <i>spl7-1</i> fruit valves	76
11. Transcriptomic profiling of <i>spl7-1</i> fruit valves indicate a loss of SPL7 pathway regulation.....	81
12. Lignin biosynthesis pathway is altered in <i>spl7-1</i> fruit valves	86
Discussion	91
Chapter 4: Role of lignin polymerizing enzymes in localized lignin deposition of endocarp <i>b</i> cells.....	99
Introduction	100
Results	106
1. Laccases are highly expressed in <i>C. hirsuta</i> fruit valves at the beginning of endocarp <i>b</i> lignification	106
2. <i>LAC4</i> , <i>LAC11</i> and <i>LAC17</i> are expressed in endocarp <i>b</i> cells of <i>C. hirsuta</i>	108
3. LACCASES co-localize precisely with lignin deposits in SCWs of endocarp <i>b</i> cells..	110
4. <i>LAC11</i> localizes to initiating asymmetric lignin deposits in SCWs of endocarp <i>b</i> cells	113
5. <i>C. hirsuta</i> laccases localize to symmetric lignin deposits in endocarp <i>b</i> SCWs of <i>A. thaliana</i>	115
6. Laccase CRISPR/Cas9 knock-out alleles have reduced lignification in SCWs of endocarp <i>b</i> cells.....	117
7. <i>PER66</i> co-localizes with lignin deposits in SCWs of endocarp <i>b</i> cells whereas <i>PER49</i> and <i>PER64</i> localize to cell walls domains in the replum	128
Discussion	130
Chapter 5: General Discussion and Future Perspectives	135
1. Lignin is an important component of endocarp <i>b</i> SCWs for explosive seed dispersal .	136
2. Explosive seed dispersal depends on SPL7 to provide sufficient Cu in the fruit	137
3. Cu-requiring laccases direct localized lignin deposition in SCWs of endocarp <i>b</i> cells	138
4. Proposed model for the mechanism of localized lignin deposition in endocarp <i>b</i> cells	139
Chapter 6: Materials and methods.....	141
1. Growing conditions and plant materials.....	142
1.1 Plant growing conditions.....	142
1.2 Plant cultivation in aeroponics system	142
1.3 Strains and lines used	143
2. Generation of transgenic plants	143

2.1 Bacterial strains.....	143
2.2 Constructs and cloning strategies.....	143
2.3 Generation of transgenic plants.....	144
3. Generation of mutant alleles	145
3.1 CRISPR/Cas9 mediated mutagenesis of <i>SPL7</i>	145
3.2 CRISPR/Cas9 mediated mutagenesis of laccases	146
4. Molecular biology methods.....	147
4.1 Fine mapping.....	147
4.2 RNA extraction and qRT-PCR.....	147
4.3 RNA sequencing	149
5. Phenotypic and ionic analysis	149
5.1 Seed dispersal experiment.....	149
5.2 Quantification of Cu concentration in fruit.....	151
6. Microscopy materials and methods.....	151
6.1 Sectioning.....	151
6.2 Phloroglucinol/HCl staining.....	151
6.3 Clearing of fruit cross sections.....	151
6.4 Light microscopy imaging	152
6.5 Confocal microscopy	152
6.6 Quantification of lignin autofluorescence	152
Bibliography.....	155
Supplementary figures	163
List of abbreviations.....	164
Acknowledgements	165
Erklärung.....	167
Curriculum vitae	168

Chapter 1: Introduction

1. Seed dispersal

Dispersal can be defined as the movement of individuals away from the habitat of their parents to settle in a new location (Nathan, 2006). This biological process occurs in animals, plants, fungi and prokaryotes. For plants, seed dispersal is often restricted to a short stage of the life cycle, but as sessile organisms, this is a crucial opportunity to move to new locations (Levin *et al.*, 2003). Compared to the range achieved by vegetative plant growth, seed dispersal can achieve much further distances over a much shorter time scale (Levin *et al.*, 2003).

Mathematical models suggested that dispersal is always beneficial for a species, even in homogenous and invariant environments, and even when it involves a high risk of mortality (Hamilton & May, 1977). The ability to disperse seeds to favourable habitats where they can germinate and develop into new adult plants influences a plant's reproductive success and, therefore, seed dispersal is expected to be under strong selection pressures (Levin *et al.*, 2003). Moreover, seed dispersal can influence population structure and dynamics by impacting gene flow, distribution range and local risk of extinction (Levin *et al.*, 2003). Through these population-scale processes, seed dispersal has the potential to influence the evolutionary processes of species distribution and diversification (Willis *et al.*, 2014).

Although dispersal of the progeny from the mother plant can be beneficial for a species by reducing kin competition and inbreeding, and by favouring the establishment in new suitable habitats, seed dispersal has costs for the plant (Levin *et al.*, 2003). Trade-offs for seed dispersal are the investment in the specialized morphologies developed to disperse the seeds, such as fleshy fruit or big winged seeds, and the risk of increased mortality for dispersed seeds. The numerous and diverse adaptations for seed dispersal that can be found in nature, despite the trade-offs, indicate how important advantage is to disperse the seeds and suggest that there are strong selection pressures to drive seed dispersal.

2. Seed dispersal in the Angiosperms

Flowering plants are also named Angiosperms, which means that they enclose the seeds in a “case”, referring to the carpels. The carpels enclosing the seed form the fruit, thus, Angiosperms are plants with fruit. The functions of the fruit are to protect the developing seeds and disperse them from the plant at maturity (Ferrándiz, 2011).

Plants have evolved very diverse fruit and seed morphologies as adaptations for a variety of seed dispersal strategies (Ferrándiz, 2011). This diversity highlights the importance of seed dispersal for plant fitness. Seed dispersal strategies can be classified depending on the nature of the dispersal vector into abiotic and biotic. Abiotic vectors include wind (anemochory) and water (hydrochory), whereas biotic vectors can be animals (zoochory) or the plants themselves (autochory) (Pijl, 1972). Autochory, or seed dispersal by a plant’s own means, is a particularly striking dispersal strategy that is driven by explosive mechanisms. Explosive seed dispersal is found in numerous plant species belonging to diverse lineages, such as in *Hevea brasiliensis* (Euphorbiaceae), *Viola* sp. (Violaceae), or *Ecballium elaterium* (Cucurbitaceae) (Ferrándiz, 2011). Although the mechanisms for explosive seed dispersal are very diverse, a common feature is that they require rapid movements.

The movement of plant organs is typically slow, since they are driven by differential growth or swelling/shrinking. For example, solar tracking by sunflowers (Atamian *et al.*, 2016) or the opening of pinecone scales (Dawson *et al.*, 1997). These processes require water movement across cell membranes or within the cell wall by diffusion (Geitmann, 2016). Therefore, the speed of diffusion restricts the speed of these movements (Skotheim & Mahadevan, 2005). In contrast, rapid movements involve the appearance of trait innovations that allow the gradual storage of potential elastic energy and the rapid release of this stored energy (Skotheim & Mahadevan, 2005). Two types of mechanisms can drive the rapid release of energy: snap-buckling, which relies on the change of geometry of a thin shell without breakage, such as in the Venus flytrap (Forterre *et al.*, 2005); and explosive fracture, which relies on a change in geometry derived from tissue breakage, such as in *Cardamine hirsuta* fruit (Hofhuis *et al.*, 2016) (Figure 1.1 A-D).

Although explosive seed dispersal has been described in many species, studies have mainly focused on the biomechanics and ecological consequences. *Cardamine hirsuta* is the only species for which we have a more comprehensive understanding of the mechanism of explosive seed dispersal (Hofhuis *et al.*, 2016).

Cardamine hirsuta is a cosmopolitan weed in the Brassicaceae, which employs an explosive mechanism to disperse its seeds. *C. hirsuta* is a close relative of the model plant *Arabidopsis thaliana*, which has non-explosive seed dispersal. These two species are genetically similar but they differ in many traits, such as leaf morphology and petal number robustness, in addition to seed dispersal strategy (Hay *et al.*, 2014). *C. hirsuta* is a small, diploid plant with a good reference genome, and can be easily cultivated and stably transformed (Gan *et al.*, 2016). Therefore, comparative studies between *C. hirsuta* and *A. thaliana* provide a powerful platform to investigate the genetic basis of phenotypic evolution. For instance, leaf shape diversity (Kierzkowski *et al.*, 2019; Vlad *et al.*, 2014), petal number robustness (McKim *et al.*, 2017; Monniaux *et al.*, 2018) and explosive seed dispersal (Hofhuis *et al.*, 2016). I use this comparative approach in my thesis, to investigate the underpinnings of one of the key morphomechanical features that drives explosive seed dispersal in *C. hirsuta*.

3. Fruit development in Brassicaceae: a morphological template for explosive seed dispersal

The fruit of *C. hirsuta* is a dehiscent silique, which is characteristic of several species of the Brassicaceae family, among them *A. thaliana*. This type of fruit originates from the fusion of two carpels that enclose the ovules. After fertilization, the outer walls of the carpels give rise to two elongated valves that enclose the seeds in the mature fruit (Figure 1.1 D). The valve tissue is called pericarp and it can be divided into three layers: exocarp (the outermost layer), mesocarp and endocarp (innermost layers) (Figure 1.1 E). The septum divides the fruit into two locules where the seeds develop. The seeds are attached to the replum, which forms a frame around the septum and contains large vascular bundles. The siliques of both *C. hirsuta* and *A. thaliana*

dehisce at maturity, meaning that the two valves separate from the rest of the fruit along a dehiscence zone. The dehiscence zone comprises two specialized cell types that differentiate at the valve margins, adjacent to the replum (Dinny *et al.*, 2005). The two cell types comprise a separation layer and a lignified layer and during dehiscence, cell walls in the separation layer degrade, allowing the valve to separate from the replum along the lignified layer (Rajani & Sundaresan, 2001).

Fruit development in *C. hirsuta* can be divided into stages that are largely equivalent to those described in *A. thaliana* (Neumann & Hay, 2020; Roeder & Yanofsky, 2006), at least until the last stages. Flower development includes the first 13 stages and, at stage 14, fertilisation occurs, which defines the beginning of fruit development. Fertilisation is followed by the elongation of the fruit at stage 15, which continues also during the next stages. At stage 16, abscission of petals and sepals occurs and the fruit continue to elongate. Stage 17 is the most extended stage and it can be subdivided. At stage 17 a, the fruit reaches its maximum length. At stage 17 b, the fruit starts to broaden to reach its final width, and dehiscence zones differentiate along the valve margins. *C. hirsuta* fruit are competent to explode from stage 17 b, therefore, dehiscence and seed dispersal occur simultaneously. In *A. thaliana*, stage 18 is defined by the yellowing and drying of the fruit and, at stage 19, fruit dehiscence takes place. Finally, during stage 20, the dry fruit tissues shatter at the slightest mechanical stimulus, dispersing the seeds. This process is termed pod shatter (Dinny *et al.*, 2005). These last stages of fruit development are not usually observed in *C. hirsuta*.

In summary, the overall morphology of the fruit is similar in *C. hirsuta* and *A. thaliana*; and both are dehiscent siliques. However, seed dispersal by pod shatter is explosive in *C. hirsuta* and non-explosive in *A. thaliana*.

4. Explosive seed dispersal in *C. hirsuta*

4.1 Mechanics of *C. hirsuta* fruit valve coiling

Seeds are dispersed by an explosive mechanism in *C. hirsuta*. At maturity, the two fruit valves separate from the replum along the dehiscence zone and rapidly coil, detaching the seeds from the septum and launching them at speeds of more than 10 ms^{-1} (Figure 1.1 A-C). By employing explosive pod shatter, *C. hirsuta* can disperse its seeds in a radius of 2 m around the plant (Hofhuis *et al.*, 2016). To actuate this rapid movement, the fruit valve requires a mechanism to generate potential elastic energy and rapidly release it as kinetic coiling energy. In a previous study in our group, the biomechanical features that allow these two processes in *C. hirsuta* were identified (Hofhuis *et al.*, 2016).

Simple perturbations were first used to investigate the mechanical properties of *C. hirsuta* fruit valves (Hofhuis *et al.*, 2016). When shallow incisions were made across the exocarp, the tissue gaped, indicating that this outer tissue layer is under tension. Given that endocarp *b* cells are lignified, this inner tissue layer is stiff and inextensible. When mature valves were detached from the fruit, they instantly coiled, however, when the inner and outer layers of the valve were separated by dissection, neither layer coiled on its own. Furthermore, when separated, the outer exocarp layer shortened in length, whereas the stiff endocarp layer conserved its length. In this way, the fruit valve acts as a bilayer: the active, outer layer shortens while the inner layer maintains its length, causing the valve to coil when detached from the fruit. Abstractly, the fruit valve can be considered as consisting of three layers with different mechanical properties: an outer exocarp layer that is under tension, a middle layer that is passive, and an inner endocarp layer that is inextensible (Hofhuis *et al.*, 2016).

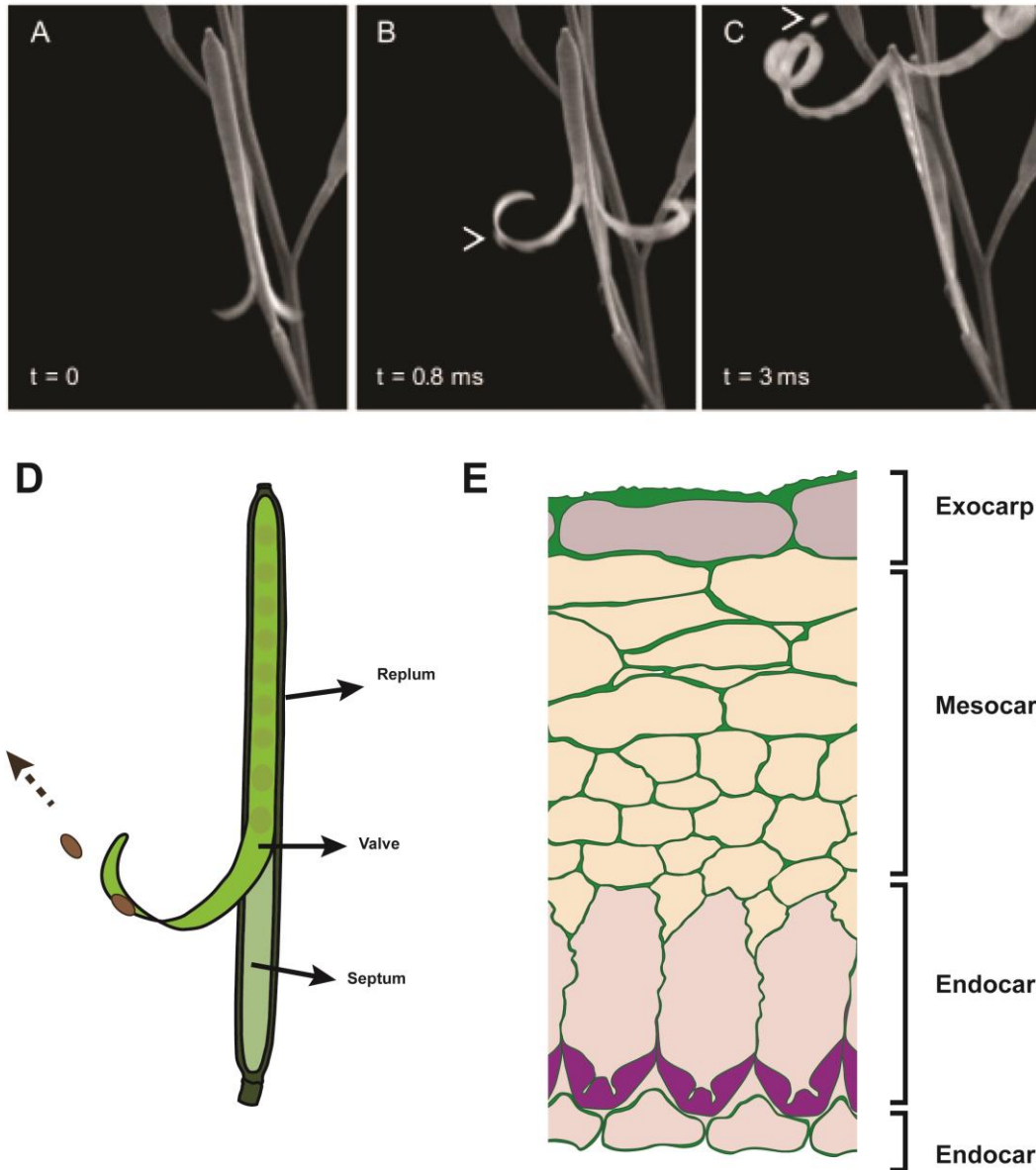


Figure 1.1: *C. hirsuta* employs an explosive mechanism to disperse its seeds. (A-C) Explosive seed dispersal in *C. hirsuta* imaged at 15,000 images per second. The two valves detach from the fruit (A), coil back (B) and launch the seeds (C). t : time between frames. Arrows indicate seeds. Image from (Hofhuis *et al.*, 2016). (D) Schematic representation of *C. hirsuta* fruit during explosive pod shatter. (E) Cartoon of *C. hirsuta* fruit valves tissue in cross section.

4.2 Elastic potential energy is built in the exocarp and stored for explosive release

Explosive seed dispersal requires the generation and storage of potential elastic energy. An important insight into this process came from the comparison of *A. thaliana* and *C. hirsuta* fruit. *A. thaliana* fruit pods are dry when they shatter, while *C. hirsuta* fruit pods remain turgid when they shatter explosively. This means that, in *C. hirsuta*, tension in the exocarp is actively generated by turgid cells. This did not fit with previous explanations that drying generates the energy for explosive seed dispersal by causing fruit tissues to deform (Beer & Swaine, 1977). Key insights into the process of turgor-driven shrinkage came from computational modelling. The authors used a finite-element model of pressurized cells to identify the cellular features that allowed shrinkage in one direction during overall expansion (Hofhuis *et al.*, 2016). These features were cell shape and anisotropy. Exocarp cells acquire a flat, square shape at maturity because they expand in width rather than length, due to directional reinforcement by cellulose microfibrils in the cell wall (Hofhuis *et al.*, 2016). These features allow the cells to shrink in length as their flat surfaces bulge, similar to an air mattress. However, while the valve is attached to the rest of the fruit, this contraction by the outer exocarp layer is resisted by the inner endocarp *b* layer that is stiff and inextensible. In this state, elastic potential energy is being generated and stored in the valve.

4.3 The endocarp *b* layer is required for explosive seed dispersal

The endocarp *b* layer was found to play a critical role in explosive pod shatter. Genetic evidence for the importance of this cell layer for explosive seed dispersal came from the identification of an endocarp *b* deletion mutant in *C. hirsuta* (Hofhuis *et al.*, 2016). Importantly, although *A. thaliana* and *C. hirsuta* fruit are both dehiscent siliques of similar overall morphology, *C. hirsuta* fruit valves have considerably more lignin in the SCWs of the endocarp *b* layer than *A. thaliana* (Hofhuis *et al.*, 2017). This difference was used by the authors to design a genetic screen for *C. hirsuta* mutants with less lignified fruit valves that resemble *A. thaliana* (*less lignin* screen). One of the mutants identified, *less lignin 2* (*lig2*), had less lignin in fruit valves because it lacked the lignified endocarp *b* layer. The *lig2* mutant is a loss of function allele of the *C. hirsuta* ortholog

of the DNA-binding protein BRASSINOSTEROID-INSENSITIVE4. Fruit of this mutant were non-explosive, which demonstrated genetically that the lignified endocarp *b* layer is required for explosive pod shatter (Hofhuis *et al.*, 2016).

4.4 The geometry of the lignified SCWs in endocarp *b* cells allows explosive energy release

Explosive seed dispersal requires the rapid release of the potential elastic energy stored in the fruit valves. In *C. hirsuta*, when the valves detach from the rest of the fruit, their stored potential elastic energy is transformed to kinetic coiling energy. However, prior to this, while still attached to the fruit, valves are bowed outwards in cross section (Figure 1.2). This curved valve configuration prevents the valve from coiling and, thus, valves first need to flatten in cross section in order to coil. This mechanism shows some analogies to a bistable “slap bracelet” toy. This toy is stable as a straight length because its curved cross section prevents it coiling, and it rapidly coils once the cross section is flattened by “slapping” it against your wrist. For the cross-sectional shape of a valve to deform from curved to flat, either the outer exocarp layer has to narrow or the inner endocarp layer has to widen (Figure 1.2). Modelling of the energy landscape of different fruit valve configurations (initially curved, transitionally flat and coiled valves in equilibrium) suggested that valves have to flatten through a passive process that does not require energy input to reproduce the coiling observed in exploded fruit valves (Hofhuis *et al.*, 2016).

It was found that the cell wall geometry of endocarp *b* cells is the key feature enabling the passive flattening of the valves in *C. hirsuta* (Hofhuis *et al.*, 2016). The geometry of the lignified SCWs in the endocarp *b* cells of *C. hirsuta* and *A. thaliana* is strikingly different. In the non-explosive fruit of *A. thaliana*, endocarp *b* SCWs are uniformly deposited and lignified on each cell face. In *C. hirsuta*, the SCWs of endocarp *b* cells are deposited and lignified asymmetrically, only on one side of the cell, in three long rods that are connected by thinner SCW domains. In cross section, these SCWs have a “U” shape with thin hinges at the base of the “U” (Figure 1.2). It was found that these hinged SCWs change from a closed to an open configuration in exploded valves. The collective ‘opening’ of each hinged endocarp *b* cell causes the endocarp *b* layer to widen, and

consequently the valves to flatten and coil (Figure 1.2) (Hofhuis *et al.*, 2016). Essentially, the SCW geometry is a design feature that imposes an ‘energy barrier’ to the system, allowing elastic potential energy to be stored in the valve until the barrier is suddenly removed, and it is rapidly transformed into kinetic coiling energy (Forterre, 2013).

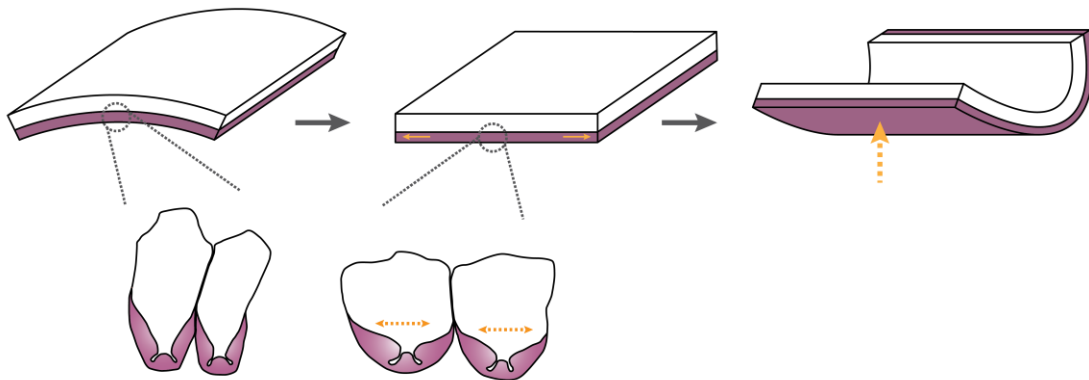


Figure 1.2: Hinged geometry of SCWs of endocarp *b* cells allows valves to flatten passively. Cartoons of fruit valves and endocarp *b* cells. (left) Fruit valve bowed outwards in cross section when attached to the fruit. (middle) Fruit valve with flat cross section when detached from the fruit. (right) fruit valve coils.

The predicted function for the hinged SCW geometry of endocarp *b* cells to release elastic potential energy, was demonstrated with a transgenic approach (Hofhuis *et al.*, 2016). The authors modified the geometry of endocarp *b* SCWs by expressing a master regulator of SCW biosynthesis, *VASCULAR-RELATED NAC-DOMAIN PROTEIN 7 (VND7)*, under the *NAC SECONDARY WALL THICKENING PROMOTING FACTOR 3 (NST3)* promoter. In the transgenic lines, transdifferentiated endocarp *b* cells and adjacent cells developed symmetrically deposited and lignified SCWs, similar to the endocarp *b* SCW geometry found in *A. thaliana*. Fruit of these lines were non-explosive, which demonstrated that the geometry of SCWs in the endocarp *b* is key for the explosive release of energy (Hofhuis *et al.*, 2016).

It was found that the appearance of asymmetric lignification in endocarp *b* cells correlated precisely with the evolution of explosive pod shatter as a seed dispersal trait in the Brassicaceae

family (Hofhuis *et al.*, 2016). Explosive seed dispersal evolved in the genus *Cardamine* and it is not found in other species of the Brassicaceae family. All species of the genus *Cardamine* with explosive seed dispersal examined by the authors had asymmetric SCWs with hinges, whereas all species examined with non-explosive seed dispersal (outside the *Cardamine* genus) had symmetric SCWs. These results indicated that the geometry of SCWs in endocarp *b* cells of *C. hirsuta* is a character innovation that drives explosive seed dispersal (Hofhuis & Hay, 2017).

In summary, it has been shown that the endocarp *b* layer plays a key role in explosive seed dispersal. Firstly, the differential contraction properties of the endocarp *b* layer and exocarp layer cause the valve to coil. Secondly, the hinged geometry of SCWs in endocarp *b* cells allows the valve to deform from a bowed configuration to a flat configuration without external energy input. Thirdly, the hinged geometry of the SCWs of endocarp *b* cells is a design feature that allows the rapid transformation of stored elastic potential energy to kinetic coiling energy. A prediction from these previous findings was that genes involved in the synthesis and/or localization of endocarp *b* SCWs were likely targets for modification during the evolution of explosive seed dispersal.

5. Plant cell walls

Cell walls are microfibril-based matrices deposited outside the plasma membrane surrounding plant cells. Cell walls provide structural support and strength and allow plants to grow in complex shapes. Moreover, plant cells are adhered together through their cell walls. As a consequence, plant cells cannot migrate and, thus, plant morphogenesis depends on directed cell division and cell growth (Cosgrove, 2005).

Cell walls have been traditionally classified into primary cell walls and secondary cell walls (SCWs). Primary cell walls start to deposit from the very initial stage of the plant cell cycle during cell division. While growing, all plant cells develop a primary cell wall, which is typically thin, flexible and highly hydrated. Primary cell walls are strong to resist the tension generated by turgor pressure but also extensible to allow cell enlargement in a controlled and directed manner (Cosgrove, 2005). Cell wall extensibility is allowed by a dynamic process involving molecular

modifications of the wall matrix, called cell wall loosening. Water uptake subsequent to cell wall loosening allows cell enlargement. Typically, primary cell walls contain the polysaccharides cellulose, hemicelluloses and pectins; and proteins. (Cosgrove, 2018).

After cell expansion has finished, only some specialized cell types develop a SCW, which provides strength and rigidity (Cosgrove, 2018). Typically, SCWs are thicker than primary cell walls and they are not extensible. SCWs are deposited between the primary cell wall and the plasma membrane and they are typically composed of the polysaccharides cellulose and hemicelluloses, and often the polyphenol lignin (Cosgrove, 2018; Kumar *et al.*, 2016). Classic examples of cell types that develop lignified SCWs are the xylem and interfascicular fibres in plant stems. Xylem tissues develop SCWs that resist the negative pressure of the water stream transported throughout the plant. SCWs develop in the interfascicular fibres to provide structural support for upright plant growth (Cosgrove, 2018). There is a wide diversity of primary and secondary cell walls that vary in their composition, structure and function (Knox, 2008).

Plant cell walls are very important resources for humans. We use them as textile, lumber, paper and also as energy resources. Non-renewable fossil energy sources, such as petroleum and gas, require millions of years to be generated. In contrast, plant resources can be regenerated in much shorter time, so they can be considered as renewable. There is an increasing interest to employ cell wall derived energy sources to help achieve a more sustainable energy usage (Lynd, 2017). However, an important obstacle for the use of cell wall derived fuels is that often cell wall components, such as lignin, are not easily decomposed into smaller molecules that can be used (they are recalcitrant) (Ragauskas & Yoo, 2018). One of the current research efforts consists on elucidating the mechanisms that regulate cell walls properties. Understanding these mechanisms can help bioengineering cell wall properties that allow a more effective use of plant resources (Ragauskas & Yoo, 2018; Zoghلامي & Paes, 2019).

Thesis aim and experimental objectives

Explosive seed dispersal is a striking trait from the point of view of biomechanics, ecology, evolution and development. It evolved independently in diverse plant groups but is not found in the model plant species *A. thaliana*. Previous work in my group has led to a comprehensive understanding of the mechanism of explosive seed dispersal found in the *A. thaliana* relative *C. hirsuta*. The aim of my thesis is to identify the genetic basis for cellular innovations that underpin explosive seed dispersal in *C. hirsuta*.

A specific prediction from previous findings is that genes involved in the localization of lignified SCWs in endocarp *b* cells were likely targets of evolutionary change during the transition from non-explosive to explosive seed dispersal in *C. hirsuta*. In my thesis project, I investigate the mechanism of localized lignin deposition in SCWs of endocarp *b* cells. For this purpose, I take advantage of a previously identified mutant in *C. hirsuta* with less lignin in endocarp *b* cells (*less lignin1 -lig1-*). I hypothesize that the gene responsible for the mutant phenotype will be involved in the biosynthesis or localization of lignin in *C. hirsuta* endocarp *b* cells. The findings of this work will contribute to our understanding of lignin patterning and polymerization, and the evolution of complex trait innovations that underpin rapid plant movements.

The experimental objectives of this thesis work are:

- (1) Characterize the *lig1* phenotype of reduced endocarp *b* lignification and whether it affects explosive seed dispersal
- (2) Identify the causal locus for the *lig1* mutant phenotype
- (3) Investigate the genetic pathway in which *LIG1* acts
- (4) Use *lig1* as an entry point to identify the mechanism of localized lignin deposition in endocarp *b* cells

**Chapter 2: Characterization and cloning
of the *less lignin1* mutant**

Introduction

One commonly used approach to investigate living systems is to generate perturbations in the system. For example, deleting something in the system and then observing the impact of this change. In genetics, this usually involves disrupting DNA sequences to cause loss of gene function. By observing the perturbed system, relative to the wild type, we can often infer gene function. In reverse genetics, a target gene is disrupted in order to infer its function in a biological process of interest. Forward genetics, on the other hand, relies on generating random perturbations in a system. For example, by using a mutagen to induce changes in the DNA. A mutagenized population is then screened to identify mutant individuals in which the biological process of interest is altered. A simple inference is that the genes mutated in these individuals function in the process of interest. By identifying these genes, we identify components of the biological process. The main advantage of a forward genetics approach is that no *a priori* assumptions are made about the genes involved in a process. Both forward and reverse genetics strategies have been widely used to investigate plant development. For instance, forward genetic screens were key for the discovery of genes involved in floral organ identity and, ultimately, for the formulation of the ABC model of floral development (Coen & Meyerowitz, 1991). Reverse genetics studies using lines from T-DNA insertion libraries have been fundamental for advances in plant development (O'Malley & Ecker, 2010).

In our group, a forward genetic screen was previously conducted in *C. hirsuta* to investigate explosive seed dispersal. A comparative strategy with the model plant *A. thaliana* was used to design the genetic screen. *A. thaliana* is a close relative of *C. hirsuta* that has non-explosive fruit (Hofhuis *et al.*, 2016). Both species have dehiscent siliques that are similar in terms of overall morphology. However, a striking difference is the amount of lignification in *C. hirsuta* compared to *A. thaliana* fruit (Hofhuis & Hay, 2017). *C. hirsuta* fruit valves have considerably more lignin in the SCWs of endocarp *b* cells than *A. thaliana*, which can be observed by whole fruit staining with phloroglucinol/HCl (Hofhuis & Hay, 2017). This difference was used to design a genetic screen for *C. hirsuta* mutants with less lignified fruit valves that resemble *A. thaliana*.

This genetic screen for mutants with less lignified fruit valves (*lig* mutants) was performed in the *C. hirsuta* Ox reference accession. To generate the mutant population for the screen, seeds were treated with the DNA mutagen ethyl methanesulfonate (EMS), and the progeny of selfed plants were screened by whole fruit staining with phloroglucinol/HCl. Mutants identified from this screen have already proven to be powerful tools to investigate explosive seed dispersal. For example, the *less lignin 2* (*lig2*) mutant has less lignified fruit valves because it lacks the endocarp *b* layer. Pod shatter in this mutant is non-explosive, which indicates that the endocarp *b* layer is required for explosive seed dispersal in *C. hirsuta* (Hofhuis *et al.*, 2016). Specifically, it is the geometry of the lignified SCWs of the endocarp *b* layer that is required for explosive seed dispersal (Hofhuis *et al.*, 2016). Therefore, it is important to investigate the mechanism by which lignin is deposited to form this specific geometry in the endocarp *b* cell layer.

In my thesis, I approached this question by taking advantage of another mutant identified in the same screen (*less lignin 1* -*lig1*-). In the *lig1* mutant, endocarp *b* cells synthesize a SCW, similar to wild type, but the SCW is dramatically less lignified. This phenotype suggests that the disrupted gene may function specifically in lignin deposition in endocarp *b* cells. One goal of this chapter is to characterize the *lig1* phenotype and explore the possible impact of reduced endocarp *b* lignin deposition on explosive seed dispersal. A second goal of this chapter is to identify the gene responsible for the *lig1* mutant phenotype. By identifying a component of the genetic network that regulates localized lignin deposition in endocarp *b* SCWs, I hope to further our understanding of this process and how it evolved in *Cardamine* to drive explosive seed dispersal.

A key methodology that I used to identify the gene responsible for the *lig1* mutant phenotype, is mapping-by-sequencing. Mapping relies on the principle of genetic linkage, whereby the closer two loci are, the more likely they are inherited together. This occurs since the probability of homologous recombination occurring between two loci during meiosis depends on the physical distance between the two loci. Thus, the phenotype generated by a causal mutation will be more likely to segregate together with linked loci that are physically adjacent in the genome. To identify linked loci, the segregation of polymorphic markers, with known physical locations in the

genome, is assessed for linkage with the mutant phenotype. This mapping is usually performed in a recombinant F₂ population, generated by a cross between polymorphic accessions. In this F₂ population, plants are classified according to the presence or absence of the mutant phenotype. Markers across the genome are genotyped to identify allelic polymorphisms, and linkage data is used to map the physical location of the mutant locus.

Identifying good genetic markers for mapping, and genotyping these markers in a mapping experiment, was traditionally a time-consuming process. But mapping-by-sequencing has helped to reduce the time and effort involved in this process (Schneeberger, 2014). By using next-generation sequencing, we can identify thousands of polymorphisms in recombinant individuals, thus increasing the resolution of mapping. Simultaneously, the allele frequencies of these markers can be calculated to find a genetic interval. By using bulked segregant analysis, whereby DNA of wild-type versus mutant recombinant individuals are bulked rather than analysed individually, only two DNA libraries are sequenced, making this methodology cost-effective. Moreover, once a genetic interval is found, candidate causal mutations can also be identified from the sequencing data. This approach is helpful in non-model organisms, since the genetic markers of a polymorphic accession can be identified during the mapping process without previous sequencing data. However, it is particularly useful in *C. hirsuta* because a reference genome (Ox accession) has been sequenced and assembled (Gan *et al.*, 2016).

In summary, I characterized the *lig1* mutant phenotype, and combined mapping-by-sequencing with a fine mapping strategy to define a genetic interval for *lig1*, and identify candidate causal mutations. I performed genetic complementation tests and generated additional loss-of-function alleles using CRISPR/Cas9 to confirm that *SQUAMOSA PROMOTER BINDING PROTEIN-LIKE 7 (SPL7)* is the causal gene responsible for the *lig1* mutant phenotype. These findings provide important insights into the mechanism patterning localized lignin deposition in endocarp *b* cells.

Results

1. Endocarp *b* secondary cell walls are less lignified in the *less lignin 1 (lig1)* mutant

One of the mutants identified in the less lignin screen was *less lignin 1 (lig1)* (Penny Sarchet thesis, 2012). To investigate the inheritance of the *lig1* phenotype, I made use of a cross between a homozygous *lig1* mutant plant (Ox accession) and the wild-type New Zealand (Nz) accession. This cross was also used for mapping the causal mutation for the *lig1* phenotype. In the F2 generation of this cross, I found a 3:1 segregation ratio of 137 phenotypically wild-type plants to 34 *lig1* mutant plants. This segregation ratio is consistent with Mendelian inheritance of a recessive allele ($\chi^2 = 2.39$, 1-degree freedom, not significantly different from expected at >10 % level). Given that *lig1* is a recessive allele, the mutant phenotype is likely to represent loss of the wild-type gene function.

The *lig1* mutant was identified in the less lignin screen because it showed decreased phloroglucinol/HCl staining in the valves of whole fruit, resembling the valves of the non-explosive species *A. thaliana*. By staining transverse sections with phloroglucinol/HCl, I found that lignification does not appear reduced in other lignified cell types in the fruit. For example, lignified xylem and fibre cells in the replum, and lignified cells in the valve margin, stain similarly with phloroglucinol/HCl in both *lig1* and wild type (Figure 2.1 A). The dehiscence zone appears to form normally in *lig1* fruit, as cells lignify at the valve margin and fruit dehisce at maturity to release seeds. This indicates that the reduction in lignin deposition is specific to the endocarp *b* cell layer in fruit valves.

Although *lig1* and *lig2* mutants are indistinguishable by whole fruit phloroglucinol/HCl staining, the endocarp *b* cell layer is absent in *lig2* (Hofhuis *et al.*, 2016), but present in *lig1* fruit. Endocarp *b* SCWs stain purple with toluidine blue in *lig1* compared to turquoise in wild type (Figure 2.1 B). Polysaccharides stain purple with toluidine blue while phenolic compounds like lignin stain turquoise (O'Brien *et al.*, 1964). Therefore, this difference in staining indicates that lignin is absent from the SCWs of *lig1*. In endocarp cells of both *lig1* and wild type, SCWs are deposited

asymmetrically forming the “U” shape thickenings with hinges that are characteristic of this cell type in *C. hirsuta* (Figure 2.1 B). In summary, *lig1* mutants specifically fail to deposit lignin in the SCWs of endocarp *b* cells.

Further observation using confocal microscopy suggests that lignin is deposited variably in the SCW of *lig1* endocarp *b* cells. Lignin exhibits autofluorescence when excited with UV light, which allows direct observation without specific staining. Overall, the SCW of *lig1* endocarp *b* cells shows reduced autofluorescence compared to wild type. Specifically, the SCW of *lig1* endocarp *b* cells exhibits variable autofluorescence in a layer-like pattern (Figure 2.1 C). Moreover, which layers of the SCW are lignified in *lig1* can differ between different endocarp *b* cells, between different fruits, and between different plants. (Figure 2.1 C) (Hofhuis, unpublished). This layer-like pattern of lignin autofluorescence is likely to reflect the progressive thickening and lignification of living endocarp *b* SCWs during the later stages of *C. hirsuta* fruit development (Hofhuis *et al.*, 2016). This differs from other lignified cell types found in xylem tissues, where lignification is cell non-autonomous and coincident with programmed cell death (Pesquet *et al.*, 2013; Smith *et al.*, 2013). Furthermore, the variable lignification observed in *lig1* indicates that “less lignin” is a plastic phenotype in this mutant. This might reflect increased sensitivity of the *lig1* mutant to changes in external conditions, whereas wild-type lignification of endocarp *b* cells is more robust.

Another phenotype in common to both *lig1* and *lig2* mutants is buckling of the fruit margin. Mature *lig1* fruit buckle along the edge of the fruit compared to the straight edge of wild-type fruit (Figure 2.1 D). By following this phenotype through development, I observed that *lig1* fruit have a straight margin throughout the earlier stages of fruit elongation, and the margin buckles during the later stages of fruit broadening, which corresponds to when endocarp *b* cells lignify (Figure 2.1 E). This suggests that buckling of the fruit margin in *lig1* may be a consequence of reduced lignification of the endocarp layer.

Finally, *lig1* fruit are shorter than wild type at maturity (Figure 2.1 F). However, I have not examined whether the difference in length is a result of differences in early stages of fruit

development or a result of changes in the last steps of maturation, when lignification of the endocarp occurs. Therefore, it is not clear whether the phenotype is linked to the reduction in lignification of the endocarp layer.

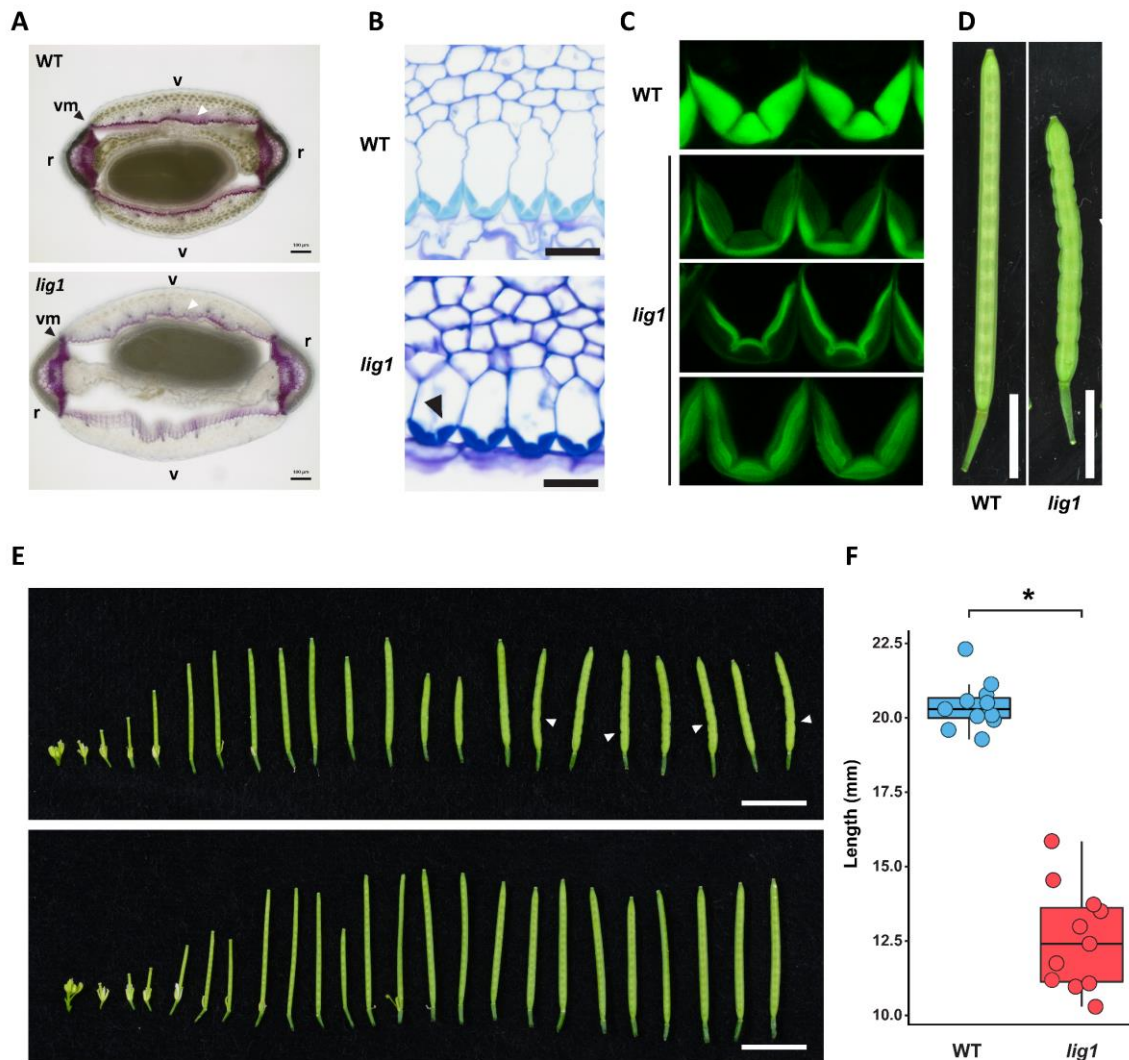


Figure 2.1: Endocarp *b* secondary cell walls are less lignified in the *less lignin 1* (*lig1*) mutant. (A) Cross sections of fruits at stage 17 a/b stained with phloroglucinol/HCl from wild type (top) and *lig1* (bottom). Plants were grown in Cu-limiting conditions (watered with collected rain water and supplemented weekly with 10 mL of 0.5 mM CuSO₄). White arrowheads indicate endocarp *b* layer. r: replum; v: valve; vm: valve margin. (B) Cross sections of fruit at stage 17 a/b stained with toluidine blue which stains polysaccharides purple and phenolic compounds, like lignin, turquoise (Obrien *et al.*, 1964). Arrowhead indicates SCWs of endocarp *b* cells in *lig1*. Images from P. Sarchet and U. Neumann (unpublished). (C) Confocal micrographs of lignin autofluorescence in endocarp *b* SCWs excited with UV 405 laser. Images from H. Hofhuis (unpublished). (D) Stage 17 a/b fruits from wild type and *lig1*. Scale bar: 5 mm. (E)

Development of flowers and siliques in wild type and *lig1* ordered by plant node. Plants were watered with collected rain water and supplemented weekly with 10 mL of 5 mM CuSO₄. Arrowheads indicate examples of the buckled edge of *lig1* fruit. Scale bar: 1 cm. (F) Box plot of fruit length of mature fruit from wild type and *lig1*. Asterisk indicates statistically significant difference (P-value < 0.05, Student's t-test) between means of genotypes (n = 11). Plants were watered with city tap water and no additional Cu was supplemented.

2. *lig1* has reduced seed dispersal range

Fruit from the *lig1* mutant are dehiscent and, in contrast to the *lig2* mutant, they are able to coil and explosively disperse seeds. We know from previous work that not only is the endocarp *b* cell layer required for explosive coiling (hence the *lig2* mutant is non-explosive), but it is the specific geometry of the endocarp *b* secondary cell wall that is necessary for this process (Hofhuis *et al.*, 2016). What is unknown is whether the material properties of the endocarp *b* secondary cell wall also contribute to explosive seed dispersal. To address this question, I measured the distribution of seeds dispersed by *lig1* mutants with reduced lignin in their endocarp *b* secondary cell walls.

For this experiment, I counted the total seeds dispersed in distance bins away from individual wild-type and *lig1* plants. I positioned each individual plant in the center of a series of concentric circles drawn on a large sheet of plastic every 25 cm, covering a 2 m radius around each plant (see Figure 6.1 in materials and methods). Plants were left to disperse seeds over a period of 6 weeks, then seeds were collected from each circular distance bin and counted. A total of 10,039 seeds were counted in this experiment (n = 4 wild-type and 4 *lig1* plants). For each plant, the percentage of total seeds in each of the distance bins was calculated. The mean and standard error for each genotype in each distance bin is indicated in Table 2.1. Significant differences between the percentage of seeds dispersed from wild-type and *lig1* plants were found at distances 75-100 and 100-125 cm, with P-values (Student's t-test) of 0.044 and 0.008 respectively (Figure 2.2). The maximum distance that seeds were dispersed was 150-175 cm for wild type and 100-125 cm for *lig1* (Figure 2.2). These results show that seeds are dispersed in a significantly reduced range in the *lig1* mutant compared to wild type. Specifically, a greater proportion of *lig1* seeds are

dispersed within 50 cm of the mother plant, and a greater proportion of wild-type seeds are dispersed further than 50 cm from the mother plant (Figure 2.2 and Table 2.1). Therefore, reduced lignin in the endocarp *b* secondary cell wall of *lig1* mutants results in a reduction of the seed dispersal range achieved by explosive valve coiling.

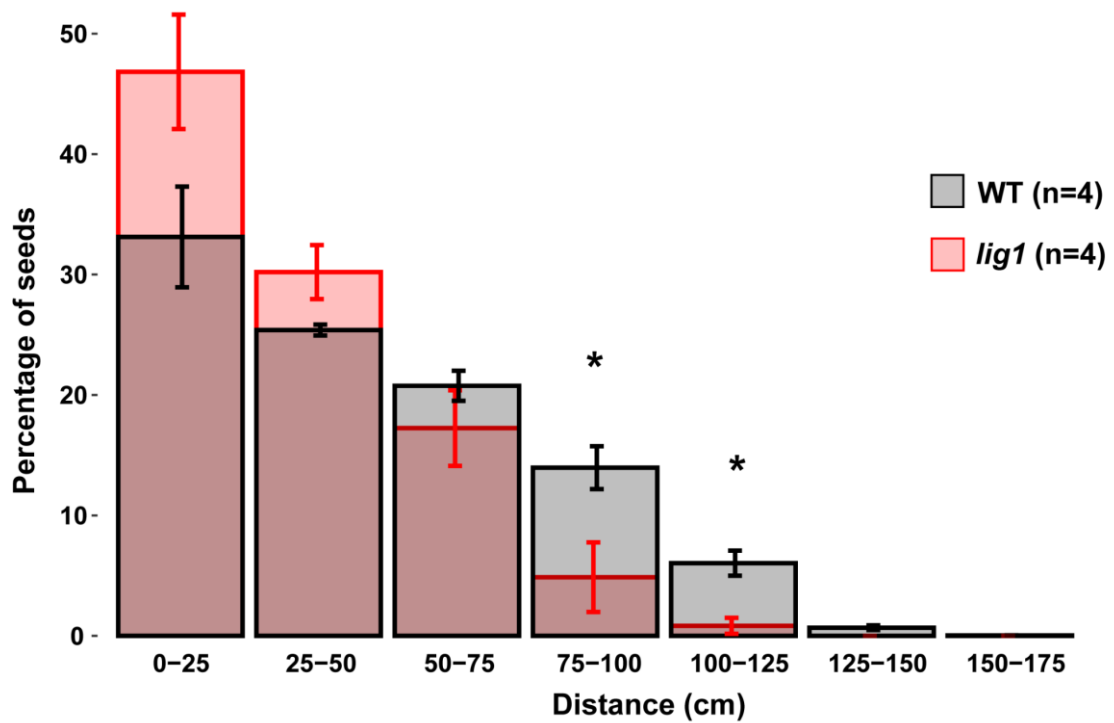


Figure 2.2: *lig1* has reduced seed dispersal range. Bar plot of percentage of seeds at distances bins. Bar plot heights indicate mean values of 4 biological replicates and error bars indicate standard deviation. Asterisks indicate statistically significant differences (P-value < 0.05, t-test) between means of genotypes (n = 4). Plants grown in Cu-limiting conditions (watered with collected rain water and supplemented weekly with 10 mL of 0.5 mM CuSO₄) to ensure fruit production with reduced endocarp *b* lignification (see Figure 2.1).

Distance bins	WT mean percentage seeds	<i>lig1</i> mean percentage seeds	WT SE	<i>lig1</i> SE
175-200	-	-	-	-
150-175	0.04	-	0.04	-
125-150	0.68	-	0.20	-
100-125	6.04	0.83*	1.04	0.67
75-100	13.96	4.87*	1.78	2.89
50-75	20.76	17.26	1.24	3.14
25-50	25.39	30.20	0.45	2.25
0-25	33.12	46.83	4.18	4.75

Table 2.1: Percentage of total seeds at each distance bin. Asterisks indicate statistically significant differences (P-value < 0.05, Student's t-test) between means of genotypes (n = 4). SE: standard error of the mean.

3. Mapping the *lig1* mutation

To identify the genetic basis of the *lig1* mutant phenotype, I first used a mapping-by-sequencing approach. The *lig1* mutant was identified from a genetic screen in the Oxford (Ox) background. To create a polymorphic mapping population, a homozygous *lig1* mutant was crossed to a wild-type plant of the New Zealand (Nz) ecotype, and an F₁ progeny plant was allowed to self-fertilize to produce an F₂ population that segregated *lig1* and wild-type plants. Plants from this F₂ population were phenotyped for the buckled margin that is characteristic of *lig1* mutant fruit. 118 plants exhibited the mutant fruit phenotype out of a total of 369 plants, indicating that the *lig1* allele is recessive. Genomic DNA was isolated from 48 plants showing the mutant phenotype and the DNA was pooled. Using the same procedure, DNA was isolated from 48 plants without the mutant phenotype and the DNA was pooled. Two genomic DNA libraries were prepared for Next Generation Sequencing, one for the mutant DNA pool and another one for the wild-type DNA pool; and they were sequenced separately by Illumina HiSeq at MIPZ Genome Center (Hugo Hofhuis, unpublished work). Sequencing reads were mapped to the Ox reference genome and single nucleotide polymorphisms (SNPs) were called against the reference sequence, including both Nz polymorphisms and EMS derived mutations (read mapping and SNP calling were performed by Dr. Xiangchao Gan). For the wild-type DNA library, sequencing results produced

a mean read coverage of approximately $43 \times$ and 96 % of the reference genome was covered at least once. For the mutant DNA library, sequencing results produced a mean read coverage of approximately $46 \times$ and 96 % of the reference genome was covered at least once. A Fisher's exact test was used to assess linkage of the SNPs identified to the phenotype and a P-value was calculated using this test for each SNP (performed by Dr. Xiangchao Gan). A region on chromosome 6 between positions Chr6:16,640,553 and Chr6:19,773,464 showed low P-values, including the two lowest P-values and 19 out of the 30 most significant SNPs (i.e. lowest P-values) (Figure 2.3). Although the genome was homogeneously sampled for SNPs, a threshold P-value was set for the analysis and, therefore, genomic regions with P-values lower than the threshold appear less sampled in Figure 2.3.

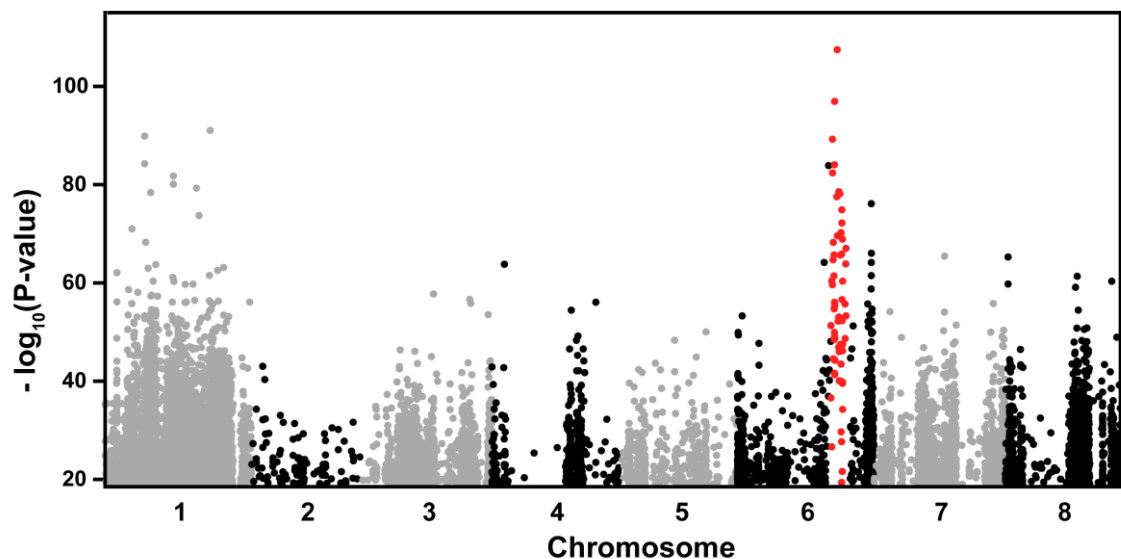


Figure 2.3: Values of $-\log_{10}(\text{P-value})$ (Fisher's exact test) of SNPs identified across the genome in the mapping-by-sequencing experiment. SNPs in the region with low P-values in chromosome 6 are shown in red.

To confirm the region of the genome identified by DNaseq, and to narrow down the genetic interval, I used a fine mapping approach. I developed several genetic markers to genotype Nz SNPs and insertions/deletions (INDELs) across the interval identified by the bulked segregant analysis. I developed these markers making use of the sequencing data available from the

DNaseq. I designed dCAPS markers to genotype SNPs and INDEL markers to genotype insertions/deletions. Markers used for mapping are listed in Table 6.5 of materials section. These genetic markers were used to genotype individuals of the F₂ mapping population that displayed a *lig1* mutant phenotype. In a first mapping experiment, stored tissue samples corresponding to individuals already phenotyped by a previous member in the group (Hugo Hofhuis, unpublished work) were genotyped. I genotyped 87 individuals exhibiting a mutant phenotype using two markers flanking the genomic region identified by DNaseq. I found 48 recombinant chromosomes out of 174 total chromosomes for SNP_16824303 (27.59 cM) and 43 recombinant chromosomes out of 174 total chromosomes for INDEL_18607525 (24.71 cM). These recombination frequencies of < 50 cM indicate that both markers are linked to the causal mutation. However, 7 individuals were homozygous for Nz alleles on both flanks of this genetic interval, suggesting the presence of mis-phenotyped individuals (i.e. wild-type plants that had been mis-scored as mutant). For further analysis, only recombinant individuals between these two markers were genotyped using 5 additional markers. These results defined a genetic interval of 1.15 cM that maps between Chr6:17,676,369 and Chr6:17,882,576 (Figure 2.4 A and C).

Although in the first mapping experiment we identified a genetic interval containing markers linked to the causal *lig1* mutation, several individuals were homozygous for Nz alleles throughout the interval. This could be due to incorrectly phenotyped plants, and since seeds were not collected from these plants, the phenotypes could not be confirmed in the next generation. Therefore, a second mapping experiment was performed using 171 new plants from the original F₂ mapping population derived from a *lig1* × Nz cross. In this mapping population, 34 plants had a buckled margin that is characteristic of *lig1* mutant fruit and 137 had wild-type fruit, indicating recessive inheritance of the *lig1* allele. Mutant plants were genotyped using two markers flanking the genomic region identified by DNaseq. For INDEL_16810437 (Chr6:16,810,437), 8 recombinant chromosomes were found in a total of 68 chromosomes (11.76 cM). For INDEL_18607525 (Chr6:18,607,525), 5 recombinant chromosomes were found in a total of 68 chromosomes (7.35 cM). These results confirm that both markers are linked to the causal mutation and validate the genomic region identified by bulked segregant DNaseq. Using 4 additional markers to genotype

the recombinant individuals, the interval of this second mapping experiment was narrowed to a 7.35 cM interval that maps between positions Chr6:17,317,339 and Chr6:18,607,525. No further recombinations were found between these positions. (Figure 2.4 B). The interval identified in the first mapping experiment is narrower (1.15 cM) and maps within the broader interval identified in the second mapping experiment (Figure 2.4 C).

To compile a list of candidate causal mutations from the SNPs present in the mapped intervals, several criteria were used. SNPs were considered candidates if they generated non-synonymous changes in annotated genes and if the SNPs were a canonical EMS-type (G to A or C to T). Furthermore, SNPs that corresponded to polymorphisms between the Ox and Nz parental ecotypes were filtered out. The candidate mutations identified in the intervals are listed in Table 2.2. Five candidate mutations were identified in the broader genetic interval from the second mapping experiment. Furthermore, two of the six candidate mutations met all the criteria mentioned above and were located in the narrower genetic interval identified in the first mapping experiment (Figure 2.4 C). One SNP was located in the gene CARHR194170, identified as the ortholog of the transcription factor *SQUAMOSA PROMOTER BINDING PROTEIN-LIKE 7* (*SPL7* -At5g18830-). The second SNP was located in CARHR194330, identified as the ortholog of *BETA-AMYLASE 9* (*BAM9* -At5g18670-).

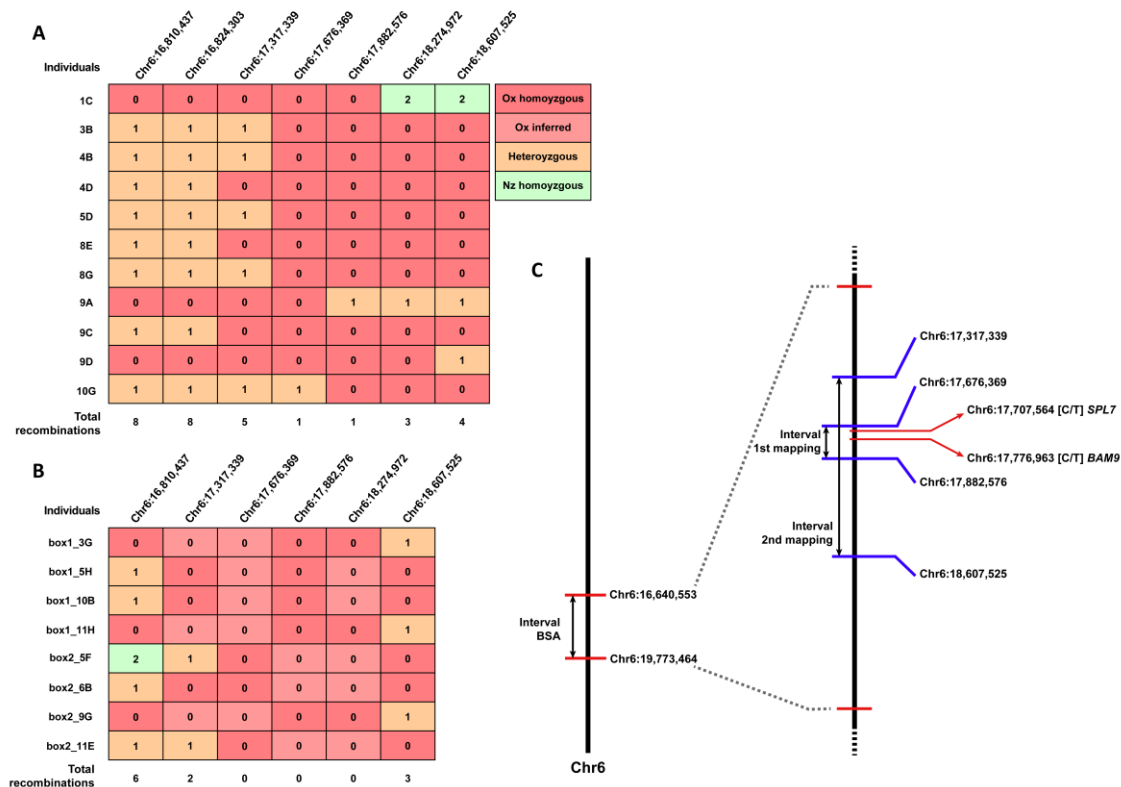


Figure 2.4: Fine mapping of *lig1* causal locus. (A) First fine mapping experiment. Table shows alleles of 11 recombinant F₂ individuals at 7 markers. Total recombinations for each position are indicated below. (B) Second fine mapping experiment. Table shows alleles of 9 individuals at 6 markers. Total recombinations for each position are indicated below. (C) Diagram summarizing results of bulked segregant DNaseq mapping and fine mapping experiments. Two candidate mutations are indicated in red.

Position	Nucleotide substitution	Amino acid substitution	<i>C. hirsuta</i> gene number	Name	<i>A. thaliana</i> reference gene number
Chr6:17,707,564	C1327T	P443S	CARHR194170	SQUAMOSA PROMOTER BINDING PROTEIN-LIKE 7 (SPL7)	AT5G18830
Chr6:17,776,963	C215T	P72L	CARHR194330	BETA-AMYLASE 9 (BAM9)	AT5G18670
Chr6:18,129,466	C1604T	T535I	CARHR195200	5-METHYLTETRAHYDROPTEROYLTRIGLUTAMATE HOMOCYSTEINE METHYLTRANSFERASE 1 (ATCIMS)	AT5G17920
Chr6:18,271,860	G340A	E114K	CARHR195560	AUGMIN SUBUNIT 7 (AUG7)	AT5G17620
Chr6:18,336,859	G686A	S229N	CARHR195780	PLETHORA4 (PLT4)	AT5G17430

Table 2.2: Candidate causal mutations of *lig1* identified in fine mapping intervals.

4. A mutation in *SQUAMOSA PROMOTER BINDING PROTEIN-LIKE 7 (SPL7)* causes the *lig1* phenotype

To identify the causal mutation underlying the *lig1* phenotype, I performed transgenic complementation tests with the two genes that I had identified containing candidate SNPs in the

fine mapping interval for *lig1*. These genes were orthologous to *BETA-AMYLASE 9* (*BAM9* - At5g18670-) and *SQUAMOSA PROMOTER BINDING PROTEIN-LIKE 7* (*SPL7* -At5g18830-). To test whether *BAM9* could complement the *lig1* phenotype, I made a construct containing the *BAM9* coding sequence, amplified from *C. hirsuta* Ox cDNA, tagged in frame with GFP, and driven by the *BAM9* promoter, amplified from *C. hirsuta* Ox genomic DNA. The construct was transformed in the *lig1* mutant background. *lig1* plants that contained the *pBAM9::BAM9:GFP* transgene had the same mutant fruit phenotype as non-transgenic *lig1* plants (Figure 2.5), indicating that *BAM9* is not the causal locus for the *lig1* mutant phenotype.

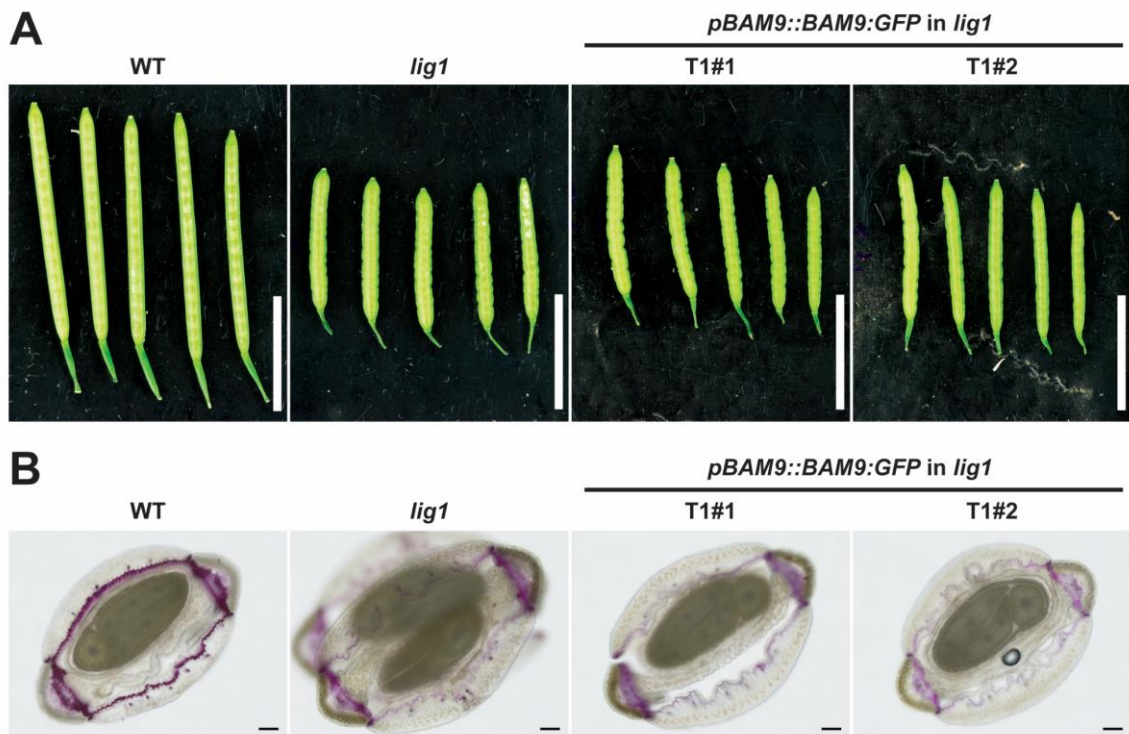


Figure 2.5: Functional complementation test of *lig1* with *BAM9*. (A) Images of fruits at stage 17 a/b from wild type, *lig1* and two independent *pBAM9::BAM9:GFP* T₁ lines in *lig1*. Plants grown in Cu-limiting conditions (watered with collected rain water and not supplemented with CuSO₄). Scale bar: 10 mm. (B) Microscope images of stage 17 a/b fruit cross sections stained with phloroglucinol/HCl. Wild type, *lig1* and two independent *pBAM9::BAM9:GFP* T₁ lines in *lig1*. Plants grown in Cu-limiting conditions (watered with collected rain water and not supplemented with CuSO₄). Scale bar: 100 μm.

5. *SPL7* complements the *lig1* mutant phenotype

The other candidate gene in the *lig1* interval encodes the transcription factor *SPL7*. This transcription factor is a central regulator of copper homeostasis and, in *A. thaliana*, loss of function *spl7* plants display a phenotype only under copper (Cu) limiting conditions (H. Yamasaki *et al.*, 2009). Therefore, to test whether *SPL7* could complement the *lig1* mutant phenotype, I grew the transgenic plants under Cu-limiting conditions. For *SPL7* complementation experiments, several constructs were used. Details and a summary of constructs used for complementation can be found in methods and Figure 2.6. One of the constructs used, carried the CDS sequence of wild-type *SPL7*, amplified from *C. hirsuta* Ox cDNA, tagged at the N-terminus with mCherry fluorescent protein and driven by the *SPL7* promoter, amplified from *C. hirsuta* Ox genomic DNA. I transformed *lig1* plants with this construct and assessed the fruit phenotype of 4 independent *pSPL7::mCherry:SPL7* lines. All 4 lines showed wild-type fruit morphology with straight margins that did not buckle at maturity (Figure 2.7 G). Furthermore, phloroglucinol staining showed that lignification of endocarp *b* secondary cell walls was restored to wild-type levels (Figure 2.7 A-F). These results indicate that *SPL7* is the causal locus for the *lig1* phenotype.

Another *SPL7* construct used for complementation experiments, contained the CDS sequence of wild-type *SPL7*, tagged at the C-terminus with YFP_{venus} fluorescent protein, and driven by the *SPL7* promoter (Figure 2.6). The fruit defects of *lig1* mutants were fully rescued to wild type in 2 independent *pSPL7::SPL7:YFP_v* lines (Figure 2.7 H), and the lignification defects were also restored similar to the *pSPL7::mCherry:SPL7* lines. This result indicates that *SPL7* fusion proteins, tagged at either the N- or C-terminus with a fluorescent protein, are sufficient to rescue the *lig1* mutant phenotype.

A third *SPL7* construct used for complementation experiments, carried a truncated N-terminal version of the *SPL7* protein, including the conserved SBP domain, but lacking the conserved IRPGC and TMD domains (Figure 2.6). This truncated protein was tagged at the C-terminus with GFP and driven by the *SPL7* promoter. The fruit defects of *lig1* mutants were fully restored to wild type in 5 independent *pSPL7::SBP:GFP* lines (Figure 2.7 G). This interesting result indicates

that the C-terminal domain of the SPL7 transcription factor, which contains the SBP DNA-binding domain, is sufficient to complement all aspects of the *lig1* mutant phenotype.

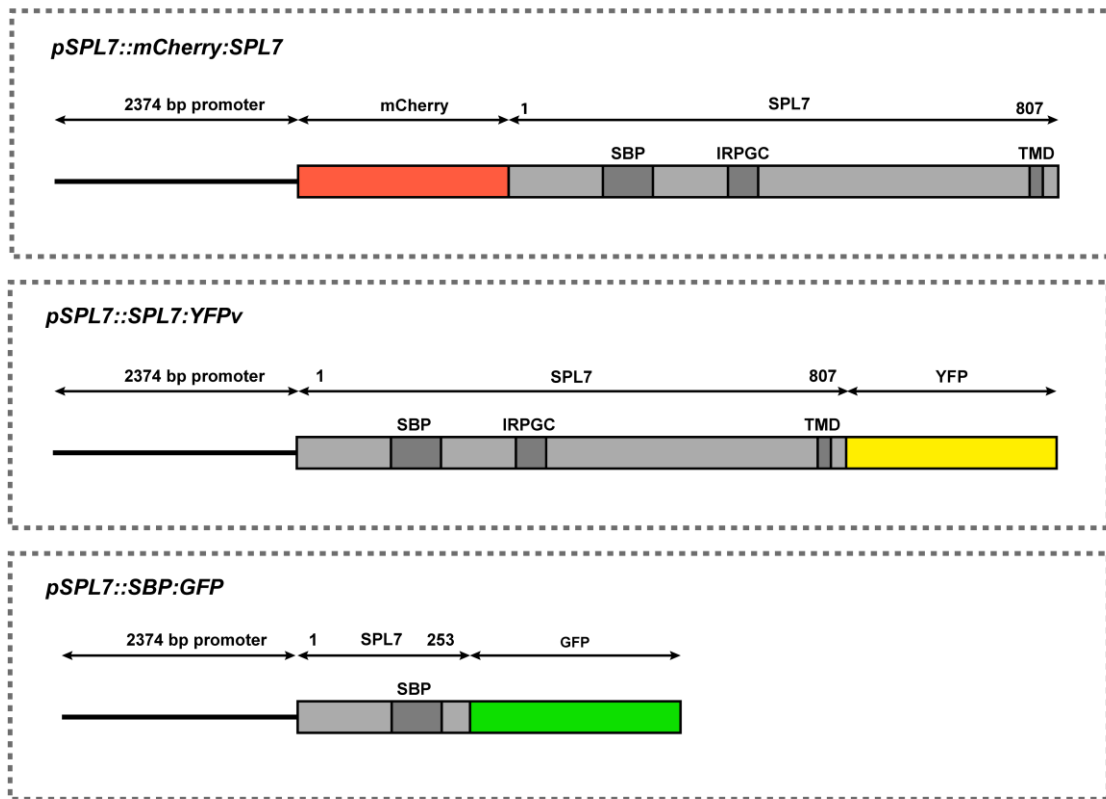


Figure 2.6: SPL7 translational fusions used in *lig1* complementation experiments. Length of promoter sequences is indicated in bp. Amino acids of the resulting protein are indicated. Conserved domains of SPL7 are marked in dark grey.

Complementation lines for these three different SPL7 constructs were used to investigate the localization of SPL7 in *C. hirsuta* fruit valves. Fluorescent signal in *pSPL7::SBP:GFP* complementation lines was detected in the valve endocarp b layer at stage 17 a/b of fruit development, when the SCW of endocarp *b* cells is lignified (Figure 2.6 I). This indicates that SPL7 accumulates in the endocarp *b* cells where the lignification defect is observed in *lig1* mutants. Importantly, the fluorescent signal in *pSPL7::SBP:GFP* complementation lines localized specifically to the nucleus in endocarp *b* cells (Figure 2.6 I). This indicates that the SBP domain of SPL7, which includes a nuclear localization signal, is sufficient for nuclear localization and complementation of the *lig1* phenotype. Although both *pSPL7::mCherry:SPL7* and

pSPL7::SPL7:YFPv constructs fully complemented the *spl7* fruit and lignification defects, I failed to reliably detect fluorescent signal in *pSPL7::mCherry:SPL7* and *pSPL7::SPL7:YFPv* complementation lines in the endocarp *b* layer or other cell types in the fruit. These results agree with previous reports in *A. thaliana*, where two full-length SPL7 proteins tagged with fluorescent markers at either the C-terminus or N-terminus fully rescued the *spl7* mutant phenotype, but could not be detected in *A. thaliana* transgenic plants (Garcia-Molina *et al.*, 2014b), suggesting rapid turnover of the protein.

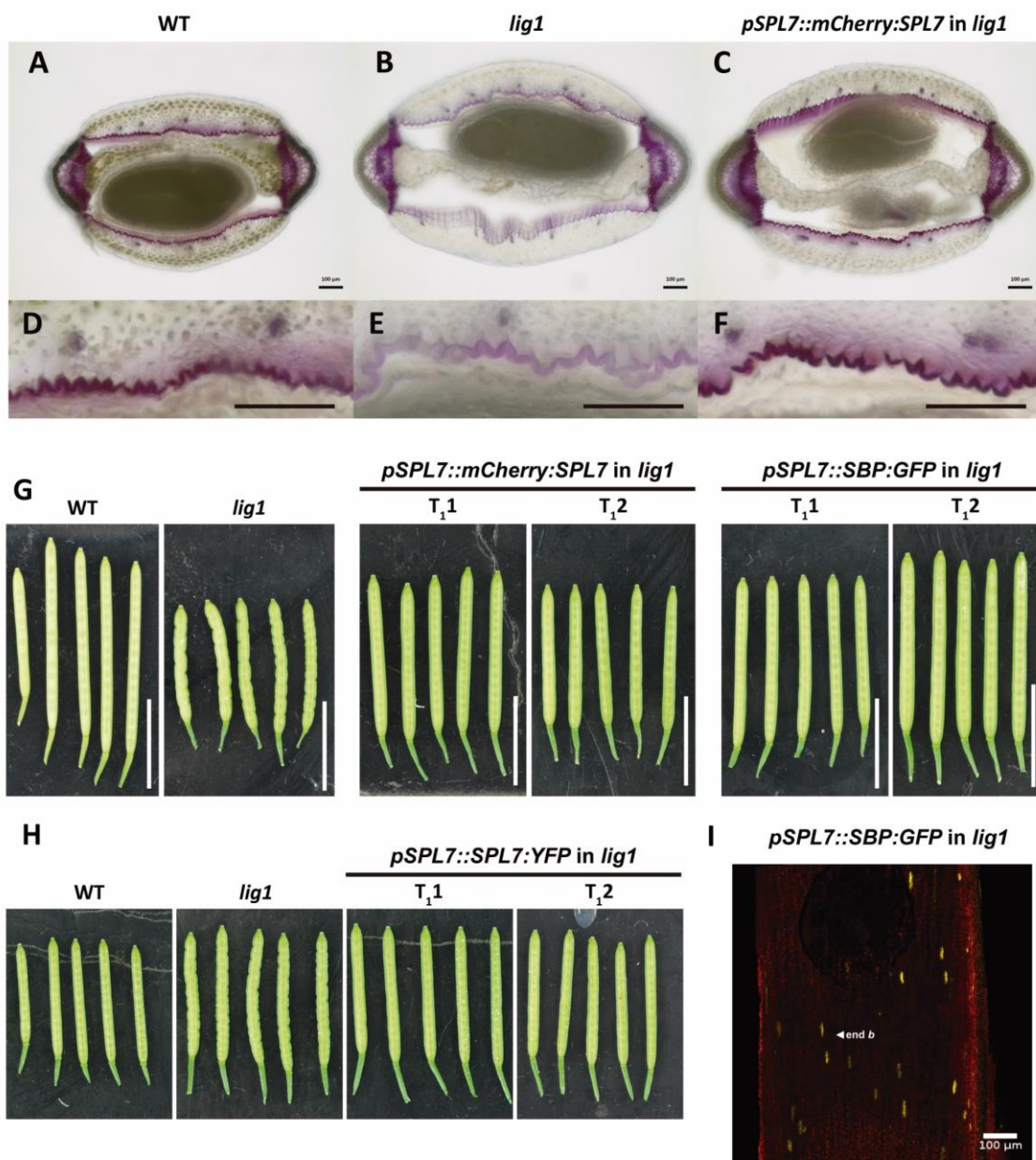


Figure 2.7: Functional complementation of *lig1* mutant phenotype with *SPL7*. (A-F) Microscope images of stage 17 a/b fruit cross sections stained with phloroglucinol/HCl. Wild type (A, D), *lig1* (B, E) and *lig1* complemented by *pSPL7::mCherry:SPL7* (C, F). Plants grown in Cu-limiting conditions (watered with collected rain water and supplemented weekly with 10 mL of 0.5 mM CuSO₄). Wild-type and *lig1* cross sections are the same as in Figure 2.1. (D-F) Zoom-in of endocarp *b* layer from the respective images A-C. Scale bars: 100 μm. (G-H) Complementation of *lig1* phenotype with three different *SPL7* constructs. (G) Fruits at stage 17 a/b from wild type and *lig1* (left), *lig1* complemented by *pSPL7::mCherry:SPL7* in two independent T₁ lines (middle, n = 4 independent lines) and *lig1* complemented by *pSPL7::SBP:GFP* in two independent T₁ lines (right, n = 5 independent lines). Plants were grown in Cu-limiting conditions (watered with collected rain water and not supplemented with additional Cu). Scale bar: 10 mm. (H) Fruits at stage 17 a/b from wild type and *lig1* (left) and *lig1* complemented by *pSPL7::SPL7:YFPv* in two independent T₁ lines (right, n = 2 independent lines). (I) Confocal micrograph of SBP:GFP localization in *lig1* valve. Valve was peeled from fruit at stage 17 a/b and placed on a slide with the inner side (endocarp layers) facing the cover slip. Background (red): autofluorescence signal in chlorophyll region. Plant not supplemented with copper. Scale bar: 100 μm. It is important to note that endocarp *b* cells are very elongated in the longitudinal direction of the fruit valve, so nuclei from adjacent cells can be located far from each other in this direction.

6. Characterization of the *lig1* mutation in *SPL7*

The causal SNP identified in *SPL7*, responsible for the *lig1* phenotype, is a nucleotide substitution of Cytosine to Thymine at position Chr6:17,707,564 (Figure 2.8 A). This mutation introduces an amino acid substitution in CARHR194170 (ortholog of the transcription factor SQUAMOSA PROMOTER BINDING PROTEIN-LIKE 7; *SPL7* -At5g18830-). This substitution converts the Proline residue at amino acid #443 in the protein to a Serine residue. This P443 residue in *SPL7* is conserved in several Brassicaceae species and other flowering plant species, and it is located in a region of overall low conservation, C-terminal to the IRPGC domain (Figure 2.8 B-D).

To explore the possible effect of this amino acid substitution on protein function, and to further characterize *SPL7* in *C. hirsuta*, I compared *C. hirsuta* *SPL7* protein to other species. *SPL7* from other species contains three conserved domains (Squamosa Promoter-Binding protein domain,

SBP; IRPGC and a transmembrane domain TMD) and their function has been characterized to some extent. To investigate whether the conserved domains of SPL7 are also present in *C. hirsuta*, I generated a multiple sequence alignment of SPL7 orthologous proteins from several flowering plant species (Figure 2.9). *C. hirsuta* and *A. thaliana* share 87.55 % amino acid sequence identity. The SBP domain is a plant-specific DNA-binding domain that is characteristic of the SBP-like (SPL) transcription factor family, which consists of 16 members in *A. thaliana* (Guo *et al.*, 2008; Xing *et al.*, 2010). Several members of the *SPL* gene family are targeted by miR156, however, *SPL7* belongs to the group of *SPLs* that are not targeted by miR156. The SBP domain contains two zinc-binding sites and a bipartite nuclear localization signal (NLS). This domain is present in *C. hirsuta* in the N-terminal part of the protein and all amino acids in the SBP pattern involved in zinc-binding (C-X₄-C-X₁₆-C-X₂-[HC]-X₁₅-C-X₂-C-X₃-H-X₁₁-C) are conserved in *C. hirsuta*. Furthermore, the residues that constitute the NLS are present in *C. hirsuta* in the same positions. Overall, only 7 amino acid substitutions are present in the region compared to the *A. thaliana* SPL7 protein in a total of 75 amino acids of SBP region. They correspond to variable amino acids in the pattern (“x residues”). Around the middle of the SPL7 protein, another conserved domain was previously identified, the IRPGC domain, which showed evidence for dimerization function in *A. thaliana* (Garcia-Molina *et al.*, 2014b). All amino acids and positions of the IRPGC signature (R-x-S-x-KL-x₄-P-x₃-P-x₂-L-x₇-L-x₇-E-x₃-R-x-GC-x₃-T) are conserved between *A. thaliana* and *C. hirsuta*. Only one amino acid is different from *A. thaliana* in a total of 69 in the entire IRPGC region. A last conserved region in the C-terminus was previously identified in *A. thaliana*, a transmembrane domain (TMD) which includes 20 residues. In *C. hirsuta*, this conserved domain is also present in the C-terminus and only the first 2 amino acids are different from *A. thaliana* (Figure 2.8).

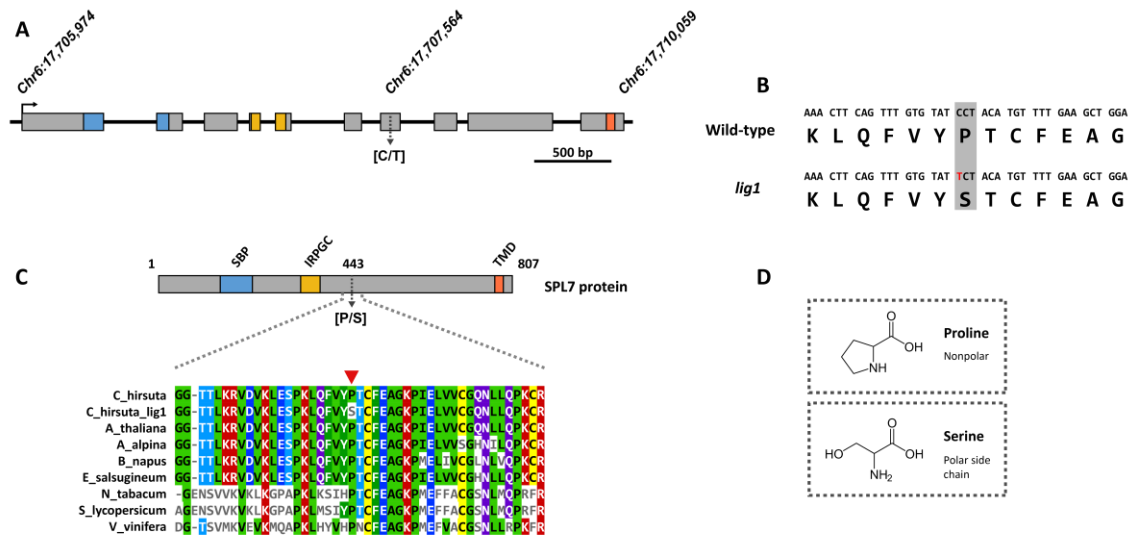


Figure 2.8: A non-synonymous nucleotide substitution in a conserved amino acid of SPL7 is a candidate mutation for the *lig1* phenotype. (A) *SPL7* genomic region showing exons and introns. Non-synonymous nucleotide substitution identified in *lig1* located in exon 7 is marked. (B) DNA and protein sequences of wild type and *lig1* in the region of the identified nucleotide substitution. (C) *C. hirsuta* SPL7 protein model and alignment of SPL7 protein sequences from several Brassicaceae species and other angiosperm species. SBP, IRPGC and TMD conserved domains are indicated in blue, yellow and orange respectively. Red arrowhead marks conserved amino acid changed in *lig1*. (D) Proline and Serine amino acid structures and their main chemical characteristic.

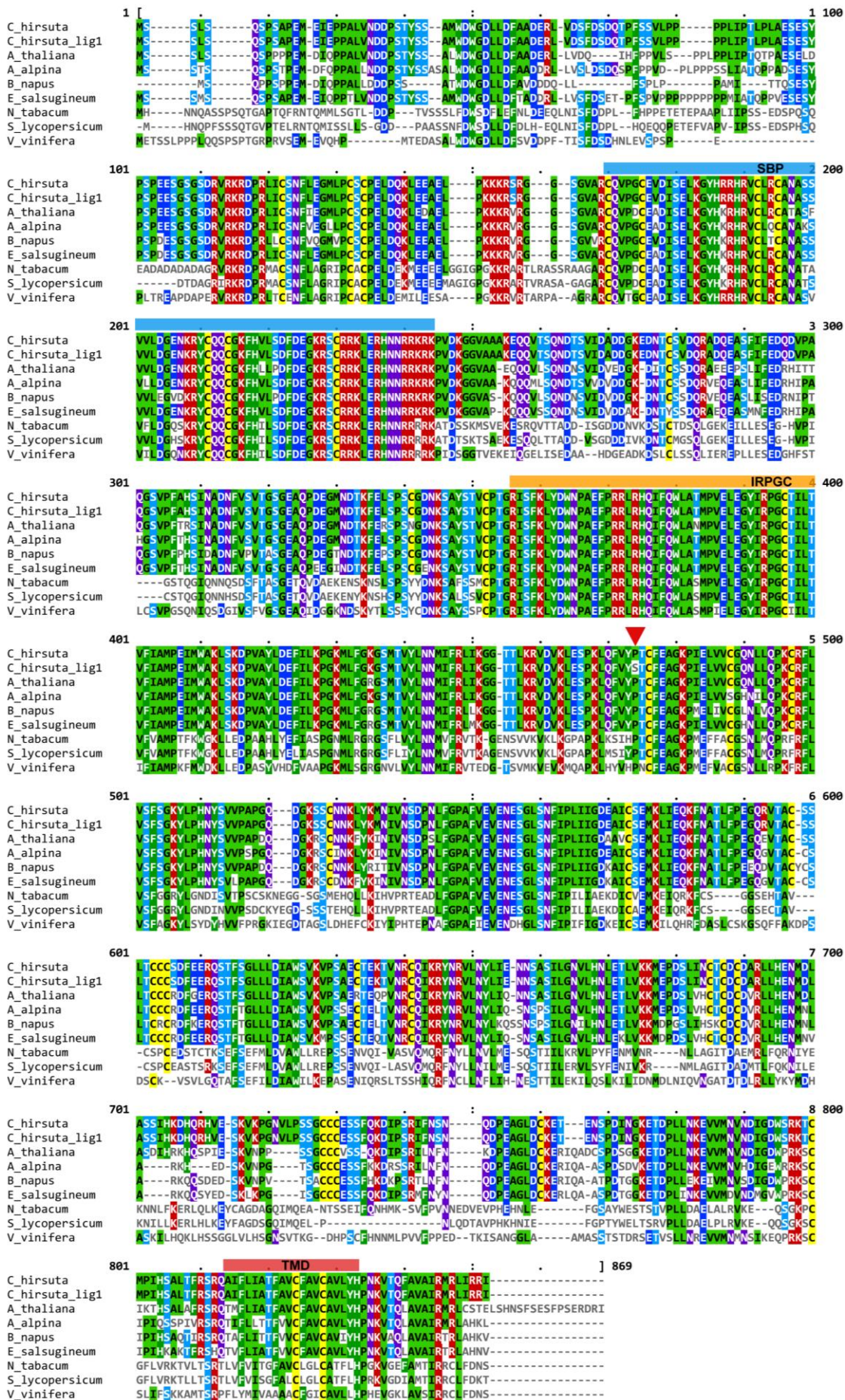


Figure 2.9: Multiple sequence alignment of SPL7 orthologous proteins. Amino-acid sequences were downloaded from GenBank and aligned using Clustal Omega alignment tool. Genbank accession numbers: *Arabidopsis thaliana* AT5G18830.3; *Arabis alpina* AGP03030.1; *Brassica napus* XP_013683534.1; *Eutrema salsugineum* XP_006400438.1; *Nicotiana tabacum* NP_001313185.1; *Solanum lycopersicum* XP_019070792.1; *Vitis vinifera* XP_002277039.1. Conserved SBP, IRPGC and TMD domains are marked. Arrowhead marks position of Proline to Serine substitution in *lig1*.

7. *SPL7* CRISPR/Cas9 allele phenocopies *lig1*

To further confirm that the *lig1* mutant phenotype is caused by loss of *SPL7* function, I generated a knockout allele of *SPL7* using CRISPR/Cas9 gene editing in *C. hirsuta* (Ox accession). In order to introduce edits that would potentially cause loss of gene function, I designed two sgRNAs to target the first exon of *SPL7* (sequences in Table 6.3 of methods section). In the T₁ generation, I identified 31 transgenic plants that were resistant to Basta. I genotyped these 31 plants by PCR amplification and sequencing of the sgRNA binding regions and found edits in the *SPL7* gene sequence in four plants. Three of these gene edits were located in the sgRNA2 binding site and one in the sgRNA1 binding site. The results of the T₁ screening are summarized in Table 2.3.

In the T₂ generation of these four edited lines, I genotyped plants to identify individuals that were homozygous for the mutation. Additionally, I tested these plants for the presence of the transgene (Cas9 presence) by PCR amplification and by insertion copy number estimation (iDNA Genetics). I identified one plant that was homozygous for the mutation and negative for the Cas9 transgene in both assays. I selected this plant (Chi_ *spl7* _T₂-19) and named the allele *spl7-2*.

The single nucleotide deletion in *spl7-2* introduces a premature stop codon in the first exon at amino acid position #67 from start codon (Figure 2.10 A, B). The resulting truncated protein lacks the conserved SBP DNA-binding domain. Homozygous *spl7-2* plants grown in Cu-limiting conditions have a buckled fruit margin, which is characteristic of *lig1* mutant fruits (Figure 2.10 C). Furthermore, cross sections of mature *spl7-2* fruits stained with phloroglucinol/HCl show reduced lignification in SCWs of the endocarp *b* layer (Figure 2.10 D). In summary, the phenotype of *spl7-2* phenocopies *lig1*, further confirming that *lig1* is a *spl7* allele. Therefore, I renamed *lig1*

as *spl7-1*. Moreover, the phenotype of both alleles is very similar, indicating that *spl7-1* is likely to represent complete loss of *SPL7* function, similar to *spl7-2*.

T₁ lines	Type of gene edit	Location of gene edit	Transgene insertion number
T ₁ 2	-1 bp (Heterozygous)	sgRNA2	10
T ₁ 7	- 2 bp (Heterozygous)	sgRNA2	42
T ₁ 17	+1bp (Heterozygous)	sgRNA1	40
T ₁ 26	+ 1bp (Heterozygous)	sgRNA2	34

Table 2.3: CRISPR/Cas9 induced gene edits identified in T₁ plants. The number of transgene insertions determined is indicated.

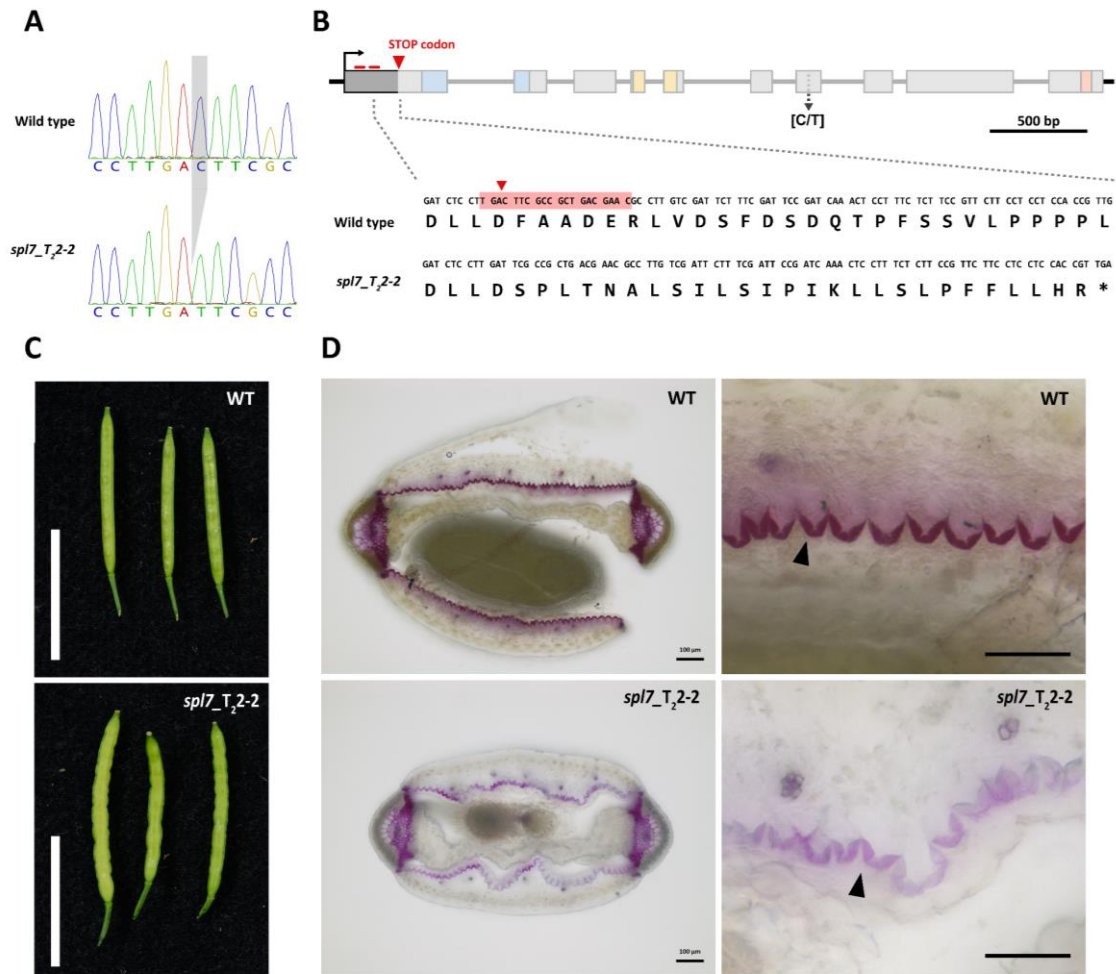


Figure 2.10: CRISPR/Cas9 knock out of *SPL7* in *C. hirsuta* shows reduced lignification in endocarp *b*. (A) Chromatograms of sgRNA2 binding site region sequenced from wild type and *spl7_T2-2*. Nucleotide deletion is indicated in grey. (B) *C. hirsuta SPL7* genomic region. SBP domain: blue, IRPGC domain: yellow and TMD domain: orange. Positions of sgRNAs binding sites and identified premature stop codon are marked in red. Position of C>T nucleic acid substitution previously identified in *lig1* is marked. DNA and amino acid sequences of wild type and *spl7_T2-2* are shown. sgRNA2 binding site is highlighted in red and arrowhead indicates position of single nucleotide deletion (C) Fruit at stage 17 a/b from wild type (top) and *spl7_T2-2* (bottom). Scale bar: 10 mm. (C and D) Plants were supplemented with 5 mM CuSO₄ at seedling stage and afterwards the treatment was stopped to ensure Cu-limiting conditions. (D) Microscope images of stage 17 a/b fruit cross sections stained with phloroglucinol/HCl from wild type (top) and *spl7_T2-2* (bottom). Arrowheads mark endocarp *b* layer. Scale bar: 100 μm.

Discussion

In this chapter, I identified a mutation in *SPL7* as causal for the *lig1* mutant phenotype. By combining mapping-by-sequencing and fine mapping, I identified a genetic interval with candidate SNPs in two loci. I used transgenic complementation tests to confirm that *SPL7* is the causal locus, since *SPL7* fusion proteins fully complemented the *lig1* mutant phenotype. A single nucleotide substitution in the *SPL7* gene was identified as the causal mutation which introduces an amino acid substitution in the middle of the *SPL7* protein sequence. This amino acid is conserved in several Brassicaceae species and other flowering plants, which suggests that this is an important residue for protein function. I further confirmed that the *lig1* phenotype is caused by loss of *SPL7* function by using CRISPR/Cas9 to generate an additional allele of *SPL7*. This *spl7-2* allele introduces an early stop codon in the first exon of *SPL7*, before the conserved SBP domain that harbours the DNA binding and nuclear localization sequences. Homozygous *spl7-2* plants had the same phenotype as *lig1*, therefore I renamed *lig1* as *spl7-1*. Moreover, the similarity between *spl7-2* and *spl7-1* phenotypes, particularly the reduced lignin deposition in endocarp *b* SCWs, indicates that the amino acid substitution in *spl7-1* causes complete loss of *SPL7* function, in the same way as deleting all functional protein domains in *spl7-2*.

Another interesting finding was the sufficiency of a truncated *SPL7* fusion protein, containing only the SBP domain, to completely rescue the *spl7-1* phenotype. The SBP domain contains the DNA binding region and a nuclear localisation signal. My results indicate that the function of *SPL7* in endocarp *b* lignification is as a transcription factor. In *A. thaliana*, a similar construct containing only the SBP domain and lacking the other conserved domains fully rescued the *spl7* mutant phenotype under copper limiting conditions (Garcia-Molina *et al.*, 2014b). Plants complemented with this GFP::SBP construct showed activation of *SPL7* targets even under Cu-replete conditions (Garcia-Molina *et al.*, 2014b), indicating a constitutive activity of the SBP domain and suggesting that other conserved domains in the *SPL7* protein are not necessary for the transcription factor activity (Garcia-Molina *et al.*, 2014b). These other domains are possibly involved in negative regulation of the *SPL7* transcription factor activity depending on Cu

availability. It has been proposed that the TMD conserved domain in the N-terminus could anchor the protein to membranes and that, under Cu-limiting conditions, ER stress-mediated cleavage in the middle of the protein could free the C-terminal part containing the SBP domain prior to its translocation to the nucleus (Garcia-Molina *et al.*, 2014b). Also, a dimerization process mediated by the IRPGC conserved domain in the middle of the protein has been proposed to act as a negative regulator. SPL7 dimerization would exclude SPL7 from the nucleus due to the large size of the homodimer (Garcia-Molina *et al.*, 2014b). However, these possibilities have not been supported by experimental evidence.

In *C. hirsuta*, I found that the C-terminal truncated SPL7 protein containing the SBP domain localizes to nuclei of SPL7-expressing cells, consistent with a conserved function of SPL7 as a transcription factor in *C. hirsuta*. In agreement with this result, in *A. thaliana*, it was reported that the SBP-GFP fusion protein localized to nuclei. Moreover, the nuclear localization of SBP was not affected in different copper concentrations (Garcia-Molina *et al.*, 2014b). I hypothesize that, in *C. hirsuta*, the truncated version of SPL7 containing only the SBP domain and lacking the other conserved domains could be freely translocated to the nucleus and act as a transcription factor in a constitutive manner. In the next chapter, I investigate what are the targets of SPL7 in the fruit valves of *C. hirsuta* to gain further insight into the role of SPL7 in endocarp *b* lignification.

Although transgenic lines carrying two different constructs of SPL7 full-length proteins, tagged at either the N-terminus or C-terminus, fully rescued the *spl7-1* mutant phenotype, I failed to detect localization of these tagged proteins in *C. hirsuta* fruit. Even in cells where SPL7 is expressed, such as those in the endocarp *b* layer, I could not reliably detect signal from the full-length tagged proteins. These results suggest rapid turnover of the protein, even in Cu-limiting conditions when SPL7 is active. My results also agree with what has been reported in *A. thaliana*, where two full-length SPL7 proteins tagged with fluorescent markers in either the C-terminus or N-terminus fully rescued the *spl7* mutant phenotype but could not be detected in *A. thaliana* transgenic plants (Garcia-Molina *et al.*, 2014b).

SPL7 is the key regulator of copper (Cu) homeostasis in plants (Anna Schulten & Krämer, 2017). I hypothesize that loss of function of this transcription factor in *C. hirsuta* results in altered copper homeostasis in the plant. Previous studies have shown a link between the plant Cu status and lignification (Printz *et al.*, 2016). For instance, Cu-deficient wheat plants showed reduced lignification in anthers resulting in decreased male fertility (Dell, 1980) and Cu-deficient *Pinus radiata* trees had reduced lignin content and altered lignin distribution in cell walls (Downes *et al.*, 1991). Conversely, Cu excess has been shown to enhance the activity of several proteins involved in lignin biosynthesis (C. C. Lin *et al.*, 2005); (Chmielowska *et al.*, 2009); (Liu *et al.*, 2014). Interestingly, laccases are Cu-requiring enzymes that can perform the last step of the lignin biosynthesis pathway (monomer polymerization) and they have been found to be required for lignification of stem tissues in *A. thaliana* (Berthet *et al.*, 2011). In the next chapter, I investigate the Cu homeostasis in *spl7* mutant fruit and the role of SPL7 in SCW lignification of endocarp *b* cells.

An interesting aspect of the reduced lignification of endocarp *b* SCWs in the *spl7-1* mutant, is its variable appearance in a layered pattern. Moreover, which layers are lignified can vary between different plants and fruit. This variable lignification suggests that the *spl7-1* mutant is more sensitive to changes in environmental conditions, whereas lignification of endocarp *b* cells in wild type is more robust. SPL7 is the key regulator of Cu homeostasis in plants (Anna Schulten & Krämer, 2017). I hypothesize that Cu homeostasis might be altered in *C. hirsuta spl7* mutants, rendering this genotype more sensitive to changes in Cu availability. Changes in Cu availability caused by loss of *SPL7* function would fit better with the variable lignification observed in the *spl7-1* mutant, rather than the loss of function of a specific enzyme in the lignin biosynthesis pathway that might have resulted in a more homogenous reduction in lignin deposition within SCWs.

Fruit of the *spl7-1* mutant are dehiscent and valves are able to rapidly coil, however, seeds are dispersed over a shorter distance than wild type, indicating that the range of explosive seed dispersal is reduced in the *spl7-1* mutant. These results add evidence for the functional importance

of the endocarp *b* for explosive seed dispersal. In particular, these results indicate that lignification of endocarp *b* SCWs is necessary for wild-type seed dispersal range. Importantly, the amount of potential elastic energy that can be stored in the fruit valve will depend on the material properties of the valve tissue. This potential elastic energy is then transformed into kinetic coiling energy. SCWs of endocarp *b* cells with reduced lignification were likely less able to resist the contraction of the exocarp layer and, therefore, less potential elastic energy was stored in the valve that could be transformed into kinetic coiling energy.

Mutant *spl7-1* fruit exhibit a buckled margin at maturity. This phenotype appears during broadening of the fruit, which corresponds also to the lignification phase of the endocarp *b* layer, suggesting that this phenotype is linked to the reduced lignification of the endocarp *b* layer. The exocarp layer in the fruit valve is under tension and it contracts when the valve is separated from the rest of the fruit. By contrast, the endocarp *b* layer is lignified and inextensible (Hofhuis *et al.*, 2016). I hypothesize that the reduced lignin deposition in the *spl7-1* mutant results in an endocarp *b* layer with less compression strength. As a consequence, part of the elastic energy generated in the exocarp layer would be released as buckling of the fruit margins. Importantly, *lig2* mutant plants, which lack the endocarp *b* layer, also had buckled margins at maturity, likely also because of reduced compression strength as a consequence of lacking the endocarp *b* layer.

In summary, in this chapter I characterized the reduced endocarp *b* SCW lignification of *lig1* mutants and I found that the range of seed dispersal was reduced in the *lig1* mutant compared to wild type, indicating the importance of SCW lignification in endocarp *b* cells for explosive seed dispersal in *C. hirsuta*. By positional cloning, transgenic complementation and the isolation of additional alleles, I demonstrated that *SPL7* was the causal locus for the *lig1* mutant phenotype, therefore, I renamed *lig1* as *spl7*. *SPL7* is the central regulator of Cu homeostasis in plants. In the next chapter, I investigate the consequences of loss of *SPL7* function on Cu homeostasis in *C. hirsuta* fruit. I also explore the consequences of loss of *SPL7* function on the transcriptome of *C. hirsuta* fruit to understand how *SPL7* regulates endocarp *b* SCW lignification.

**Chapter 3: Role of SPL7 in lignin
deposition of endocarp *b* cells**

Introduction

In the previous chapter, I found that a mutation in *SPL7* is the basis for the *lig1* mutant phenotype. I found that the amino acid substitution in *spl7-1* results in the same phenotype as the *spl7-2* allele, which lacks all conserved domains, indicating that both alleles are loss of function. *SPL7* is the key regulator of copper homeostasis in plants. In this chapter, I examine the conservation of *SPL7* function in *C. hirsuta* as a central regulator of copper homeostasis. Furthermore, I investigate the role of *SPL7* in endocarp *b* lignification.

Metal micronutrients are present as cofactors in numerous plant proteins and they are involved in most plant biological processes such as metabolism, gene regulation, signalling, and reproduction (Hansch & Mendel, 2009). For instance, a considerable proportion of the metal micronutrients iron (Fe), zinc (Zn), manganese (Mn) and copper (Cu) are allocated to proteins involved in photosynthesis (Yruela, 2013), highlighting the importance of these metals for plant biochemistry. Since plants are sessile organisms, they rely on the availability of these nutrients in the rhizosphere and they often grow in soils with deficient or excess concentrations of these metals. Metals such as Fe and Cu act in electron transport and redox processes. However, when in excess, these redox properties can make them harmful because of uncontrolled production of reactive oxygen species (ROS) (Halliwell & Gutteridge, 1984). As a consequence, plants have evolved a tight homeostasis regulation by acquisition, distribution and storage of these metal micronutrients (Hansch & Mendel, 2009).

Copper (Cu) is an essential micronutrient for nearly all eukaryotic organisms (Printz *et al.*, 2016). Copper can cycle between an oxidized (Cu^{2+}) and a reduced state (Cu^{1+}) when present as a cofactor in proteins. This characteristic is used by plants in electron transport and redox reactions (Printz *et al.*, 2016). In plants, Cu is involved in several functions (Burkhead *et al.*, 2009) including photosynthesis (Weigel *et al.*, 2003), respiration (Carr & Winge, 2003), antioxidant activity, hormone perception (Rodriguez *et al.*, 1999) and cell wall metabolism (Berthet *et al.*, 2011). However, when Cu ions are present in excess, redox cycling between Cu^{1+} and Cu^{2+} can

catalyse the production of highly toxic ROS and cause cellular damage (Halliwell & Gutteridge, 1984). Therefore, copper homeostasis is tightly controlled in plants.

SQUAMOSA PROMOTER-BINDING PROTEIN-LIKE 7 (SPL7) encodes a transcription factor that shares a highly conserved DNA-binding domain - SQUAMOSA PROMOTER-BINDING (SBP) domain - with other gene family members. This family of DNA binding proteins were first identified in *Antirrhinum majus* as transcriptional regulators of the MADS-box gene *SQUAMOSA* (Klein *et al.*, 1996). Genes that contain an SBP domain are found exclusively in the green plant lineage, from green algae to flowering plants (S. D. Zhang *et al.*, 2015). Sixteen SBP-like (SPL) proteins are encoded in the *A. thaliana* genome. Based on size and sequence similarity, *SPL* genes can be divided into two groups (Guo *et al.*, 2008; Xing *et al.*, 2010). *SPL7* belongs to the group of genes that encode larger proteins, more than 800 amino acids, and contain at least 10 exons. This group also includes *SPL1*, *SPL12*, *SPL14* and *SPL16*. The second group, consists of 11 genes that encode smaller proteins, less than 400 amino acids, and contain 4 or less exons. These small *SPL* genes, with the exception of *SPL8*, are targeted for post-transcriptional degradation by miR156, which regulates developmental phase transitions in plants (Huijser & Schmid, 2011; Wang *et al.*, 2009; Wu *et al.*, 2009). Importantly, the large *SPL* genes, including *SPL7*, are not miR-targeted (Xing *et al.*, 2010). All *SPL* family members contain the characteristic SBP-domain. This domain contains a bipartite nuclear localization signal (NLS) and 8 conserved cysteine and histidine residues, which are organized in two Zn-finger like structures that are essential for DNA binding (Birkenbihl *et al.*, 2005; Yamasaki *et al.*, 2004). *SPL* proteins bind DNA sequences with a core GTAC motif (Birkenbihl *et al.*, 2005).

In the alga *Chlamydomonas reinhardtii*, *COPPER RESPONSE REGULATOR 1 (CRR1)* is homologous to *SPL7* (Kropat *et al.*, 2005). Under copper limiting conditions, *CRR1* is required for switching from a copper-dependent photosynthetic electron transfer chain to an iron-based one. *CRR1* downregulates plastocyanin, which uses copper as cofactor, and promotes cytochrome c6, that contains iron (Eriksson *et al.*, 2004; Quinn & Merchant, 1995). In *Arabidopsis*, the function of *SPL7* to regulate copper homeostasis is conserved. However, in land plants, unlike in

Chlamydomonas, Cu-containing plastocyanin (PC) carries out the essential function of electron transport to photosystem I and cannot be replaced (Weigel *et al.*, 2003). Therefore, Cu availability needs to be ensured for photosynthesis and autotrophic growth. Under copper limiting conditions, the SBP domain of *SPL7* binds to GTAC motifs of copper responsive elements (CuREs) in promoters of Cu-responsive genes, increasing their expression (Birkenbihl *et al.*, 2005; H. Yamasaki *et al.*, 2009).

SPL7 function can be divided in two pathways. Firstly, *SPL7* promotes copper uptake by inducing Cu reduction and transport in roots. *SPL7* promotes gene expression of FERRIC REDUCTASE OXIDASE 4 (*FRO4*) and *FRO5*, which reduce copper from Cu^{2+} to Cu^{1+} in roots (Bernal *et al.*, 2012). Reduced Cu (Cu^{1+}) can be transported by members of the COPPER TRANSPORTER (*COPT*) family, and the expression of several gene family members (*COPT1*, *COPT2* and *COPT6*) is promoted by *SPL7* under copper deficiency (Jung *et al.*, 2012; Yamasaki *et al.*, 2009). Secondly, *SPL7* promotes Cu economization by inducing gene silencing of presumably non-essential proteins and, for some of these proteins, the replacement of their function by proteins using alternative cofactors. This system is based on the Cu-miRNAs, which are promoted by *SPL7* in copper deficiency. They include miR397, miR398, miR408 and miR857, which target transcripts of Cu-containing proteins such as laccases, Cu/Zn superoxide dismutases (*CSDs*) and plantacyanin (*ARPN*). While chloroplastic Cu/Zn superoxide dismutase (*CSD2*) is downregulated in copper deficiency by *SPL7*, iron superoxide dismutase *FSD1* is upregulated, which represents a mechanism of functional replacement to ensure Cu availability for plastocyanin (PC) in the chloroplast (Bernal *et al.*, 2012; Yamasaki *et al.*, 2007; Yamasaki *et al.*, 2009).

SPL7 was shown to be expressed constitutively in *A. thaliana* across developmental stages and at high levels in roots (Figure S1) (Yamasaki *et al.*, 2009) and it was found that *SPL7* expression is independent of the Cu supply in the soil (Yamasaki *et al.*, 2009). Therefore, a post-transcriptional mechanism of activation has been hypothesized to regulate its activity depending on Cu-availability. In *C. reinhardtii*, DNA binding of SBP is inhibited by high concentrations of copper (Sommer *et al.*, 2010). In plants, there is no evidence for a direct interaction between *SPL7* and

Cu that can alter SPL7 binding activity, although it has been hypothesized that SPL7 might interact with Cu-complexes that could result in an inhibition of DNA binding (Garcia-Molina *et al.*, 2014b). The SBP region in the N-terminus of SPL7 contains an NLS and a DNA binding domain. Additionally, two other conserved regions have been identified in SPL7. One, is a transmembrane domain (TMD) located in the C-terminal region. In a transient expression system, this domain is sufficient to localize GFP to membranes. Furthermore, SPL7 showed a dual localization when transiently expressed in tobacco leaves, since SPL7 tagged at the N-terminus localized to the nucleus whereas SPL7 tagged in C-terminus localized to endomembranes, including the endoplasmic reticulum (ER) (Garcia-Molina *et al.*, 2014b). The protein sizes of these two tagged versions examined by Western blot suggested a cleavage of the protein. It was shown that ER stress is increased under Cu-deficiency and it has been proposed that ER stress could trigger cleavage of SPL7 prior to translocation of the C-terminal part to the nucleus, where it can act as a transcription factor (Garcia-Molina *et al.*, 2014b).

Other mechanisms have been investigated that can influence the activity of SPL7. It was shown that SPL7 can homodimerize *in vivo* and it was proposed that dimerization may occur through another conserved domain present around the middle of the protein, the IRPGC domain (Garcia-Molina *et al.*, 2014b). Furthermore, it was found that SPL7 can interact with a protein containing a Kin17 DNA/RNA binding domain, suggesting a link between Cu deprivation and oxidative stress signalling pathways (Garcia-Molina *et al.*, 2014a). SPL7 was also shown to interact with ELONGATED HYPOCOTYL 5 (HY5) and indicated a crosstalk between Cu and light signalling pathways (H. Zhang *et al.*, 2014).

In this chapter, I generated transcriptional reporters of *SPL7* to study the expression pattern in *C. hirsuta* fruit. By using ICP-MS, I measured the Cu concentration in *spl7* mutant fruit and compared it to wild type. I used RNA-seq to characterize the transcriptional profile of *spl7* versus wild-type fruit valves and explored whether the SPL7 pathway is affected in *C. hirsuta*. I also examined this RNA-seq data for changes in the expression of genes involved in lignin biosynthesis to investigate the reduced lignification of endocarp *b* cells in the *spl7* mutant.

Results

1. *SPL7* is expressed constitutively in *C. hirsuta* throughout development with higher expression in roots

To explore the functions of *SPL7* in *C. hirsuta*, first, I examined *SPL7* gene expression in different parts of the plant and at different developmental stages. For this purpose, I used RNA sequencing data collected in several experiments performed in my Department (experiments performed in the department and collected and curated by Dr. Xiangchao Gan in an internal database). *SPL7* is expressed in all organs and developmental stages analysed and its expression does not differ strongly (Figure 3.1). Nevertheless, *SPL7* expression in roots is around 2 times higher than in other parts of the plant. In all aerial organs, *SPL7* expression levels are very similar. This indicates constitutive expression of *SPL7* with higher expression in roots.

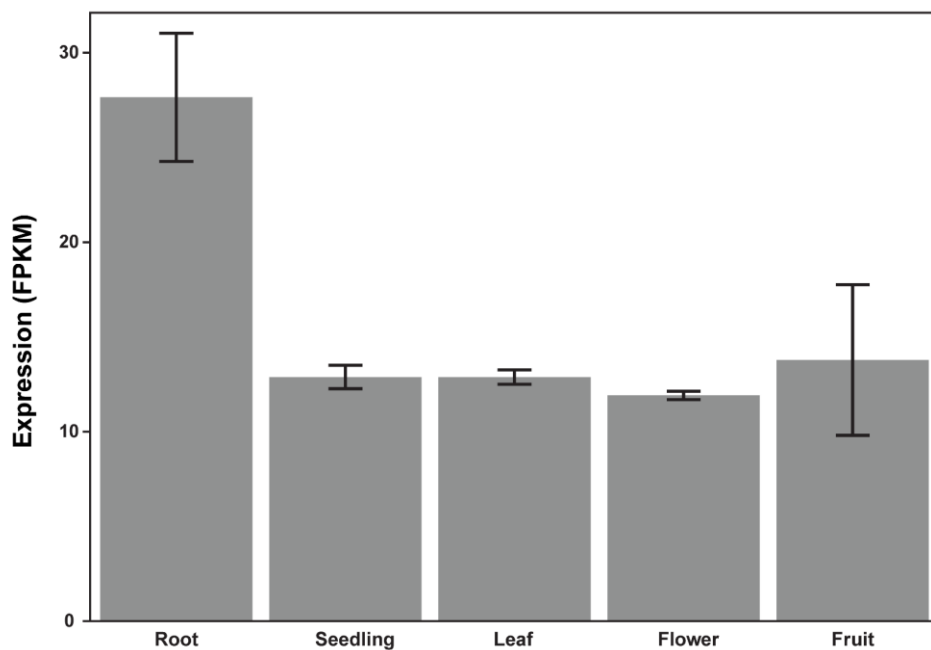


Figure 3.1: *SPL7* expression throughout *C. hirsuta* development. *SPL7* expression data in FPKM. Data from several different RNAseq projects in the department. Root: roots from 14 days old seedling grown in $\frac{1}{2}$ MS agar under short day (n = 3). Seedling: whole vegetative part from 14 days old seedlings grown in $\frac{1}{2}$ MS agar under short day (n = 3). Leaf: developing leaf of plant growing in long day (n = 3). Flower: stage 9 flowers from plant in long day (n = 2). Fruit: stage 16 fruit from plant in long day (n = 2).

2. *SPL7* is expressed in lignifying cell types of *C. hirsuta* fruits

To investigate the expression pattern of *SPL7* in *C. hirsuta* fruits, I generated a transcriptional reporter where I fused the promoter of *SPL7* with a three-copy GFP protein (*pSPL7::3xGFP*). I introduced the resulting construct into *C. hirsuta* wild-type plants via Agro-mediated transformation.

SPL7 is highly expressed in endocarp *b* cells at stage 17 ab, when SCWs of these cells are lignified (Figure 3.2 A). *SPL7* is also expressed in the valve margin adjacent to the replum. This tissue differentiates as the dehiscence zone and contains a lignified cell layer (Figure 3.2 B). Expression of *SPL7* is not detectable in the endocarp *a* or exocarp layers of the valve, or in the outer layers of the replum (Figure 3.2 B). Given that *SPL7* is expressed in the endocarp *b* layer, this suggests that *SPL7* may be required locally for the lignification of SCWs in these cells.

It is important to note that the 3xGFP signal in all these cell types is detected in nuclei despite the fact that the protein lacks any annotated nuclear localization signal (NLS). Additionally, I analysed the GFP protein sequence searching for predicted NLS using the cNLS mapper online software tool (Kosugi *et al.*, 2009) This analysis predicted a low score for putative nuclear localization signals with a maximum of 3, which indicates no exclusive nuclear localization of the protein. Although I do not expect that the unpredicted nuclear localization of 3xGFP produces any change in the *SPL7* expression pattern, I confirmed my results with a new *SPL7* promoter reporter. To generate this second transcriptional reporter, I fused the promoter of *SPL7* with a single-copy GFP protein and including an annotated nuclear localization signal (*pSPL7::GFP-NLS*). I introduced the resulting construct into *C. hirsuta* wild-type plants via Agro-mediated transformation.

Consistent with the results obtained with the previous construct, *SPL7* is highly expressed in endocarp *b* cells at stage 17 a/b, when SCWs of these cells are lignified (Figure 3.2 C-E). Expression of *SPL7* is detected in the valve margin in peeled valves (Figure 3.2 C). The GFP-NLS signal is localized to nuclei, as expected since this construct carries a nuclear localization

signal. Therefore, I reasoned that both constructs (*pSPL7::GFP-NLS* and *pSPL7::3xGFP*) are equivalent to investigate the pattern of *SPL7* expression. I also confirmed that *SPL7* expression is not detectable in the unlignified endocarp *a* layer at fruit stage 17 a/b (Figure 3.2 C-E), as I had occasionally observed low levels of expression in this cell type.

In summary, *SPL7* is expressed in endocarp *b* cells at stage 17 a/b, when SCWs are lignified, suggesting a local role in the lignification process. Moreover, *SPL7* is expressed in the valve margin, which contains a lignified cell type. These results suggest a role for *SPL7* in the lignification of cell types in the fruit valves of *C. hirsuta*. *SPL7* expression is absent, or too low to be detected with the settings used, in other non-lignified cell types in the fruit, suggesting specificity of *SPL7* expression to lignified cells in the fruit.

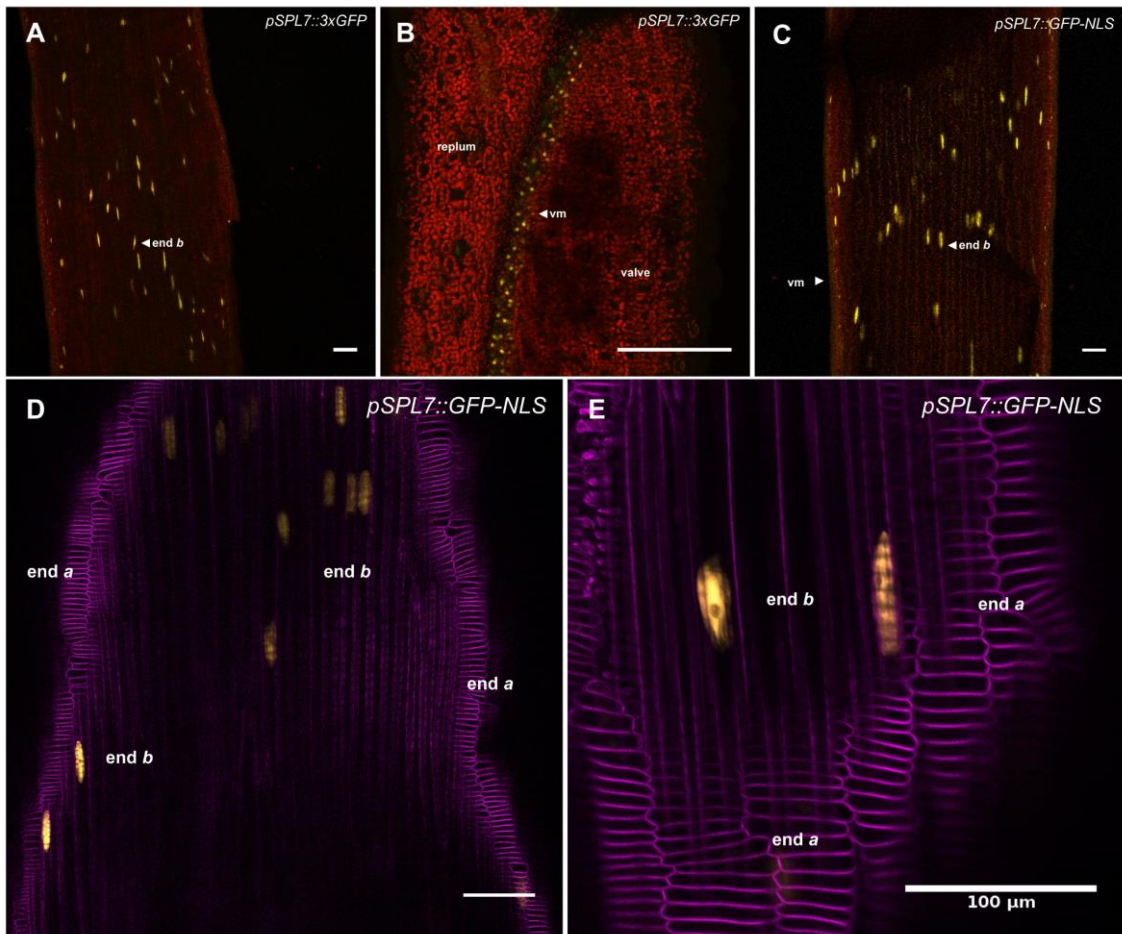


Figure 3.2: *SPL7* is expressed in the endocarp *b* layer at stage 17 a/b. Confocal micrographs showing *SPL7* expression in *C. hirsuta* fruit. Valves were peeled from fruit at stage 17 a/b and placed on a slide with the inner side (endocarp layers) facing the cover slip (A, C, D and E), or the outer layers of intact fruit were imaged (B). The transgenic lines used were *pSPL7::3xGFP* (A and B), *pSPL7::GFP-NLS* (C) and the F₁ of a cross between *pSPL7::GFP-NLS* and *pChUBI::PM:tdTomato* (D and E). Chlorophyll: red (A-C), 3xGFP: yellow (A and B), GFP-NLS: yellow (C-E), PM:tdTomato: magenta (D and E). Endocarp *a*: end *a*, endocarp *b*: end *b*, valve margin: vm. Scale bars: 100 μm. Note that endocarp *b* cells are very elongated in the longitudinal direction of the fruit valve and highly endo-reduplicated, so nuclei are very large and elongated, and nuclei in adjacent cells can be located far from each other in the longitudinal direction.

3. SPL7 is necessary for copper homeostasis in *C. hirsuta* fruit

SPL7 is the key regulator of copper homeostasis in plants and, in *A. thaliana*, loss of function *spl7* plants display a phenotype only under copper limiting conditions. Therefore, I investigated whether Cu homeostasis is affected in *spl7-1* fruits of *C. hirsuta*. For this purpose, I measured the concentration of Cu in fruits of different genotypes, under different conditions of Cu availability, by inductively coupled plasma mass spectrometry (ICP-MS). These measurements were done in collaboration with Dr. Sabine Metzger at the Mass Spectrometry platform, University of Cologne.

Cardamine hirsuta wild type, *spl7-1* and two independent complementation lines (*pSPL7::SPL7:YFPv* in *spl7-1*) were grown in soil under two different Cu conditions: supplemented and not supplemented. Mature fruits were collected and Cu concentration was analysed by ICP-MS. In non-supplemented soil, fruit from *spl7-1* plants had four times less Cu concentration (1.96 mg/Kg of dry biomass) than wild-type fruit (7.79 mg/Kg). This difference is significant at $P < 0.05$ (Figure 3.3). The Cu concentration in fruit was rescued in *pSPL7::SPL7:YFPv* complementation lines to wild-type levels (complementation line 1), or even to higher levels (complementation line 2), (7.64 mg/Kg and 11.05 mg/Kg respectively, Figure 3.3). These results indicate that *spl7-1* fruit have less copper and that transgenic expression of SPL7 fully complements the Cu concentration to wild-type levels in the fruit of two independent lines.

In soil that was supplemented weekly with 20 mL of 5 mM CuSO₄, the fruit of all genotypes had a higher Cu concentration than fruit from non-supplemented plants (Figure 3.3). In this treatment, fruits from *spl7-1* had a Cu concentration comparable to that of wild-type fruit grown in soil with no Cu supplementation (Figure 3.3). This indicates that Cu supplementation to the soil can increase the Cu concentration in *spl7-1* fruit. In these conditions of Cu supplementation, wild-type fruit still had a higher Cu concentration (11.13 mg/Kg) than *spl7-1* fruit (8.99 mg/Kg), although the difference was smaller than when these genotypes were grown on non-supplemented soil (Figure 3.3). In these Cu-supplemented conditions, *pSPL7::SPL7:YFPv* transgenic lines fully complemented the Cu concentration of *spl7-1* fruit and even increased the Cu concentration above

wild-type levels in fruits from complementation line 2 (Figure 3.3). In summary, these results indicate that SPL7 is necessary for the homeostasis of Cu observed in *C. hirsuta* fruit in response to Cu deprivation.

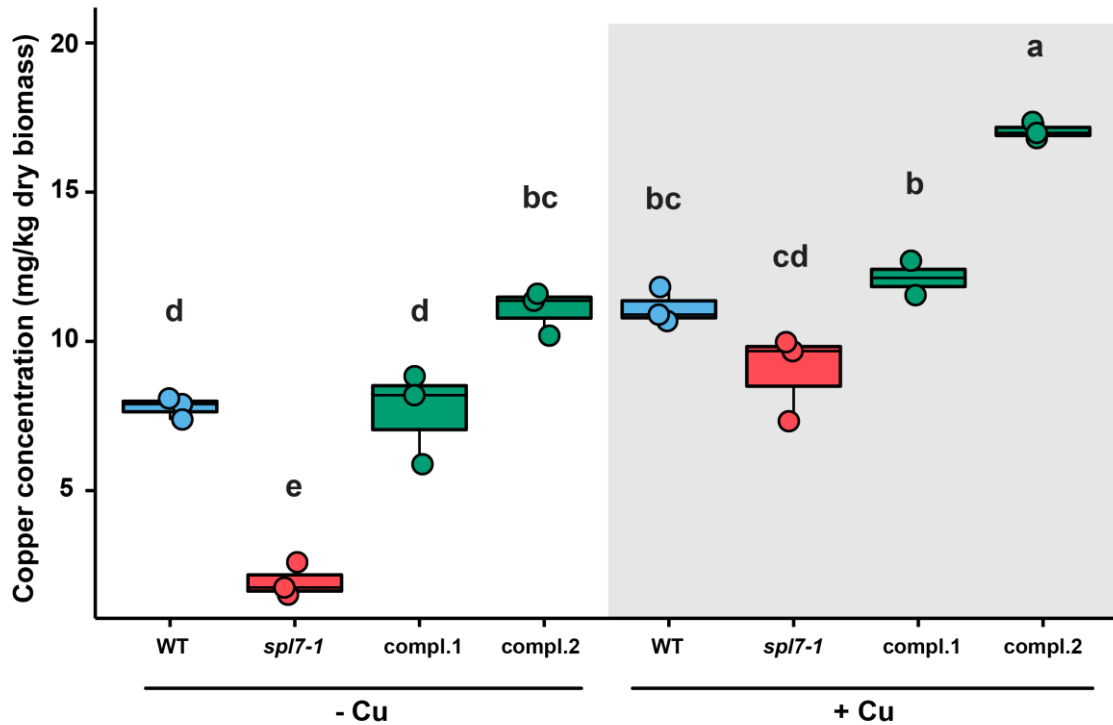


Figure 3.3: SPL7 is necessary for copper homeostasis in *C. hirsuta* fruits. Copper concentration in mature fruits measured by ICP-MS. Plants were grown on soil watered with collected rain water and supplemented weekly either with 20 mL of 5 mM CuSO₄ (+Cu) or with 20 mL of Millipore water (-Cu). WT: wild type; compl: T₂ plants of complementation lines (*pSPL7::SPL7:YFP_v* in *spl7-1* background) from two independent insertion lines with 1 insertion in T₁ (compl.1) and 3 insertions in T₁ (compl.2). Different letters denote statistically significant differences (P < 0.05) between means based on ANOVA (Tukey's HSD). One outlier data point was removed from the analysis since the value of Cu concentration was abnormally high (30.84 mg/Kg). The difference of this value to the mean value of the other replicates in its condition (18.71) was more than 10 times higher than the standard deviation in any of the conditions in the experiment.

4. *SPL7* is sufficient to increase Cu concentration in *C. hirsuta* fruit

It was evident that the Cu concentration in *spl7-1* fruit was fully complemented in *pSPL7::SPL7:YFPv* transgenic lines. In addition, it was interesting that one of the complementation lines (line 2) showed a higher Cu concentration than wild type in both Cu-supplemented and non-supplemented conditions (Figure 3.3). The number of transgene insertions, and therefore the number of *SPL7* gene copies in the genome, had been estimated in T₁ plants of both complementation lines used in this previous experiment (iDNA genetics, see materials and methods). Complementation line T₁-1 was estimated to contain 1 transgene insertion whereas line T₁-2 was estimated to contain 3 insertions of the transgene. The higher concentration of copper in the line that contained more copies of *SPL7*, suggested that increasing *SPL7* activity above wild-type levels might also increase the Cu concentration above the levels found in wild type fruit.

To test this hypothesis, we measured the Cu concentration in fruit of genotypes carrying different copies of functional *SPL7* (in collaboration with Patrizia Kroll as part of her MSc thesis, UoC). The genotypes used for this experiment were: wild-type *C. hirsuta*, which contains two alleles of *SPL7*; *spl7-1*, which contains no functional alleles of *SPL7*; and complementation lines (*pSPL7::SPL7:YFPv* in *spl7-1*) carrying different copies of *SPL7*. To obtain plants with a different number of transgene insertions (*SPL7* copies) two independent complementation lines were used. As mentioned above, the T₁-1 plant was estimated to contain 1 transgene copy and the T₁-2 plant was estimated to contain 3 transgene copies. Thus, we grew T₂ progeny of these lines that segregated for the transgene insertion and estimated the number of transgene copies in different plants (iDNA genetics). We found that the 3 transgene copies in T₁-2 segregated as a single locus since we could only find plants carrying 3 or 6 copies. Based on copy number estimation, we identified plants that carried 1 copy of *SPL7* (T₂-1 heterozygote), 2 copies of *SPL7* (T₂-1 homozygote), 3 copies of *SPL7* (T₂-2 heterozygote), and 6 copies of *SPL7* (T₂-2 homozygote). Importantly, all *pSPL7::SPL7:YFPv* plants also carry 2 mutant alleles of *SPL7* that are non-functional (*SPL7* copies with one amino acid substitution in *spl7-1*).

Once plants with different numbers of *SPL7* gene copies were identified, we analysed whether an increased number of *SPL7* copies was associated with higher *SPL7* gene expression in fruit by quantitative RT-PCR (using Clathrin as reference housekeeping gene) (Figure 3.4 A). We found that wild-type and *spl7-1* fruit have comparable levels of *SPL7* expression. This indicates that, in *spl7-1*, the accumulation of mutant *SPL7* transcripts is not affected. Therefore, the amino acid substitution in *spl7-1* affects *SPL7* protein function but not *SPL7* gene expression. Furthermore, *pSPL7::SPL7:YFPv; spl7-1* plants with either 1 or 2 transgene copies of *SPL7* have higher *SPL7* gene expression than wild type and *spl7-1*, although the difference is not statistically significant. This would reflect the combined expression of functional *SPL7* transgenes and non-functional *spl7-1* alleles. More importantly, *pSPL7::SPL7:YFPv; spl7-1* fruit from line T₂-2 have significantly higher *SPL7* gene expression than wild-type fruit. Transgenic lines carrying 3 or 6 functional copies of *SPL7* have increasingly higher levels of *SPL7* gene expression (Figure 3.4 A). These results indicate that the dosage of *SPL7* is positively correlated with the expression of *SPL7* in fruits of these genotypes. We obtained the same trends when using a second housekeeping gene (*TIP41*) and a different primer pair to amplify *SPL7* (data not shown here), indicating that this finding is robust.

Next, we investigated whether the dosage of *SPL7* was associated with Cu concentration in the fruit. We found a linear relationship between increasing *SPL7* dose and increasing Cu concentration (Figure 3.4). *spl7-1* fruits had the lowest Cu concentration of all genotypes. This difference is significant at $P < 0.05$. *SPL7::SPL7:YFPv; spl7-1* fruit with 1 functional copy of *SPL7* had a lower Cu concentration than wild type, although the difference was not statistically significant. *SPL7::SPL7:YFPv; spl7-1* fruit with 2 functional copies of *SPL7* had a slightly higher Cu concentration than wild-type fruit, although the difference was not statistically significant. *SPL7::SPL7:YFPv; spl7-1* fruit carrying 3 functional copies of *SPL7* had a higher Cu concentration than wild-type fruit. This difference is significant at $P < 0.05$. Finally, the highest Cu concentration was found in *SPL7::SPL7:YFPv; spl7-1* fruit carrying 6 functional copies of *SPL7*, although this concentration was only slightly higher than that in fruit with 3 copies of *SPL7* (Figure 3.4 B). These results indicate that the expression of *SPL7* is sufficient to increase Cu

concentration above wild-type levels in *C. hirsuta* fruit. Moreover, Cu concentration shows a dose-response relationship to *SPL7* activity in the fruit.

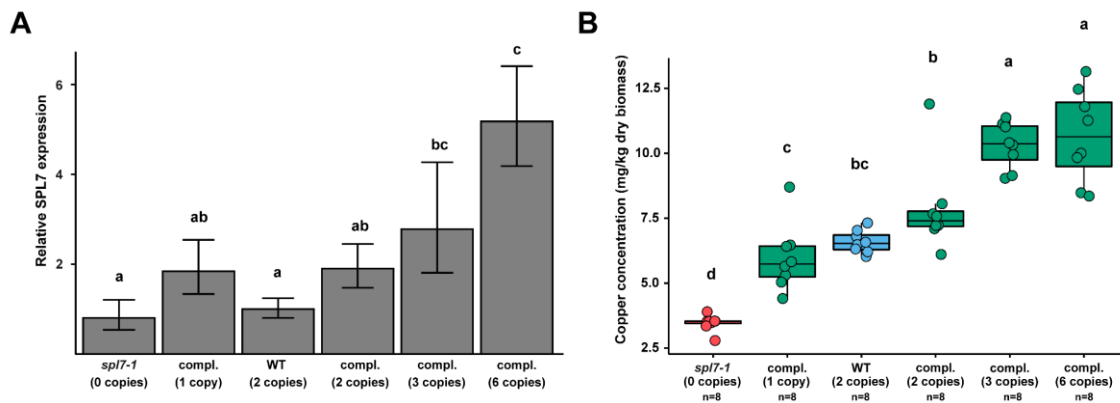


Figure 3.4: *SPL7* is sufficient to increase copper concentration in *C. hirsuta* fruits. (A) Relative *SPL7* gene expression (relative to wild-type value) calculated by quantitative RT-PCR in mature fruit of genotypes with different copy numbers of functional *SPL7* gene copies, both endogenous and transgenes. *SPL7* expression was normalized to the expression of the housekeeping gene *Clathrin*. The number of functional copies is indicated. Different letters denote statistically significant differences ($P < 0.05$) between means based on ANOVA (Tukey's HSD). (B) Copper concentration in fruit of different genotypes carrying varying numbers of functional *SPL7* gene copies measured by ICP-MS. Different letters denote statistically significant differences ($P < 0.05$) between means based on ANOVA (Tukey's HSD). WT: wild type; compl: complementation lines (*pSPL7::SPL7:YFP_v* in *spl7-1* background). Plants were grown on soil in Cu-limiting conditions (watered with collected rain water and supplemented weekly with 10 mL of 1 mM CuSO_4).

Taken together, my results showed that *SPL7* is necessary and sufficient to increase Cu concentration in *C. hirsuta* fruit. In these experiments, I also observed that supplementing copper to the soil increases Cu concentration in the fruit. This was observed both in wild-type and *spl7-1* plants. In this section, I aim to further investigate the relationship between Cu supply and Cu concentration in fruits.

Cu bioavailability in soils can vary depending on properties of the soil such as pH and content of organic material (Mengel *et al.*, 2001). Therefore, it is difficult to achieve precise control over the

concentration of Cu supplied to plants that are grown on soil. To obtain a tighter control over the Cu concentration supplied to *C. hirsuta* plants in my experiments, I developed an aeroponics system (in collaboration with Patrizia Kroll as part of her MSc thesis, UoC). In this system, *C. hirsuta* seedlings were established in an inert material and their roots grew into dark aeroponic chambers. An automatic watering system ensured that plant roots were routinely sprayed in the chambers with nutrient solution to ensure optimal growth. We directly supplied different concentrations of Cu via the nutrient solution, thus ensuring that the concentration of Cu supplied was bioavailable (see Materials and Methods for details). Two independent, replicated experiments were performed using this aeroponics system (Patrizia Kroll, MSc thesis, UoC). We measured the Cu concentration in fruit of wild-type and *spl7-1* plants grown in different concentrations of Cu by ICP-MS.

I found that Cu concentration in the fruit showed a linear increase in response to increased Cu supply in both wild-type and *spl7-1* genotypes (Figure 3.5). Three different concentrations of Cu were supplied as CuSO₄ in the nutrient solutions, that spanned a 10-50 fold concentration difference in the two experiments. The difference in fruit Cu concentration between each condition was significant at $P < 0.05$ for both genotypes (Figure 3.5). In wild-type fruit, the range of Cu concentrations measured in experiments one and two was 6.38 and 8.64, respectively. In *spl7-1* fruit, a smaller range of Cu concentrations (2.23 and 6.47) was measured in experiments one and two, respectively. Moreover, the Cu concentration in wild-type fruit was higher than in *spl7-1* fruits in all conditions analysed (Figure 3.5). These results show that the concentration of Cu in the fruit is dependent on the concentration of Cu supplied during growth, over a range of 0.1 μM – 5 μM Cu. They also show that *spl7* fruit accumulate significantly less Cu than wild type.

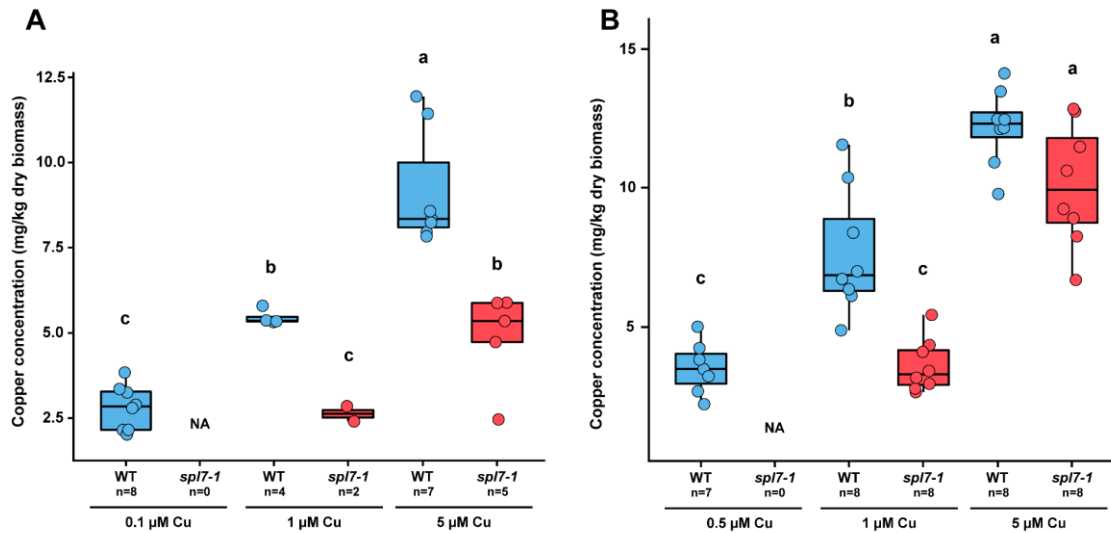


Figure 3.5: Copper concentration in the fruit is directly proportional to the copper supplied during plant growth. Cu concentration measured by ICP-MS and shown as mg/kg dry weight in mature fruits of wild type and *spl7-1*. Different letters denote statistically significant differences ($P < 0.05$) between means based on ANOVA (Tukey's HSD). Plants were grown in an aeroponics system with Cu concentrations supplied directly to roots via CuSO_4 concentration in the nutrient solution. The lowest concentration of Cu supplied in the first experiment was 0.1 μM , while in the second experiment it was 0.5 μM . This change was made to try to stimulate fruit formation in the *spl7-1* mutant. However, neither concentration was sufficient for *spl7-1* plants to produce fruit. NA (not applicable) indicates the absence of fruit in *spl7-1* in these conditions.

5. Cu supplementation to soil rescues endocarp *b* lignification in *spl7*

In the previous sections, I found that *spl7-1* fruit have reduced Cu concentration, which can be complemented to wild-type levels by expressing a *SPL7* transgene. Cu concentrations were measured in mature fruit when the endocarp *b* cell layer was lignified. Furthermore, I found that Cu supplementation during plant growth could increase the concentration of Cu in fruit.

In this section, I investigate whether Cu supplementation to the soil can rescue the reduced lignification of endocarp *b* cells in *spl7-1* fruit. I grew *spl7-1* plants in Cu-supplemented soil and in soil without Cu supplementation. Fruit from *spl7-1* plants that were not supplemented with Cu show the characteristic fruit phenotype of buckled margins at maturity, whereas fruit from *spl7-*

l plants grown in Cu-supplemented soil exhibit the wild-type phenotype of straight margins at maturity (Figure 3.6 A). I examined lignification of the endocarp *b* layer in these plants by staining cross sections of mature fruit with phloroglucinol/HCL. *spl7-1* fruit showed reduced staining in the endocarp *b* cell layer, compared to wild type, when grown in non-supplemented soil. However, lignification of the endocarp *b* cell layer was restored to wild-type levels in *spl7-1* fruit when plants were grown in soil supplemented with Cu (Figure 3.6 B). These results indicate that Cu supplementation to the soil can fully rescue the reduced lignification of endocarp *b* cells in *spl7-1* mature fruit.

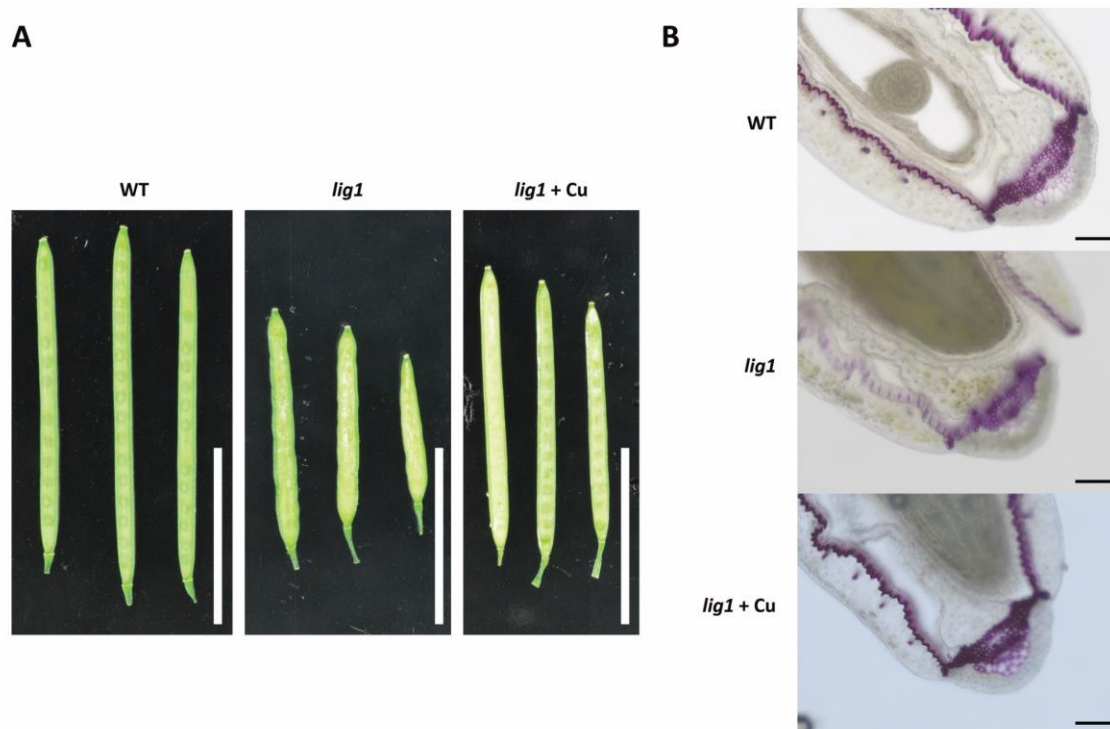


Figure 3.6: Copper supplementation to soil rescues the *spl7-1* phenotype. (A) Stage 17 a/b fruits. Scale bar: 10 mm. (B) Microscope images of 100 μm fruit cross sections from stage 17 a/b fruits stained with phloroglucinol/HCl. Scale bar: 100 μm (A and B) Plants were grown on soil watered with tap water. Additionally, soil was supplemented with either 20 mL of 5 mM CuSO_4 (+Cu) or 20 mL of water (control). For two weeks, soil was supplemented weekly and, to ensure enough copper availability during fruit lignification, the following week, soil was supplemented three consecutive days (last day 30 mL were applied). Wild-type fruits and sections are only shown as reference of phenotype, since wild-type plants were not treated in the same experiment.

6. Reduced growth of *spl7-1* plants in Cu-limiting conditions

The *spl7* allele was identified in a mutant screen for less lignified fruit valves (*less lignin* screen). Characterization of the mutant showed that this *less lignin* phenotype was due to reduced lignification of the endocarp *b* cell layer in the fruit valve. The mutant also showed a morphological phenotype late in fruit development where the margins buckled. However, mutant plants showed no other obvious developmental defects, apart from a slightly shorter stature than wild-type plants.

However, when I started growing plants in the new greenhouse facilities at MPIPZ, I observed that *spl7-1* mutant plants had a very reduced stature compared to wild-type plants. This reduction in height was specific to *spl7-1* plants as the stature of wild-type plants did not differ in the new greenhouse facilities. One difference between greenhouses is that plants in the new facilities are watered with rain water collected on-site, whereas plants in the other facilities are watered with city tap water. In this section, I examined whether a further reduction in Cu availability is responsible for the reduced stature of *spl7-1* plants watered with collected rain water. I grew wild-type and *spl7-1* plants in the new greenhouse facilities, i.e. watered with collected rain water (Cu-limiting) and supplemented the soil with different concentrations of CuSO₄ (0 mM, 1 mM or 5 mM). I found that the average fresh weight of *spl7-1* plants (0.07 ± 0.03 g) was dramatically reduced compared to wild-type plants (3.59 ± 1.10 g) when the soil was not supplemented with additional Cu (Figure 3.7 A). Similarly, the average height of *spl7-1* plants was approximately 5 % of wild type in non-Cu supplemented soil (Figure 3.7 A, C). The biomass and height of *spl7-1* plants progressively increased when the soil was supplemented with 1 mM CuSO₄ and 5 mM CuSO₄ (Figure 3.7). In soil supplemented with 5 mM CuSO₄, the average fresh weight of *spl7-1* plants is approximately 77 % of wild type and average height is approximately 86 % of wild type (Figure 3.7). These results indicate that *spl7-1* mutant plants have significantly reduced stature when grown in Cu-limiting conditions, and that regular supplementation with 5 mM CuSO₄ rescues this phenotype. However, the range of CuSO₄ concentrations used to supplement the soil in this experiment did not fully rescue the height and fresh weight of *spl7-1* plants to wild-type values.

Another interesting observation, is that wild-type plants grown in soil supplemented with 5 mM CuSO₄ showed a significant reduction in height and fresh weight compared to growth in lower Cu conditions (81.9 % average height and 64.1 % average fresh weight of wild-type plants in non-Cu soil, Figure 3.7). This suggests that the high Cu conditions in this experiment may have a toxic effect on wild-type plant growth. In contrast to wild-type plants, the height and weight of *spl7-1* plants continued to increase on soil with higher levels of Cu supplementation. This might

reflect a reduced ability of *spl7-1* plants to uptake copper, and therefore, toxic levels might not be reached in the mutant when grown on soil supplemented with 5 mM CuSO₄. This fits my previous observations that *spl7-1* fruit accumulate lower concentrations of Cu than wild type (Figure 3.7). However, I did not measure Cu concentration in plant tissues in this experiment.

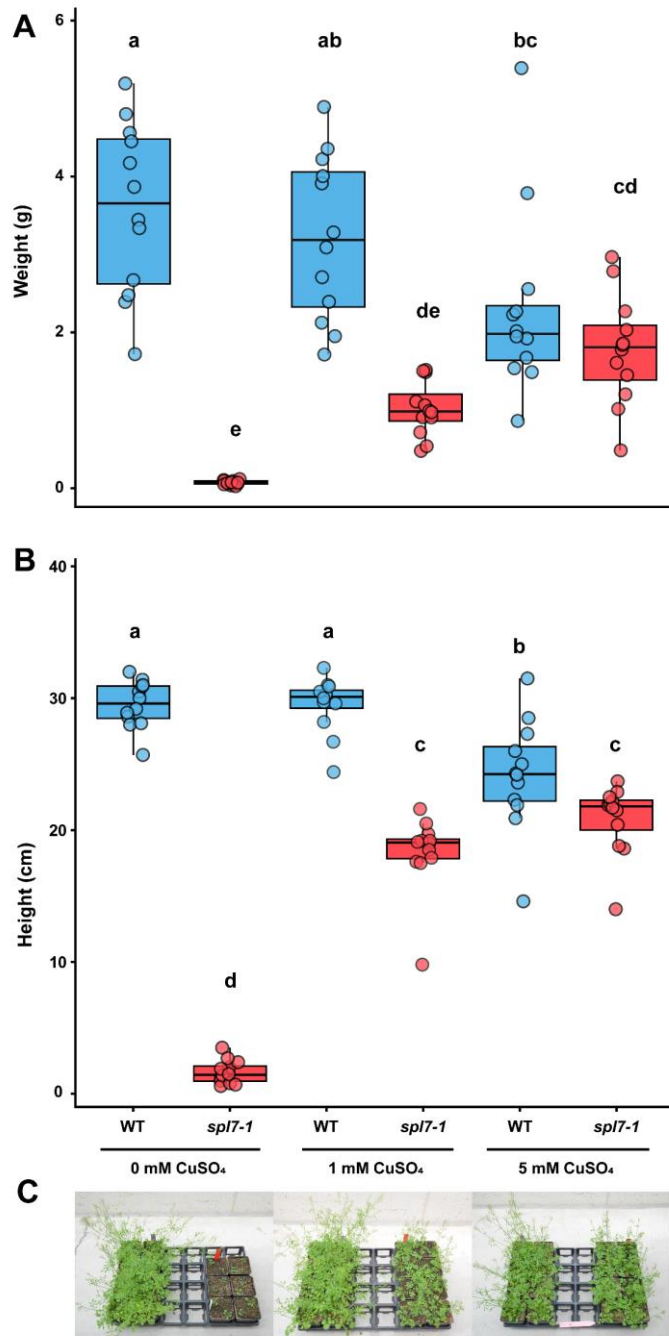


Figure 3.7: In Cu limiting conditions, *spl7-1* plants are shorter and have reduced growth compared to wild type. 7 weeks-old plants grown in three different Cu conditions. Soil was supplemented regularly with 20 mL of different concentration of CuSO₄ solution (0 mM, 1 mM or 5 mM). (A) Fresh weight of plant aerial parts (n = 12). (B) Height of plants (n = 12). (C) Images of plants at the day of phenotype analysis. Different letters denote statistically significant differences (P < 0.05) between means based on ANOVA (Tukey's HSD).

7. Lignification is not reduced in roots and stems of *spl7-1* plants under Cu-limiting conditions

Given that *spl7-1* plants showed significantly reduced growth under Cu-limiting conditions (irrigation with collected rain water), I investigated whether pleiotropic lignification defects could be responsible for the reduction in plant height and weight. In this experiment, I examined the lignification of root and stem tissues in *spl7-1* compared to wild-type plants, and compared the lignification in these tissues to lignification in the fruit.

To assess the lignification of multiple plant tissues, I wanted to use experimental conditions where *spl7-1* plants were relatively easy to work with. In Cu-limiting conditions (irrigation with collected rain water), *spl7-1* plants were very short (average height 1.6 cm, Figure 3.7 B), which would make it difficult to investigate stem tissues. On the other hand, when the soil was supplemented with 1 mM CuSO₄, *spl7-1* plants grew much taller (average height 18.3 cm), but still showed reduced stature compared to wild-type (Figure 3.7 B). Therefore, I followed an experimental design where I regularly supplemented wild-type and *spl7-1* plants with 0.1 mM CuSO₄ to ensure a minimal amount of stem growth in *spl7-1* plants, but a significant reduction in stature compared to wild type.

I used phloroglucinol/HCl to specifically stain lignified cell walls in plant tissues grown under these low Cu conditions (soil supplemented with 0.1 mM CuSO₄). The fruit of *spl7-1* plants showed reduced lignification in the endocarp *b* layer, but not in other lignified cell types in the replum and valve margin when compared to wild type (Figure 3.8 A). Vascular bundles and fibres in the stems of *spl7-1* plants showed comparable levels of lignification to wild-type stems in cross section (Figure 3.8 B). Similarly, the stele tissue of *spl7-1* roots showed comparable levels of lignification to wild-type roots (Figure 3.8 C). Therefore, lignification is deficient in *spl7-1* plants only in the fruit endocarp *b* cell layer, and not in other plant tissues, under the conditions of Cu supply in this experiment. These results indicate that, in contrast to other lignified cell types, endocarp *b* SCWs have a higher requirement for SPL7 activity in response to Cu deprivation, or a higher sensitivity to Cu levels in the absence of SPL7. Moreover, the reduction in stem girth

observed in *spl7* plants compared to wild type (Figure 3.8 B), in the low Cu conditions of this experiment, was not associated with reduced lignification. In summary, I found no evidence that a qualitative decrease in the lignification of stem or root tissues was responsible for the reduced stature of *spl7-1* plants grown in Cu-limiting conditions.

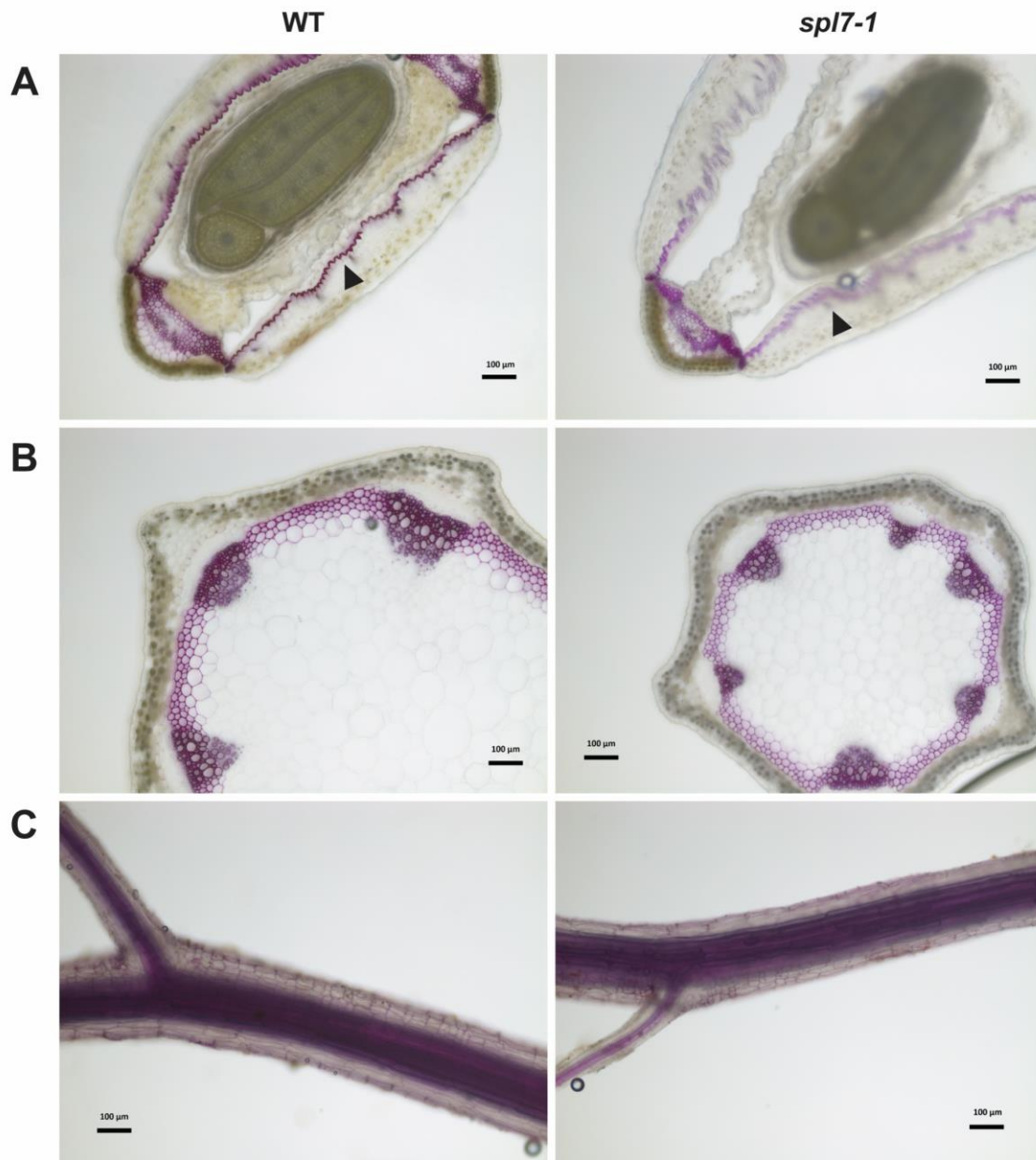


Figure 3.8: Lignification is specifically reduced in the endocarp *b* layer and not in other tissues of the fruit, stem or root in *spl7-1* under low Cu conditions. (A) Cross sections of stage 17 a/b fruits stained with phloroglucinol/HCl. Arrowheads indicate endocarp *b* layer. (B) cross sections of stems at the last internode stained with phloroglucinol/HCl. (C) Roots stained with phloroglucinol/HCl. Plants were grown on soil in Cu-limiting conditions (watered with collected rain water and supplemented weekly with 0.1 mM CuSO₄). Scale bars: 100 µm.

8. Endocarp *b* secondary cell walls are less lignified in the *A. thaliana spl7* mutant

In *A. thaliana* fruit, the SCWs of endocarp *b* cells are also lignified (Spence *et al.*, 1996). However, endocarp *b* cells are smaller and have less lignin content in *A. thaliana* than in *C. hirsuta* (Hofhuis & Hay, 2017; Hofhuis *et al.*, 2016). Furthermore, the geometry of lignin deposition is different in these species. In *A. thaliana*, lignin is deposited symmetrically in endocarp *b* cells, whereas in *C. hirsuta*, lignin is deposited asymmetrically in a “U”-shape pattern with thin hinges. This specific pattern of lignin deposition in endocarp *b* cells of *C. hirsuta* is required for explosive seed dispersal (Hofhuis *et al.*, 2016).

To understand whether *SPL7* function is conserved between *C. hirsuta* and *A. thaliana*, I explored whether lignification is reduced in the endocarp *b* cells of *A. thaliana spl7* mutants in low Cu conditions. To my knowledge, fruit lignification in *A. thaliana spl7* mutants has not been examined in previous studies. I grew *A. thaliana* wild-type Col-0 and loss of function *spl7* mutant plants (*spl7-2* allele; SALK-125385) in soil irrigated with tap water but not supplemented with Cu. Then, I used phloroglucinol/HCl to specifically stain lignified cell walls in transverse sections of mature fruit. I found that lignin staining was reduced in *spl7-2* mutant fruit compared to wild type (Figure 3.9). In particular, the lignification of endocarp *b* cells was considerably reduced in *spl7-2* fruit (Figure 3.9). The lignification of cells at the valve margin was also reduced in *A. thaliana spl7-2* fruit, unlike in *C. hirsuta spl7* mutants, where the lignification of the valve margin is not particularly affected (Figure 3.9). These results indicate that *SPL7* is required for endocarp *b* lignification in *A. thaliana* under Cu-limiting conditions.

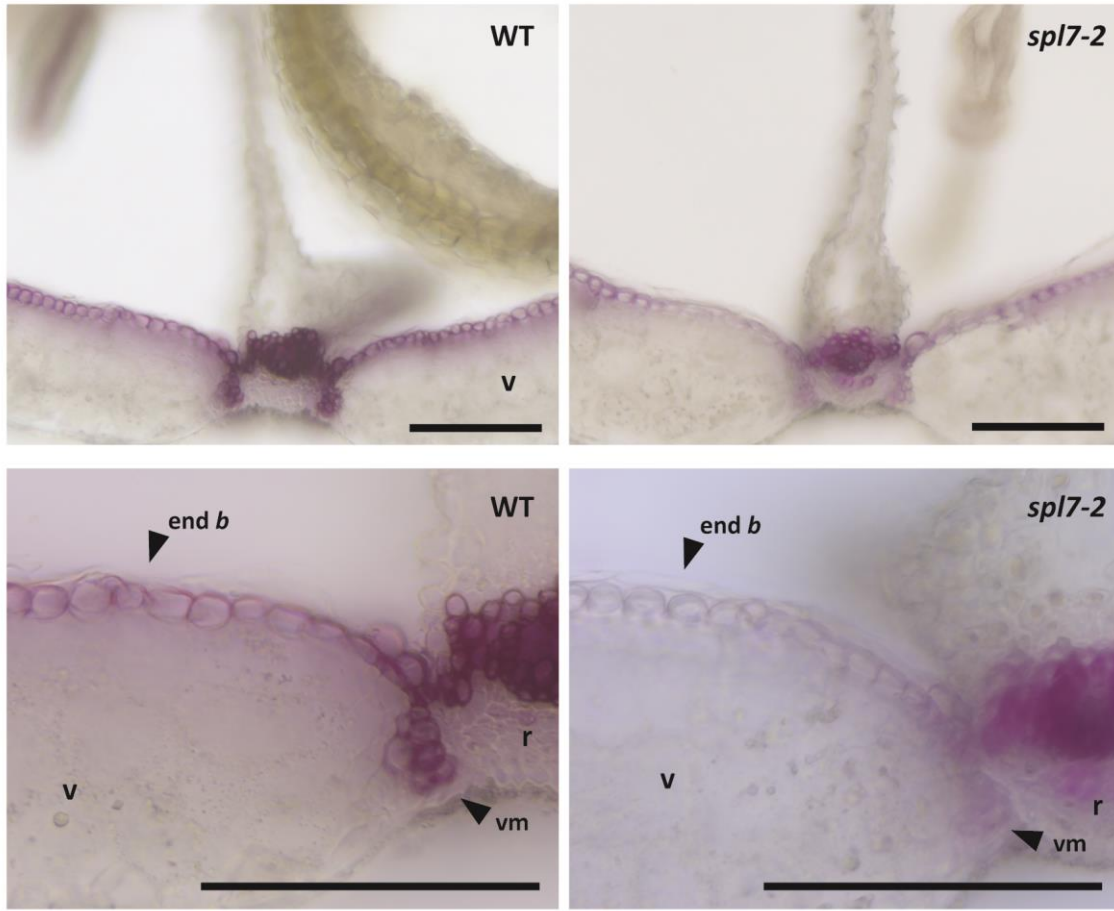


Figure 3.9: *A. thaliana* loss of function allele *spl7-2* has reduced endocarp *b* lignification in low Cu conditions. Microscope images of 100 μm cross sections from mature fruit stained with phloroglucinol/HCl, *A. thaliana* Col-0 WT (left) and *spl7-2* mutant allele in Col-0 background (right). Arrowheads indicate endocarp *b* layer. Seeds were germinated in ½ MS media, seedlings were transferred to soil and watered with tap water. Soil was not supplemented with additional Cu. end *b*: endocarp *b*, v: valve, r: replum, vm: valve margin. Scale bars: 100 μm.

9. Components of SPL7 pathway are conserved in *C. hirsuta*

In the previous chapter, I showed that the SPL7 protein is highly conserved in *C. hirsuta*. In particular, the SBP region is conserved, which defines SPL proteins and contains the DNA binding domain and nuclear localization signal. Therefore, I expect that the function of SPL7 is conserved in *C. hirsuta* as a transcription factor. Given this assumption, I examined whether known targets of SPL7 in *A. thaliana* are also present in *C. hirsuta*. In previous studies, a pathway regulated by SPL7 has been characterized (Anna Schulten & Krämer, 2017). SPL7 is proposed to

act as a switch that responds to copper deprivation by activating genes involved in copper homeostasis (Bernal *et al.*, 2012). Additionally, SPL7 activates the expression of a group of miRNAs, known as the Cu-miRNAs, which includes miR397, miR398, miR408 and miR857 (Abdel-Ghany & Pilon, 2008; H. Yamasaki *et al.*, 2007; H. Yamasaki *et al.*, 2009; H. Zhang *et al.*, 2014). These Cu-miRNAs target mRNAs encoding copper-requiring proteins. To examine whether genes activated by SPL7, and genes post-transcriptionally regulated by the Cu-miRNAs, have orthologs in *C. hirsuta*, I made use of reciprocal best BLAST hits between *A. thaliana* known targets and *C. hirsuta* annotated genes. I assume that genes identified by this method are likely orthologs in these closely related species. This approach is possible since a reference genome for *C. hirsuta* has been sequenced and assembled; and genes have been annotated. I identified 17 genes in *C. hirsuta* out of 19 searched. The results of this analysis are summarized in Table 3.1. Reciprocal best BLAST hit failed to identify two genes, *FRO5* and *COPT6* in the reference genome of *C. hirsuta*. However, when using the BLAST tool against a new *C. hirsuta* genome assembly (M. Awad and X. Gan, unpublished work), sequences of high similarity to *A. thaliana* *FRO5* and *COPT6* were identified in *C. hirsuta*. However, since this new *C. hirsuta* genome assembly has not been validated or annotated yet, I will not analyse these two genes further here.

Abbreviation	<i>A. thaliana</i> gene number	Description	<i>C. hirsuta</i> gene number
CSD1	AT1G08830	Superoxide dismutase [Cu-Zn]	CARHR008750
CSD2	AT2G28190	Superoxide dismutase [Cu-Zn]	CARHR121080
CCS	AT1G12520	copper chaperone for SOD1	CARHR012800
Cox5b.1	AT3G15640	cytochrome c oxidase subunit Vb	CARHR090730
LAC2	AT2G29130	laccase 2	CARHR122430
LAC4	AT2G38080	laccase 4	CARHR132660
LAC17	AT5G60020	laccase 17	CARHR273650
LAC7	AT3G09220	laccase 7	CARHR083560
LAC3	AT2G30210	laccase 3	CARHR123520
LAC12	AT5G05390	laccase 12	CARHR207840
LAC13	AT5G07130	laccase 13	CARHR206010
ARPN	AT2G02850	plantacyanin	CARHR145280
FSD1	AT4G25100	Superoxide dismutase [Fe]	CARHR232490
COPT1	AT5G59030	copper transporter 1	CARHR285590
COPT2	AT3G46900	copper transporter 2	CARHR155490
FRO4	AT5G23980	ferric reduction oxidase 4	CARHR189580
YSL2	AT5G24380	metal-nicotianamine transporter YSL2	CARHR189040
FRO5	AT5G23990	ferric reduction oxidase 4	Identified
COPT6	AT5G23990	copper transporter 6	Identified

Table 3.1: All genes in the SPL7 pathway have orthologs in *C. hirsuta*. Genes regulated by SPL7 in *A. thaliana* and corresponding reciprocal best BLAST hit *C. hirsuta* genes. High confidence orthologs of *A. thaliana* FRO5 and COPT6 were identified by this method in a new *C. hirsuta* genome assembly (M. Awad and X. Gan, unpublished work).

In the reference *C. hirsuta* genome, miRNAs have not been annotated yet. Therefore, I used the BLAST tool to search for *C. hirsuta* sequences similar to *A. thaliana* miRNA genomic and mature sequences. Once regions with sequence similarity were found, I aligned *C. hirsuta* and *A. thaliana* sequences and examined sequence conservation and synteny of the loci identified.

BLAST results for *MIR397A* and *MIR397B* identified two genomic regions with identity above 80 % (81.31 and 81.00 % respectively). The mature miRNA sequence found at both loci in *C. hirsuta* is identical to miR397a from *A. thaliana*. However, one locus is located next to the miR857 sequence identified in *C. hirsuta* by BLAST. Both *MIR397B* and *MIR857* loci are physically adjacent in *A. thaliana*. Therefore, the sequence identified for *MIR397B* by BLAST is likely to be the *C. hirsuta* ortholog of *MIR397B* despite having one nucleotide substitution in the mature miRNA sequence (Figure 3.10).

A genomic region with 71.89 % identity to *MIR408* was identified in *C. hirsuta* by BLAST. The mature miRNA sequence is fully conserved between species. Additionally, a gene adjacent to *MIR408* in *A. thaliana* is orthologous of the gene adjacent to the sequence identified by BLAST in *C. hirsuta*. Therefore, this sequence is likely the *C. hirsuta* ortholog of *MIR408* based on synteny and sequence identity (Figure 3.10).

The genomic stem-loop region of *MIR857* is larger than the other Cu-miRNAs. A region in *C. hirsuta* with 71.89 % identity to *MIR857* was identified by BLAST. This locus is located next to the region identified for miR397b as mentioned above. The miR857 mature sequence is fully conserved between both species. Therefore, based on synteny and sequence identity, this sequence is likely the *C. hirsuta* ortholog of miR857 (Figure 3.10).

C. hirsuta genomic regions with identity above 80% were identified by BLAST for *MIR398A* (87.62 %) and *MIR398B* (85.34 %). The gene adjacent to *MIR398A* in *A. thaliana* is ortholog of the gene adjacent to *C. hirsuta* sequence identified by BLAST. Similarly, the gene adjacent to *MIR398B* in *A. thaliana* is ortholog of the gene adjacent to *C. hirsuta* sequence identified by BLAST. The mature miR397a sequence differs between species in the first nucleotide, while the mature miR397b sequence is fully conserved. Therefore, these sequences represent the *C. hirsuta* orthologs of *MIR397A* and *MIR397B*, however, no region of high percentage identity was found for *MIR397C* in *C. hirsuta* (Figure 3.10).

pairing is fully conserved between species. In *C. hirsuta*, the *LAC4* mRNA target sequence is complementary to miR397a with the exception of one base mismatch and one G:U wobble base pair (Figure 3.11). In *A. thaliana*, 1 mismatch and 2 wobble pairs are described (Abdel-Ghany & Pilon, 2008).

Next, I analysed the *ARPN* gene in *C. hirsuta*, which is a confirmed target of miR408 in *A. thaliana*. The *ARPN* mRNA is complementary to miR408 except for two mismatches in *C. hirsuta* (Figure 3.11). The *ARPN* target sequence and pairing with miR408 is identical in both *C. hirsuta* and *A. thaliana* (Abdel-Ghany & Pilon, 2008).

I analysed the mRNA sequence of *LAC7* in *C. hirsuta*, which is targeted by miR857 in *A. thaliana*. In *C. hirsuta*, the *LAC7* mRNA and miR857 sequences are complementary except for 1 mismatch and 2 wobble pairs (Figure 3.11). In *A. thaliana*, 2 mismatches and 1 wobble pair were identified (Abdel-Ghany & Pilon, 2008).

Finally, I analysed the *CSD2* gene in *C. hirsuta*, which is targeted by miR398b in *A. thaliana* (H. Yamasaki *et al.*, 2007). The *CSD2* mRNA and miR398b sequences are complementary except for 2 mismatches and four wobble pairings in *C. hirsuta* (Figure 3.11). Both the *CSD2* mRNA and miR398b sequences are entirely conserved between *C. hirsuta* and *A. thaliana*. *CSD1* is a target of miR398a and miR398b in *A. thaliana* (Bouche, 2010). I searched the mRNA of *CSD1* for complementary sequences to miR398a and miR398b in *C. hirsuta*, however, I couldn't identify a clear target sequence.

These results indicate conservation of the sequence pairings between Cu-miRNAs and several mRNA targets in *C. hirsuta*. This suggests that post-transcriptional regulation mediated by Cu-miRNAs is possible in *C. hirsuta*. However, further experiments, such as analysis of target cleavage, would still be needed to confirm this regulation.

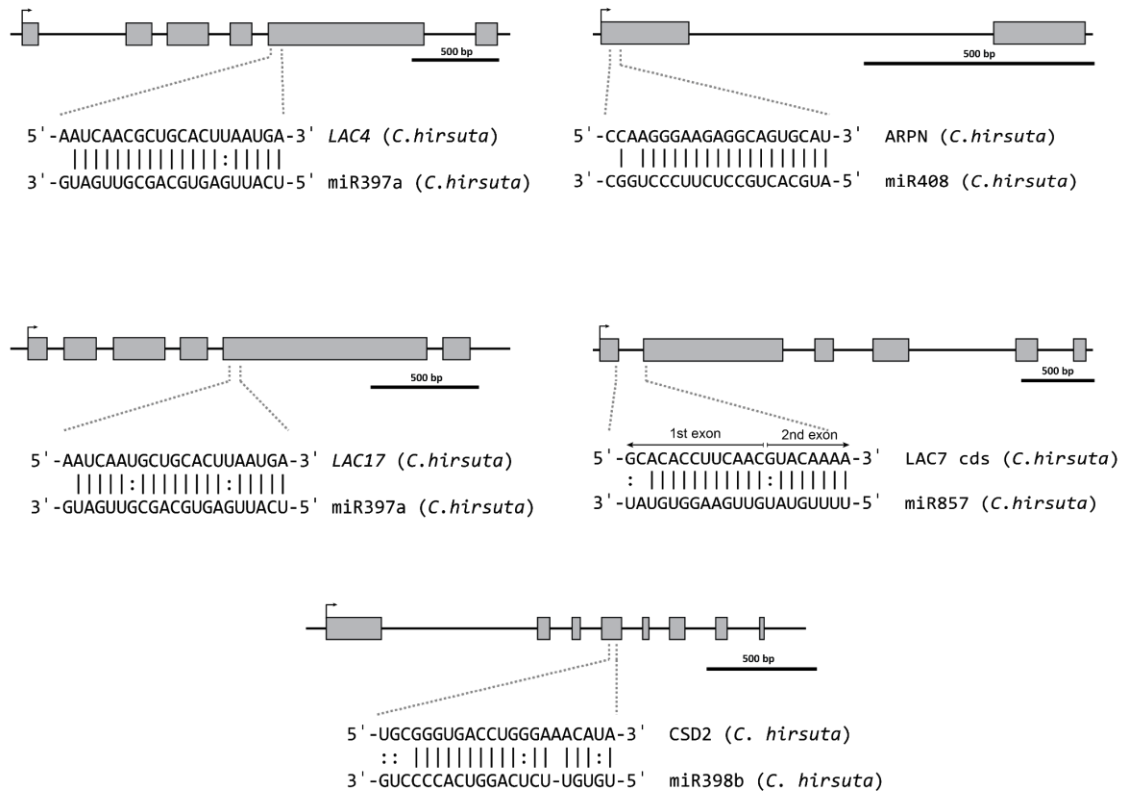


Figure 3.11: Predicted mRNA target sequences for miRNAs miR397, miR398, miR408 and miR857 are highly conserved in several *C. hirsuta* genes. Complementary pairing of miRNA sequences (3' to 5') and mRNA sequences of putative targets (5' to 3'). Gene models with exons (grey boxes) and introns (black line between exons) are depicted. The complementary mRNA and miRNA sequences are shown below the gene model. Vertical dashes indicate perfect pairing and dots indicate G:U wobble pairing.

10. Transcriptomic profiling of wild-type and *spl7-1* fruit valves

Lignification of endocarp *b* SCWs starts during fruit stage 17, when fruit have reached their full length and they start to broaden in width. We reasoned that genes involved in lignin monomer biosynthesis and localized polymerization within the cell wall would be highly expressed at this initial stage of lignification. To gain insights into the mechanism of localized lignin deposition in *C. hirsuta* endocarp *b* cells, a transcriptomic profile of wild-type and *spl7-1* fruit valves at stage 17 was generated using RNA-sequencing (RNA-seq). Given that lignification of endocarp *b* cells is reduced in the *spl7-1* mutant, I aimed to identify which genes might be involved in localized

lignin deposition by comparing differentially expressed genes between these two genotypes. Moreover, I used this comparison to investigate the specific role of *SPL7* in this process.

For RNA-sequencing of wild-type and *spl7-1* fruit valves, the valves were dissected from fruit at stage 17, when lignin deposition initiates in the SCWs of endocarp *b* cells. RNA was extracted from approximately 15 pooled valves for each biological replicate. Synthesized cDNA from the RNA samples was used to prepare libraries that were subjected to RNA sequencing using the HiSeq2500 Illumina platform at the MPIPZ Genome Centre. Three biological replicates per genotype were sequenced separately (see materials and methods). Sample preparation, RNA extraction and cDNA synthesis were performed by Dr. Hugo Hofhuis (unpublished work). Library preparation and sequencing was performed at the MPIPZ Genome Centre. The alignment of sequence reads, assessment of RNA-seq data quality, and analysis of differential gene expression were conducted via a bioinformatics pipeline set up by Dr. Xiangchao Gan (Department of Comparative Development and Genetics, MPIPZ). Specifically, paired-end reads were aligned to the *C. hirsuta* reference genome using TopHat2 (Kim *et al.*, 2013) and raw read counts were quantified with HTSeq v0.5.4 (Anders *et al.*, 2015). Principal component analysis (PCA) and hierarchical clustering were used to visualize the overall similarity between samples and assess RNA-seq data quality. PCA analysis shows that biological replicates of each genotype cluster together and that the *spl7-1* and wild-type clusters are separated (Figure 3.12 A). Hierarchical clustering also shows that *spl7-1* samples are more similar to each other than they are to wild-type samples (Figure 3.12 B). Taken together, these results indicate a good quality of the data that fits the experimental design.

To test for differential gene expression between genotypes in this RNA-seq experiment, the software package DESeq from Bioconductor (Anders & Huber, 2010) was used. A total of 128 differentially expressed genes (DEGs) were found between wild-type and *spl7-1* fruit valves using the criteria of adjusted P-value < 0.05. Of these genes, 53 are downregulated and 75 are upregulated in *spl7-1* fruit valves (Figure 3.12). These results are summarized using a volcano

plot to show the change in expression (log₂ fold change) and adjusted P-value for all genes analysed (Figure 3.12). All DEGs are listed in Table 3.2.

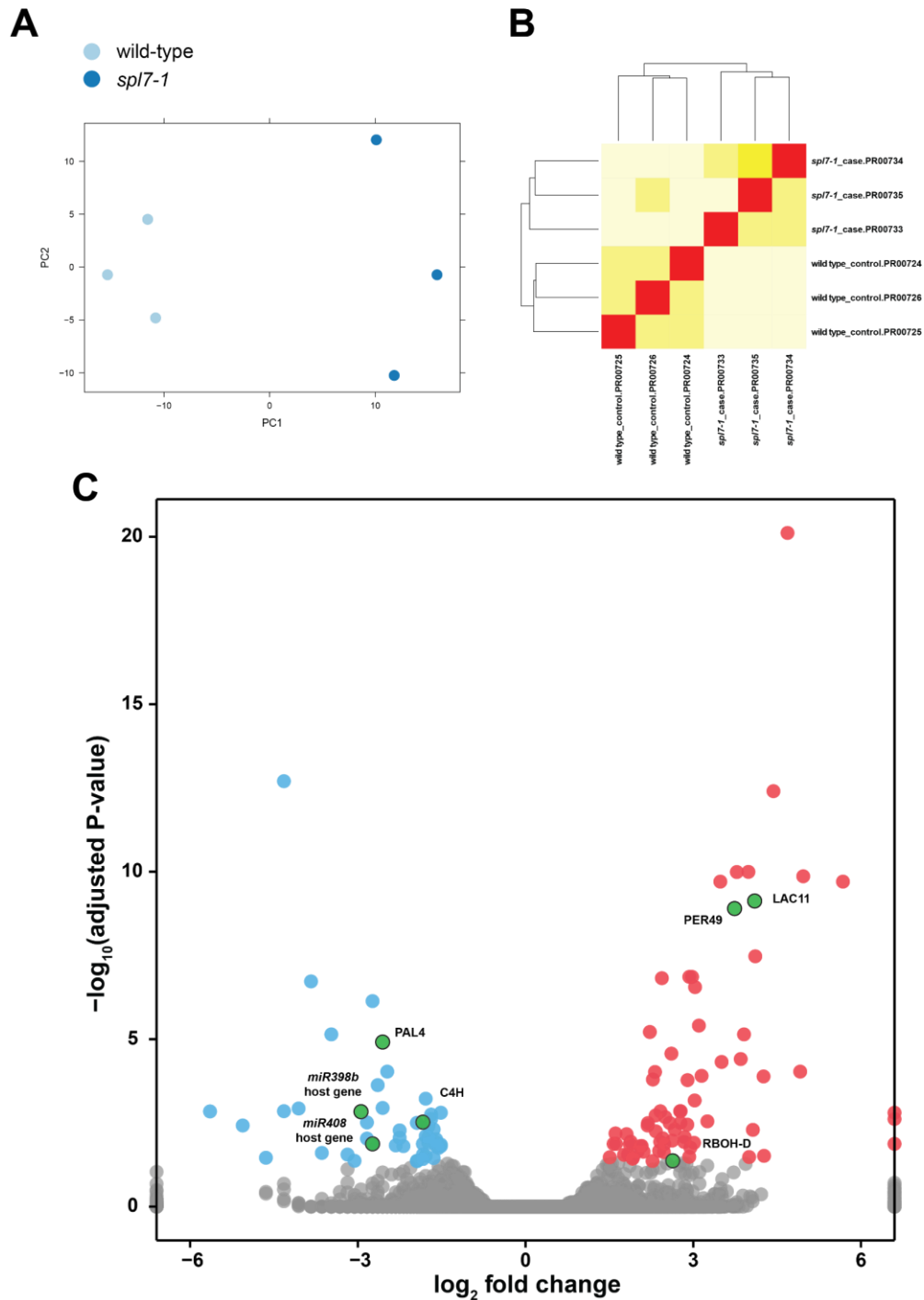


Figure 3.12: Quality assessment of RNA sequencing data and differential gene expression between wild type and *spl7-1* fruit valves. (A) PCA plot of the samples. (B) Heatmap of the sample-to-sample distance and hierarchical clustering of the samples. (C) Volcano plot showing differential expression of genes between wild-type and *spl7-1* fruit valves shown as log₂ fold change. In blue, genes with adjusted P-

value < 0.05 and log2 fold change < -1.5. In red, genes with adjusted P-value < 0.05 and log2 fold change > 1.5. Several differentially expressed genes related to lignin biosynthesis or SPL7 pathway are highlighted in green. For visualization purposes, values of log2 fold change < -6 were set to -6 and values of log2 fold change > 6 were set to 6.

<i>C. hirsuta</i> gene number	Mean normalized counts	Wild-type normalized counts	<i>spl7-1</i> normalized counts	log2 fold change	Adjusted P-value	<i>A. thaliana</i> gene number	Name	Description
CARHR054840	174.01	13.01	335	4.69	7.65E-21	Unknown	Unknown	Unknown
CARHR080320	65.04	123.3	6.77	-4.19	1.98E-13	Unknown	Unknown	Unknown
CARHR163920	56.06	4.96	107.17	4.43	3.93E-13	AT3G54020	AtPDC1	inositol phosphotransferase 1
CARHR003450	43.89	5.21	82.57	3.99	1.01E-10	AT1G04110	SDD1	Subtilase-like protein
CARHR108340	57.83	7.85	107.81	3.78	1.02E-10	AT2G17840	ERD7	sensescence/dehydration related protein
CARHR244410	27.05	1.68	52.42	4.97	1.37E-10	AT4G36010	AT4G36010	pathogenesis-related thaumatin family protein
CARHR215040	58.55	9.61	107.49	3.48	1.97E-10	AT5G37770	TCH2	calcium-binding protein CML24
CARHR224840	23.75	0.91	46.58	5.68	1.97E-10	AT4G18070	AT4G18070	uncharacterized protein
CARHR210090	23.75	3.54	60.68	4.1	7.47E-10	AT5G03260	LAC11	laccase 11
CARHR24760	23.75	5.23	69.85	3.74	1.25E-09	AT4G36430	AT4G36430	peroxidase 49
CARHR012310	23.75	3.27	56.49	4.11	3.35E-08	AT1G11960	AT1G11960	putative ERD4 protein
CARHR083850	23.75	14.25	112.25	2.98	1.37E-07	AT3G09440	AT3G09440	protein heat shock protein 70-3
CARHR193940	23.75	13.02	99.25	2.93	1.37E-07	AT5G19050	AT5G19050	esterase/lipase domain-containing protein
CARHR020900	23.75	119.51	648.09	2.44	1.51E-07	AT1G20450	ERD10	dehydrin ERD10
CARHR124080	23.75	50.91	3.73	-3.77	1.88E-07	Unknown	Unknown	Unknown
CARHR111500	23.75	10.38	84.96	3.03	2.78E-07	Unknown	Unknown	Unknown
CARHR280930	23.75	91.16	13.38	-2.77	7.28E-07	AT5G66770	AT5G66770	scarecrow-like protein 4
CARHR071750	23.75	7.78	66.73	3.1	3.93E-06	AT1G78280	AT1G78280	transferase
CARHR223690	23.75	77.04	359.83	2.22	6.10E-06	AT4G17090	BMY8	beta-amylase 3
CARHR037910	23.75	37.83	3.42	-3.47	7.18E-06	AT1G48300	AT1G48300	uncharacterized protein
CARHR235440	23.75	2.32	34.85	3.91	7.18E-06	AT4G27720	AT4G27720	major facilitator protein
CARHR084820	23.75	102.97	17.83	-2.53	1.22E-05	AT3G10340	PAL4	phenylalanine ammonia-lyase 4
CARHR071760	23.75	11.95	72.91	2.61	2.70E-05	AT1G78290	AT1G78290	serine/threonine-protein kinase SRK2C
CARHR067720	23.75	1.78	25.64	3.85	3.91E-05	AT1G74450	AT1G74450	uncharacterized protein
CARHR166160	23.75	2.3	26.17	3.51	4.78E-05	Unknown	Unknown	Unknown
CARHR149720	23.75	61.64	10.85	-2.51	9.28E-05	Unknown	Unknown	Unknown
CARHR224130	23.75	0.651	19.59	4.91	9.28E-05	AT4G17483	AT4G17483	palmitoyl protein thioesterase family protein
CARHR008960	23.75	20.63	102.71	2.32	9.52E-05	AT1G09070	(AT)SRC2	uncharacterized protein
CARHR107880	23.75	4.89	43.38	3.15	0.000124	AT2G17650	AT2G17650	putative AMP-binding protein
CARHR158030	23.75	1.24	23.77	4.26	0.000129	AT3G49160	AT3G49160	pyruvate kinase
CARHR000900	23.75	20.81	100.9	2.28	0.00016	AT1G01470	LEA14	putative desiccation-related protein LEA14
CARHR200270	23.75	6.04	44.97	2.9	0.000167	AT5G13200	AT5G13200	GEM-like protein 5
CARHR243330	23.75	54.15	8.89	-2.61	0.000236	AT4G35050	MS13	histone-binding protein RBBP4
CARHR060970	23.75	244.79	71.29	-1.78	0.000598	AT1G68290	ENDO 2	endonuclease 2
CARHR018790	23.75	4.06	33.02	3.05	0.000674	AT1G18210	AT1G18210	putative calcium-binding protein CML27
CARHR086500	23.75	39.64	6.89	-2.53	0.00113	AT3G11950	AT3G11950	homogentisate solanesyltransferase
CARHR166510	23.75	18.32	1.08	-4.08	0.00117	AT3G56360	AT3G56360	uncharacterized protein
CARHR069150	23.75	15.92	0.757	-4.39	0.00141	AT1G75750	GASA1	gibberellin-regulated protein 1
CARHR211020	23.75	4.53	30.82	2.77	0.00141	AT5G02390	AT5G02390	uncharacterized protein
CARHR255310	23.75	4.7	32.16	2.77	0.00141	AT4G11280	ACS6	1-aminocyclopropane-1-carboxylate synthase 6
CARHR081720	23.75	8.78	46.69	2.41	0.00142	AT3G07120	AT3G07120	RING/U-box domain-containing protein
CARHR090510	23.75	15.27	0.263	-5.86	0.00143	AT3G15460	AT3G15460	ribosomal RNA processing brix domain-containing protein
CARHR198760	23.75	35.22	4.74	-2.89	0.00146	AT5G14550	AT5G14550	Core-2/1-branching beta-1,6-N-acetylglucosaminyltransferase family protein
CARHR173540	23.75	412.75	142.51	-1.53	0.00156	Unknown	Unknown	Unknown
CARHR259270	23.75	0	10.65	Inf	0.00157	AT4G08160	AT4G08160	glycosyl hydrolase family 10 protein / carbohydrate-binding domain-containing protein
CARHR280550	23.75	222.89	68.98	-1.69	0.00178	AT5G67100	ICU2	DNA polymerase alpha catalytic subunit
CARHR139300	23.75	8.27	41.53	2.33	0.00189	AT2G44140	AT2G44140	cysteine protease ATG4a
CARHR195780	23.75	7.23	40.85	2.5	0.00212	AT5G17430	BBM	AP2-like ethylene-responsive transcription factor BBM
CARHR112650	23.75	332.25	102.03	-1.7	0.00241	AT2G21660	CCR2	glycine-rich RNA-binding protein 7
CARHR263290	23.75	0	10.35	Inf	0.00241	Unknown	Unknown	Unknown
CARHR276300	23.75	2.45	23.39	3.25	0.00284	AT5G62520	SRO5	RCD one 5-like protein
CARHR123940	23.75	156.08	43.55	-1.84	0.003	AT2G30490	ATC4H	trans-cinnamate 4-monooxygenase
CARHR073470	23.75	27.18	3.88	-2.81	0.00306	AT1G79700	AT1G79700	AP2-like ethylene-responsive transcription factor
CARHR106280	23.75	78.63	20.49	-1.94	0.00316	AT2G15960	AT2G15960	uncharacterized protein
CARHR152270	23.75	4.08	27.82	2.77	0.00316	Unknown	Unknown	Unknown
CARHR166170	23.75	7.04	41.98	2.58	0.00317	AT3G56090	FER3	ferritin 3
CARHR172490	23.75	11.86	54.12	2.19	0.0032	AT3G62150	PGP21	ABC transporter B family member 21
CARHR022580	23.75	3.71	27.53	2.89	0.00355	AT1G22230	AT1G22230	uncharacterized protein
CARHR027290	23.75	12.58	57.07	2.18	0.00377	AT1G27770	PEA1	autoinhibited Ca ²⁺ -ATPase 1
CARHR086390	23.75	15.44	0.526	-4.87	0.00377	AT3G11840	PUB24	plant U-box 24 protein
CARHR184430	23.75	141.35	42.83	-1.72	0.00395	AT5G47860	AT5G47860	uncharacterized protein
CARHR234660	23.75	158.47	50.89	-1.64	0.00492	Unknown	Unknown	Unknown
CARHR158540	23.75	4.32	27.48	2.67	0.00494	AT3G49530	ANAC062	NAC domain-containing protein 62
CARHR224330	23.75	0.935	15.66	4.07	0.00509	AT4G17615	ATCBL1	calcineurin B-like protein 1
CARHR133020	23.75	47.88	10.16	-2.24	0.00528	AT2G38400	AGF3	alanine:glyoxylate aminotransferase 3
CARHR191150	23.75	7.23	36.36	2.33	0.00563	AT5G22380	NAC090	NAC domain-containing protein 90
CARHR206210	23.75	83.28	254.41	1.61	0.00651	AT5G06940	AT5G06940	probably inactive leucine-rich repeat receptor-like protein kinase
CARHR178340	23.75	21.88	76.47	1.81	0.00685	Unknown	Unknown	Unknown

Table 3.2: List of differentially expressed genes between wild-type and *spl7-1* fruit valves. Genes with an adjusted P-value < 0.05 are listed. Continued in next page.

CARHR277920	23.75	91.9	26.9	-1.77	0.00787	AT5G64000	SAL2	SAL2 phosphatase
CARHR187810	23.75	87.21	25.95	-1.75	0.00826	AT5G25560	AT5G25560	CHY and CTCHY and RING-type zinc finger protein
CARHR245740	23.75	2.8	20.16	2.85	0.00838	AT4G37360	CYP81D2	cytochrome P450, family 81, subfamily D, polypeptide 2
CARHR222610	23.75	43.8	9.31	-2.23	0.00877	Unknown	Unknown	Unknown
CARHR036230	23.75	5.77	31.62	2.45	0.00908	AT1G45145	ATTRX5	thioredoxin H5
CARHR014020	23.75	25.87	3.62	-2.84	0.00927	AT1G13640	AT1G13640	phosphatidylinositol 3-and 4-kinase-like protein
CARHR181660	23.75	371.92	132.93	-1.48	0.00942	AT5G42750	BK11	BRI1 kinase inhibitor 1
CARHR221670	23.75	107.75	36.09	-1.58	0.00976	Unknown	Unknown	Unknown
CARHR242700	23.75	3.84	23.7	2.63	0.0106	AT4G34150	AT4G34150	calcium-dependent lipid-binding domain-containing protein
CARHR284960	23.75	13	47.89	1.88	0.0115	AT5G42330	AT5G42330	uncharacterized protein
CARHR015540	23.75	6.88	36.57	2.41	0.0116	AT1G15000	scpl50	serine carboxypeptidase-like 50
CARHR129900	23.75	2.84	20.29	2.84	0.0117	AT2G35660	CTF2A	CTF2A like oxidoreductase
CARHR238480	23.75	161.34	53.19	-1.6	0.0121	AT4G30610	BRS1	carboxypeptidase D
CARHR106220	23.75	72.64	21.97	-1.73	0.0124	AT2G15890	MEE14	maternal effect embryo arrest 14 protein
CARHR287570	23.75	2.43	19.64	3.01	0.0124	Unknown	Unknown	Unknown
CARHR116920	23.75	0	8.4	Inf	0.0133	AT4G25490	CBF1	dehydration-responsive element-binding protein 1B
CARHR166060	23.75	24.01	73.83	1.62	0.0133	AT3G55980	ATSZF1	zinc finger CCH domain-containing protein 47
CARHR202620	23.75	66.57	198.72	1.58	0.0133	AT5G10700	AT5G10700	Peptidyl-tRNA hydrolase II (PTH2) family protein
CARHR271410	23.75	56.53	16.03	-1.82	0.0133	AT5G57655	AT5G57655	xylose isomerase
CARHR279620	23.75	18.86	2.82	-2.74	0.0133	AT5G65660	AT5G65660	hydroxyproline-rich glycoprotein family protein
CARHR213880	23.75	17.8	64.76	1.86	0.0135	Unknown	Unknown	Unknown
CARHR211030	23.75	4.72	26.39	2.48	0.0135	AT5G02370	AT5G02370	kinesin family member 22
CARHR142390	23.75	28.45	4.39	-2.7	0.0136	AT2G47020	AT2G47020	Peptide chain release factor 1
CARHR001810	23.75	445.46	156.35	-1.51	0.0141	AT1G02500	MAT1	S-adenosylmethionine synthetase 1
CARHR256820	23.75	31.57	6.34	-2.32	0.0148	Unknown	Unknown	Unknown
CARHR022760	23.75	172.09	56.52	-1.61	0.0154	AT1G22410	AT1G22410	class-II DAHP synthetase-like protein
CARHR056310	23.75	7.95	33.52	2.08	0.0154	AT2G12190	AT2G12190	putative cytochrome P450
CARHR009280	23.75	14.3	59.37	2.05	0.0156	AT1G09320	AT1G09320	agenet domain-containing protein
CARHR224970	23.75	136.05	47.31	-1.52	0.0156	AT4G18210	ATPUP10	purine permease 10
CARHR226160	23.75	28.92	6.28	-2.2	0.0156	AT4G19370	AT4G19370	uncharacterized protein
CARHR101520	23.75	1.99	15.39	2.95	0.0173	AT3G25180	CYP82G1	cytochrome P450, family 82, subfamily G, polypeptide 1
CARHR198580	23.75	72.07	24.37	-1.56	0.0176	AT5G14730	AT5G14730	uncharacterized protein
CARHR106410	23.75	4.9	25.65	2.39	0.0215	Unknown	Unknown	Unknown
CARHR001330	23.75	10.25	44.29	2.11	0.0229	AT1G01140	CIPK9	CBL-interacting serine/threonine-protein kinase 9
CARHR205420	23.75	7.54	30.25	2.01	0.0229	AT5G07730	AT5G07730	uncharacterized protein
CARHR092300	23.75	4.03	22.4	2.47	0.0235	AT2G18790	PHYB	phytochrome B
CARHR187060	23.75	12.74	1.08	-3.56	0.0249	AT5G26340	MSS1	sugar transport protein 13
CARHR089710	23.75	10.88	38.71	1.83	0.0279	AT3G14760	AT3G14760	uncharacterized protein
CARHR128270	23.75	15.28	1.76	-3.12	0.0279	AT2G34180	CIPK13	CBL-interacting serine/threonine-protein kinase 13
CARHR206000	23.75	209.34	75.88	-1.46	0.0279	AT5G07140	AT5G07140	protein kinase family protein
CARHR142510	23.75	41.13	11.33	-1.86	0.0281	AT2G47130	AT2G47130	Rossmann-fold NAD(P)-binding domain-containing protein
CARHR009320	23.75	13.48	45.7	1.76	0.0284	AT1G09350	AtGolS3	galactinol synthase 3
CARHR226210	23.75	52.63	15.42	-1.77	0.0302	AT4G19420	AT4G19420	putative Pectinacetyltransferase
CARHR015550	23.75	0.617	11.88	4.27	0.0304	AT1G15010	AT1G15010	uncharacterized protein
CARHR026730	23.75	8.55	0	Inf	0.0305	AT1G24400	AATL2	lysine histidine transporter 2
CARHR235200	23.75	2.47	18.8	2.93	0.0325	AT4G27520	ENODL2	early nodulin-like protein 2
CARHR066620	23.75	0.651	10.4	4	0.033	AT1G73600	AT1G73600	putative phosphoethanolamine N-methyltransferase 3
CARHR242030	23.75	45.01	128.01	1.51	0.0335	AT4G33930	AT4G33930	glycine-rich protein
CARHR013880	23.75	12.32	46.73	1.92	0.0346	AT1G13560	AAPT1	ethanolaminephosphotransferase
CARHR170630	23.75	9.57	0.41	-4.54	0.0346	AT3G60310	AT3G60310	uncharacterized protein
CARHR022930	23.75	62.57	19.72	-1.67	0.0354	Unknown	Unknown	Unknown
CARHR103580	23.75	8.15	30.73	1.91	0.037	AT2G05940	AT2G05940	kinase-like protein
CARHR196390	23.75	43.49	12.32	-1.82	0.0377	AT5G16770	MYB9	myb domain protein 9
CARHR194820	23.75	139.27	50.99	-1.45	0.0381	AT5G18240	ATMYR1	myb-related protein 1
CARHR168130	23.75	41.25	10.86	-1.93	0.0427	AT3G57800	AT3G57800	transcription factor bHLH60
CARHR172500	23.75	15.57	1.91	-3.02	0.0427	AT3G62160	AT3G62160	HXXXD-type acyl-transferase-like protein
CARHR264480	23.75	80.56	207.47	1.36	0.0427	Unknown	Unknown	Unknown
CARHR284360	23.75	2.87	17.8	2.63	0.0427	AT5G47910	ATRBOHD	respiratory burst oxidase-D
CARHR063180	23.75	4.49	21.69	2.27	0.0434	AT1G70090	GATL9	putative galacturosyltransferase-like 9
CARHR124750	23.75	31.18	8	-1.96	0.0439	AT2G31150	AT2G31150	ATP binding / ATPase

11. Transcriptomic profiling of *spl7-1* fruit valves indicate a loss of SPL7 pathway regulation

To gain insight into the role of *SPL7* in endocarp *b* SCW lignification, I examined how the *SPL7* pathway was affected in the RNA-seq comparison of *spl7-1* versus wild-type fruit valves. For all genes identified in the *SPL7* pathway in *A. thaliana* that have clear orthologs in *C. hirsuta* (see previous section), I collected the values of gene expression in wild-type and *spl7-1* fruit valves as well as the change in expression in *spl7-1* valves (log₂ fold change). *SPL7* is activated in response to Cu-deficiency to regulate genes involved in Cu homeostasis (Schulten & Krämer, 2017). Genes regulated by *SPL7* activity can be divided in two groups. First, *SPL7* promotes expression of genes involved in Cu uptake and mobilisation. Second, *SPL7* promotes expression of the Cu-miRNAs, which target mRNAs of Cu-requiring proteins that are likely to be non-essential for the plant. A summary of expression data for these genes in *spl7-1* versus wild-type fruit valves can be found in Table 3.3.

It is important to note that this RNA-seq experiment was performed before I discovered that the *lig1* mutant phenotype was caused by loss of *SPL7* gene function. Therefore, the Cu supplied to plants in this experiment was not monitored. However, the *spl7-1* fruit that were used for RNA extraction exhibited the mutant phenotype, so I reasoned that plants were grown in Cu-deficient soil. Previously, I have described that only additional supplementation of Cu to *spl7-1* plants grown on soil can rescue the lignification of endocarp *b* SCWs. Given that plants experienced Cu-deficiency in this experiment, *SPL7* activity would be necessary for endocarp *b* lignification. Following this logic, I expected to find differences in the expression of genes in the *SPL7* pathway between wild type and *spl7-1*.

Firstly, *SPL7* is expressed in fruit valves of wild type at low levels (Table 3.3). The expression of *SPL7* is slightly reduced in the fruit valves of the *spl7-1* mutant, although the difference is not statistically significant. These results indicate that *SPL7* is expressed in the *spl7* mutant. This is expected in the *spl7* mutant since the mutation identified only generates a single amino acid substitution.

For some genes in the SPL7 pathway, no expression was found either in wild-type or *spl7-1* fruit valves (normalized counts = 0). These genes include *COPT2*, *FRO4*, *LAC3* and *LAC7* (Table 3.3). I confirmed the absence of expression of these genes in *C. hirsuta* fruit with an additional RNA-seq dataset from stage 16 fruit (Gan *et al.*, 2016). *LAC12*, *LAC13*, *ARPN*, and *YSL2* gene expression was found to be low in wild-type and *spl7-1* fruit valves since the mean of normalized counts in both genotypes is below 5 for these genes (Table 3.3). Many of the genes regulated by SPL7 have been identified in studies that sampled roots, seedlings and shoots (Bernal *et al.*, 2012; H. Yamasaki *et al.*, 2009). Therefore, it is not surprising that some of these genes are not expressed, or expressed at very low levels, in fruit valves.

However, other genes in the SPL7 pathway show expression in *C. hirsuta* fruit valves. For example, the Cu/Zn superoxide dismutases *CSD1* and *CSD2*, which are both targets of miR398 and are downregulated under Cu-deficiency in a SPL7-dependent manner in *A. thaliana* (Abdel-Ghany & Pilon, 2008). In *C. hirsuta spl7-1* fruit valves, transcripts of *CSD1* and *CSD2* are more abundant than in wild type (Table 3.3 and Figure 3.13). This is the expected response in a *spl7* mutant, where a failure to upregulate miR398 in response to Cu-deficiency would result in upregulation of *CSD1* and *CSD2* gene expression. In *A. thaliana*, *FSD1* gene expression is upregulated by SPL7 in response to Cu-deficiency, in what is thought to be a compensatory mechanism to replace *CSD1* and *CSD2* function (Abdel-Ghany *et al.*, 2005; Yamasaki *et al.*, 2007). Therefore, *FSD1* activation is expected to be absent in a *spl7* mutant. In agreement with this, I found that *FSD1* gene expression in *C. hirsuta* fruit valves is downregulated in *spl7-1* compared to wild type (Table 3.3 and Figure 3.13). Taken together, these results suggest that the economization of Cu through downregulation of Cu/Zn SODs and upregulation of Fe SOD1 is lost in fruit valves of *C. hirsuta spl7-1*.

Two other genes that are expressed in fruit valves, *COPPER CHAPERONE FOR SOD1 (CCS)* and cytochrome c oxidase subunit 5b (*COX5b.1*), are targets of miR398 in *A. thaliana* (H. Yamasaki *et al.*, 2007). I found that these genes are not differentially expressed between *spl7-1* and wild-type fruit valves (Table 3.3 and Figure 3.13). These results indicate that SPL7-dependent

economization through downregulation of these genes is not taking place in *C. hirsuta* fruit valves under the Cu conditions used in this experiment.

Three laccases (*LAC2*, *LAC4* and *LAC17*) that are targets of miR397, are highly expressed in *C. hirsuta* fruit valves. Transcripts of these genes are more abundant in *spl7-1* than in wild-type fruit valves (Table 3.3 and Figure 3.13). This is the expected response in a *spl7* mutant, where a failure to upregulate miR397 in response to Cu-deficiency would result in upregulation of these laccase genes.

Other genes that are predicted targets of Cu-miRNAs show low or no expression in *C. hirsuta* fruit valves as mentioned above. *LAC7* is a target of miR857 but is not expressed in *C. hirsuta* valves. *LAC3*, *LAC12*, *LAC13* and *ARPN* are targets of miR408, but are not expressed (*LAC3*) or expressed at low levels (*LAC12*, *LAC13* and *ARPN*) in *C. hirsuta* fruit valves. Nevertheless, expression of *LAC12*, *LAC13* and *ARPN* is slightly downregulated in *spl7-1* compared to wild type (Table 3.3 and Figure 3.13), which is not the expected response to Cu-deficiency in a *spl7* mutant.

In addition to economising Cu, *SPL7* regulates Cu homeostasis by promoting the expression of genes involved in Cu uptake and mobilisation. *C. hirsuta* orthologs of two of these genes, *COPT2* and *FRO4*, are not expressed in fruit valves. However, *COPT1* is expressed in fruit valves, and its expression is slightly downregulated in *spl7-1* compared to wild type (Table 3.3 and Figure 3.13). This is the expected response to Cu-deficiency in a *spl7* mutant. The expression of two other genes do not fit this expectation: *YELLOW STRIPE LIKE 2* (*YSL2*) and *COPPER CHAPERONE* (*CCH*) are both upregulated in *spl7-1* valves compared to wild type (Table 3.3 and Figure 3.13). Although expression of *YSL2* is below 2 normalized counts in both genotypes and should be discounted. Upregulation of *CCH* gene expression in *spl7-1* fruit valves suggests that this gene can be regulated independently of *SPL7*.

In summary, my results indicate that regulation of the canonical *SPL7* pathway is lost in *spl7-1* fruit valves in *C. hirsuta*. This is particularly evident for *SPL7* targets that act to economise Cu;

for example, the switch from Cu/Zn SODs to Fe SOD1 is lost in *spl7-1* fruit, and the repression of *LAC2*, *LAC4* and *LAC17* gene expression is lost in *spl7-1* fruit.

It is important to note that RNA libraries were not prepared to include small RNA molecules, such as miRNAs, in this experiment. Therefore, expression of Cu-miRNAs could not be directly assessed. Moreover, Cu-miRNA-encoding genes have not been annotated in the *C. hirsuta* reference genome, so sequence reads for these transcripts are not analysed by the bioinformatics pipeline used here. However, previous studies have shown that the expression of miRNA-encoding genes located in non-translated regions of host genes, such as in introns and UTR regions, are often coregulated with the expression of their host genes (Yang *et al.*, 2012). In Figure 3.10, I described a *C. hirsuta* genomic region with high identity to *A. thaliana* *MIR389B* sequence. This genomic region in *C. hirsuta* is located in the 3'UTR of the gene CARHR198760 (ortholog of At5g14550). I found that this gene is downregulated in fruit valves of *spl7-1* compared to wild type (log₂ fold change value of -2.89). The difference in expression is statistically significant (adjusted P-value of 0.0014). If expression of the *C. hirsuta* *MIR398b* gene is coregulated with its host gene, CARHR198760, these results could reflect the loss of *MIR398b* upregulation by SPL7 in response to Cu-deprivation in *spl7-1* fruit valves. I also described a *C. hirsuta* genomic region with high identity to *A. thaliana* *MIR408* sequence (Figure 3.10). This genomic region in *C. hirsuta* is located in the 3'UTR of the gene CARHR142390 (ortholog of At2g47020). I found that this gene is also downregulated in fruit valves of *spl7-1* compared to wild type (log₂ fold change value of -2.7). The difference in expression is statistically significant (adjusted P-value of 0.0136). If expression of the *C. hirsuta* *MIR408* gene is coregulated with its host gene CARHR142390, this could reflect the loss of *MIR408* upregulation by SPL7 in response to Cu-deprivation in *spl7-1* fruit valves. The *C. hirsuta* genomic regions with high identity to the other *A. thaliana* Cu-miRNA (miR397a, miR397b, miR398a and miR857a) sequences, are all in regions annotated as intergenic. Therefore, these putative Cu-miRNA-encoding genes are not located in obvious host genes. Genes adjacent to these putative Cu-miRNA-encoding genes, either upstream or downstream, are not significantly differentially expressed in *spl7-1* fruit valves. Therefore, I could not use coregulation to indirectly assess the expression of these putative Cu-

miRNA-encoding genes. To directly measure the response of Cu-miRNAs to Cu-deprivation, it will be necessary to repeat this RNA-seq experiment using libraries that include small RNA molecules.

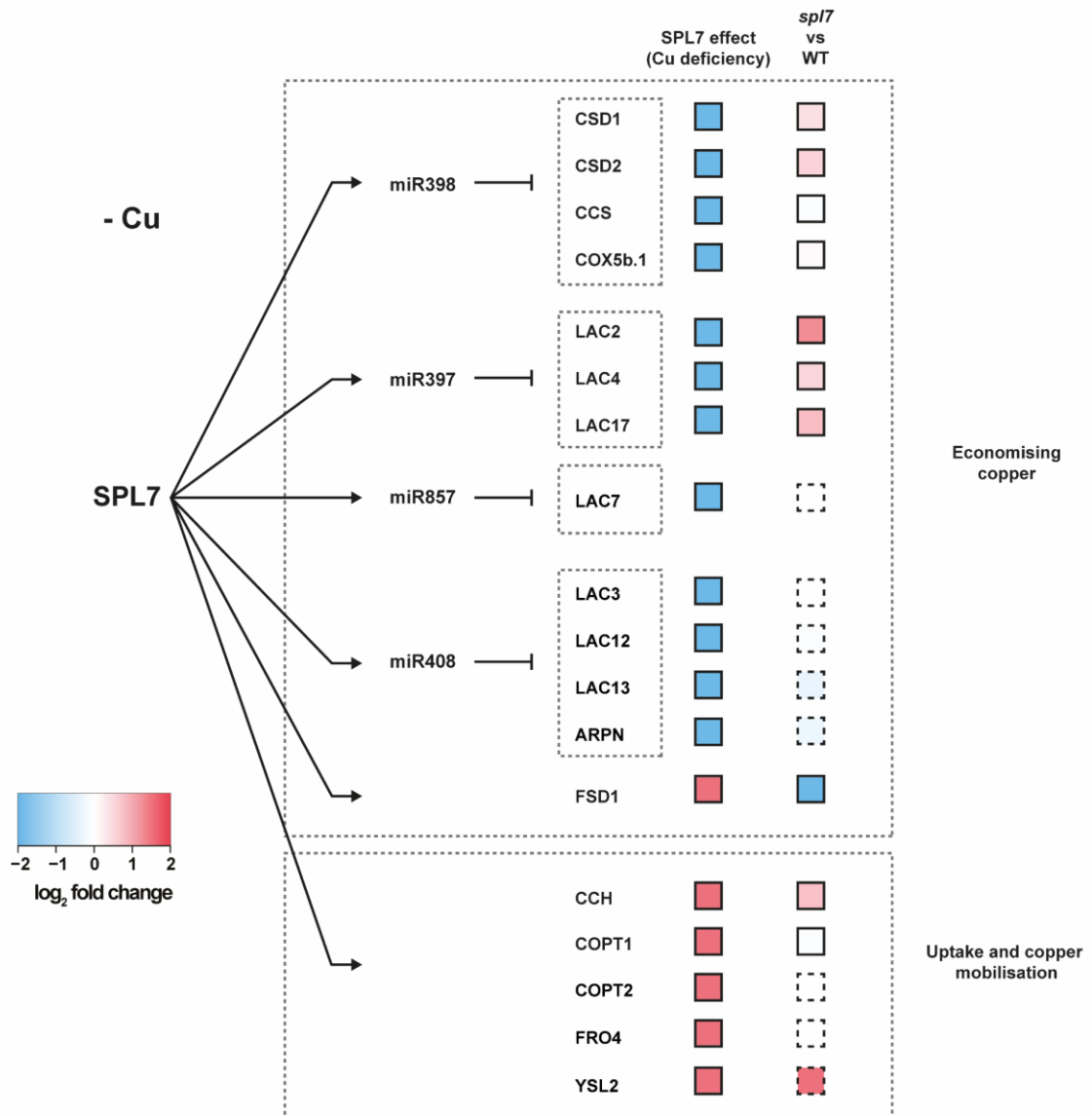


Figure 3.13: SPL7 pathway is altered in *C. hirsuta spl7-1* fruit valves. Diagram showing SPL7 pathway identified in *A. thaliana* as in (Schulten & Krämer, 2017). Expected effect of SPL7 on gene transcript levels (under Cu deficiency) is indicated in two different colours: upregulation (red) and downregulation via Cu-miRNAs (blue). Experimentally determined change in expression in RNA-seq data comparing *spl7-1* and wild-type fruit valves is indicated. Values of log₂ fold change were represented into a heat map scale and mapped to the diagram of SPL7 pathway. Squares with dashed outline indicate that the mean of normalized counts for the gene is < 5.

<i>C. hirsuta</i> gene number	Mean normalized counts	Wild-type normalized counts	<i>spl7-1</i> normalized counts	log2 fold change	Adjusted P-value	<i>A. thaliana</i> gene number	Name	Description
CARHR194170	4.44	4.99	3.89	-0.36	1	AT5G18830	SPL7	squamosa promoter-binding-like protein 7
CARHR008750	22.24	18.9	25.58	0.437	1	AT1G08830	CSD1	Superoxide dismutase [Cu-Zn]
CARHR121080	16.16	13	19.33	0.573	1	AT2G28190	CSD2	Superoxide dismutase [Cu-Zn]
CARHR012800	9.47	9.71	9.23	-0.07	1	AT1G12520	CCS	copper chaperone for SOD1
CARHR090730	9.54	9.27	9.81	0.0814	1	AT3G15640	Cox5b.1	cytochrome c oxidase subunit Vb
CARHR122430	41.6	24.28	58.92	1.28	0.192	AT2G29130	LAC2	laccase 2
CARHR132660	263.87	215.46	312.29	0.536	1	AT2G38080	LAC4	laccase 4
CARHR273650	109.79	79.52	140.05	0.817	0.733	AT5G60020	LAC17	laccase 17
CARHR083560	0	0	0	NA	NA	AT3G09220	LAC7	laccase 7
CARHR123520	0	0	0	NA	NA	AT2G30210	LAC3	laccase 3
CARHR207840	0.274	0.284	0.263	-0.11	1	AT5G05390	LAC12	laccase 12
CARHR206010	4.5	5.06	3.94	-0.36	1	AT5G07130	LAC13	laccase 13
CARHR145280	2.35	2.61	2.1	-0.31	1	AT2G02850	ARPN	plantacyanin
CARHR232490	7.94	12.58	3.29	-1.93	0.757	AT4G25100	FSD1	Superoxide dismutase [Fe]
CARHR285590	9.17	9.43	8.92	-0.08	1	AT5G59030	COPT1	copper transporter 1
CARHR155490	0	0	0	NA	NA	AT3G46900	COPT2	copper transporter 2
CARHR189580	0	0	0	NA	NA	AT5G23980	FRO4	ferric reduction oxidase 4
CARHR189040	1.1	0.568	1.63	1.52	1	AT5G24380	YSL2	metal-nicotianamine transporter YSL2
CARHR166400	31.055	23	39.11	0.766	1	AT3G56240	CCH	Cu chaperone

Table 3.3: Differential expression of *SPL7* gene and *SPL7* regulated genes in *spl7-1* fruit valves relative to wild type.

12. Lignin biosynthesis pathway is altered in *spl7-1* fruit valves

To investigate which genes are associated with the lignification of endocarp *b* SCWs in *C. hirsuta*, I took advantage of the RNA-seq data from stage 17 wild-type and *spl7-1* fruit valves. At this stage, lignification of endocarp *b* SCWs is starting in wild type, but is reduced in *spl7-1*. I examined the differential expression of genes involved in the lignin biosynthesis pathway between wild-type and *spl7-1* fruit valves.

I identified *C. hirsuta* orthologs of *A. thaliana* genes involved in the lignin biosynthesis pathway (Zhao & Dixon, 2011), and collected the expression values for these gene in wild-type and *spl7-1* fruit valves as well as the change in expression in *spl7-1* valves relative to wild type (log2 fold change). Some steps in the lignin biosynthesis pathway can be performed by several members of the same enzyme family, therefore, I included the expression data for all *C. hirsuta* gene family members that encode enzymes involved in lignin biosynthesis. Since some gene families contain many members and some of these genes are not expressed, or expressed at low levels, in fruit valves, I filtered out genes with a mean of normalized counts lower than 10. After filtering, all steps of the lignin biosynthesis pathway are represented by at least one gene (Table 3.4 and Figure 3.14).

The lignin biosynthesis pathway can be divided into two parts according to the location in the cell where the enzymatic steps take place. Most of the steps of the pathway take place in the cytosol where the three different lignin monomers (monolignols) are produced. Once synthesized, monolignols are exported to the apoplast where they undergo a final step of oxidation performed by laccases or peroxidases (second part of the pathway). I found that two genes contributing to monomer biosynthesis in the cytosol are significantly downregulated in *spl7-1* fruit valves relative to wild type. These genes encode enzymes that perform the first and second steps of monolignol biosynthesis, *PHENYLALANINE AMMONIA-LYASE 4 (PAL4)* and *CINNAMATE 4-HYDROXYLASE (C4H)* respectively (Figure 3.14). Furthermore, other members of the *PAL* gene family and most of the genes involved in the first steps of monolignol biosynthesis are downregulated in fruit valves of *spl7-1* (Figure 3.14). This is the case for most gene family members of *PAL*, *C4H*, *4CL*, *HCT*, *C3H*, *CCR*, *F5H* and *COMT*, although the difference in expression is not statistically significant. All genes in the dataset belonging to the *CAD* gene family, which perform the last step of monolignol biosynthesis, are upregulated in *spl7-1* fruit valves, although the differences are not statistically significant (Figure 3.14). Taken together, these results suggest that monolignol biosynthesis is negatively regulated in fruit valves of the *spl7-1* mutant and that this negative regulation is observed in the first steps of the pathway.

I found that two genes encoding oxidases that polymerize monolignols, *LACCASE11 (LAC11)* and *PEROXIDASE49 (PER49)*, are upregulated in *spl7-1* fruit valves (Figure 3.14). The change in expression is similar for *LAC11* and *PER49* (log₂ fold change values of 4.1 and 3.74 respectively, Table 3.4). The change in expression is statistically significant for both genes and they are among the 10 genes with lowest P-value (Figure 3.12 and 3.14 and Table 3.4). These genes encode members of the two families of enzymes that can perform the last step of the lignin biosynthesis pathway in the apoplast (monolignol polymerization). Other members of the laccases and peroxidases are upregulated, with the exception of one laccase and one peroxidase which are downregulated (Figure 3.14). However, changes in expression of other members is not statistically significant. Taken together, these results suggest that genes required to polymerize monolignols in the cell wall are upregulated in *spl7-1* fruit valves.

Although not part of the canonical lignin biosynthesis pathway, an additional gene that encodes a NADPH oxidase, *RESPIRATORY BURST OXIDASE HOMOLOG D (RBOHD)*, is upregulated (log₂ fold change of 2.62) in fruit valves of *spl7-1* relative to wild type (Figure 3.14). This difference in expression is statistically significant (P-value of 0.043). This enzyme is involved in the generation of reactive oxygen species, leading to the production of H₂O₂, which is the substrate of peroxidases. It has been shown that this enzyme is required for lignification of the abscission zone in *A. thaliana* flowers (Lee *et al.*, 2018) and for lignification of the Casparian strip in the root endodermis (Fujita *et al.*, 2020). This result further suggests that genes required for lignin polymerization are upregulated in *spl7-1* fruit valves.

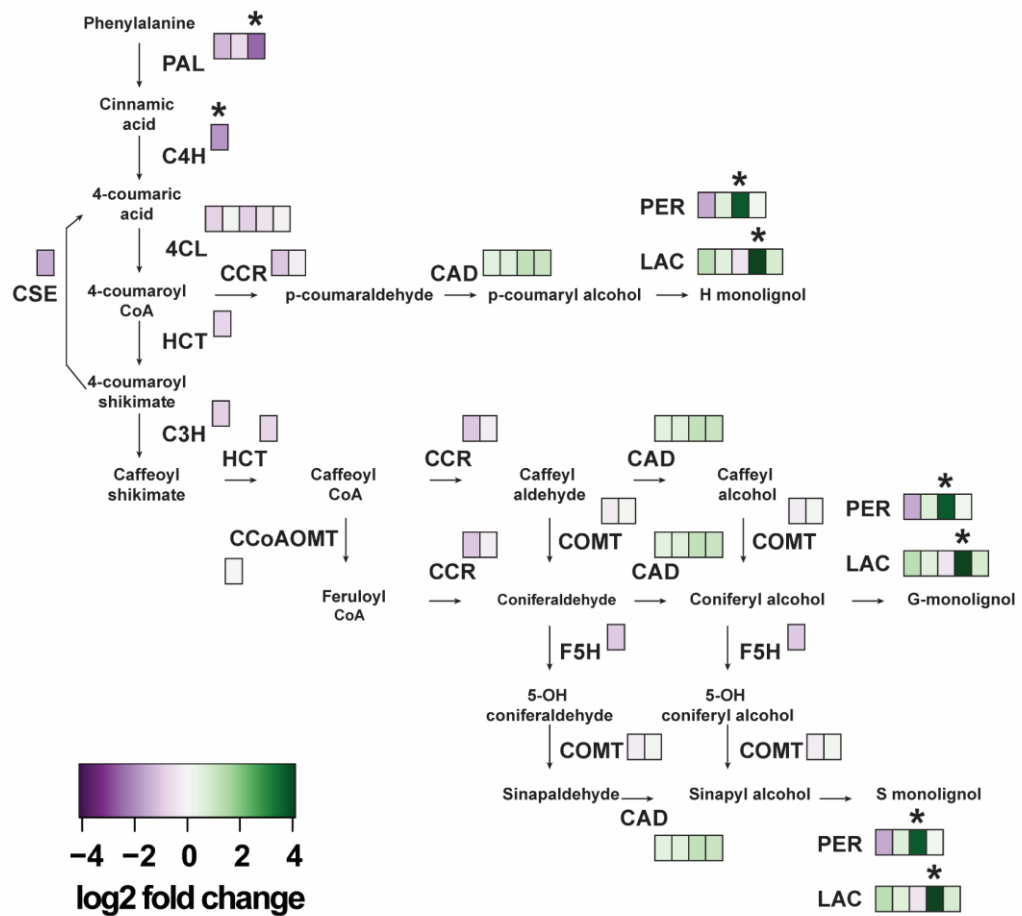


Figure 3.14: Lignin biosynthesis pathway is altered in *spl7-1* fruit valves. Differential gene expression between fruit valves of wild type and *spl7-1* obtained from RNA-seq. Values of log₂ fold change were represented with a heat map scale and mapped to a diagram of the lignin biosynthesis pathway as in (Zhao & Dixon, 2011). On each biosynthesis reaction, each rectangle represents a gene potentially involved. To avoid presenting genes with no expression or very low expression, a mean value of normalized counts >10 (mean of normalized counts in wild type and *spl7-1*) was set as a threshold, and only genes with a higher value are presented in this figure. Asterisks denote statistically significant differences in gene expression between wild type and *spl7-1* (adjusted p-value < 0.05). Importantly, genes can be involved in several different steps of the pathway leading to the synthesis of the different monolignols. These genes and their log₂ fold change values are represented in all steps where they are potentially involved.

<i>C. hirsuta</i> gene number	Wild-type normalized counts	<i>lig1</i> normalized counts	Mean normalized counts	log2 fold change	Adjusted P-value	<i>A. thaliana</i> gene number	Enzyme type	Description
CARHR131540	204.14	81.17	142.66	-1.33	0.0599	AT2G37040	PAL	phenylalanine ammonia-lyase
CARHR289320	70.38	45.43	57.9	-0.63	1	AT3G53260	PAL	
CARHR084820	102.97	17.83	60.4	-2.53	0.0000122	AT3G10340	PAL	
CARHR123940	156.08	43.55	99.82	-1.84	0.003	AT2G30490	C4H	cinnamate-4-hydroxylase
CARHR041840	80.19	44.43	62.31	-0.85	0.973	AT1G51680	4CL	4-coumarate--CoA ligase
CARHR097130	39.75	43.59	41.67	0.133	1	AT3G21230	4CL	
CARHR020950	32.26	17.64	24.95	-0.87	1	AT1G20500	4CLlike	4-coumarate--CoA ligase-like
CARHR020980	57.94	42.97	50.45	-0.43	1	AT1G20510	4CLlike	
CARHR070710	37.95	34.78	36.36	-0.13	1	AT1G77240	4CLlike	
CARHR046060	56.65	33.78	45.21	-0.75	1	AT5G48930	HCT	hydroxycinnamoyl-CoA shikimate/ quininate hydroxycinnamoyl transferase
CARHR136000	68.93	37.23	53.08	-0.89	0.98	AT2G40890	C3H	4-coumarate-shikimate/ quininate-ester 3 hydroxylase
CARHR242190	75.79	79.21	77.5	0.0636	1	AT4G34050	CCoAOMT	caffeoyl-CoA-ortho-methyl-transferase
CARHR244620	34.65	17.48	26.07	-0.99	1	AT4G36220	F5H	ferulate-5 hydroxylase
CARHR267360	74.31	63.53	68.92	-0.23	1	AT5G54160	COMT	5-hydroxyconiferaldehyde / alcohol ortho-methyltransferase
CARHR006410	16.78	18.52	17.65	0.143	1	AT1G51990	COMT-like	similarity to 5-hydroxyconiferaldehyde / alcohol ortho-methyltransferase
CARHR016460	35.18	17.25	26.22	-1.03	1	AT1G15950	CCR	cinnamyl CoA reductase
CARHR238360	13.25	11.71	12.48	-0.18	1	AT4G30470	CCR-like	similarity to cinnamyl CoA reductase
CARHR242560	57	79.95	68.48	0.488	1	AT4G34230	CAD	cinnamyl alcohol dehydrogenase
CARHR065600	11.23	17.06	14.14	0.603	1	AT1G72680	CAD-like	similarity to cinnamyl alcohol dehydrogenase
CARHR246390	8.06	18.26	13.16	1.18	0.973	AT4G37980	CAD-like	
CARHR247380	7.12	14.77	10.95	1.05	1	AT4G39330	CAD-like	
CARHR122430	24.28	58.92	41.6	1.28	0.192	AT2G29130	LAC	laccase
CARHR132660	215.46	312.29	263.87	0.536	1	AT2G38080	LAC	
CARHR141920	54.97	41.16	48.07	-0.42	1	AT2G46570	LAC	
CARHR210090	3.54	60.68	32.11	4.1	7.47E-10	AT5G03260	LAC	
CARHR273650	79.52	140.05	109.79	0.817	0.733	AT5G60020	LAC	
CARHR128150	19.77	6.71	13.24	-1.56	0.387	AT2G34060	PER	peroxidase
CARHR228770	123.7	194.46	159.08	0.653	1	AT4G21960	PER	
CARHR244760	5.23	69.85	37.54	3.74	1.25E-09	AT4G36430	PER	
CARHR264810	39.47	44.61	42.04	0.176	1	AT5G51890	PER	
CARHR042920	55.91	19.69	37.8	-1.51	0.173	AT1G52760	CSE	

Table 3.4: Expression of genes involved in lignin biosynthesis. Genes with a mean of normalized counts below 10 were not included in this dataset.

Discussion

SPL7 is expressed at comparable levels in several tissues and developmental stages in *C. hirsuta*, such as seedlings, developing leaves and young fruit; and expression is approximately two times higher in roots than in aerial organs. These results agree with the expression profile found in *A. thaliana*, where *SPL7* shows constitutive expression throughout different tissues and developmental stages and a higher expression in roots (Figure S1) (Yamasaki *et al.*, 2009). The expression pattern found in *C. hirsuta* fits with the functions of *SPL7* in Cu homeostasis described in previous studies (Schulten & Krämer, 2017). *SPL7* promotes Cu uptake in the roots; and it promotes Cu mobilisation and Cu economization, which might be important in different organs of the plant.

Although *SPL7* expression data was available for several tissues and developmental stages in *A. thaliana* (Figure S1) (Yamasaki *et al.*, 2009), to my knowledge, *SPL7* expression data was lacking for fruit valves at lignification stage both in *A. thaliana* and *C. hirsuta*. Using data from an RNAseq experiment of wild-type and *spl7-1* fruit valves, I found that *SPL7* is expressed in *C. hirsuta* fruit valves at stage 17, when lignin deposition in the endocarp *b* SCWs is initiating. Also, *SPL7* is not differentially expressed in the *spl7-1* fruit valves compared to wild type. This is expected since the causal mutation for *spl7-1* mutant phenotype is a single amino acid change.

To my knowledge, there was no previous data on cell specific expression of *SPL7* in fruit of *A. thaliana* or *C. hirsuta*. I found that *SPL7* is highly expressed in the endocarp *b* cells of *C. hirsuta* fruit at stage 17 a/b, when SCWs are lignified. These results suggest that *SPL7* might have a local role in lignification of endocarp *b* cells. I could detect *SPL7* expression also in the valve margin, which contains a lignified cell type. These results suggest a local role of *SPL7* in lignification of these cell types in *C. hirsuta* fruit. Lignification of endocarp *b* SCWs is reduced in *spl7-1*, whereas, lignification of the valve margin does not seem reduced by phloroglucinol/HCl staining, suggesting that lignification of SCWs of the endocarp *b* is more sensitive to the loss of *SPL7* activity than other cell types. In *A. thaliana*, I observed that both the endocarp *b* layer and the

valve margin are less lignified in Cu-limiting conditions, indicating that SPL7 is necessary for lignification of both cell types and suggesting that the higher sensitivity of the endocarp *b* layer to loss of SPL7 activity is specific to *C. hirsuta*.

The Cu concentrations in fruit of wild-type *C. hirsuta* plants grown in an aeroponics system ranged from 2.8 µg/g of dry weight, in the lowest Cu supply, to 12.17 µg/g, in the highest Cu supply. In shoots of *A. thaliana* wild-type plants, Cu concentration ranged from just less than 2 µg/g of dry weight, in Cu-limiting conditions, to approximately 8 µg/g when grown in media supplemented with 0.5 µM CuSO₄ (Schulten & Krämer, 2017). These results indicate that Cu concentrations in fruit of *C. hirsuta* are comparable to the Cu concentrations found in other organs in *A. thaliana*, when grown in a range of Cu supply between Cu-deficiency and Cu-sufficiency. Therefore, *C. hirsuta* fruit do not accumulate unusually high or low Cu concentrations and Cu homeostasis operates in *C. hirsuta* fruit over a range of Cu concentrations that are similar to those reported in *A. thaliana*.

In soil not supplemented with Cu, *spl7* fruit have four times less Cu concentration than wild-type fruit and I showed that transgenic expression of *SPL7* fully complements the Cu concentration to wild-type levels in the fruit of two independent transgenic lines. My results are in contrast with the Cu concentrations found in several organs of the *spl7* mutant in *A. thaliana*. For instance, in a previous study in *A. thaliana*, it was reported that Cu concentrations in roots and stems of *spl7* mutants grown in Cu-deficient media were approximately 20 % and 50 % higher than in wild type (Bernal *et al.*, 2012). In these Cu-deficient conditions, growth of *A. thaliana spl7* plants was reduced compared to wild type, likely because they are unable to economize Cu for processes essential for growth (Bernal *et al.*, 2012). Therefore, the higher Cu concentration per tissue dry weight in *spl7* versus wild type, may reflect the significant reduction in *spl7* tissue dry weight. Moreover, 3-week-old seedlings of *A. thaliana spl7* mutant grown in media under Cu-limiting conditions had a Cu concentration slightly higher than wild-type seedlings (Yamasaki *et al.*, 2009). In another study, shoots of 3-week-old *spl7* seedlings grown in Cu-deficient media had a Cu concentration similar to that of wild type (Schulten *et al.*, 2019). The increased or comparable

Cu levels found in different tissues of the *A. thaliana spl7* mutant contrasts with the strong reduction in Cu concentration that I found in *C. hirsuta spl7* fruit. My results indicate that *C. hirsuta spl7* fruit are less able to accumulate Cu under low Cu supply than vegetative tissues of *A. thaliana spl7*, suggesting that Cu mobilisation to the fruit is more sensitive to the loss of SPL7 function. However, Cu concentration of *A. thaliana spl7* mutant fruit has not been reported and it may be that I achieved more sensitivity simply because I sampled a single organ type at a single developmental stage, rather than the whole shoots, roots or seedlings used previously. In addition, it is possible that the growth and elongation of *spl7* fruit is less impaired than shoots, roots or seedlings, therefore the calculation of Cu concentration is not so biased by large differences in tissue dry weight between *spl7* and wild type.

I found that Cu supplementation to growing plants increases the Cu concentration in *spl7* mutant fruit, indicating that Cu supplementation can bypass loss of SPL7 function to increase Cu concentration in the fruit, at least to some degree. My results agree with previous studies in *A. thaliana*, where increased Cu supply to the growth media increased Cu concentration in *spl7* mutant seedlings (H. Yamasaki *et al.*, 2009), and in *spl7* mutant roots and stems (Bernal *et al.*, 2012). I showed that Cu supplementation to wild-type *C. hirsuta* plants also increases Cu concentration in wild-type fruit. This is also in agreement with previous results in *A. thaliana*, where increased Cu supply resulted in increased tissue Cu concentrations in wild type (Bernal *et al.*, 2012; Yamasaki *et al.*, 2009). Nevertheless, I found that Cu concentration in *spl7-1* mutant fruit was lower than in wild type when supplied with the same concentration of Cu. I observed this difference in fruit Cu concentration in response to a range of supplied Cu that spanned a 5-fold concentration difference. My results indicate that increased Cu supply cannot fully rescue the Cu concentration in fruit of the *spl7-1* mutant, suggesting that Cu uptake cannot be fully bypassed by Cu supplementation, and that Cu mobilisation to the fruit is impaired in the *spl7* mutant.

My results indicate that increased Cu supply can increase Cu concentration in fruit. Furthermore, I found that Cu supplementation to the soil, in sufficient concentrations, can fully rescue the

reduced endocarp *b* lignification in the *spl7* mutant. This result indicates that Cu supplementation to the soil, when applied in adequate concentrations is sufficient to bypass SPL7 function for lignification of endocarp *b* cells. Therefore, reduced Cu availability is responsible for the reduced lignification of endocarp *b* SCWs in the *spl7* mutant, and it is not due to other putative functions of SPL7. Interestingly, although endocarp *b* SCWs are less lignified in the *spl7* mutant in Cu limiting conditions, lignification of the root stele and fibres and vascular bundles in the stem do not appear reduced compared to wild type when examined by phloroglucinol/HCl staining. These results suggest that endocarp *b* SCWs have a higher specificity for SPL7 activity in response to Cu deprivation, or a higher sensitivity to Cu levels in the absence of SPL7 than other cell types. This sensitivity may reflect particularities of SPL7-dependent Cu mobilisation or economization in the fruit.

Another interesting observation is that, only frequent supplementation with high concentrations of Cu to the soil was sufficient to rescue lignification of *spl7* endocarp *b* cells, whereas the stature defects were rescued at lower Cu supply. Although the Cu concentration in fruit was not measured in the experiment where endocarp *b* lignification was rescued by Cu supply to the soil, I observed that supplementation with the same Cu concentration, but applied less frequently, does not rescue the *spl7* fruit phenotype. These preliminary observations suggest that even when *spl7* fruit might have Cu levels comparable to those of wild-type fruit, lignification might be still reduced in endocarp *b* cells. However, to investigate these preliminary observations, further experiments are required in which the Cu concentration of fruit, and the restoration of endocarp *b* lignification, are assessed for a range of supplied Cu concentrations. Nevertheless, this hypothesis fits with the results that I obtained from the transcriptomic profiling of wild-type and *spl7-1* fruit valves, where I observed that the Cu economization pathway regulated by SPL7 is lost in *spl7-1* fruit valves. Reduced Cu economization could translate to less Cu availability for a Cu-dependent lignification of the endocarp *b* SCWs in the *spl7-1* mutant.

In this chapter, I generated a transcriptomic profile of wild-type versus *spl7* mutant fruit valves at stage 17 by using RNA-seq data. At this stage of fruit development, lignification of endocarp *b*

SCWs is starting. Given that *SPL7* is expressed in the endocarp *b* of the fruit valves, I used this transcriptomic comparison to investigate the specific role of *SPL7* in the lignification process. It is important to note that this is the first time that a transcriptomic profile has been generated for fruit valves in *C. hirsuta*. Moreover, to my knowledge, the transcriptome of fruit valves in the *A. thaliana spl7* mutant has not been profiled before. Thus, differences to *A. thaliana* could reflect organ or species-specific differences.

SPL7 is the central regulator of Cu homeostasis (Anna Schulten & Krämer, 2017). Under Cu-limiting conditions, *SPL7* is activated and it promotes the expression of Cu-responsive genes. Firstly, *SPL7* promotes the expression of genes that encode Cu transporters and chaperones to increase Cu uptake in the roots and mobilisation throughout the plant. Secondly, *SPL7* promotes the expression of the so-called Cu-miRNAs that target Cu-requiring proteins with non-essential functions to economize Cu for essential processes that cannot be replaced. By examining RNA-seq data from wild-type and *spl7* mutant fruit valves, I found that some of the elements in the canonical *SPL7* pathway are lost in fruit valves of the *spl7* mutant. Expression of several genes that are targets of the Cu-miRNAs is increased in the *spl7* mutant, which might reflect a loss of *SPL7*-dependent downregulation. This is particularly evident for several laccases and for the Cu-SODs. Conversely, expression of the gene encoding the Fe-SOD is downregulated in *spl7* mutant fruit valves, reflecting a loss of upregulation by *SPL7*. Taken together, these results indicate that Cu economization in a *SPL7*-dependent manner is lost in fruit valves of the *spl7* mutant.

On the other hand, several genes known to be regulated by *SPL7* in Cu deficiency in *A. thaliana* are not expressed or are very low expressed in the fruit valves, suggesting organ specific differences. For instance, *FRO4* has been found to reduce Cu in *A. thaliana* roots (Bernal *et al.*, 2012) and it is not expressed in *C. hirsuta* fruit valves. Importantly, *SPL7* targets in *A. thaliana* have been identified in roots, stem and seedlings (Bernal *et al.*, 2012; H. Yamasaki *et al.*, 2009; H. Zhang *et al.*, 2014), thus it is not surprising that some of these genes are not expressed in fruit.

Although in this study I have not aimed to identify new *SPL7*-regulated genes specific of the fruit valves, which might have not been identified in previous studies in other organs, I plan to use the

data from the transcriptomic profiling of wild-type and *spl7* fruit valves for this purpose. For instance, I plan to compile a list of known Cu transporters and other proteins involved in Cu homeostasis, such as in (Peñarrubia *et al.*, 2015) and examine whether these genes are differentially expressed in fruit valves. However, as mentioned in the results section, the RNA-seq comparing wild-type and *spl7* fruit valves was performed before I discovered that the *lig1* mutant phenotype was caused by loss of *SPL7* gene function. Therefore, the Cu supplied to plants in this experiment was not monitored. Although, I was able to identify changes in expression of genes already known to be regulated by *SPL7*, this dataset might not be powerful enough to identify new *SPL7*-regulated genes specific to the fruit valve. In addition, miRNA sequencing libraries were not included in the RNA-seq study that I analysed here. Therefore, expression of the *SPL7*-regulated Cu-miRNAs could not be directly assessed. For future work, I plan to design an experiment to address all of these issues. In addition to growing plants in controlled Cu conditions and preparing both miRNA and RNA-seq libraries, I plan to optimize power and specificity by including a chemically inducible *SPL7* expression system (Moore *et al.*, 2006), which I have already generated, to identify new putative *SPL7* regulated genes in the fruit valve of *C. hirsuta*. Furthermore, it will be useful to prepare and sequence degradome libraries to confirm targets of the Cu-miRNAs in *C. hirsuta* fruit valves and, in this way, identify putative new targets that are specific to fruit valves (Lin *et al.*, 2019).

Lignification of endocarp *b* SCWs starts during fruit stage 17, so I reasoned that genes involved in lignin monomer biosynthesis and localized polymerization within the cell wall would be highly expressed at this initial stage of lignification. Compared to wild type, I found that the expression of several genes encoding lignin biosynthesis enzymes was altered in the *spl7* fruit valves. On one hand, the first steps of the monolignol biosynthesis pathway are downregulated in the *spl7* mutant, suggesting a negative feedback from reduced lignification to regulate lignin biosynthesis at the transcript level. These results agree with previous studies in mutants with reduced lignification in *A. thaliana*. For example, double laccase knock-out alleles (*lac4 lac17*) have reduced lignification in stem tissues, which coincided with a reduction in expression of several genes involved in the lignin biosynthesis pathway (Berthet *et al.*, 2011). On the other hand, the

last step of monolignol biosynthesis and the monolignol polymerization step are upregulated in the *spl7* mutant. I interpret these results as a compensatory mechanism to increase lignin polymerization in the *spl7* mutant. Interestingly, several laccases are expressed at higher levels in the *spl7* mutant compared to wild type, although the difference is not statistically significant. This upregulation is an expected consequence of loss of *SPL7* function, where Cu-miRNAs that target laccases are not upregulated. However, *LAC11*, which has not been found to be targeted by Cu-miRNAs, is expressed approximately 20 times higher in *spl7* fruit valves compared to wild type and the difference in expression is statistically significant. Therefore, the upregulation of genes involved in monolignol polymerization may reflect both compensation for reduced lignification and the loss of *SPL7*-regulated Cu homeostasis.

In summary, in this chapter, I have shown that *C. hirsuta spl7* fruit have less Cu than wild type, and that Cu supplementation to growing plants can fully rescue the lignification of endocarp *b* SCWs. I hypothesize that some step of the lignin biosynthesis pathway might be affected by the reduced Cu availability in the fruit. Among the enzymes that potentially catalyse the different steps of lignin biosynthesis, one family of enzymes (laccases) are annotated as Cu binding proteins (copper ion binding, GO:0005507) (The Gene Ontology, 2019). Interestingly, laccases are Cu-requiring enzymes that perform the last step of the lignin biosynthesis pathway (monolignol oxidation). In the next chapter, I will explore the hypothesis that laccase activity might be impaired in the *spl7* fruit due to reduced Cu availability, translating to reduced lignin deposition in SCWs of endocarp *b* cells.

**Chapter 4: Role of lignin polymerizing
enzymes in localized lignin deposition of
endocarp *b* cells**

Introduction

Secondary cell walls (SCWs) are deposited and lignified asymmetrically in *C. hirsuta* endocarp *b* cells, forming a "U" shape with thin hinges at the base of the "U". This specific geometry of lignified SCWs is required for explosive seed dispersal in *C. hirsuta* (Hofhuis *et al.*, 2016). Endocarp *b* SCWs in the *spl7* mutant have less lignin relative to the wild type, and the range of seed dispersal is reduced in this mutant, indicating that lignification of endocarp *b* SCWs is necessary for wild-type seed dispersal range. In this chapter, I investigate the role of lignin polymerizing enzymes in localized lignin deposition in endocarp *b* cells of *C. hirsuta*.

Lignin is a phenolic polymer composed mainly of p-hydroxycinnamyl alcohols (monolignols) that is deposited in cell walls, conferring mechanical reinforcement and hydrophobicity (Liu *et al.*, 2018). The appearance of lignified cell walls coincided with the emergence of vascular land plants and it has been considered a key factor in their colonization of terrestrial environments (Weng & Chapple, 2010). Lignin is essential in the SCWs of vascular tissues to provide mechanical support and, thus, allow upright plant growth and water transport (Barros *et al.*, 2015). However, lignin deposition is not restricted to vascular tissues, but it occurs in different cell types and it is involved in diverse processes, e.g. seed protection, abscission of organs and in the response to biotic and abiotic stress (Barros *et al.*, 2015).

Lignin forms intricate subcellular patterns in the walls of certain lignified cell types, and localized lignin deposition is often key for cellular function. For example, in protoxylem tracheary elements (TEs) that are produced during primary growth, lignin is deposited in SCWs that follow annular or helical patterns, which are important to allow the cells to function as water conduits, resisting hydraulic pressures, while still allowing cell elongation during organ growth (Karam, 2005; Schuetz *et al.*, 2014). In the root endodermis, the Casparian strip is a lignin structure that is deposited in a median position between cells in a band-like pattern. Collective deposition of the Casparian strip in the endodermis forms a diffusion barrier in the root to control selective uptake of molecules from the soil. (Lee *et al.*, 2013). Lignin subcellular localization and monolignol

composition are often cell-specific, meaning that it is difficult to generalize about the regulation of localized lignin deposition. As a consequence of this, the regulation of localized lignin deposition remains still only partially understood (Barros *et al.*, 2015). In this chapter, I aim to gain insight into the mechanism of localized lignin deposition in endocarp *b* SCWs of *C. hirsuta* and compare the results to other lignified cell types.

The lignin biosynthesis pathway can be divided into two steps: monolignol biosynthesis and monolignol polymerization. Monolignols are synthesized from phenylalanine through the phenylpropanoid pathway in the cytosol (Bonawitz & Chapple, 2010), and they are exported to the apoplast where they are activated by oxidation. This final step of oxidation can be catalysed by enzymes that belong to two different families, peroxidases and laccases. Currently, it is accepted that lignin is polymerized in cell walls by oxidative coupling of the active oxidized monolignols (Barros *et al.*, 2015).

Directed monolignol export to lignifying cell wall domains could be a mechanism to regulate localized lignin deposition. However, studies using tagged monolignols indicated that monolignols are highly mobile in the apoplast (Schuetz *et al.*, 2014; Tobimatsu & Schuetz, 2019). Furthermore, exogenous application of monolignols, that are mobile in the apoplast, did not perturb the lignin deposition pattern in transdifferentiated protoxylem TEs (Schuetz *et al.*, 2014) or the localization of the lignified Casparian strip in the root endodermis (Naseer *et al.*, 2012). These results suggested that directed monolignol export is not required for localized lignin deposition. Alternatively, the localization of oxidative enzymes in precise cell wall domains has been proposed as a mechanism to direct localized lignin deposition. Two families of enzymes (laccases and peroxidases) can mediate the oxidation of monolignols *in vitro* and there is evidence for a role in lignification *in planta* for both enzyme families (Tobimatsu & Schuetz, 2019).

Type III peroxidases (PERs) are heme-containing glycoproteins that reduce H₂O₂ to oxidize a wide variety of substrates, including monolignols. Peroxidases have an N-terminal peptide signal, indicating that these proteins are guided through the secretory pathway (Barros *et al.*, 2015). PERs are a big group of enzymes, comprising 73 members in *A. thaliana* (Tognolli *et al.*, 2002;

Welinder *et al.*, 2002). Catalytic redundancy of this large enzyme family is likely the reason why the function of many members has not yet been described. Nevertheless, several studies have shown evidence for the involvement of certain PERs in lignification. In *A. thaliana* stems, single and double knock-out alleles of *PER2*, *PER4*, *PER25*, *PER71* and *PER72* genes showed partial reductions of total lignin content, cell wall structure defects and altered lignin monomer composition, indicating a role for these peroxidases in stem lignification (Fernandez-Perez *et al.*, 2015; Herrero *et al.*, 2013; Shigeto *et al.*, 2015; Shigeto *et al.*, 2013). *PER64* localizes to Casparian strip domains in the *A. thaliana* root endodermis and knockdown of *PER64* via amiRNA resulted in a delayed formation of the lignified Casparian strip, suggesting a role in localized lignin deposition in this cell type (Lee *et al.*, 2013). More recently, (Rojas-Murcia *et al.*, 2020) reported that, in a quintuple *per* mutant, formation of the Casparian strip is abolished, proving genetically the requirement for peroxidases in the development of the lignified Casparian strip.

Importantly, peroxidases require H_2O_2 as a co-substrate for oxidation. NADPH oxidases (in plants, Respiratory burst oxidase homologs -RBOHs-) catalyse the production of superoxide (O_2^-), which can be dismutated into H_2O_2 by enzymatic and non-enzymatic activity (Barros *et al.*, 2015). It was found that RBOHF localized to the Casparian strip domain in the *A. thaliana* root endodermis and that formation of the lignified Casparian strip was delayed in loss-of-function *rboh* mutants (Lee *et al.*, 2013), indicating that production of reactive oxygen species (ROS) is necessary for Casparian strip formation. Casparian strip membrane domain proteins (CASPs) are required for localized formation of the Casparian strip and they are necessary for localization of *PER64* (Lee *et al.*, 2013; Roppolo *et al.*, 2011). It was proposed that CASPs scaffold peroxidases and ROS-producing enzymes, such as RBOHs, in the Casparian strip domain and that localization of these enzymes guides localized lignin deposition (Lee *et al.*, 2013).

Laccases (LACs) are multi-copper glycoproteins that, unlike PERs, reduce O_2 to H_2O in order to oxidize several substrates, among them monolignols (Barros *et al.*, 2015). Laccases bind four copper atoms that are arranged in sites with distinct spectroscopic characteristics. One Cu ion is

located in site T₁ and the other three Cu ions are located in a cluster (one T₂ site and two T₃ sites). The Cu ion in T₁ participates in the oxidation of the substrate and the three Cu ions in the cluster participate in the reduction of O₂ to H₂O (Wang *et al.*, 2015). Laccases have an N-terminal peptide signal, indicating that these proteins are guided through the secretory pathway (Barros *et al.*, 2015). 17 genes that encode laccases have been identified in the genome of *A. thaliana* (McCaig *et al.*, 2005). Direct genetic evidence for the role of LACs in lignification was found in the double mutant *lac4 lac17* in *A. thaliana*, which exhibited collapsed xylem vessels, reduced lignin content and altered monolignol composition in mature stems (Berthet *et al.*, 2011). This was further confirmed in a triple knock-out allele, *lac4 lac11 lac7*, which showed a further reduction in lignin content in the stem and growth arrest (Zhao *et al.*, 2013). In *A. thaliana*, *lac15* mutant showed a 30 % decrease in seed lignin content, indicating that LAC15 is required for lignification in seeds (Liang *et al.*, 2006).

Interestingly, in the triple laccase mutant *lac4 lac11 lac17*, Casparian strip lignification is not affected, suggesting that divergent mechanisms of lignification operate in different cell types and indicating that the activity of laccases and peroxidases is not redundant (Zhao *et al.*, 2013). *LAC4*, *LAC11* and *LAC17* are not expressed or are expressed at very low levels in the root endodermis (Rojas-Murcia *et al.*, 2020). Nevertheless, loss of function of 9 endodermis-expressed laccases (*lac1 lac3 lac5 lac7 lac8 lac9 lac12 lac13 lac16*), several of which localize to the site of Casparian strip formation, had no detectable effect on Casparian strip formation or lignification, which suggested that laccases are not required for Casparian strip lignification (Rojas-Murcia *et al.*, 2020).

Although, some studies point toward a cell-specific requirement of laccases versus peroxidases, it was reported that knocking out both PERs and LACs resulted in defects in cell walls of xylem TEs (Herrero *et al.*, 2013; Zhao *et al.*, 2013). To explain the requirement of both families of enzymes for lignification of certain cell types, it has been proposed that laccases and peroxidases act sequentially in cell wall lignification (Barros *et al.*, 2015). This hypothesis was supported by the observation that scavenging of H₂O₂, required for peroxidase activity, inhibited the release of

lignin in cell cultures of Norway spruce, while an enrichment of oligolignols was found. The interpretation of the authors is that, H₂O₂-independent laccases initiate the generation of oligolignols, whereas peroxidases continue polymerization of lignin from these compounds (Laitinen *et al.*, 2017).

Alternatively, it has been proposed that the activity of laccases versus peroxidases might be spatially regulated in the cell wall. In agreement with this model, in stem tissue of *A. thaliana*, it was found that LAC4 localizes to thick SCWs of fibres, whereas PER64 localizes to the middle lamella and cell corners in between fibre cells (Chou *et al.*, 2018). Furthermore, Fluorescence Recovery After Photobleaching (FRAP) experiments showed that LAC4 was immobile in SCWs of fibres but mobile in primary cell walls, suggesting that this anchoring in the SCW underpins lignin deposition (Chou *et al.*, 2018). In a very recent study, the localization of several LACs and PERs was assessed at different stages and cell types during *A. thaliana* stem maturation (Hoffmann *et al.*, 2020). It was found that PERs and LACs co-localize in cell wall domains and that localization of these oxidative enzymes is spatially and temporarily regulated. Furthermore, it was found that even though some PERs localize to non-lignified cell walls in the stem, ROS production is restricted to lignifying cells. These results suggest that localized ROS production is an additional mechanism for tissue-scale spatial regulation of lignification (Hoffmann *et al.*, 2020).

In summary, previous studies addressing the mechanisms of lignification in different cell types point toward diverse regulation. On one hand, different cell types seem to require either laccases or peroxidases for lignification of their cell walls (Rojas-Murcia *et al.*, 2020), whereas other cell types seem to require the activity of both families (Herrero *et al.*, 2013; Zhao *et al.*, 2013). Although in stem tissue of *A. thaliana*, PERs and LACs co-localize in cell wall domains at certain developmental stages, studies with knock-out alleles of either PERs or LACs indicate non-redundant activity of these enzyme families in lignification of stem tissue (Herrero *et al.*, 2013; Zhao *et al.*, 2013). As mentioned previously, peroxidases and laccases are two large families of

enzymes, with catalytic redundancy, which makes it particularly challenging to uncover individual gene functions (Barros *et al.*, 2015).

In this chapter, I investigate the mechanism of localized lignin deposition in SCWs of endocarp *b* cells of *C. hirsuta*. I focus on the last step of the lignin biosynthesis pathway as a candidate mechanism for localized lignin deposition. Furthermore, I explore whether laccases or peroxidases contribute to lignification of endocarp *b* SCWs, or whether both are required. Importantly, endocarp *b* SCWs of the *spl7* mutant have less lignin relative to wild type.

Results

1. Laccases are highly expressed in *C. hirsuta* fruit valves at the beginning of endocarp *b* lignification

In the previous chapter, I found that *spl7-1* fruit have a reduced Cu concentration compared to wild type, and that transgenic expression of *SPL7* fully complements the Cu concentration to wild-type levels in the mutant fruit. Furthermore, I showed that Cu supplementation can fully rescue lignification of SCWs of endocarp *b* cells in the *spl7-1* mutant. Reduced Cu availability in *spl7-1* fruit may affect lignin biosynthesis at certain enzymatic steps. Interestingly, laccases are lignin polymerizing enzymes that require Cu for their activity, since they bind four Cu atoms necessary for the oxidation of substrates. Therefore, I hypothesize that a reduction in laccase activity due to reduced Cu availability in *spl7-1* fruit, is responsible for the reduced lignification observed in endocarp *b* SCWs of the *spl7* mutant.

To test this hypothesis, first, I examined the expression of laccase gene family members in fruit valves of wild type and *spl7-1* mutant. For this purpose, I made use of the RNA-seq data from fruit valves at stage 17 described in the previous chapter. In *A. thaliana*, 17 laccase genes have been identified (McCaig *et al.*, 2005). Analysis by reciprocal best BLAST hit, indicated that orthologs of at least 15 LACs are present in the genome of *C. hirsuta*. Three laccases (*LAC3*, *LAC7* and *LAC16*) are not expressed in wild-type or *spl7-1* fruit valves (normalized counts = 0) (Figure 4.1). Six other laccases (*LAC1*, *LAC5*, *LAC8*, *LAC10*, *LAC12* and *LAC13*) have low expression in fruit valves of wild type and *spl7-1* mutant (mean of normalized counts < 5) (Figure 4.1). *LAC2*, *LAC4*, *LAC6*, *LAC11*, *LAC15* and *LAC17* have higher expression in *C. hirsuta* fruit valves (mean of normalized counts > 5) (Figure 4.1). *LAC4* and *LAC17* are the most highly expressed laccases in fruit valves of both wild type and *spl7-1* mutant. *LAC11* is upregulated in fruit valves of *spl7-1* mutant relative to wild type (log₂ fold change of 4.1) and the difference in expression of this gene is statistically significant (P-value among the 10 lowest from the RNA-seq analysis) (Figure 4.1 and Table 3.2). These results show that laccases are expressed in fruit

valves at stage 17, when lignification of SCWs in endocarp *b* cells is starting, suggesting a role in lignification. Also, these results show large differences in expression among different laccase members in wild-type valves, suggesting that only a subset of laccases might contribute to fruit valve lignification.

Peroxidases are another family of enzymes that can polymerize lignin monomers. These enzymes are heme-containing proteins and they do not require Cu to oxidize monolignols. To explore whether these enzymes might contribute to lignification of the endocarp *b* SCWs of *C. hirsuta*, I examined expression of peroxidases using data from the RNA-seq experiment of wild-type and *spl7-1* fruit valves. In *A. thaliana*, 73 genes encoding peroxidases have been identified (Tognolli *et al.*, 2002). Analysis by reciprocal best BLAST hit, indicated that at least 62 orthologs are present in the genome of *C. hirsuta*. I collected expression data of these orthologs and I found that 31 peroxidases were not expressed in fruit valves (normalized counts = 0 in both genotypes). 22 peroxidases have low expression in fruit valves of wild type and *spl7-1* mutant (mean of normalized counts < 5) (Figure 4.1). Finally, 9 peroxidases show expression in fruit valves (mean of normalized counts > 5) (Figure 4.1). Among these PERs, *PER42* and *PER66* are the highest expressed peroxidases in fruit valves. Furthermore, *PER49* is highly upregulated in fruit valves of *spl7-1* mutant relative to wild type (log₂ fold change of 3.74) and the difference in expression of this gene is statistically significant (P-value among the 10 lowest from the RNA-seq analysis).

Taken together, my results indicate that several laccases and peroxidases are expressed in fruit valves, suggesting that they might contribute to fruit valve lignification. Only 14.5 % of the peroxidases examined have expression levels above 5 normalized counts, whereas a higher proportion of laccases (40 %) have expression levels above 5 normalized counts. These results might indicate a larger contribution of laccases in fruit valve lignification. I consider that the highly expressed genes, *LAC4* and *LAC17*, are good candidates to contribute to lignification of endocarp *b* cells in the fruit valves of *C. hirsuta*. Also, the highly expressed genes *PER42* and *PER66*, could contribute to lignification of endocarp *b* cells in the fruit valves of *C. hirsuta*. Interestingly, *LAC11* and *PER49* are upregulated in *spl7-1* fruit valves. These results might reflect

a compensatory mechanism to increase lignin polymerization in the *spl7-1* mutant. I decided to focus on genes that are highly expressed or that are upregulated in the *spl7-1* fruit valves to investigate lignin polymerization of endocarp *b* SCWs.

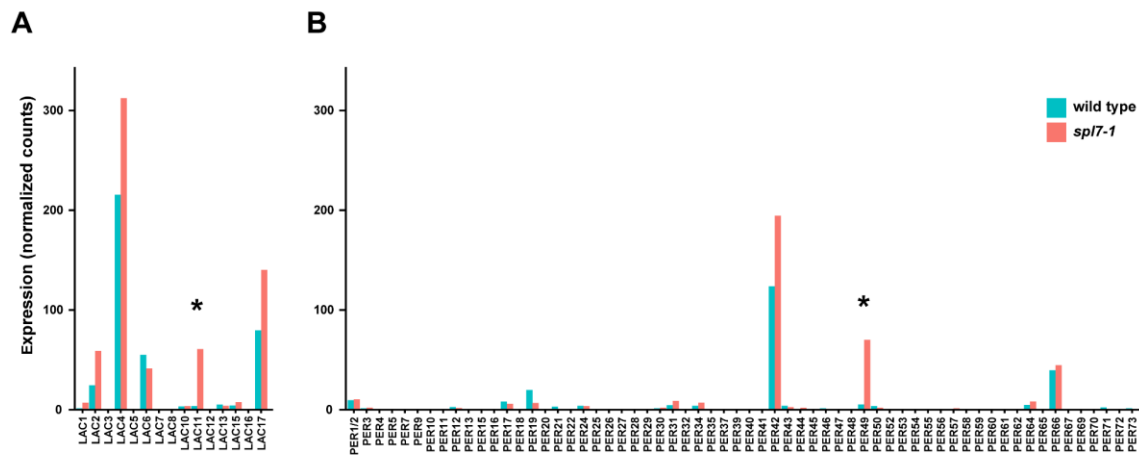


Figure 4.1: Expression of laccases and peroxidases in *C. hirsuta* wild-type and *spl7-1* fruit valves. Gene expression of laccases and peroxidases in fruit valves of wild-type and *spl7-1* fruit valves from RNA-seq data. Barplot of normalized counts of laccases (A) and peroxidases (B). Asterisks indicate statistically significant differences in gene expression between genotypes (Adjusted P-value < 0.05).

2. *LAC4*, *LAC11* and *LAC17* are expressed in endocarp *b* cells of *C. hirsuta*

Several laccases were found to be highly expressed in *C. hirsuta* fruit valves. *LAC4* and *LAC17* were the most highly expressed laccases, suggesting a role in lignification of SCWs in fruit valves. *LAC11* was found to be strongly upregulated in fruit valves of the *spl7-1* mutant. Although I found that these laccases are expressed in fruit valves of *C. hirsuta*, there is no available information for gene expression at a cell-type specific scale. Therefore, to investigate whether laccases that are highly expressed in fruit valves, are specifically expressed in the endocarp *b* layer, I generated transcriptional reporters for *LAC4*, *LAC11* and *LAC17* and transformed *C. hirsuta* wild-type plants with these constructs. To generate the transcriptional reporters, I fused the promoters of these genes with GFP-NLS (GFP containing a nuclear localization signal). I used 3696 bp of promoter sequence for *pLAC4::GFP-NLS*, 3252 bp of promoter sequence for *pLAC11::GFP-*

NLS, and 2885 bp of promoter sequence for *pLAC17::GFP-NLS*. The resulting constructs were introduced into *C. hirsuta* wild-type plants via Agro-mediated transformation.

LAC4, *LAC11* and *LAC17* are highly expressed in endocarp *b* cells at stage 17 ab, when SCWs of these cells are lignified (Figure 4.2 A-D). These three laccases are also expressed in the lignified layer of the valve margin (Figure 4.2 A-D). Expression of *LAC4* is not detectable in the non-lignified exocarp of the fruit valves (Figure 4.2 E). These results indicate that laccases are expressed in the endocarp *b* layer, which suggests a possible role in lignification of SCWs in these cells.

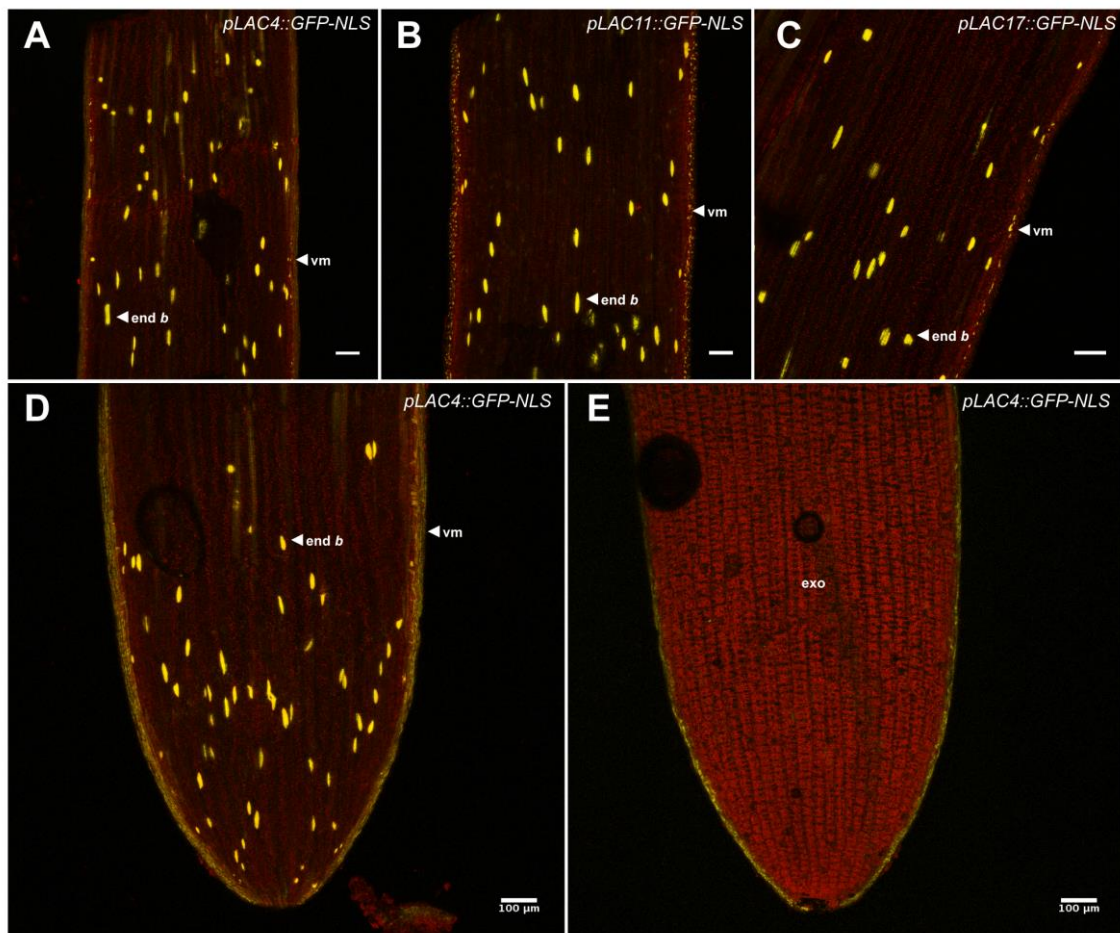


Figure 4.2. *LAC4*, *LAC11* and *LAC17* are expressed in the endocarp *b* layer and lignified valve margin in *C. hirsuta* fruit valves. (A-E) Confocal micrograph showing expression pattern of three laccases in fruit valves. Valves were peeled from fruit at stage 17 a/b and placed on a slide with the inner side (endocarp layers) facing the cover slip (A-D) or with the outer (exocarp) layer facing the cover slip (E). Background (red): autofluorescence signal in chlorophyll region. (A, D and E) *pLAC4::GFP-NLS*, (B) *pLAC11::GFP-*

NLS and (C) *pLAC17::GFP-NLS*. end *b*: endocarp *b*, vm: valve margin, exo: exocarp. Background fluorescence: chlorophyll. Scale bar: 100 μ m.

3. LACCASES co-localize precisely with lignin deposits in SCWs of endocarp *b* cells

I found that *LAC4*, *LAC11* and *LAC17* genes are expressed in endocarp *b* cells of the fruit valve. SCWs are deposited and lignified asymmetrically in endocarp *b* cells, forming a “U” shape with thin hinges at the base of the “U”. If these laccase enzymes contribute to lignin polymerization of endocarp *b* SCWs, I would expect that they accumulate precisely in the cell wall domains where lignin is deposited.

To test this hypothesis, I generated translational reporters of these three laccases. I fused the proteins with mCherry at the C-terminus and used their native promoters to drive expression (*pLAC4::LAC4:mCherry*, *pLAC11::LAC11:mCherry* and *pLAC17::LAC17:mCherry*). I introduced the constructs into *C. hirsuta* wild-type plants via Agro-transformation and analysed localization of the tagged proteins in transverse sections of fruit at stage 17 a/b.

I found that all three laccases (*LAC4*, *LAC11* and *LAC17*) localize to lignified cell walls in the fruit (Figure 4.3). *LAC4*-mCherry and *LAC17*-mCherry localize to lignified cell walls in the replum, valve margin, vascular bundles of the valve and in the endocarp *b* layer (Figure 4.3). *LAC11*-mCherry localization is specific to cell walls in the fruit valve, with the exception of a few cell walls in the centre of the lignified replum. In the fruit valve, it localizes to the endocarp *b*, valve margin and vascular bundles (Figure 4.3). I found that the three laccases (*LAC4*, *LAC11* and *LAC17*) precisely co-localize with lignin deposits in SCWs of endocarp *b* cells (Figure 4.4). This precise co-localization of the tagged proteins with lignin deposits, suggests that laccases might direct localized lignin deposition in the endocarp *b* SCWs.

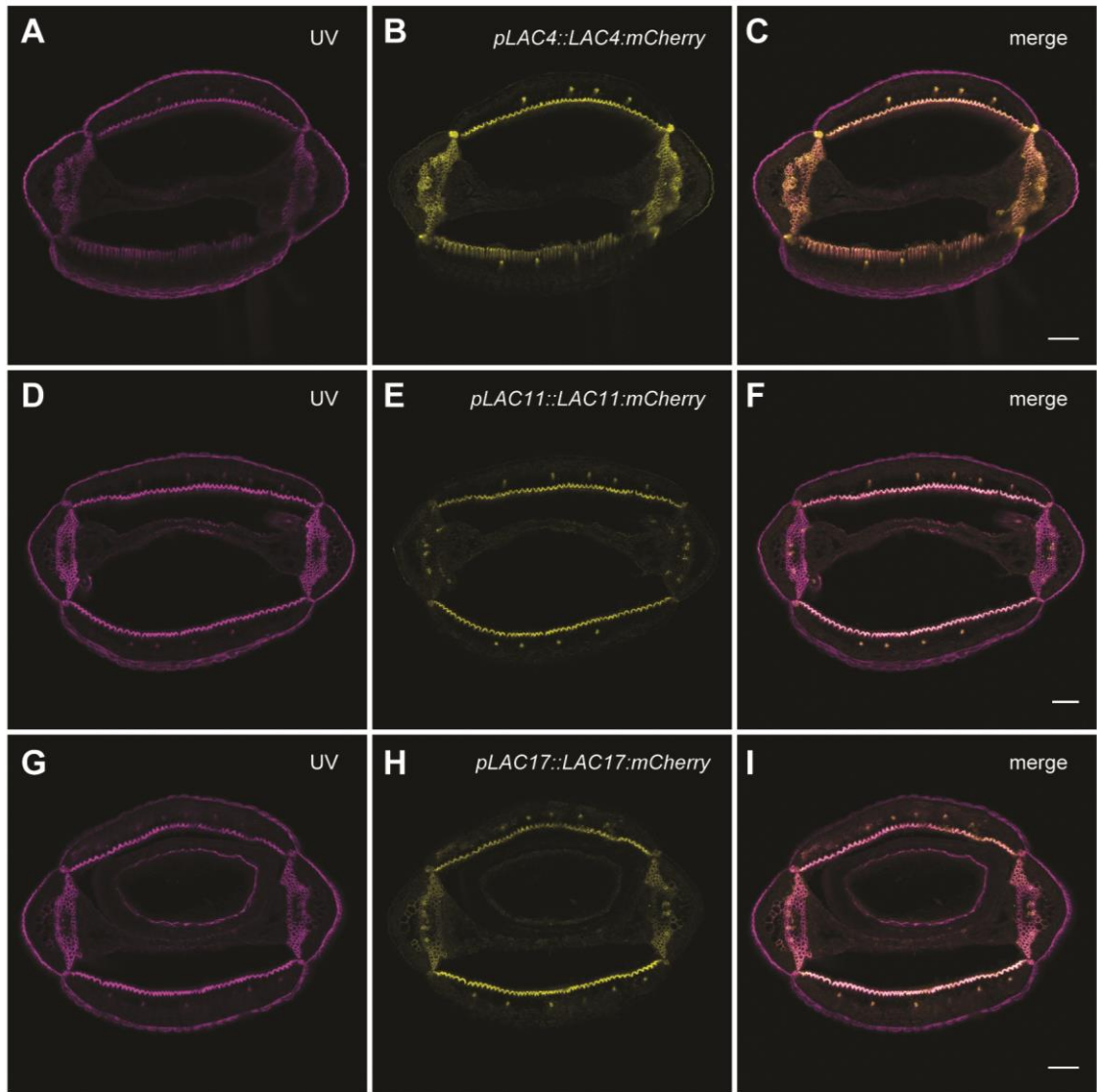


Figure 4.3: LAC4, LAC11 and LAC17 localize to lignified SCWs in the fruit. Confocal micrographs showing localization of laccases in fruit cross sections at stage 17 a/b from plants carrying LAC-mCherry fusions driven by their own promoter. (A, D and G) Autofluorescence under UV 405 laser. (B, E and H) mCherry signal from LAC:mCherry fusions. (C, F and I) Merge images. Scale bars: 100 μ m.

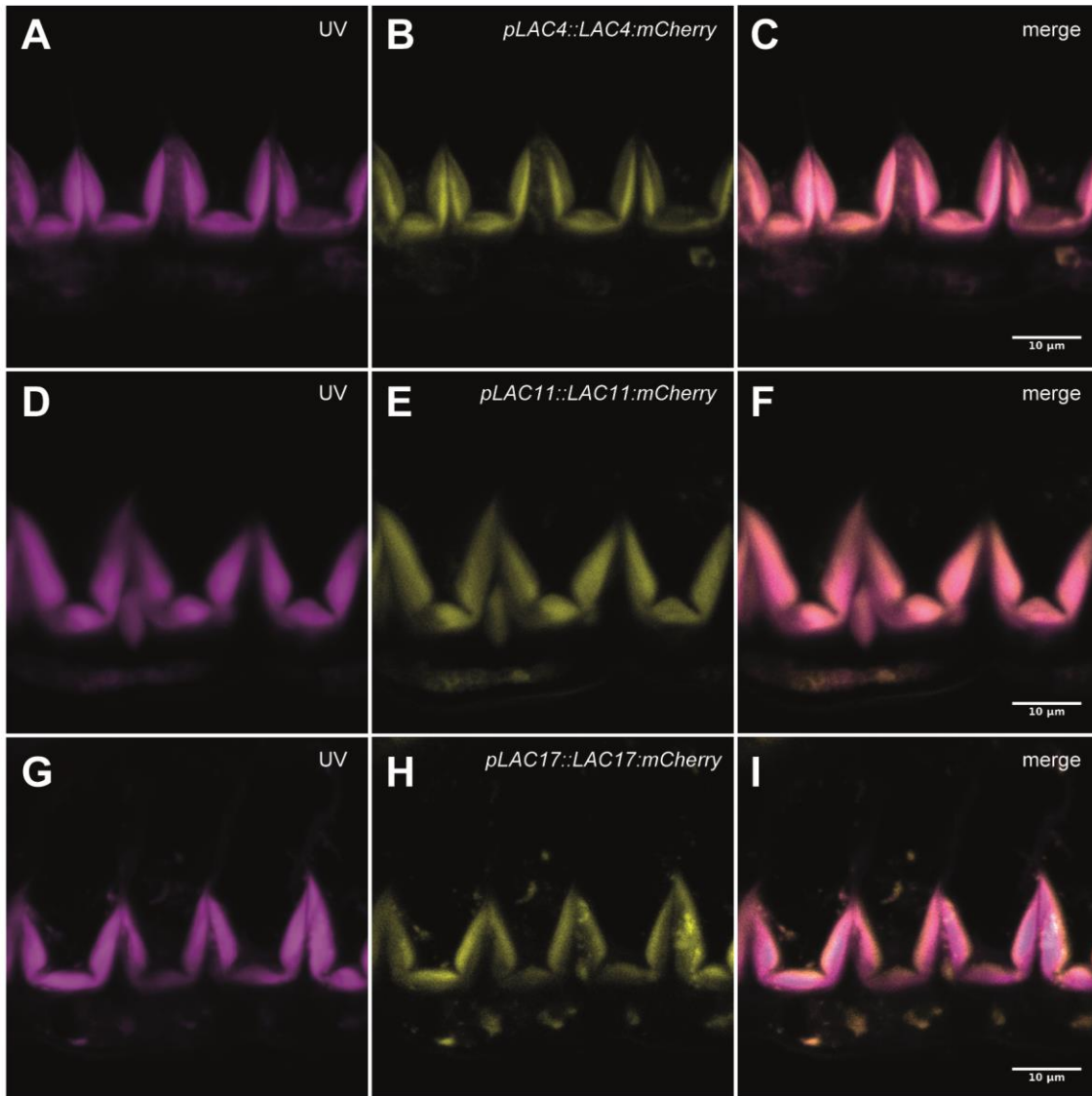


Figure 4.4: LAC4, LAC11 and LAC17 localize to lignin deposits in endocarp *b*. Confocal micrographs showing localization of laccases in endocarp *b* cells in *C. hirsuta* stage 17 a/b fruit cross sections. (A, D and G) UV405 autofluorescence signal. (B, E and H) mCherry signal from LAC:mCherry fusions. (C, F and I) Merge images. Scale bar: 10 μm .

4. LAC11 localizes to initiating asymmetric lignin deposits in SCWs of endocarp *b* cells

Three laccases co-localize with lignin deposits in SCWs of endocarp *b* cells. Localization of the translational LAC:mCherry fusions was assessed at stage 17a/b, when SCWs were already considerably thickened and lignified (several μm thickness). Thickening and lignification of SCWs in *C. hirsuta* endocarp *b* cells is progressive, starting at stage 17 (Hofhuis *et al.*, 2016). I reasoned that, if these enzymes contribute to localized lignin deposition in endocarp *b* SCWs, they would co-localize with lignin deposits from the initial stages of SCW lignification.

To test this hypothesis, I assessed localization of the LAC11:mCherry fusion in cross sections of fruit at stage 17, which corresponds to the initiation of lignin deposition in SCWs of endocarp *b* cells. I found that LAC11:mCherry co-localizes to the very initial lignin deposits in SCWs of endocarp *b* cells, when lignin autofluorescence is detectable only in a very thin layer (Figure 4.5). LAC11:mCherry shows a polar localization pattern on the inner cell face at this initial stage, and it co-localizes with lignin deposits throughout the subsequent thickening and lignification of SCWs. Co-localization of lignin and LAC11:mCherry signals is continuous throughout all stages analysed (Figure 4.5). These results suggest that laccases pre-pattern the localized lignin deposition in the endocarp *b* layer, and direct localized lignin deposition throughout the thickening of SCWs.

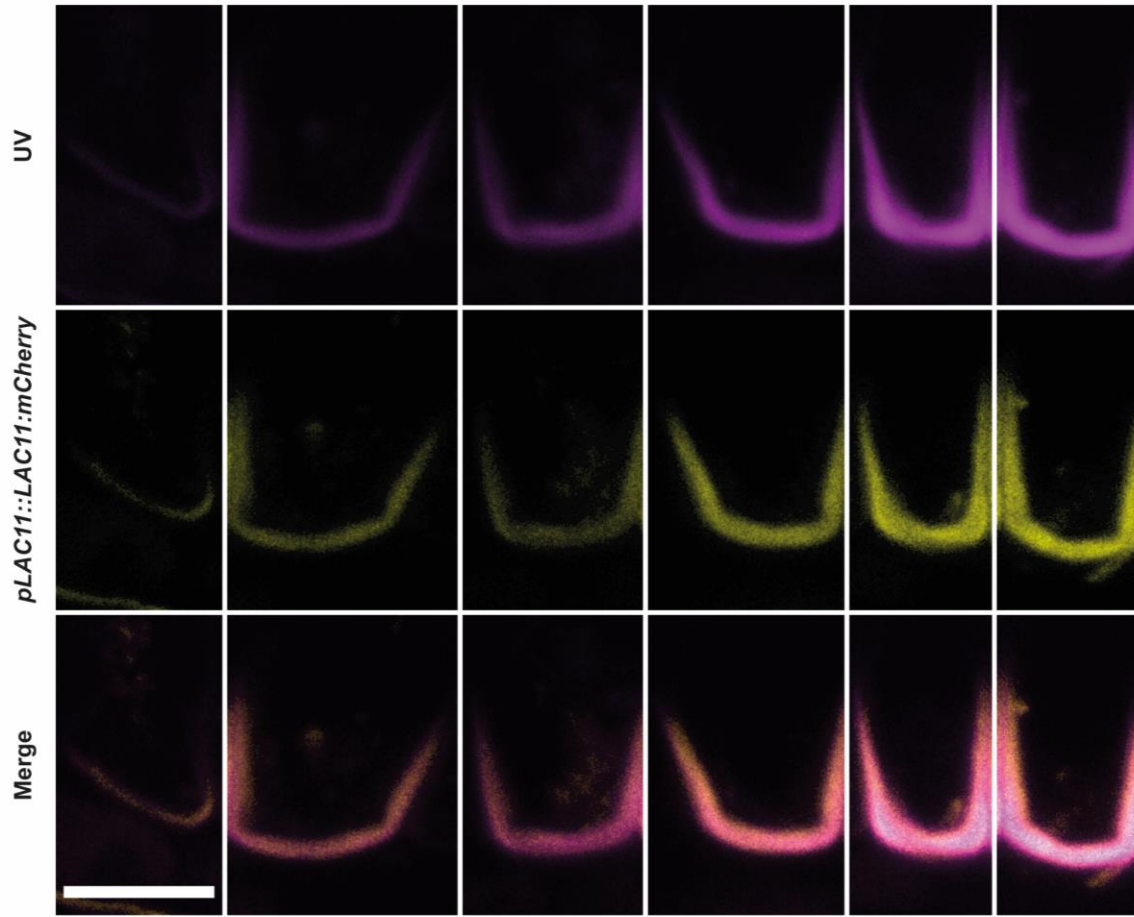


Figure 4.5: LAC11 co-localizes with the earliest detection of lignin in SCWs of endocarp *b* cells.

Localization pattern of *pLAC11::LAC11:mCherry* in endocarp *b* cells of *C. hirsuta* fruit at stage 17. Confocal micrographs show UV405 autofluorescence (top panel), LAC11:mCherry signal (middle panel) and merge images (bottom panel). Images are crops of individual endocarp *b* cells from several micrographs. Images were obtained from cross section fixed and cleared (ClearSee) as described in methods section. Scale bar: 10 μm .

5. *C. hirsuta* laccases localize to symmetric lignin deposits in endocarp *b* SCWs of *A. thaliana*

In *C. hirsuta*, SCWs are deposited and lignified asymmetrically in endocarp *b* cells, forming a “U” shape pattern with thin hinges. This particular geometry of lignified SCWs in endocarp *b* cells is required for explosive seed dispersal (Hofhuis *et al.*, 2016). Importantly, explosive seed dispersal evolved in the Cardamine genus, and all species examined in this group showed asymmetric SCW deposition with a hinged geometry (Hofhuis *et al.*, 2016). *A. thaliana* is a close relative of *C. hirsuta* and seed dispersal is non-explosive in this species. In *A. thaliana*, SCWs are deposited and lignified symmetrically in every cell wall in endocarp *b* cells. In a wide sample of Brassicaceae species, it was found that those species with non-explosive seed dispersal had symmetric SCW deposition in endocarp *b* cells, whereas those species with explosive seed dispersal (belonging to the genus Cardamine) had asymmetric SCW deposition. These results indicated that this change in SCW pattern was strictly associated with the gain of explosive seed dispersal in Cardamine.

I found that three laccases precisely co-localize with asymmetric lignin deposits in SCWs in *C. hirsuta* endocarp *b* cells, suggesting that laccases might direct localized lignin deposition in these cells. I reasoned that, if laccases contributed to the divergent pattern of lignin deposition found in explosive vs non-explosive species, then laccases would localize differently between *C. hirsuta* and *A. thaliana*.

To investigate whether asymmetrically localized *C. hirsuta* laccases localize differently in *A. thaliana*, and to investigate whether the information for asymmetric localization is encoded in the laccase gene sequences (*cis*), or due to a change in the species-specific regulatory environment (*trans*), I performed an interspecies gene transfer experiment (Nikolov & Tsiantis, 2015). I introduced three *C. hirsuta* LAC:mCherry fusions under the control of their own *C. hirsuta* promoter into *A. thaliana* plants and examined localization in endocarp *b* SCWs. The transgenes introduced in *A. thaliana* are: *pChLAC4::ChLAC4:mCherry*, *pChLAC11::ChLAC11:mCherry* and *pChLAC17::ChLAC17:mCherry*.

I found that ChLAC4:mCherry and ChLAC17:mCherry fusions are expressed in the fruit valve of *A. thaliana* (Figure 4.6). These results indicate that the *C. hirsuta* promoter sequences of *LAC4* and *LAC17* are active in *A. thaliana* fruit valves. I could not detect signal from ChLAC11:mCherry, suggesting that the *C. hirsuta* promoter sequence of *LAC11* might not be active in *A. thaliana* fruit valves, or that the transgene is silenced in the lines analysed. For example, the authors of a study in *A. thaliana* reported that they were not able to examine lines carrying the construct *pAtLAC11::AtLAC11:mCherry* due to strong silencing of the transgene (Hoffmann *et al.*, 2020).

ChLAC4:mCherry and ChLAC17:mCherry fusions co-localize with symmetric lignin deposits in SCWs of endocarp *b* cells in *A. thaliana* (Figure 4.6). These results indicate that *C. hirsuta* laccases are secreted into the apoplast and they localize to SCWs in *A. thaliana*. However, these *C. hirsuta* laccases localize according to the symmetric pattern of SCW deposition in *A. thaliana*. This result indicates that the positional cue for the asymmetric localization of *C. hirsuta* laccases in endocarp *b* cells is not *cis*-encoded, but rather depends on the species-specific regulatory environment.

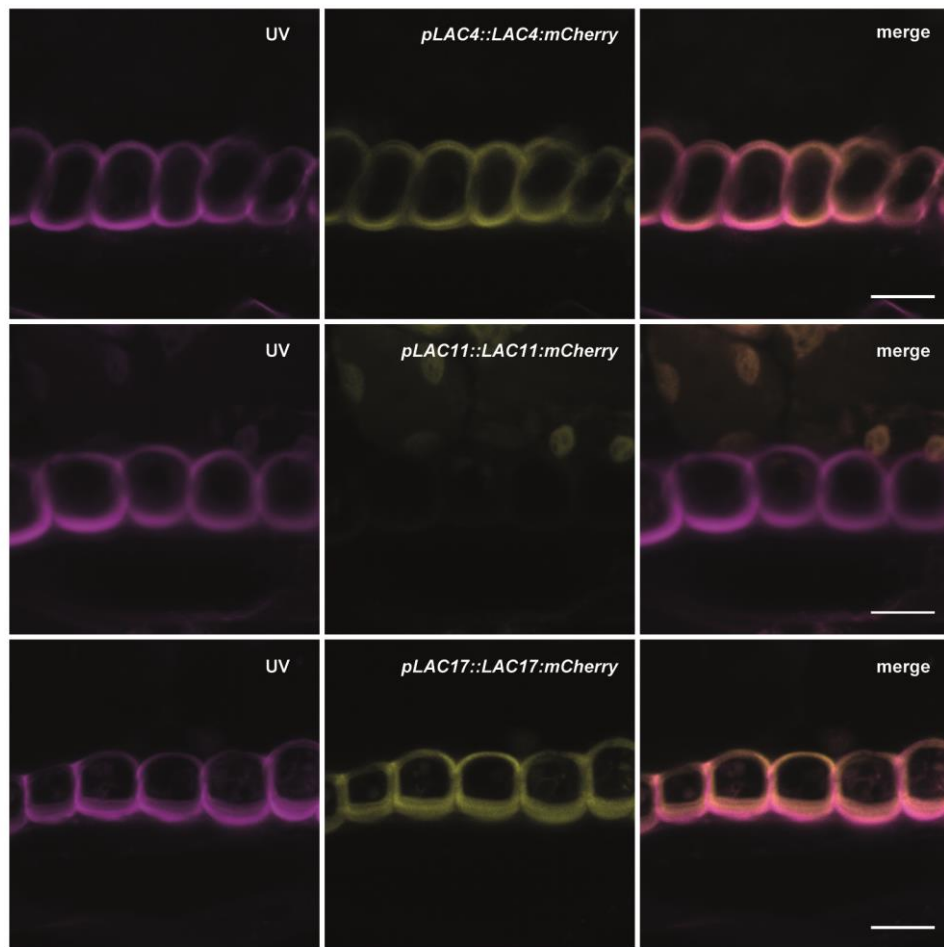


Figure 4.6: *C. hirsuta* laccases co-localize with symmetric lignin deposits in endocarp *b* SCWs of *A. thaliana*. Localization pattern of *C. hirsuta* laccases in endocarp *b* cells of *A. thaliana* mature fruit. Confocal micrographs show UV405 autofluorescence (left), LAC:mCherry signal (middle) and merge (right). Images were obtained from cross section fixed and cleared (ClearSee) as described in methods section. Scale bars: 10 μ m.

6. Laccase CRISPR/Cas9 knock-out alleles have reduced lignification in SCWs of endocarp *b* cells

I identified three laccases (*LAC4*, *LAC11* and *LAC17*) that are expressed in endocarp *b* cells and I found that these three laccases co-localize with lignin deposits in SCWs of endocarp *b* cells, suggesting a role in directing localized lignin deposition. To test whether these laccases are indeed required for lignification of SCWs of endocarp *b* cells, I generated knock-out alleles of *LAC4*, *LAC11* and *LAC17* by CRISPR/Cas9 mutagenesis in *C. hirsuta* (Ox accession).

I designed sgRNAs to target exons of the three laccases (two sgRNAs to target each laccase) with the aim of generating a triple laccase mutant as well as single and double mutants of the three laccases. I cloned a multiple sgRNA construct containing the six sgRNAs (sequences in Table 6.4 of methods section) together with the Cas9 gene, driven by an egg cell-specific promoter. I transformed wild-type *C. hirsuta* plants with this construct (for cloning details see Materials and methods). By including all sgRNAs in one construct I had the potential to generate edits in all three laccases in a single individual plant. Nevertheless, I expected differences in the efficiency of the different sgRNAs to recruit Cas9 and drive DNA cleavage, which meant that I should also obtain single and double mutants in different lines. I used a seed coat fluorescent marker to select for transgene insertion in the T₁ generation and its absence in the T₂ generation.

I sowed 40 T₁ seeds that displayed a fluorescent seed coat and I genotyped plants grown from these seeds by PCR amplification and sequencing of the six sgRNA binding regions. I used TIDE software to identify DNA edits and to estimate zygosity of the edits in the T₁ generation (Brinkman *et al.*, 2014). I found that 7 independent T₁ plants had DNA edits in at least one laccase gene sequence. The results of the T₁ screening are summarized in Table 4.1. Out of the 7 total plants with edits, 4 T₁ plants had edits in only one laccase, whereas, T₁-15 and T₁-27 had edits in two laccase genes. I found that T₁-23 had edits in all three laccase genes.

	LAC4		LAC11		LAC17		Transgene insertion number
	sgRNA1	sgRNA2	sgRNA1	sgRNA2	sgRNA1	sgRNA2	
T ₁ -14				-1 / 0			4
T ₁ -15		-1 / +1		-1 / -3			2
T ₁ -22		-4 / 0					6
T ₁ -23		-1 / 0		-1 / 0	+1 / +1		13
T ₁ -24		-1 / +2					3 to 4
T ₁ -27				-6 / 0	+1 / 0		2
T ₁ -30		-1 / 0					1

Table 4.1: Overview of DNA edits identified in T₁ plants of CRISPR/Cas9 lines targeting *LAC4*, *LAC11* and *LAC17*. TIDE analysis was used to identify edits in sgRNA binding regions of *LAC4*, *LAC11* and *LAC17*. The nucleotide insertions and deletions identified are indicated. Zeros indicate wild-type genotype. Transgene insertion number was estimated in these plants (iDNA genetics).

In the T₁-23 plant, I identified a single nucleotide deletion in the *LAC4* sgRNA2 binding region (deletion of an A at genomic position 1333 from start codon) present only in one copy of the gene. Therefore, this allele is heterozygous. This single nucleotide insertion in *LAC4* sgRNA1 binding region results in a premature stop codon, which generates a 212 amino acid truncated protein (346 amino acid-short peptide) (Figure 4.7 A and B). This truncated protein lacks several amino acids that coordinate the Cu ions that are essential for the redox activity of laccases. Therefore, I expect that the mutation is a knock-out allele of *LAC4*.

In the same plant (T₁-23), I identified a single nucleotide deletion in *LAC11* sgRNA2 binding region (deletion of a C at position 1162) present only in one copy of the gene. Therefore, this allele is heterozygous. The edit was identified as a single nucleotide insertion using TIDE software, however, visual inspection of the sequencing chromatogram indicates a single nucleotide deletion. The single nucleotide insertion identified in *LAC11* sgRNA2 binding region results in a premature stop codon, which generates a 244 amino acid truncated protein (317 amino acid-short peptide) (Figure 4.7 C and D). Similar, to the *lac4* mutant allele, I expect that the mutation in *LAC11* is a knock-out allele since the truncated protein would lack several amino acids that coordinate the Cu ions.

In the same plant (T₁-23), I identified a single nucleotide insertion in the *LAC17* sgRNA1 binding region (a T insertion between genomic positions 431 and 432). The sequencing and TIDE analysis indicate that the edit is present in both copies of the gene (biallelic for 1 nucleotide insertion) and therefore it is equivalent to a homozygous edit. This single nucleotide insertion in the *LAC17* sgRNA1 binding region results in a premature stop codon, which generates a 92 amino acid truncated protein (478 amino acid-short peptide) (Figure 4.7 E and F). I expect that the mutation in *LAC17* is a knock-out allele since the truncated protein would lack several amino acids coordinating the Cu ions.

In summary, in line T₁-23, I found edits in all three laccases that lead to premature stop codons. In *LAC17* the edit identified is present in both copies (biallelic for the same mutation). In *LAC4* and *LAC11*, edits are present in one copy, whereas the other copy shows the wild-type genotype.

Thus, by selfing this single plant, it is possible to derive a homozygous triple mutant of laccases 4, 11 and 17 as well as a single and two double mutant combinations. Therefore, I decided to focus my analyses on this line (T₁-23).

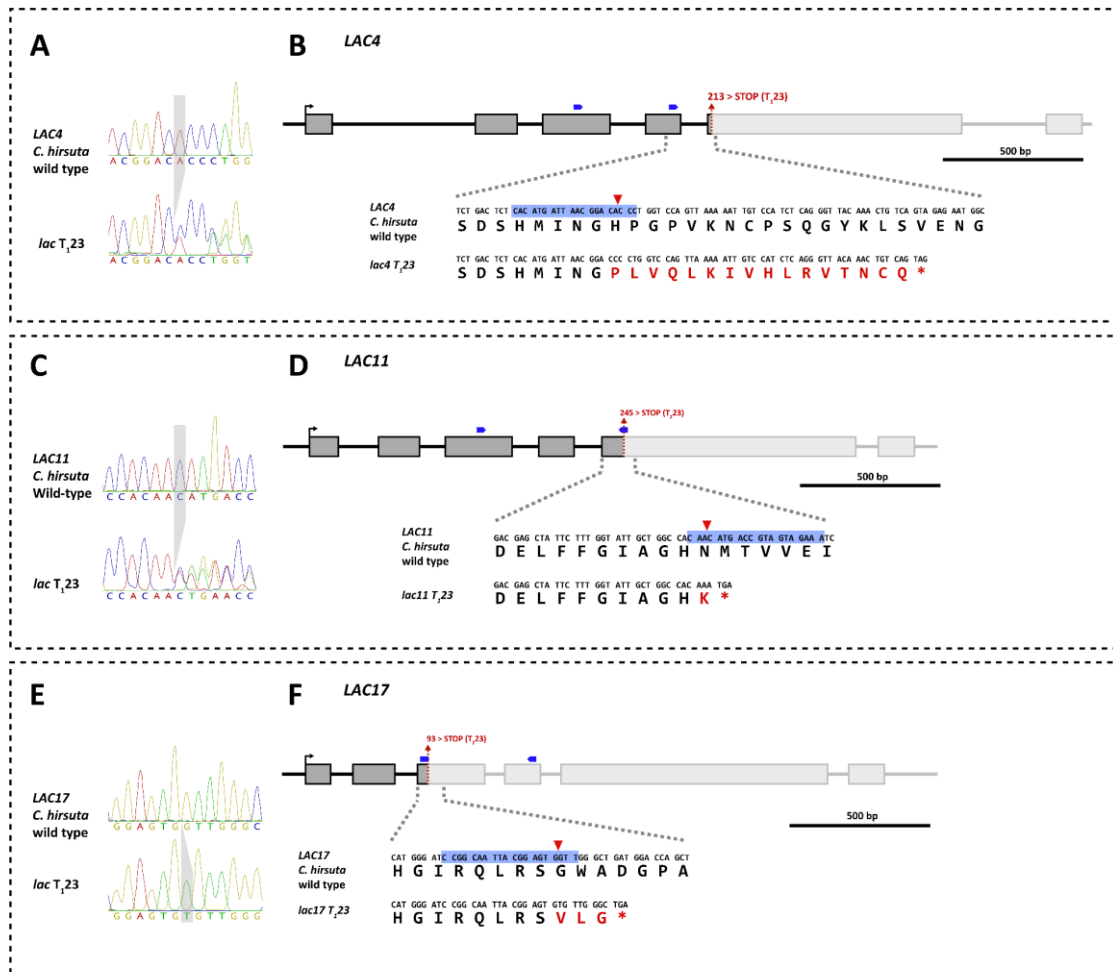


Figure 4.7: Generation of knock-out alleles of three laccases in *C. hirsuta* using CRISPR/Cas9. Edits identified in plant T₁23. (A, C and E) Chromatograms of sgRNA binding regions from wild type and *lac* T₁23. Nucleotide changes are highlighted in gray. (B, D and F) Gene models of *LAC4*, *LAC11* and *LAC17*. DNA and amino acid sequences of wild type and *lac* T₁23 are shown. sgRNA binding sites are indicated in blue in the DNA sequences and in the gene models. Red arrowheads indicate expected position of Cas9 cleavage. Premature stop codon positions identified are indicated. Red font indicates change in the amino acid sequence.

To identify different combinations of stable laccase mutants, I screened T₂-23 seeds that segregated for the Cas9 transgene insertion and identified non-fluorescent seeds, indicating that they were transgene-free. Additionally, I genotyped the T₂ plants for Cas9 by PCR amplification to confirm the absence of transgene insertion. When I grew *lac* mutant T₂-23 plants, I observed growth arrest after the appearance of one or two small leaves in some of the plants (Figure 4.8

A). The growth of other T₂-23 plants was not different from wild type. Growth arrest at a very early stage of plant development was also found in the triple mutant *lac4 lac11 lac17* in *A. thaliana* (Zhao *et al.*, 2013). Although the phenotype I observed is very similar to the phenotype reported in the mutant *lac4 lac11 lac17* in *A. thaliana*, I could not genotype the plants with growth arrest in this experiment due to the small size of the plants. Furthermore, plants that showed growth arrest didn't produce fruit and, thus, I could not assess lignification of the endocarp *b* layer. The mutant *lac4 lac11 lac17* in *A. thaliana* produced a stem that did not grow more than approximately 1 cm, and only occasionally produced fruit, which were much smaller than the wild type (Zhao *et al.*, 2013). I decided to sow *lac* mutant T₂-23 seeds in tissue culture boxes containing MS media with the aim of reducing stress on the putative triple mutant plants and favouring a minimum of growth to assess lignification. In these boxes, I identified a plant with mutations in all three laccases in homozygosity (*lac4 lac11 lac17*). This plant produced small stems but not fruit. Cross sections of stem tissue from the triple *lac* mutant plant stained with phloroglucinol/HCl show reduced lignification and collapsed xylem vessels (Figure 4.8 B). These results indicate that laccases are required for lignification of stem tissues in *C. hirsuta*, in agreement with the results found in *A. thaliana* (Berthet *et al.*, 2011; Zhao *et al.*, 2013).

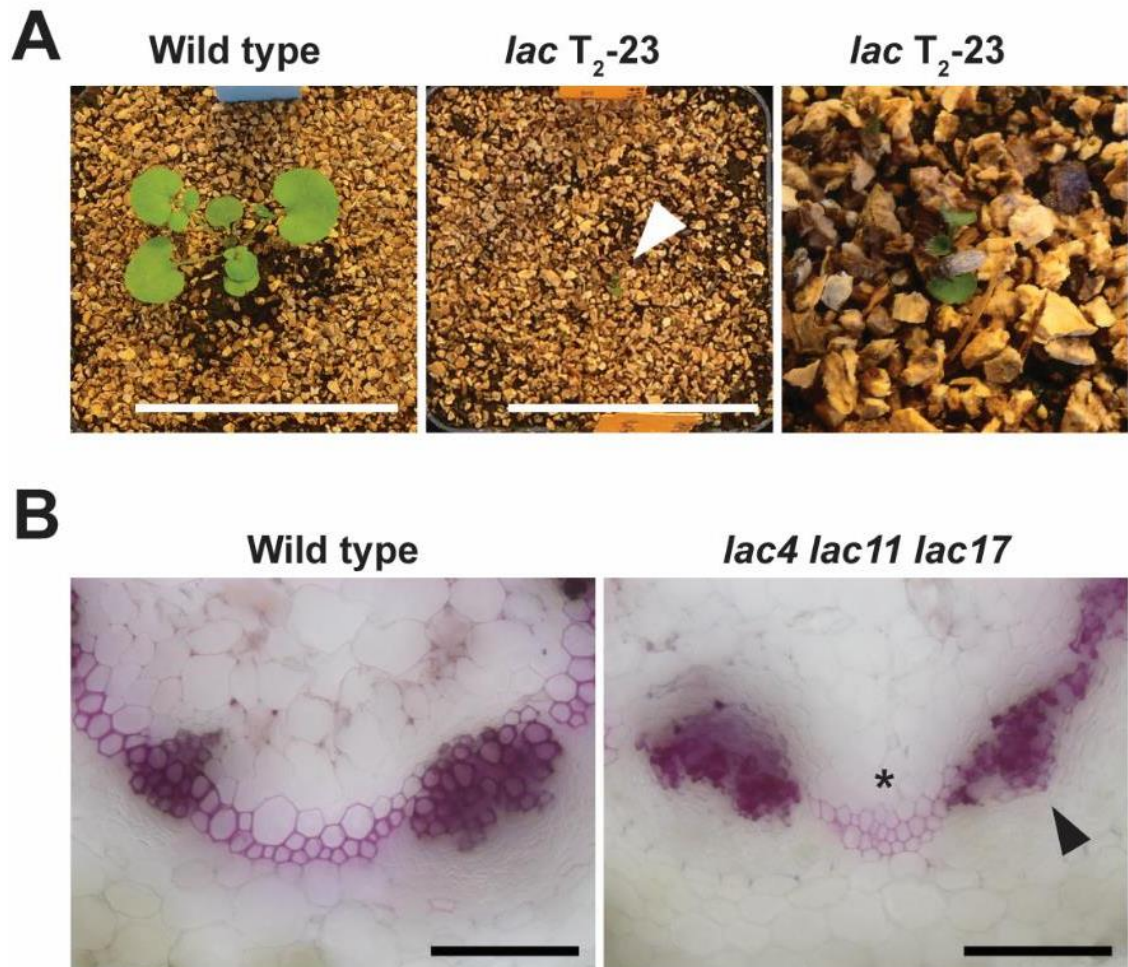


Figure 4.8: Triple *lac4 lac11 lac17* mutant has reduced stem tissue lignification and collapsed xylem vessels. (A) 2 weeks-old wild-type (left) and putative *lac4 lac11 lac17* T₂-23 plant (middle and close-up of this image on right). Arrowhead indicates putative *lac4 lac11 lac17* T₂-23 plant with growth arrest. Scale bars: 5 cm. (B) Phloroglucinol/HCl staining of stem cross sections from 4 months-old plants grown in MS media culture boxes. Asterisk marks reduced lignification of fibres in *lac4 lac11 lac17* mutant. Arrowhead indicates collapsed xylem vessels in *lac4 lac11 lac17* mutant. Scale bars: 100 μm.

As I described before, other *lac* T₂-23 plants were indistinguishable from wild type. Among these plants, I identified one plant in which mutations in *LAC4* and *LAC17* were in homozygosity and the mutation in *LAC11* was in heterozygosity, thus, 5 gene copies of laccases were mutated in this plant (*lac4 lac11+/- lac17*). This plant has a buckled fruit margin (Figure 4.9 A), which is also characteristic of *spl7* mutant fruits. Cross sections of mature *lac4 lac11+/- lac17* fruits stained with phloroglucinol/HCl show lack of lignification in some cells of the replum and a slight reduction of lignification in the endocarp *b* layer (Figure 4.9 B). These results indicate a role for laccases in lignification of *C. hirsuta* fruit.

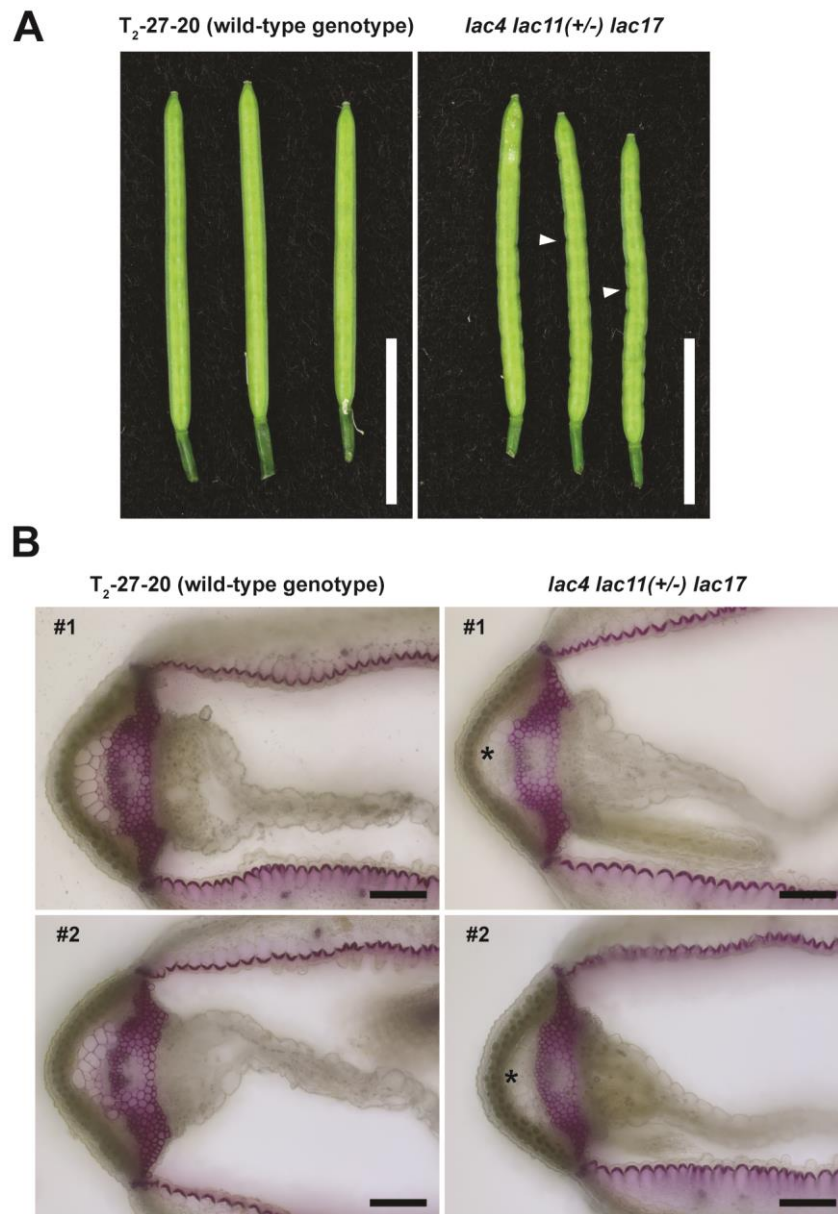


Figure 4.9: Knock-out alleles in 5 copies of laccases (*lac4 lac11(+/-) lac17*) lack lignification in cells of the replum and have slight reduction of lignification in endocarp *b* cells. (A) Mature fruit from T_2 -27-20 (wild-type genotype) and *lac4 lac11(+/-) lac17* mutant grown in long-day conditions. Arrowheads indicate buckled margins in the *lac4 lac11(+/-) lac17* mutant fruit. Scale bars: 1 cm. (B) Cross sections of mature fruit stained with phloroglucinol/HCl from T_2 -27-20 (wild-type genotype) and *lac4 lac11(+/-) lac17* mutant plants grown in long-day conditions. Images show sections from two different fruits from one plant for each genotype. Asterisks mark lack of lignification in the replum of the *lac4 lac11(+/-) lac17* mutant. Scale bars: 100 μ m.

In *A. thaliana*, the double mutant *lac4 lac17* showed reduced phloroglucinol/HCl staining in stem tissues under long-day conditions, however, a semi-dwarf phenotype and collapsed xylem vessels in the stem were observed only under continuous light conditions (Berthet *et al.*, 2011). Therefore, I grew *C. hirsuta lac* mutant plants in continuous light to investigate whether lignification of the *lac4 lac11+/- lac17* mutant endocarp *b* layer was further reduced. I sowed segregating T₃ seeds from line T_{223-3 lac4(+/-) lac11(+/-) lac17} (Cas9 free) in continuous light conditions and identified plants with *lac4 lac11+/- lac17* genotype. When grown under continuous light conditions, cross sections of mature *lac4 lac11+/- lac17* fruit stained with phloroglucinol/HCl showed a clear reduction of lignification in the endocarp *b* layer (Figure 4.10 A). By quantifying lignin autofluorescence intensity in the *lac4 lac11+/- lac17* mutant, I measured reduced lignification in the SCWs of endocarp *b* cells relative to wild type (Figure 4.10 B and C). The reduction in mean fluorescence intensity (mean gray value) and the reduction in the maximum intensity (maximum gray value) were statistically significant (Figure 4.10 B and C). These results indicate that laccases are necessary for wild-type lignification of endocarp *b* SCWs under continuous light conditions. Although, fruit of the *lac4 lac11+/- lac17* mutant have explosive pod shatter, I don't know whether the reduced lignification in the endocarp *b* layer affects seed dispersal. In future work, I plan to complement the laccase CRISPR/Cas9 mutant alleles with a LAC transgene to validate that reduced lignification is caused by loss of laccase function.

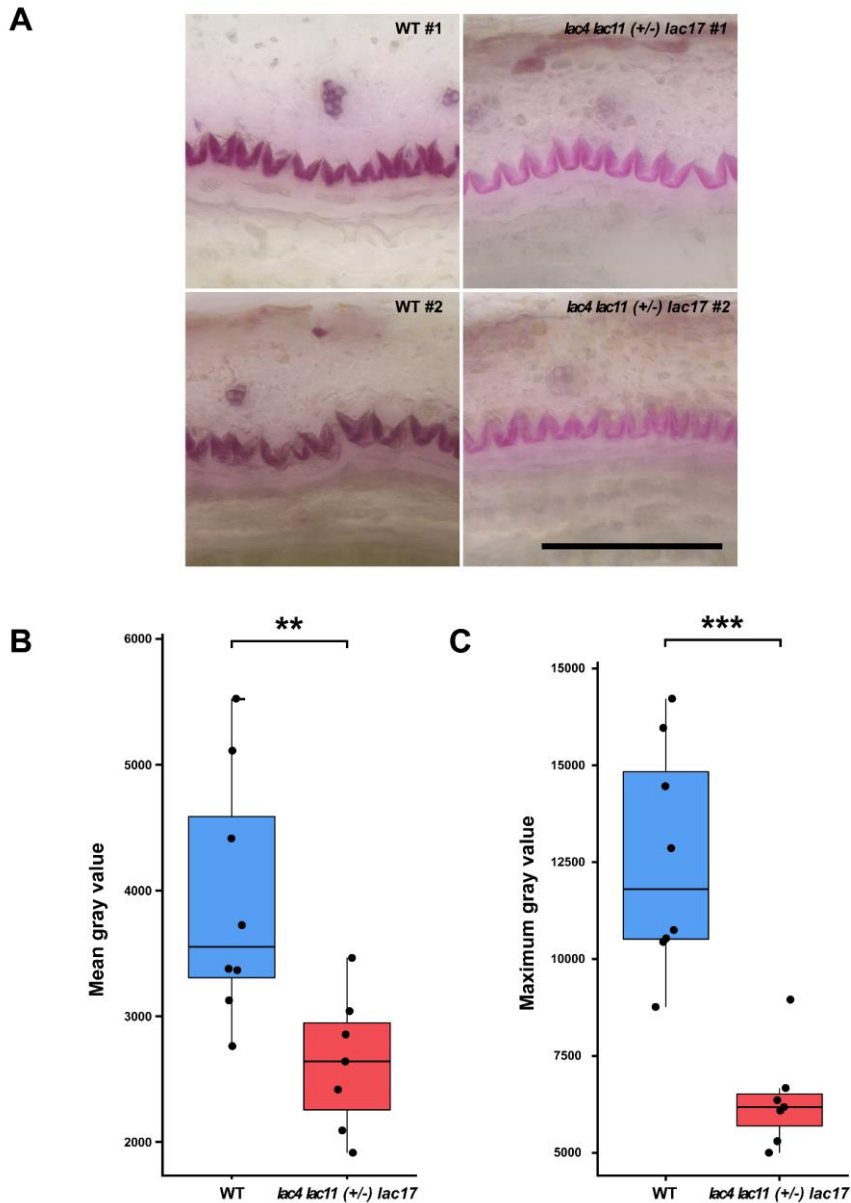


Figure 4.10: Mutant *lac4 lac11*^{+/-} *lac17* fruit show reduced lignification in SCWs of endocarp *b* cells.

(A) Cross sections of mature fruit stained with phloroglucinol/HCl from two wild-type plants and two *lac4 lac11*^{+/-} *lac17* mutant plants grown in continuous light conditions. Scale bar: 100 μ m. (B) Lignin autofluorescence intensity measured in endocarp *b* cells in cross sections of mature fruit of plants grown in continuous light conditions. 4 wild-type plants and 4 *lac4 lac11*^{+/-} *lac17* mutant plants were analysed. For each plant, one or two regions containing a few endocarp *b* cells were analysed. Detailed analysis information in methods part. Asterisks indicate statistically significant differences (*P-value < 0.05, **P-value < 0.01, ***P-value < 0.001, Student's t-test) between means of genotypes.

7. PER66 co-localizes with lignin deposits in SCWs of endocarp *b* cells whereas PER49 and PER64 localize to cell walls domains in the replum

Several peroxidases were found to be expressed in *C. hirsuta* fruit valves. *PER42* is the peroxidase with highest expression in the fruit valves of *C. hirsuta*. *PER64* and *PER66* are also expressed in fruit valves, although at lower levels than *PER42*. *PER49* was found to be strongly upregulated in fruit valves of the *spl7-1* mutant. If peroxidases contribute to lignin polymerization of endocarp *b* SCWs, I would expect that they accumulate precisely in the cell wall domains where lignin is deposited. To test this hypothesis, I generated translational reporters of these four peroxidases. I fused the proteins with mCherry at the C-terminus and used their native promoters to drive expression (*pPER42::PER42:mCherry*, *pPER49::PER49:mCherry*, *pPER64::PER64:mCherry* and *pPER66::PER66:mCherry*). I introduced the constructs into *C. hirsuta* wild-type plants via Agro-transformation and analysed localization of the tagged proteins in transverse sections of fruit at stage 17 a/b.

PER66:mCherry precisely co-localizes with lignin deposits in SCWs of endocarp *b* cells (Figure 4.11 A-C), suggesting a role in lignification of this cell type. Moreover, *PER66-mCherry* localization is specific to the endocarp *b* cell layer in the fruit, with the exception of a few cell walls in the centre of the lignified replum (not appreciable on Figure 4.11 E). Within the SCW, *PER66-mCherry* appears localized to the inner layers (more recently deposited) suggesting a possible spatial specificity of *PER66* function in endocarp *b* SCW lignification.

PER49 and *PER64* localize to cell corners between lignified cells in the replum (Figure 4.11 G-L). *PER49-mCherry* localizes only in cell corners of a few cells in the replum, whereas *PER64* localizes more broadly in lignified cells in the replum (Figure 4.11 G-L). Importantly, *PER64* and *PER49* do not localize throughout the lignified SCW in these cells, but rather to cell corners, and possibly the middle lamella between adjacent cells for *PER64* (Figure 4.11 G-L). I did not detect signal from *PER49-mCherry* or *PER64-mCherry* in SCWs of endocarp *b* cells, suggesting that these peroxidases do not contribute to lignification of endocarp *b* cells.

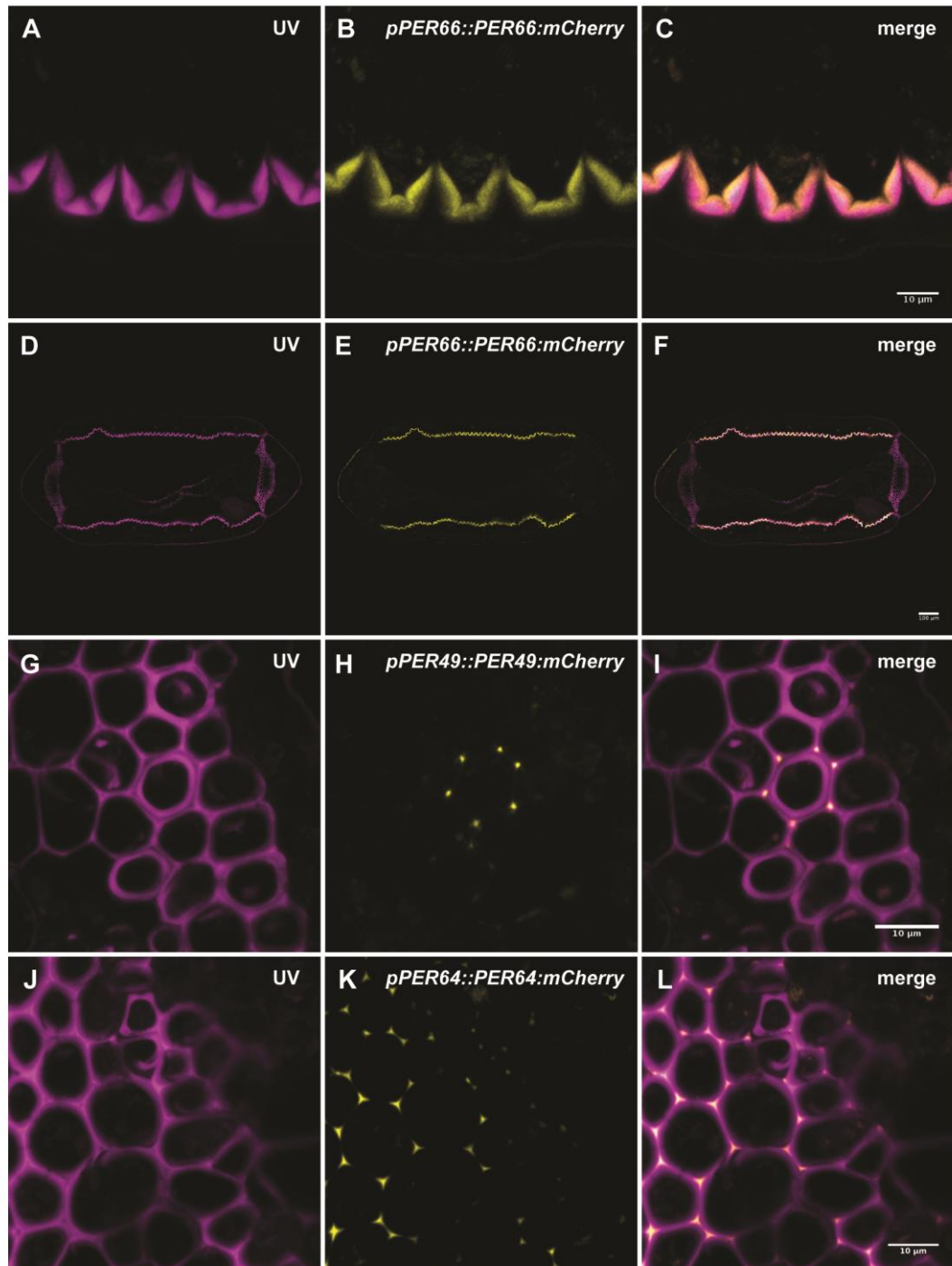


Figure 4.11. PER66 localizes to lignin deposits in SCWs of endocarp *b* cells; and PER49 and PER64 localize to cell corners between lignified cells in the replum. Confocal micrographs showing localization of peroxidases in *C. hirsuta* stage 17 a/b fruit cross sections. (A-C) PER66 localization in endocarp *b* cells. (D-F) PER66-mCherry localization in cross section of whole fruit. (G-I) PER49-mCherry localization in the replum. (J-L) PER64-mCherry localization in the replum. (A, D, G and J) UV405 autofluorescence signal. (B, E, H and K) mCherry signal from PER:mCherry fusions. (C, F, I and L) Merge images. Scale bars: 10 μm (C, I and L), 100 μm (F).

Discussion

In this chapter, I aimed to identify the role of lignin polymerizing enzymes in localized lignin deposition in endocarp *b* cells of *C. hirsuta*. By generating translational reporter lines, I found three laccases that precisely co-localized with lignin deposits in SCWs of endocarp *b* cells. I further characterized one of these laccases (LAC11) and I found that it co-localized with lignin deposits from the initial stage of lignin deposition and throughout thickening and lignification of the SCWs. I showed that CRISPR/Cas9 knock-out alleles of these laccases have reduced lignification in endocarp *b* cells under continuous light conditions, indicating that laccases are necessary for wild-type lignification of endocarp *b* cells. I plan to perform a complementation test with the laccases wild-type sequences to validate that the reduced lignification is indeed caused by loss of laccase function.

My results indicate that the precise localization of three monolignol-oxidases - LAC4, LAC11 and LAC17 - in SCWs of endocarp *b* cells directs localized lignin deposition. In this section, I discuss my findings on the mechanism of lignin deposition in endocarp *b* cells and I compare them with the models of lignification that have been investigated in other cell types, mainly focusing on the vasculature TEs and the Casparian strip in the root endodermis.

I examined the expression levels of laccase- and peroxidase-encoding genes in the fruit valve of *C. hirsuta* at the initial stages of endocarp *b* lignification and I found that *LAC4* and *LAC17* are the highest expressed laccases in *C. hirsuta* fruit valves. This profile of laccase expression resembles the one described in *A. thaliana* inflorescence stems, where *LAC4* and *LAC17* are the highest expressed laccases (Berthet *et al.*, 2011). In contrast to this, *LAC4* and *LAC17* expression levels are very low in the root endodermis cells of *A. thaliana* (Rojas-Murcia *et al.*, 2020).

To my knowledge, this is the first study to examine localization of lignin polymerizing enzymes (laccases or peroxidases) in Brassicaceae siliques. Of the three laccases that I examined (LAC4, LAC11 and LAC17), all co-localized with lignin deposits in SCWs of endocarp *b* cells. In contrast to this, out of a total of three peroxidases expressed in the fruit valve, only one peroxidase co-

localized with lignin deposits in the SCWs of endocarp *b* cells, whereas two peroxidases localized to cell corners in lignified cells in the replum and were not detected in cell wall domains of endocarp *b* cells. In *A. thaliana*, LAC4 and LAC17 were found to localize to SCWs of fibres and xylem vessels in the stem (Hoffmann *et al.*, 2020). My results indicate that the localization of laccases to SCW domains is conserved in endocarp *b* cells of *C. hirsuta* fruit valves. Furthermore, laccases co-localized with subcellular precision to the asymmetric lignin deposits of endocarp *b* cells in *C. hirsuta* and were absent from the non-lignified parts of the cell wall (likely primary cell walls). In *A. thaliana*, LAC4 and LAC17 co-localized with discrete lignified SCW domains in induced protoxylem TEs and were absent from the adjacent primary cell wall domains (Schuetz *et al.*, 2014). My results indicate a mechanism of localized lignin deposition via precise localization of phenoloxidases. By an interspecies gene transfer experiment, I found that *C. hirsuta* laccases adopted a symmetric pattern of localization in *A. thaliana* endocarp *b* cells, suggesting that asymmetric localization of laccases in *C. hirsuta* endocarp *b* cells is an innovation that might have contributed to the trait novelty of explosive seed dispersal in the Brassicaceae.

I found that one peroxidase (PER66) localized to lignified SCWs in endocarp *b* cells. In *Zinnia elegans*, a homolog of the *A. thaliana* gene *PER66* localized to SCWs of TEs (Sato *et al.*, 2006). Of the three peroxidases examined here, only PER66 localized to SCWs in endocarp *b* cells, whereas the other two peroxidases (PER49 and PER64) localized to cell corners and possibly the middle lamella in lignified cells in the replum. Similarly, in the *A. thaliana* stem, PER64 localized to cell corners and the middle lamella in between lignified fibre cells (Chou *et al.*, 2018). A previous study in *A. thaliana* showed similar findings to mine, where out of three peroxidases examined, only one peroxidase (PER72) localized to SCWs in lignified cells of the stem, whereas the other two localized to cell corners and middle lamella (Hoffmann *et al.*, 2020). My results suggest that only PER66 is a candidate peroxidase to contribute to endocarp *b* lignification.

I found that the *C. hirsuta lac4 lac11(+/-) lac17* mutant had reduced lignification in SCWs of endocarp *b* cells in continuous light conditions and that the triple *lac4 lac11 lac17* mutant had reduced lignification in fibres and collapsed xylem vessels in the stem. In *A. thaliana*, mature

stems of the double mutant *lac4 lac17* had reduced lignification in fibres and collapsed vessels (Berthet *et al.*, 2011); and mature stems of the triple *lac4 lac11 lac17* mutant had further reduced lignification in the stem (Zhao *et al.*, 2013). In contrast to this, formation of the lignified Casparian strip is not affected in the triple *lac4 lac11 lac17* mutant in *A. thaliana* (Zhao *et al.*, 2013). Furthermore, loss of function of 9 endodermis-expressed laccases had no detectable effect on Casparian strip formation or lignification (Rojas-Murcia *et al.*, 2020). Taken together, my results suggest that the mechanism of lignin polymerization in SCWs of endocarp *b* cells in *C. hirsuta* has similarities to that of the SCWs of lignified cell types in the stem and is different from that of the lignified Casparian strip in cell walls of the root endodermis.

Lignification of endocarp *b* cells is reduced in the *lac4 lac11(+/-) lac17* mutant under continuous light conditions, however, phloroglucinol/HCl staining shows that lignification is not completely abolished. One possibility to explain the remaining lignification is that the wild-type *LAC11* allele in the *lac4 lac11(+/-) lac17* mutant accounts for the lignification observed. Unfortunately, I was unable to find conditions where the triple *lac4 lac11 lac17* mutant produced fruit, thus, I could not assess whether the additional loss of the second copy of *LAC11* results in a complete lack of lignification in the endocarp *b* SCWs. To test this hypothesis, I have generated a *LAC11*-mCherry dexamethasone-inducible construct and I plan to introduce it in the triple mutant background (*lac4 lac11 lac17*). In future work, I intend to continuously provide *LAC11* activity by dexamethasone application in the triple *lac4 lac11 lac17* mutant during vegetative growth and flowering to ensure the production of fruit. After flowering, I intend to cease dexamethasone application and assess lignification of the endocarp *b* cells of the triple mutant fruit.

Another possibility to explain why lignification of SCWs of endocarp *b* cells is not completely abolished in the *lac4 lac11(+/-) lac17* mutant is that peroxidases also contribute to lignification. Although my results indicate that the function of laccases in endocarp *b* lignification is not redundant with peroxidases, since in the *lac4 lac11(+/-) lac17* mutant, peroxidases didn't rescue the lignification, peroxidases might account for the remaining lignification in this mutant. To investigate the contribution of peroxidases to lignification, I plan to generate a CRISPR/Cas9

knock-out allele of *PER66*, the peroxidase that co-localized with lignin deposits in endocarp *b* SCWs, and assess lignification of endocarp *b* cells. *PER42* was the peroxidase with highest expression levels in *C. hirsuta* fruit valves; unfortunately, I could not recover any transgenic T₁ line of the PER42-mCherry translational fusion construct. In future work, I plan to attempt transformation again to assess whether PER42 localizes to endocarp *b* SCWs and if it is the case generate CRISPR/Cas9 knock-out alleles.

Interestingly, I found that knock-out alleles of laccases phenocopy the buckled margin of the *spl7* mutant fruit. The *C. hirsuta* fruit valve is under tension while it is attached to the fruit. The outer exocarp layer contracts while the inner endocarp *b* layer can't contract because it is lignified and inextensible, and this differential contraction produces tension (Hofhuis *et al.*, 2016). Before pod shatter, the fruit valve is attached to the replum which also contains lignified cell types. I hypothesize that the reduced lignification in fruit tissues of these mutants leads to reduced mechanical strength and, therefore, part of the elastic potential energy generated in the exocarp is released as buckling of the fruit margins. In the *lac4 lac11(+/-) lac17* mutant, lignification of the endocarp *b* layer is reduced and lignification of a cell type in the outer part of the replum is abolished, whereas lignification of this cell type in the replum does not appear reduced in the *spl7* mutant. Moreover, the same buckled fruit margin phenotype is observed in the *lig2* mutant, where the endocarp *b* layer is specifically missing (Hofhuis *et al.*, 2016). In future work, it will be interesting to formulate and test a biomechanical hypothesis for how a reduction in endocarp *b* lignification can result in a buckled fruit margin.

Reduction in laccase transcript levels, mediated by miR397 activity, was previously linked to reduced lignification in non-domesticated rice relatives compared to domesticated rice cultivars (Swetha *et al.*, 2018). In *A. thaliana*, transgenic lines overexpressing miR397 reduced *LAC4* transcript levels, which also resulted in reduced lignification (Wang *et al.*, 2014). By examining RNA-seq data, I found that laccase gene expression is not reduced but slightly increased in the *spl7-1* mutant fruit compared to wild type, suggesting that lower expression of laccase genes is not responsible for the reduced lignification of endocarp *b* cells in the *spl7-1* mutant. In future

work, I plan to validate this result by introducing LAC-mCherry fusions that I have generated into the *spl7-1* mutant background, and examining whether they localize correctly to the less lignified SCW domains of endocarp *b* cells.

In this chapter, I found that three laccases pre-pattern the asymmetric lignin deposition in *C. hirsuta* endocarp *b* cells and I found evidence that they are required for lignification. These findings provide a mechanism for the localized lignin deposition in endocarp *b* cells. Laccases use Cu to oxidize lignin monomers and, previously, I found that *spl7* mutant fruit have a reduced concentration of Cu. In future work, I plan to establish a laccase purification and activity assay to test whether reduced laccase activity in the *spl7* mutant fruit is responsible for the reduced lignification of endocarp *b* cells. In addition to the requirement of Cu for laccase-catalysed oxidation, reduced Cu availability in the *spl7-1* mutant might have other post-transcriptional effects on laccase function. It has been proposed that Cu binding can affect protein folding and protein stability (Arioz & Wittung-Stafshede, 2018). Furthermore, proteins can bind different metal ions depending on their relative availability in a specific cell compartment (Tottey *et al.*, 2008). Ultimately, reduced Cu availability likely results in laccase proteins lacking the Cu metal cofactor (apoproteins) that would not be functional. Therefore, I hypothesize that laccase proteins accumulate in SCWs of endocarp *b* cells and that they have reduced activity as a consequence of one or several of these factors.

Chapter 5: General Discussion and Future Perspectives

Species in all phylogenetic groups have evolved adaptations for dispersal since, to a varying magnitude, dispersal is essential for the success of all species. For plants, as sessile organisms, seed dispersal is a key opportunity to move and colonize new locations. The importance of seed dispersal is illustrated by the numerous and diverse adaptations that can be found in nature, from the winged seeds of maple tree, to the explosive fruit of *C. hirsuta*. Explosive seed dispersal is a remarkable means of dispersing the plant's progeny that relies on rapid movements. A major goal in biology is to identify the genetic basis of complex trait innovations, such as explosive seed dispersal in *C. hirsuta*. Previous work in my group investigating this trait at cellular, tissue and organ scales resulted in a comprehensive understanding of the mechanics of explosive seed dispersal in *C. hirsuta* (Hofhuis *et al.*, 2016). Here, I identified genetic mechanisms contributing to the cellular innovations that underpin explosive seed dispersal in *C. hirsuta*.

1. Lignin is an important component of endocarp *b* SCWs for explosive seed dispersal

The endocarp *b* layer plays a key role in explosive seed dispersal (Hofhuis *et al.*, 2016). Firstly, the differential contraction of the exocarp layer and endocarp *b* layer cause the coiling of the valves. Secondly, the SCW geometry of endocarp *b* cells is crucial for the explosive release of the potential elastic energy stored in the fruit valve. Here, I find that defective lignin deposition in endocarp *b* SCWs of the *spl7* mutant resulted in a reduced distance of seed dispersal compared to wild type. This key result indicated that lignification of endocarp *b* SCWs significantly contributes to explosive seed dispersal in *C. hirsuta*. Lignin deposition confers rigidity and strength to compression to SCWs (Cosgrove, 2018). For instance, in xylem vessels, lignified SCWs allow these cells to resist the strong negative pressures of the water stream (Cosgrove, 2018). Importantly, the amount of potential elastic energy that can be stored in the fruit valve will depend on the material properties of the valve tissue. SCWs of endocarp *b* cells with reduced lignification were likely less able to resist the contraction of the exocarp layer and, therefore, less potential elastic energy was stored in the valve that could be transformed into kinetic coiling

energy. My findings demonstrate that the amount of lignin in the endocarp *b* SCW is an important determinant of effective seed dispersal in *C. hirsuta*.

In future work, it would be interesting to quantify the mechanical properties of the less lignified endocarp *b* layer in the *spl7* mutant and compare them to the wild type. Furthermore, it would be interesting to include the measurements of the mechanical properties into the fruit valve mathematical models that have been used to investigate explosive seed dispersal in *C. hirsuta* (Hofhuis *et al.*, 2016) and test whether the outcomes of the model match the observed reduced seed dispersal distance of the *spl7* mutant.

2. Explosive seed dispersal depends on SPL7 to provide sufficient Cu in the fruit

I found that SPL7 regulates the Cu concentration in *C. hirsuta* fruit. First, *spl7* mutant fruit have less Cu concentration than wild type in a wide range of Cu supplies. Moreover, I found that SPL7 is sufficient to increase Cu concentration in the fruit in a dose-dependent manner. These results indicated that SPL7 mediates Cu homeostasis in *C. hirsuta* fruit. Importantly, Cu concentration in the growing media positively correlated with the Cu concentration in the fruit of both wild type and *spl7* mutant; and Cu supplementation to growing *spl7* mutant plants fully rescued the lignification defects, indicating that Cu is required for lignification of endocarp *b* SCWs. My findings together, imply a link between Cu homeostasis, regulated by SPL7, and explosive seed dispersal in *C. hirsuta*.

Interestingly, I found evidence for a higher sensitivity of *C. hirsuta* fruit for the loss of SPL7 function compared to other parts of the plant. First, I observed that lignification of SCWs of endocarp *b* cells is reduced in response to a range of supplied Cu concentrations that has no effect on the lignification of stem and root tissues. Second, I find that the Cu concentration in fruit of *spl7* is strongly reduced, whereas Cu concentrations in seedlings, roots and shoots, of *A. thaliana spl7* mutant were similar or higher compared to wild type (Bernal *et al.*, 2012; A. Schulten *et al.*, 2019; Yamasaki *et al.*, 2009). However, a comparison between organs in either *C. hirsuta* or *A. thaliana spl7* is needed to interpret this finding.

Furthermore, I found that *SPL7* is expressed in endocarp *b* cells when SCWs are lignified, and it is not expressed in other non-lignified cell types in the fruit valve at this stage. This observation suggests a possible local role of *SPL7* in endocarp *b* lignification. Interestingly, I found that the *SPL7* pathway of Cu economization was lost in *spl7* fruit valves. I hypothesize that restoration of *SPL7*-dependent economization and mobilisation of Cu within the fruit might be sufficient to rescue lignification of endocarp *b* SCWs. By using a chemically inducible *SPL7* expression system, that I have already generated, I plan to investigate in future studies whether *SPL7* is sufficient to rescue the lignification defects of the *spl7* mutant when locally expressed in the fruit. Furthermore, I plan to use this system to identify putative *SPL7* target genes that are specifically regulated in the fruit valve of *C. hirsuta*.

3. Cu-requiring laccases direct localized lignin deposition in SCWs of endocarp *b* cells

I found that three lignin-polymerizing laccases (LAC4, LAC11 and LAC17), which are Cu-requiring enzymes, are expressed in endocarp *b* cells, where they accumulate precisely in SCWs to pre-pattern lignin deposition. I generated knock-out alleles of these three laccases and found that plants with 5 mutant laccase alleles had reduced lignification in SCWs of the endocarp *b* layer. These two key results together, indicate that laccases direct localized lignin deposition in endocarp *b* cells of *C. hirsuta*. I found that *C. hirsuta* laccases localize symmetrically to endocarp *b* SCWs when expressed in the non-explosive species *A. thaliana*, suggesting that a novel, asymmetric pattern of laccase localization evolved during the transition from non-explosive to explosive seed dispersal in *C. hirsuta*.

Interestingly, the laccase mutant plants phenocopy the reduced lignification in endocarp *b* SCWs of the *spl7* mutant. Laccases are Cu-requiring enzymes, thus, they act downstream of *SPL7*, which regulates Cu homeostasis. This suggests that reduced lignification in the *spl7* mutant is likely to be caused by reduced laccase activity due to low Cu concentrations in the fruit as consequence of altered Cu homeostasis. In future work, I plan to measure whether laccase activity is reduced in the *spl7* mutant fruit to test this hypothesis.

I found that genes encoding several laccases are highly expressed in the fruit valve at the onset of endocarp *b* lignification, whereas only a small number of peroxidase genes are expressed. Three laccases precisely co-localized with lignin deposits in SCWs of endocarp *b* cells whereas only one out of the three fruit valve-expressed peroxidases that I examined co-localized with lignin deposition in endocarp *b* SCWs. These results suggest that heme-containing peroxidases might have a minor role in endocarp *b* SCW lignification compared to the Cu-requiring laccases. To further investigate the possible contribution of peroxidases to endocarp *b* SCW lignification, I plan to generate a knock out allele of *PER66* by using CRISPR/Cas9.

By generating and characterizing knock-out alleles for three laccase genes and fluorescently-tagged fusion proteins for three laccases and three peroxidases, my work provides valuable resources to investigate questions about development, mechanics and cell wall biology in *C. hirsuta* and in a comparative context with *A. thaliana*. To my knowledge, it is the first time that the localization of lignin-polymerizing enzymes has been investigated in the fruit of any Brassicaceae species, including *A. thaliana*. As such, my work will contribute generally to the understanding of cell wall lignification.

4. Proposed model for the mechanism of localized lignin deposition in endocarp *b* cells

To summarize my findings, I propose a model for the mechanism of localized lignin deposition in SCWs of endocarp *b* cells. At the initial stage of SCW deposition, Cu-requiring laccases accumulate asymmetrically in the cell walls to precisely pre-pattern lignin deposition. Throughout endocarp *b* development, laccases direct localized lignin deposition in the asymmetric SCW. Localized lignin deposition is dependent on *SPL7* to regulate Cu homeostasis in *C. hirsuta* fruit. I propose that laccase activity is reduced in the *spl7* mutant due to decreased Cu availability. Finally, the lack of lignin in the composition of endocarp *b* SCWs translates into reduced seed dispersal range in the *spl7* mutant. Therefore, explosive seed dispersal depends on the *SPL7* pathway to provide sufficient copper to the fruit for localized lignin deposition mediated by the precise localization of Cu-requiring laccases.

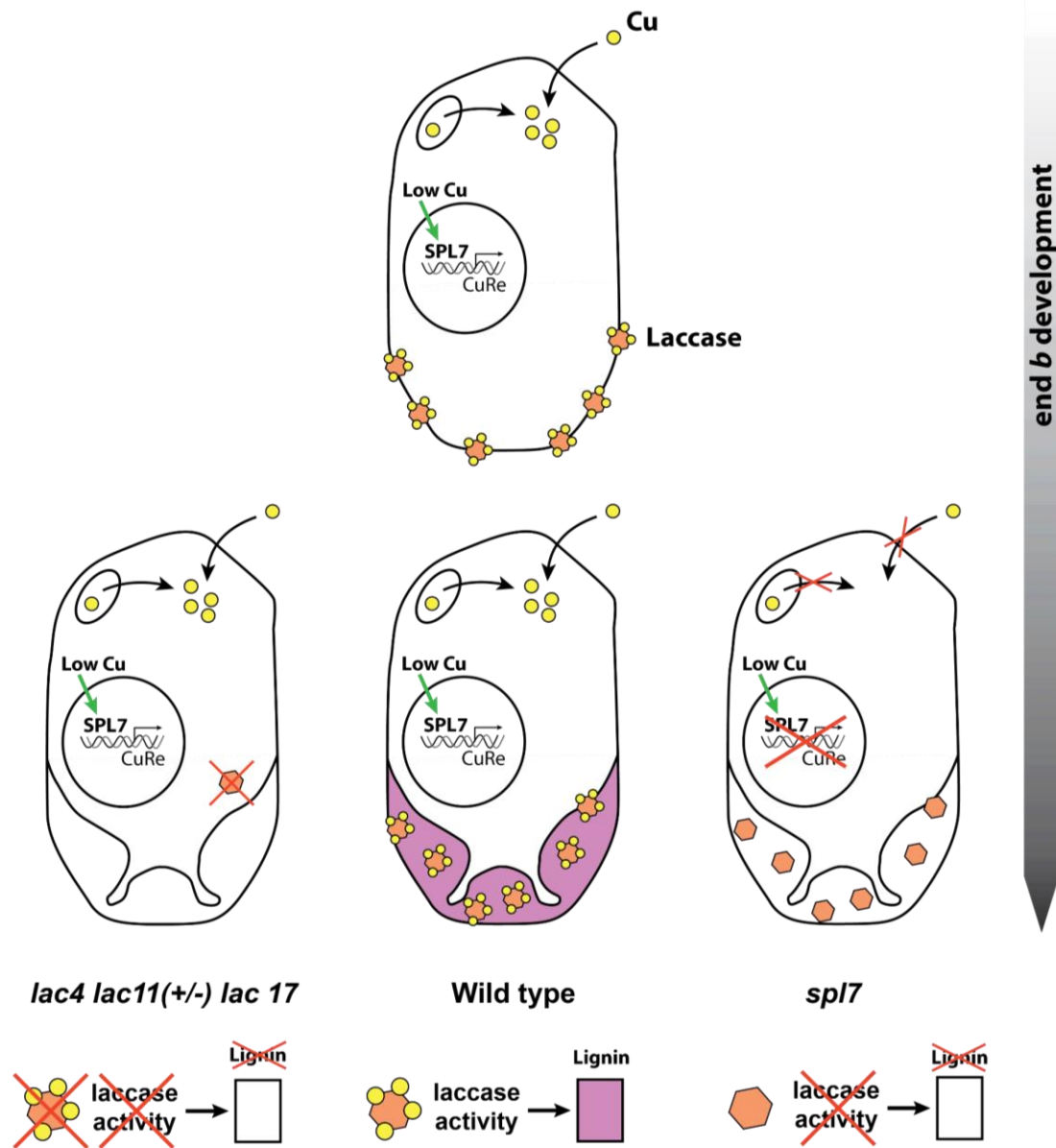


Figure 5.1: Proposed model for the mechanism of localized lignin deposition in endocarp *b* cells.

(middle) Wild type scenario. Under Cu limiting conditions SPL7 is activated and promotes expression of Cu responsive elements CuRe genes to increase uptake, mobilisation and economization of Cu (these three processes are represented by the two arrows bringing Cu). At the initial stage of SCW deposition, Cu-requiring laccases localize asymmetrically to precisely pre-pattern lignin deposition. Throughout endocarp *b* development, laccases direct localized lignin deposition in the asymmetric SCW. (right) *spl7* mutant scenario. Loss of function of SPL7 translates in reduced Cu availability since Cu uptake, mobilisation and economisation are not promoted. Laccase activity is not possible due to the reduced Cu availability and translates into lack of lignin deposition. (left) In laccase knock out alleles, laccase proteins do not accumulate in endocarp *b* SCWs which translates in reduced lignin deposition.

Chapter 6: Materials and methods

1. Growing conditions and plant materials

1.1 Plant growing conditions

Plants were grown at the Max Planck Institute for Plant Breeding Research in Cologne, Germany.

Plants grown on soil were cultivated in greenhouse chambers with controlled environment in long-day conditions (LD) (days: 20 °C, 16 h; nights: 18 °C, 8 h) or continuous-light conditions (days: 17°C, 24 h). *Cardamine hirsuta* seeds were stratified in the dark for 10 days at 4°C before being placed in the light. *Arabidopsis thaliana* seeds were stratified on soil in the dark for 3 days at 4°C before being placed in the light.

For in vitro cultivation of wild-type and CRISPR/Cas9 *lac* mutant T₂23 plants, seeds were placed in closed culture boxes containing ½ MS media without sucrose. Boxes were placed in the dark for 10 days at 4°C before being placed in the light under LD conditions.

Cu supplementation was performed by applying different concentration of CuSO₄ to the soil surface.

1.2 Plant cultivation in aeroponics system

Plants were grown in small permeable pots filled with inert material (perlite). The pots were fit through holes on the top part of large, dark, enclosed tanks, thus, the roots were inside the tank and the aerial parts of the plants outside the tank (EZ-CLONE Plant Cloning System -EZClone company-). Nutrient solution was sprayed inside the box to irrigate the roots four times a day during 15 min. This was performed with an OASE Aquarius Universal 180 Statuary and Fountain pump and a HortiPots Clone Machine Spray Nozzle Manifold with 12 Red Micro Sprayers with 360 Degree Fan Jet Spray Pattern connected to the fountain pump. Irrigation solutions contained all nutrients used in the greenhouse conditions and different concentrations of Cu depending on the treatment. Cu concentrations were adjusted by adding CuSO₄ to the solutions. During plant growth the pH of the solutions was adjusted and kept in a range of 5.5 – 6.0 pH. In a first experiment, seeds were germinated directly on the pot surface and, in a second experiment, seeds

were germinated in ½ MS media plates supplemented with 0.5 µM CuSO₄ and then transferred to the pots in the aeroponics system.

1.3 Strains and lines used

The strains used in this study were: *Arabidopsis thaliana* Col-0 (Columbia, USA) and *Cardamine hirsuta* (herbarium specimen voucher Hay 1 (OXF) described in (A. Hay & Tsiantis, 2006)).

Allele	Reference
<i>lig1 (spl7-1)</i>	Generated by Penny Sarchet
<i>spl7-2</i>	Generated in this study
<i>lac4 lac11 lac17</i>	Generated in this study

Table 6.1: Mutant alleles used in this study

2. Generation of transgenic plants

2.1 Bacterial strains

The bacterial strain *Escherichia coli* DH10B was used for plasmid amplification. *Agrobacterium tumefaciens* GV3101 and C58 strains were used for *C. hirsuta* and *A. thaliana* transformation.

2.2 Constructs and cloning strategies

To generate transcriptional and translational fusions of *SPL7*, a 2374 bp promoter sequence was amplified from *C. hirsuta* Ox genomic DNA. To amplify the coding sequence (CDS) of *SPL7*, I used cDNA previously synthesized from *C. hirsuta* extracted RNA. To generate the constructs *pSPL7::GFP-NLS*, *pSPL7::3xGFP*, *pSPL7::mCherry:SPL7* and *pSPL7::SPL7(ΔSBP):GFP* the GreenGate system was used (Lampropoulos *et al.*, 2013). The different entry vector combinations were cloned in the destination vector pGGZ003. Construct *pSPL7::SPL7:YFPv* was generated using MultiSite Gateway with plasmids generated in (Galinha *et al.*, 2007). Three entry vectors containing the promoter, coding sequence and YFPvenus tag were cloned into the binary vector pGIII0125-R4R3 which contained the norflurazon selection. *SPL7* translational fusion constructs

used in *lig1* complementation experiments are summarized in **Figure ???**. Primers used for cloning are listed in Table 6.6.

To generate transcriptional and translational reporters of three laccases (LAC4, LAC11 and LAC17), promoter regions were amplified from *C. hirsuta* Ox genomic DNA: *LAC4* (3696 bp), *LAC11* (3252 bp) and *LAC17* (2885 bp). cDNA synthesized from *C. hirsuta* Ox RNA was used to amplify the coding sequences (CDS). The GreenGate system was used to generate constructs: *pLAC4::GFP-NLS*, *pLAC11::GFP-NLS*, *pLAC17::GFP-NLS*, *pLAC4::LAC4:mCherry*, *pLAC11::LAC11:mCherry* and *pLAC17::LAC17:mCherry*. The entry vector combinations were cloned into binary vectors pGGZ003 or pGGZwf01. Primers used for cloning are listed in Table 6.6.

To generate translational reporters of three peroxidases (PER49, PER64 and PER66), promoter regions were amplified from *C. hirsuta* Ox genomic DNA: *PER49* (958 bp, whole intergenic region), *PER64* (2888 bp) and *PER66* (3292 bp). cDNA synthesized from *C. hirsuta* Ox RNA was used to amplify the coding sequences (CDS). The GreenGate system was used to generate the constructs: *pPER49::PER49:mCherry*, *pPER64::PER64:mCherry* and *pPER66::PER66:mCherry*. The entry vector combinations were cloned into binary vector pGGZ003. Primers used for cloning are listed in table 6.6.

2.3 Generation of transgenic plants

Plants were transformed with *Agrobacterium tumefaciens* strains *GV3101* or *C58* by the floral dip method (Clough & Bent, 1998). T₁ seeds from transformed plants were screened for transgene insertion by using Basta resistance, Norflurazon resistance or seed coat fluorescent marker. T₂ and T₃ lines were obtained by self-fertilization. To identify homozygous plants from single insertion lines, two approaches were used: (1) Analysis of the segregation ratios of resistance markers and (2) determination of the number of transgene insertion copies (iDNA Genetics). Transgenic lines generated in this study are listed in Table 6.2.

Line	Background	Reference	Independent transgenic lines characterized
<i>pSPL7::SBP-SPL7:GFP</i>	<i>C. hirsuta lig1</i>	Generated in this study	5
<i>pSPL7::mCherry:SPL7</i>	<i>C. hirsuta lig1</i>	Generated in this study	4
<i>pSPL7::SPL7:YFPv</i>	<i>C. hirsuta lig1</i>	Generated in this study	2
<i>pBAM9::BAM9:GFP</i>	<i>C. hirsuta lig1</i>	Generated in this study	4
<i>pSPL7::3xGFP</i>	<i>C. hirsuta</i> wild type Ox	Generated in this study	2
<i>pSPL7::GFP-NLS</i>	<i>C. hirsuta</i> wild type Ox	Generated in this study	6
<i>pLAC4::GFP-NLS</i>	<i>C. hirsuta</i> wild type Ox	Generated in this study	7
<i>pLAC11::GFP-NLS</i>	<i>C. hirsuta</i> wild type Ox	Generated in this study	11
<i>pLAC17::GFP-NLS</i>	<i>C. hirsuta</i> wild type Ox	Generated in this study	12
<i>pLAC4::LAC4:mCherry</i>	<i>C. hirsuta</i> wild type Ox	Generated in this study	13
<i>pLAC11::LAC11:mCherry</i>	<i>C. hirsuta</i> wild type Ox	Generated in this study	5
<i>pLAC17::LAC17:mCherry</i>	<i>C. hirsuta</i> wild type Ox	Generated in this study	3
<i>pPER49::PER49:mCherry</i>	<i>C. hirsuta</i> wild type Ox	Generated in this study	1
<i>pPER64::PER64:mCherry</i>	<i>C. hirsuta</i> wild type Ox	Generated in this study	4
<i>pPER66::PER66:mCherry</i>	<i>C. hirsuta</i> wild type Ox	Generated in this study	2
<i>pLAC4::LAC4:mCherry</i>	<i>A. thaliana</i> wild type Col-0	Generated in this study	16
<i>pLAC17::LAC17:mCherry</i>	<i>A. thaliana</i> wild type Col-0	Generated in this study	3

Table 6.2: Transgenic lines used in this study

3. Generation of mutant alleles

3.1 CRISPR/Cas9 mediated mutagenesis of *SPL7*

For directed mutagenesis using CRISPR/Cas9, a similar strategy as in (Kamei *et al.*, 2020) was followed, although with several modifications. All possible sgRNA positions for the PAM site "GG" in the *SPL7* genomic sequence were identified using ChopChopv2 (Labun *et al.*, 2016). Two sgRNAs were selected from the list based on location, high efficiency and minimum off-target prediction (Table 6.3). A MultiSite Gateway cloning method was used to assemble two entry vectors into a destination vector. Two sgRNAs present in a previously existing Gateway-compatible entry vector were mutagenized (GenScript) to obtain the sequence of the two chosen sgRNAs. Each of the sgRNAs were located downstream of a copy of the *A. thaliana* U6 RNA polIII promoter to drive their expression. The other entry vector used contained the gene encoding an Arabidopsis codon optimised spCas9 protein (Fauser *et al.*, 2014) downstream of an egg cell-specific promoter (Wang *et al.*, 2015) to drive expression in egg cells and very initial stages of embryo development. These two entry vectors were assembled via LR reaction in a destination vector containing the Basta resistance locus for plant selection pPZP200-BASTA-GW (Dr. Claire Kamei, unpublished work). The vector was transformed into wild-type *C. hirsuta* (Ox strain) plants by *Agrobacterium tumefaciens* (strain *GV3101*)-mediated floral dip, as previously

described. T₁ Basta-resistant plants were genotyped for Cas9-derived mutations in *SPL7*. Primers were designed to amplify 700 bp regions including sgRNAs sequences. PCR products were sequenced and then analysed using the Tracking of Indels by DEcomposition (TIDE) software (Brinkman *et al.*, 2014). T₂ plants were genotyped for homozygous mutations and absence of Cas9 insertion.

	Target sequence	Strand	Expected cut position (bp from ATG)
sgRNA1	ATCCCCATCGGCGCCTGAGAT TGG	Positive	35
sgRNA2	GTTCGTCAGCGGCGAAGTCA AAG	Negative	120

Table 6.3: sgRNAs used to knock out *SPL7* using CRISPR/Cas9. PAM sites are marked in bold italics.

3.2 CRISPR/Cas9 mediated mutagenesis of laccases

All possible sgRNA positions for the PAM site "GG" in the genomic sequences were identified using ChopChopv2 (Labun *et al.*, 2016). Two sgRNAs were selected from the list based on location, high efficiency and minimum off-target prediction (Table 6.4). A MultiSite Gateway cloning method was used to assemble two entry vectors into a destination vector. One entry vector contains a single ubiquitin promoter from *Petroselinum crispum* (parsley, pPcUbi) (Fauser *et al.*, 2014) to drive expression of the 6 sgRNAs in a tRNA-gRNA system (polycistronic) and a single terminator downstream. The other entry vector used contained the gene encoding an Arabidopsis codon-optimised spCas9 protein (Fauser *et al.*, 2014) downstream of an egg cell-specific promoter (Wang *et al.*, 2015) to drive expression in egg cells and very initial stages of embryo development. These two entry vectors were assembled via LR reaction in destination vector pPZP200-pFAST-RFP-GW (Dr. Claire Kamei, unpublished work) containing a seed coat marker for plant selection. The vector was transformed into wild-type *C. hirsuta* (Ox strain) plants by *Agrobacterium tumefaciens* (strain *GV3101*)-mediated floral dip, as previously described. Fluorescent T₁ seeds were selected and germinated. T₁ plants were genotyped for mutations by PCR amplification and sequencing of PCR products. Sequencing results were analysed using the Tracking of Indels by DEcomposition (TIDE) software (Brinkman *et al.*, 2014). T₂ plants were

genotyped to find homozygous alleles. The presence of Cas9 insertion in T₂ plants was assessed by one or several methods (evaluation of seed fluorescence, PCR amplification (primer sequences in Table ???) and transgene copy number determination (iDNA Genetics)).

Target gene name	<i>C. hirsuta</i> gene number	Target sequence	Strand	Expected cut position (bp from ATG)
LACCASE 4	CARHR132660	sgRNA1 GCCAACGTGGAACGCTCTGG TGG	Positive	987
		sgRNA2 CACATGATTAACGGACACC TGG	Positive	1334
LACCASE 11	CARHR210090	sgRNA1 CCGGACAACGCGGGACCCT TGG	Positive	615
		sgRNA2 TTTCTACTACGGTCATGTT TGG	Negative	1162
LACCASE 17	CARHR273650	sgRNA1 CCGGCAATTACGGAGTGGT TGG	Positive	415
		sgRNA2 GAGCAGTTGTATAACGGACC AGG	Negative	821

Table 6.4: sgRNAs used to knock out laccases using CRISPR/Cas9 mutagenesis method. PAM sites are marked in bold italics.

4. Molecular biology methods

4.1 Fine mapping

Marker name	Position	Primer sequences
INDEL_16810437 (Ox + 53 bp)	Chr6:16,810,437	F CAATTCATAGTTGGGATGCTCTCTC R CGGGCGGACACAATAGTTTA
SNP_16824303 (dCAPS/XbaI cuts Nz)	Chr6:16,824,303	F CACATCTTTAAACAAATGCCGATCTA R ACAACCGCGCTTTTATTCAT
INDEL_17317339 (Ox + 21 bp)	Chr6:17,317,339	F TTGTTGTGAAACTTATTTTGTGGTC R AATAACCGCCATTTTAAACAATTC
SNP_17676369 (dCAPS/ScaI cuts Ox)	Chr6:17,676,369	F TGTAATGGAAGTGGGAACAGAAAGTA R CCATAATCTTTATTAGCACATCGAG
INDEL_17882576 (Ox + 65 bp)	Chr6:17,882,576	F TCCACGTGGGGTAAAAATAATG R CCTGAATCTGGTGTCTGAGC
SNP_18274972 (dCAPS/XbaI cuts Ox)	Chr6:18,274,972	F TCTTCTCCTGATTTCTACATTCTA R TCCGTATTAATCAAATCGAAGC
INDEL_18607525 (Ox + 31 bp)	Chr6:18,607,525	F CACAAGTCGTCGTCTCTTGC R CCCGTTCCATGAATCTGTT

Table 6.5: Primer sequences of markers used for *lig1* fine mapping. INDEL and dCAPS markers are shown. Genome sequence locations in *C. hirsuta* reference genome are indicated.

4.2 RNA extraction and qRT-PCR

RNA extraction was performed using the Spectrum™ Plant Total RNA kit (Sigma-Aldrich) following the manufacturer's protocol. cDNA synthesis was performed using SuperScript IV Reverse Transcriptase (Invitrogen). A 2-step qRT-PCR was performed with the DNA-specific dye SYBR Green (Power SYBR green PCR master mix kit; Applied Biosystem) in a QuantStudio 5 PCR machine (Applied Biosystems).

Experiments were performed in triplicate from three biological samples consisting of two pooled matured fruits each. Expression levels were estimated by using the comparative Ct method (Pfaffl, 2001) and were normalized against values obtained for the housekeeping gene Clathrin (CARHR174880). Primers used are listed in Table 6.6.

Usage	Primer name		Primer sequence
Cloning of pSPL7 GreenGate	pSPL7/fullF	F	GGTCTCAACCTTAACCACCACCAAAGGTAACAA
	pSPL7/fullR	R	GGTCTCATGTTCTGAGTCTTCTCAATTCATAAAATTC
Cloning of SPL7 CDS GreenGate	cdsSPL7.F	F	GGTCTCAGGCTCCATGCTTCTCTGTCGCAATCC
	cdsSPL7stopR	R	GGTCTCACTGATTAATTCGCGTATCAATCTCATC
Cloning of SBP (SPL7) GreenGate	SBPcdsSPL7.R	R	GGTCTCACTGACTGGTCAACAGAGCATGTATTATCTT
Cloning of pSPL7 Gateway Tech	pSPL7.attB4.F	F	GGGGACAACCTTTGTATAGAAAAGTTGCTTAACCACCACCAAAGGTA
	pSPL7.attB1r.R	R	GGGGACTGCTTTTTTGTACAAAACCTGCCTGAGTCTTCTTCAATTC
Cloning of SPL7 CDS Gateway Tech	cdsSPL7.attB1.F	F	GGGGACAAGTTTGTACAAAAAAGCAGGCTTAATGCTTCTCTGTGCGAA
	SPL7NoStopB2.R	R	GGGGACCACCTTTGTACAAGAAAGCTGGGTAATTCGCGTATCAATCTC
Cloning pLAC4 GreenGate	proLAC4.F	F	GGTCTCAACCTCAACATTGTAATGGACTTGAATCT
	proLAC4.R	R	GGTCTCATGTTCCCTCTAGCTCTCTATTCTCTCT
Cloning pLAC11 GreenGate	proLAC11.F1	F	GGTCTCAACCTATAACTTTTCAAAGTCTCGACCTTTTT
	proLAC11.R1	R	GGTCTCAGTCCACAAGATTGAAAATGAAGCAT
	proLAC11.F2	F	GGTCTCTGGACTCAATTATCGATAAATCTACACAT
	proLAC11.R2	R	GGTCTCATGTTTCCCGTCAATCTTCCGGIT
Cloning pLAC17 GreenGate	proLAC17.F	F	GGTCTCAACCTGAAACAGATTTTGATTCTCTCTCAA
	proLAC17.R	R	GGTCTCATGTTTTAAGTGAAGCTTGGAAACCCG
Cloning LAC4 CDS GreenGate	cdsLAC4.F	F	GGTCTCAGGCTCCATGGGATCTCATATGGTTTGG
	cdsLAC4NoStopR	R	GGTCTCACTGAACATTTGGGAAGATCCTTAGGC
Cloning LAC11 CDS GreenGate	cdsLAC11.F	F	GGTCTCAGGCTCCATGAAGATCATCCGAGTCCCG
	cdsLAC11NoStop	R	GGTCTCACTGAGCAGCAGCGGATAGTCTTTAGG
Cloning LAC17 CDS GreenGate	cdsLAC17.F	F	GGTCTCAGGCTCCATGGCGTTTCAGCTTCTCTCT
	cdsLAC17NoStop	R	GGTCTCACTGAGCATTTGGGCAAGTCTGC
Cloning of pPER42 GreenGate	proPER42.F1	F	AACAGGTCTCAACCTTGCTTGGTATTGAATCTTTTCAGG
	proPER42.R1	R	AACAGGTCTCGTGTTCATTGAGTGCATTAGTGGACC
Cloning of pPER42 GreenGate	proPER42.F2	F	AACAGGTCTCTGACACCAAAATCCAAAACCTTGGTGAT
	proPER42.R2	R	AACAGGTCTCATGTTTTTCTCTTCTCTGCTCTCACT
Cloning of pPER49 GreenGate	proPER49.F	F	AACAGGTCTCAACCTAGACTTGGACTTTGCTACGC
	proPER49.R	R	AACAGGTCTCATGTTTACTTTCAACAAGAAGATGAGGAA
Cloning of pPER64 GreenGate	proPER64.F	F	AACAGGTCTCAACCTTGCCATTAAGAGGAGGTTACAA
	proPER64.R	R	AACAGGTCTCATGTTTTCAGCAAAATGTTTCGAAATC
Cloning of pPER66 GreenGate	proPER66.F	F	AACAGGTCTCAACCTTATTTAACGTGTAATGGGGTTTTT
	proPER66.R	R	AACAGGTCTCATGTTTTTGGATGATGCAGAAGAAGAAGC
Cloning of PER42 CDS GreenGate	cdsPER42.F	F	AACAGGTCTCAGGCTCCATGGGAGGAAAAGTTTGGATG
	cdsPER42NoStop	R	AACAGGTCTCACTGAGTGGTCTTGTGTCGAGATT
Cloning of PER49 CDS GreenGate	cdsPER49.F	F	AACAGGTCTCAGGCTCCATGGCAAGACTCACTAGCTTTC
	cdsPER49NoStop	R	AACAGGTCTCACTGAAGAGTTTATCTTCTGCAATCTTTC
Cloning of PER64 CDS GreenGate	cdsPER64.F	F	AACAGGTCTCAGGCTCCATGAATGCAAAATATACTGATCAATCTC
	cdsPER64NoStop	R	AACAGGTCTCACTGAGCGAACCTCTCTGCAATTA
Cloning of PER66 CDS GreenGate	cdsPER66.F	F	AACAGGTCTCAGGCTCCATGTCATTTCTCGAAAGGACTCA
	cdsPER66NoStop	R	AACAGGTCTCACTGAGTTGATGAAGCGAGTTTTAA
qRT-PCR Clathrin (CARHR174880)	qPCR_Clathrin_F	F	TCGATTGCTTGGTTTGGAAAGATAAGA
	qPCR_Clathrin_R	R	TCTCTCCCATTGTTGAGATCAACTC
qRT-PCR SPL7	qPCR_SPL7_F2	F	TGAAGCTCAGCCAGATGAAGG
	qPCR_SPL7_R2	R	CGTGGGAACCTGCTGCTGATT
pEC-CAS9 genotyping	CF72	F	AGCCCTAAACAGACCCACT
	CR74	R	GAATGACTCTTCGAGCCTGTG

Table 6.6: Primer sequences used for cloning, qRT-PCR and Cas9 insertion genotyping.

4.3 RNA sequencing

For RNA-sequencing of wild-type and *spl7-1* fruit valves, the valves were dissected from fruit at stage 17. RNA was extracted from approximately 15 pooled valves for each biological replicate. cDNA synthesis was performed with SuperScript III Reverse Transcriptase (Invitrogen) from the RNA samples. cDNA was subjected to sequencing using the HiSeq2500 Illumina platform at the MPIPZ Genome Centre. 20,000,000 reads were requested for each library. Three biological replicates per genotype were sequenced separately. Sample preparation, RNA extraction and cDNA synthesis were performed by Hugo Hofhuis (unpublished work).

5. Phenotypic and ionic analysis

5.1 Seed dispersal experiment

Wild-type and *lig1* plants were grown for 7 weeks, watered with collected rain water and supplemented weekly with 0.2 mM CuSO₄ (Cu limiting conditions). When siliques started to develop, 4 wild-type and 4 *lig1* plants were staked upright and moved to a cabinet with big empty tables to measure distance of seed dispersal. At this point, plant height was measured from the base to the first fruit on main stem. On average, wild-type plants were 6 cm higher than *lig1* plants (Table 6.7), therefore, pots containing *lig1* plants were placed 6 cm higher than wild-type ones. This adjustment eliminated the effect of plant height on dispersal distance. Pots were positioned at the centre of concentric rings drawn on a large sheet of plastic. Circles were drawn at increasing distance (15 cm, 25 cm and every 25 cm until 200 cm). Additionally, each plant was passed through a hole on a petri dish placed at the base of the plant to collect seeds falling directly below the plant. Set up of the experiment is shown in Figure 6.1. Plants were left to disperse seeds for 6 weeks. Following seed dispersal, seeds were collected separately from each ring and counted. The

tables that were used for the experiment had a width of only 1 m, therefore for bins of distances further than 1 m, the whole circular ring area could not be sampled (grey areas on Figure 6.1 A). For these distance rings, the percentage of area sampled with respect to total ring area was calculated and the number of seeds was corrected proportionally to the area sampled.

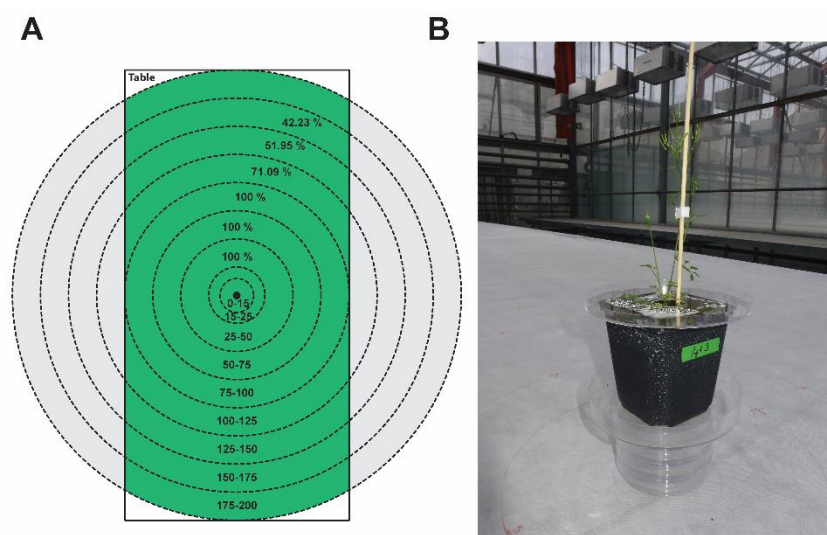


Figure 6.1: Set up of seed dispersal experiment. (A) Diagram showing set up of seed dispersal experiment. Distance bins and percentages of ring area covered in the experiment are indicated. (B) Image of a *lig1* plant staked upright and placed 6 cm above the table surface for the experiment.

Plant	Height (cm)	Plant	Height (cm)
WT-1	17	<i>lig1</i> -1	10
WT-2	16	<i>lig1</i> -2	12
WT-3	17	<i>lig1</i> -3	11
WT-4	16	<i>lig1</i> -4	9
Mean Wt	16.5	Mean <i>lig1</i>	10.5

Table 6.7: Height of plants from the base of the plant to the first fruit in the main stem when placed for the seed dispersal experiment.

5.2 Quantification of Cu concentration in fruit

Mature fruit were harvested and dried overnight in a vacuum desiccator Alpha 1-4 LSCplus (Martin Christ™). 5 to 7 fruit were pooled for each replicate. Dried fruit samples were weighed and digested with 1 mL of 67% nitric acid in a water bath at 98 °C. Digested samples were diluted by adding 9 mL of milliQ water to reach a final acid concentration of < 5 %. Empty tubes were weighed before transferring the samples. Samples were filtered into the tubes using CellTrics disposable filters of 20 µm diameter (SYSMEX) and tubes containing the samples were weighed again. Samples were analysed by Inductively Coupled Plasma Mass Spectrometry (ICP-MS) at the Mass Spectrometry platform, University of Cologne. Measurements of Cu ion content were normalized by the dilution factor of the sample using the formula: Dilution factor = weight full tube - weight empty tube/dry weight sample.

6. Microscopy materials and methods

6.1 Sectioning

Fruit or stem were embedded in 1.5 mL tubes containing 5 or 10 % low melt agarose (Hi-Pure Low agarose, biogene Ltd). Sample sectioning was performed in a Leica Vibratome VT1000 S.

6.2 Phloroglucinol/HCl staining

Samples were incubated in 2% Phloroglucinol dissolved in 95 % ethanol for 10 min, staining solution was removed and samples were treated with 10 N HCl for 1 min. Afterwards, samples were transferred to 1 N HCl solution until imaging. Samples were mounted in 1 HCl solution on slides with a cover slip. Adapted from (Mitsuda *et al.*, 2007).

6.3 Clearing of fruit cross sections

Some cross sections of fruit from LAC:mCherry transgenic lines were fixed and cleared. The protocol in (Ursache *et al.*, 2018) was followed. Fixation was performed with 4%

paraformaldehyde for 30 min to 1 hour, including 20 min vacuum treatment (in some cases). After fixation samples were cleared with ClearSee solution for 3-4 days in darkness with gentle agitation. Cleared cross sections were mounted in ClearSee solution for imaging in a CLSM.

6.4 Light microscopy imaging

Light microscopy images were taken with Zeiss Axio Imager M2 microscope using dry objectives. Images were acquired as single plane images in some cases. For other samples, a Z-stack was acquired and the built-in software ZEN 2 (Zeiss) was used to generate “Extended depth of focus” images.

6.5 Confocal microscopy

Confocal imaging was performed with a CLSM TCS SP8 (Leica) confocal microscope using dry objective HC PL FLUOTAR 10x/0.30, and water immersion objectives: HC PL APO CS2 20x/0.75; HC PL APO CS2 40x/1.10; HC PL APO CS2 63x/1.20. All images were acquired with a pinhole of 1 AU and a scanner speed of 400 Hz. Parameters used for each fluorophore are described in Table 6.8.

Fluorophore	Excitation (nm)	Emission (nm)
Lignin autofluorescence	405	440-510
GFP	488	(500-550), (492-540)
tdTomato	561	570-620
mCherry	594	600-640
Chlorophyll	488	650-730

Table 6.8: Excitation and emission parameters used for the different fluorophores.

6.6 Quantification of lignin autofluorescence

Images for lignin autofluorescence measurements were taken using a CLSM TCS SP8 (Leica). Laser line UV405 was used for excitation of lignin and autofluorescence emission was recorded in 440-510 nm range. Z-stack images were taken in 12 bit making sure that no areas were overexposed (setting visualization of maximum tones to 70% and adjusting gain and laser power

to avoid overexposed areas). Settings were adjusted for a wild-type sample first and then they were kept constant for the rest of the samples. Fiji software (Schindelin *et al.*, 2012) was used to analyse fluorescence intensity. Z-stack images were projected using the method “Sum slices”, a threshold of 950 was chosen to avoid background signal. The values of Area, Mean and Max intensity were recorded for each sample.

Bibliography

- Abdel-Ghany, S. E., Muller-Moule, P., Niyogi, K. K., Pilon, M., & Shikanai, T. (2005). Two P-type ATPases are required for copper delivery in *Arabidopsis thaliana* chloroplasts. *Plant Cell*, *17*(4), 1233-1251.
- Abdel-Ghany, S. E., & Pilon, M. (2008). MicroRNA-mediated systemic down-regulation of copper protein expression in response to low copper availability in *Arabidopsis*. *J Biol Chem*, *283*(23), 15932-15945.
- Alvim Kamei, C. L., Pieper, B., Laurent, S., Tsiantis, M., & Huijser, P. (2020). CRISPR/Cas9-Mediated Mutagenesis of RCO in *Cardamine hirsuta*. *Plants (Basel)*, *9*(2).
- Anders, S., & Huber, W. (2010). Differential expression analysis for sequence count data. *Genome Biol*, *11*(10), R106.
- Anders, S., Pyl, P. T., & Huber, W. (2015). HTSeq--a Python framework to work with high-throughput sequencing data. *Bioinformatics*, *31*(2), 166-169.
- Arioz, C., & Wittung-Stafshede, P. (2018). Folding of copper proteins: role of the metal? *Q Rev Biophys*, *51*, e4.
- Atamian, H. S., Creux, N. M., Brown, E. A., Garner, A. G., Blackman, B. K., & Harmer, S. L. (2016). Circadian regulation of sunflower heliotropism, floral orientation, and pollinator visits. *Science*, *353*(6299), 587-590.
- Barros, J., Serk, H., Granlund, I., & Pesquet, E. (2015). The cell biology of lignification in higher plants. *Ann Bot*, *115*(7), 1053-1074.
- Beer, T., & Swaine, M. D. (1977). Theory of Explosively Dispersed Seeds. *New Phytologist*, *78*(3), 681-694.
- Bernal, M., Casero, D., Singh, V., Wilson, G. T., Grande, A., Yang, H., Dodani, S. C., Pellegrini, M., Huijser, P., Connolly, E. L., Merchant, S. S., & Kramer, U. (2012). Transcriptome sequencing identifies SPL7-regulated copper acquisition genes FRO4/FRO5 and the copper dependence of iron homeostasis in *Arabidopsis*. *Plant Cell*, *24*(2), 738-761.
- Berthet, S., Demont-Caulet, N., Pollet, B., Bidzinski, P., Cezard, L., Le Bris, P., Borrega, N., Herve, J., Blondet, E., Balzergue, S., Lapierre, C., & Jouanin, L. (2011). Disruption of LACCASE4 and 17 results in tissue-specific alterations to lignification of *Arabidopsis thaliana* stems. *Plant Cell*, *23*(3), 1124-1137.
- Birkenbihl, R. P., Jach, G., Saedler, H., & Huijser, P. (2005). Functional dissection of the plant-specific SBP-domain: overlap of the DNA-binding and nuclear localization domains. *J Mol Biol*, *352*(3), 585-596.
- Bonawitz, N. D., & Chapple, C. (2010). The genetics of lignin biosynthesis: connecting genotype to phenotype. *Annu Rev Genet*, *44*, 337-363.
- Bouche, N. (2010). New insights into miR398 functions in *Arabidopsis*. *Plant Signal Behav*, *5*(6), 684-686.
- Brinkman, E. K., Chen, T., Amendola, M., & van Steensel, B. (2014). Easy quantitative assessment of genome editing by sequence trace decomposition. *Nucleic Acids Res*, *42*(22), e168.
- Burkhead, J. L., Reynolds, K. A., Abdel-Ghany, S. E., Cohu, C. M., & Pilon, M. (2009). Copper homeostasis. *New Phytol*, *182*(4), 799-816.
- Carr, H. S., & Winge, D. R. (2003). Assembly of cytochrome c oxidase within the mitochondrion. *Acc Chem Res*, *36*(5), 309-316.

- Chmielowska, J., Deckert, J., & Diaz, J. (2009). Activity of peroxidases and phenylalanine ammonia-lyase in lupine and soybean seedlings treated with copper and an ethylene inhibitor. *BIOLOGICAL LETTERS*, 45, 59-67.
- Clough, S. J., & Bent, A. F. (1998). Floral dip: a simplified method for *Agrobacterium*-mediated transformation of *Arabidopsis thaliana*. *Plant J*, 16(6), 735-743.
- Coen, E. S., & Meyerowitz, E. M. (1991). The war of the whorls: genetic interactions controlling flower development. *Nature*, 353(6339), 31-37.
- Cosgrove, D. J. (2005). Growth of the plant cell wall. *Nat Rev Mol Cell Biol*, 6(11), 850-861.
- Cosgrove, D. J. (2018). Primary walls in second place. *Nat Plants*, 4(10), 748-749.
- Dawson, J., Vincent, J. F. V., & Rocca, A. M. (1997). How pine cones open. *Nature*, 390(6661), 668-668.
- Dell, B. (1980). Male Sterility and Anther Wall Structure in Copper-deficient Plants. *Ann. Bot.*, 48, 599-608.
- Dinneny, J. R., Weigel, D., & Yanofsky, M. F. (2005). A genetic framework for fruit patterning in *Arabidopsis thaliana*. *Development*, 132(21), 4687-4696.
- Downes, G. M., Ward, J. V., & Turvey, N. D. (1991). Lignin Distribution across Tracheid Cell-Walls of Poorly Lignified Wood from Deformed Copper Deficient *Pinus-Radiata* (D Don). *Wood Science and Technology*, 25(1), 7-14.
- Eriksson, M., Moseley, J. L., Tottey, S., Del Campo, J. A., Quinn, J., Kim, Y., & Merchant, S. (2004). Genetic dissection of nutritional copper signaling in *Chlamydomonas* distinguishes regulatory and target genes. *Genetics*, 168(2), 795-807.
- Fausser, F., Schiml, S., & Puchta, H. (2014). Both CRISPR/Cas-based nucleases and nickases can be used efficiently for genome engineering in *Arabidopsis thaliana*. *Plant J*, 79(2), 348-359.
- Fernandez-Perez, F., Pomar, F., Pedreno, M. A., & Novo-Uzal, E. (2015). Suppression of *Arabidopsis* peroxidase 72 alters cell wall and phenylpropanoid metabolism. *Plant Sci*, 239, 192-199.
- Ferrández, C. (2011). Fruit structure and diversity. In *Encyclopedia of Life Sciences (ELS)*
- Forterre, Y. (2013). Slow, fast and furious: understanding the physics of plant movements. *J Exp Bot*, 64(15), 4745-4760.
- Forterre, Y., Skotheim, J. M., Dumais, J., & Mahadevan, L. (2005). How the Venus flytrap snaps. *Nature*, 433(7024), 421-425.
- Fujita, S., De Bellis, D., Edel, K. H., Koster, P., Andersen, T. G., Schmid-Siegert, E., Denervaud Tendon, V., Pfister, A., Marhavy, P., Ursache, R., Doblaz, V. G., Barberon, M., Daraspe, J., Creff, A., Ingram, G., Kudla, J., & Geldner, N. (2020). SCHENGEN receptor module drives localized ROS production and lignification in plant roots. *EMBO J*, 39(9), e103894.
- Galinha, C., Hofhuis, H., Luijten, M., Willemsen, V., Blilou, I., Heidstra, R., & Scheres, B. (2007). PLETHORA proteins as dose-dependent master regulators of *Arabidopsis* root development. *Nature*, 449(7165), 1053-1057.
- Gan, X., Hay, A., Kwantes, M., Haberer, G., Hallab, A., Ioio, R. D., Hofhuis, H., Pieper, B., Cartolano, M., Neumann, U., Nikolov, L. A., Song, B., Hajheidari, M., Briskine, R., Kougioumoutzi, E., Vlad, D., Broholm, S., Hein, J., Meksem, K., Lightfoot, D., Shimizu, K. K., Shimizu-Inatsugi, R., Imprialou, M., Kudrna, D., Wing, R., Sato, S., Huijser, P., Filatov, D., Mayer, K. F., Mott, R., & Tsiantis, M. (2016). The *Cardamine hirsuta* genome offers insight into the evolution of morphological diversity. *Nat Plants*, 2(11), 16167.

- Garcia-Molina, A., Xing, S., & Huijser, P. (2014a). A conserved KIN17 curved DNA-binding domain protein assembles with SQUAMOSA PROMOTER-BINDING PROTEIN-LIKE7 to adapt Arabidopsis growth and development to limiting copper availability. *Plant Physiol*, *164*(2), 828-840.
- Garcia-Molina, A., Xing, S., & Huijser, P. (2014b). Functional characterisation of Arabidopsis SPL7 conserved protein domains suggests novel regulatory mechanisms in the Cu deficiency response. *BMC Plant Biol*, *14*, 231.
- Geitmann, A. (2016). Actuators Acting without Actin. *Cell*, *166*(1), 15-17.
- Guo, A. Y., Zhu, Q. H., Gu, X., Ge, S., Yang, J., & Luo, J. (2008). Genome-wide identification and evolutionary analysis of the plant specific SBP-box transcription factor family. *Gene*, *418*(1-2), 1-8.
- Halliwell, B., & Gutteridge, J. M. (1984). Oxygen toxicity, oxygen radicals, transition metals and disease. *Biochem J*, *219*(1), 1-14.
- Hamilton, W. D., & May, R. M. (1977). Dispersal in Stable Habitats. *Nature*, *269*(5629), 578-581.
- Hansch, R., & Mendel, R. R. (2009). Physiological functions of mineral micronutrients (Cu, Zn, Mn, Fe, Ni, Mo, B, Cl). *Current Opinion in Plant Biology*, *12*(3), 259-266.
- Hay, A., & Tsiantis, M. (2006). The genetic basis for differences in leaf form between Arabidopsis thaliana and its wild relative Cardamine hirsuta. *Nat Genet*, *38*(8), 942-947.
- Hay, A. S., Pieper, B., Cooke, E., Mandakova, T., Cartolano, M., Tattersall, A. D., Ioio, R. D., McGowan, S. J., Barkoulas, M., Galinha, C., Rast, M. I., Hofhuis, H., Then, C., Plieske, J., Ganal, M., Mott, R., Martinez-Garcia, J. F., Carine, M. A., Scotland, R. W., Gan, X., Filatov, D. A., Lysak, M. A., & Tsiantis, M. (2014). Cardamine hirsuta: a versatile genetic system for comparative studies. *Plant J*, *78*(1), 1-15.
- Herrero, J., Fernandez-Perez, F., Yebra, T., Novo-Uzal, E., Pomar, F., Pedreno, M. A., Cuello, J., Guera, A., Esteban-Carrasco, A., & Zapata, J. M. (2013). Bioinformatic and functional characterization of the basic peroxidase 72 from Arabidopsis thaliana involved in lignin biosynthesis. *Planta*, *237*(6), 1599-1612.
- Hoffmann, N., Benske, A., Betz, H., Schuetz, M., & Samuels, A. L. (2020). Laccases and peroxidases co-localize in lignified secondary cell walls throughout stem development. *Plant Physiol*.
- Hofhuis, H., & Hay, A. (2017). Explosive seed dispersal. *New Phytol*, *216*(2), 339-342.
- Hofhuis, H., Moulton, D., Lessinnes, T., Routier-Kierzkowska, A. L., Bomphrey, R. J., Mosca, G., Reinhardt, H., Sarchet, P., Gan, X., Tsiantis, M., Ventikos, Y., Walker, S., Goriely, A., Smith, R., & Hay, A. (2016). Morphomechanical Innovation Drives Explosive Seed Dispersal. *Cell*, *166*(1), 222-233.
- Hruz, T., Laule, O., Szabo, G., Wessendorp, F., Bleuler, S., Oertle, L., Widmayer, P., Gruissem, W., & Zimmermann, P. (2008). Genevestigator v3: a reference expression database for the meta-analysis of transcriptomes. *Adv Bioinformatics*, *2008*, 420747.
- Huijser, P., & Schmid, M. (2011). The control of developmental phase transitions in plants. *Development*, *138*(19), 4117-4129.
- Jung, H. I., Gayomba, S. R., Rutzke, M. A., Craft, E., Kochian, L. V., & Vatamaniuk, O. K. (2012). COPT6 is a plasma membrane transporter that functions in copper homeostasis in Arabidopsis and is a novel target of SQUAMOSA promoter-binding protein-like 7. *J Biol Chem*, *287*(40), 33252-33267.
- Karam, G. N. (2005). Biomechanical model of the xylem vessels in vascular plants. *Ann Bot*, *95*(7), 1179-1186.

- Kierzkowski, D., Runions, A., Vuolo, F., Strauss, S., Lymbouridou, R., Routier-Kierzkowska, A. L., Wilson-Sanchez, D., Jenke, H., Galinha, C., Mosca, G., Zhang, Z., Canales, C., Dello Iorio, R., Huijser, P., Smith, R. S., & Tsiantis, M. (2019). A Growth-Based Framework for Leaf Shape Development and Diversity. *Cell*, *177*(6), 1405-1418 e1417.
- Kim, D., Pertea, G., Trapnell, C., Pimentel, H., Kelley, R., & Salzberg, S. L. (2013). TopHat2: accurate alignment of transcriptomes in the presence of insertions, deletions and gene fusions. *Genome Biol*, *14*(4), R36.
- Klein, J., Saedler, H., & Huijser, P. (1996). A new family of DNA binding proteins includes putative transcriptional regulators of the *Antirrhinum majus* floral meristem identity gene SQUAMOSA. *Mol Gen Genet*, *250*(1), 7-16.
- Knox, J. P. (2008). Revealing the structural and functional diversity of plant cell walls. *Curr Opin Plant Biol*, *11*(3), 308-313.
- Kosugi, S., Hasebe, M., Tomita, M., & Yanagawa, H. (2009). Systematic identification of cell cycle-dependent yeast nucleocytoplasmic shuttling proteins by prediction of composite motifs. *Proc Natl Acad Sci U S A*, *106*(25), 10171-10176.
- Kropat, J., Tottey, S., Birkenbihl, R. P., Depege, N., Huijser, P., & Merchant, S. (2005). A regulator of nutritional copper signaling in *Chlamydomonas* is an SBP domain protein that recognizes the GTAC core of copper response element. *Proc Natl Acad Sci U S A*, *102*(51), 18730-18735.
- Kumar, M., Campbell, L., & Turner, S. (2016). Secondary cell walls: biosynthesis and manipulation. *J Exp Bot*, *67*(2), 515-531.
- Labun, K., Montague, T. G., Gagnon, J. A., Thyme, S. B., & Valen, E. (2016). CHOPCHOP v2: a web tool for the next generation of CRISPR genome engineering. *Nucleic Acids Res*, *44*(W1), W272-276.
- Laitinen, T., Morreel, K., Delhomme, N., Gauthier, A., Schiffthaler, B., Nickolov, K., Brader, G., Lim, K. J., Teeri, T. H., Street, N. R., Boerjan, W., & Karkonen, A. (2017). A Key Role for Apoplastic H₂O₂ in Norway Spruce Phenolic Metabolism. *Plant Physiol*, *174*(3), 1449-1475.
- Lampropoulos, A., Sutikovic, Z., Wenzl, C., Maegele, I., Lohmann, J. U., & Forner, J. (2013). GreenGate---a novel, versatile, and efficient cloning system for plant transgenesis. *PLoS One*, *8*(12), e83043.
- Lee, Y., Rubio, M. C., Alassimone, J., & Geldner, N. (2013). A mechanism for localized lignin deposition in the endodermis. *Cell*, *153*(2), 402-412.
- Lee, Y., Yoon, T. H., Lee, J., Jeon, S. Y., Lee, J. H., Lee, M. K., Chen, H., Yun, J., Oh, S. Y., Wen, X., Cho, H. K., Mang, H., & Kwak, J. M. (2018). A Lignin Molecular Brace Controls Precision Processing of Cell Walls Critical for Surface Integrity in Arabidopsis. *Cell*, *173*(6), 1468-1480 e1469.
- Levin, S. A., Muller-Landau, H. C., Nathan, R., & Chave, J. (2003). The ecology and evolution of seed dispersal: A theoretical perspective. *Annual Review of Ecology Evolution and Systematics*, *34*, 575-604.
- Liang, M., Davis, E., Gardner, D., Cai, X., & Wu, Y. (2006). Involvement of AtLAC15 in lignin synthesis in seeds and in root elongation of Arabidopsis. *Planta*, *224*(5), 1185-1196.
- Lin, C. C., Chen, L. M., & Liu, Z. H. (2005). Rapid effect of copper on lignin biosynthesis in soybean roots. *Plant Science*, *168*(3), 855-861.
- Lin, S. S., Chen, Y., & Lu, M. J. (2019). Degradome Sequencing in Plants. *Methods Mol Biol*, *1932*, 197-213.
- Liu, Q., Luo, L., & Zheng, L. (2018). Lignins: Biosynthesis and Biological Functions in Plants. *Int J Mol Sci*, *19*(2).

- Liu, Q., Zheng, L., He, F., Zhao, F., Shen, Z., & Zheng, L. (2014). Transcriptional and physiological analyses identify a regulatory role for hydrogen peroxide in the lignin biosynthesis of copper-stressed rice roots. *Plant and soil*(387), 323-336.
- Lynd, L. R. (2017). The grand challenge of cellulosic biofuels. *Nat Biotechnol*, 35(10), 912-915.
- McCaig, B. C., Meagher, R. B., & Dean, J. F. (2005). Gene structure and molecular analysis of the laccase-like multicopper oxidase (LMCO) gene family in *Arabidopsis thaliana*. *Planta*, 221(5), 619-636.
- McKim, S. M., Routier-Kierzkowska, A. L., Monniaux, M., Kierzkowski, D., Pieper, B., Smith, R. S., Tsiantis, M., & Hay, A. (2017). Seasonal Regulation of Petal Number. *Plant Physiol*, 175(2), 886-903.
- Mengel, K., Kirkby, E. A., Kosegarten, H., & Appel, T. (2001). Soil Copper. In K. Mengel, E. A. Kirkby, H. Kosegarten, & T. Appel (Eds.), *Principles of Plant Nutrition* (pp. 599-611). Dordrecht: Springer Netherlands.
- Mitsuda, N., Iwase, A., Yamamoto, H., Yoshida, M., Seki, M., Shinozaki, K., & Ohme-Takagi, M. (2007). NAC transcription factors, NST1 and NST3, are key regulators of the formation of secondary walls in woody tissues of *Arabidopsis*. *Plant Cell*, 19(1), 270-280.
- Monniaux, M., Pieper, B., McKim, S. M., Routier-Kierzkowska, A. L., Kierzkowski, D., Smith, R. S., & Hay, A. (2018). The role of APETALA1 in petal number robustness. *Elife*, 7.
- Moore, I., Samalova, M., & Kurup, S. (2006). Transactivated and chemically inducible gene expression in plants. *Plant J*, 45(4), 651-683.
- Naseer, S., Lee, Y., Lapierre, C., Franke, R., Nawrath, C., & Geldner, N. (2012). Casparian strip diffusion barrier in *Arabidopsis* is made of a lignin polymer without suberin. *Proc Natl Acad Sci U S A*, 109(25), 10101-10106.
- Nathan, R. (2006). Long-distance dispersal of plants. *Science*, 313(5788), 786-788.
- Neumann, U., & Hay, A. (2020). Seed coat development in explosively dispersed seeds of *Cardamine hirsuta*. *Ann Bot*, 126(1), 39-59.
- Nikolov, L. A., & Tsiantis, M. (2015). Interspecies Gene Transfer as a Method for Understanding the Genetic Basis for Evolutionary Change: Progress, Pitfalls, and Prospects. *Front Plant Sci*, 6, 1135.
- O'Malley, R. C., & Ecker, J. R. (2010). Linking genotype to phenotype using the *Arabidopsis* unimutant collection. *Plant J*, 61(6), 928-940.
- O'Brien, T. P., Feder, N., & McCully, M. E. (1964). Polychromatic Staining of Plant Cell Walls by Toluidine Blue O. *Protoplasma*, 59(2), 368-&.
- Penarrubia, L., Romero, P., Carrio-Segui, A., Andres-Borderia, A., Moreno, J., & Sanz, A. (2015). Temporal aspects of copper homeostasis and its crosstalk with hormones. *Front Plant Sci*, 6, 255.
- Pesquet, E., Zhang, B., Gorzsas, A., Puhakainen, T., Serk, H., Escamez, S., Barbier, O., Gerber, L., Courtois-Moreau, C., Alatalo, E., Paulin, L., Kangasjarvi, J., Sundberg, B., Goffner, D., & Tuominen, H. (2013). Non-cell-autonomous postmortem lignification of tracheary elements in *Zinnia elegans*. *Plant Cell*, 25(4), 1314-1328.
- Pfaffl, M. W. (2001). A new mathematical model for relative quantification in real-time RT-PCR. *Nucleic Acids Res*, 29(9), e45.
- Pijl, L. v. d. (1972). *Principles of dispersal in higher plants* (2nd ed.). Berlin, New York etc.: Springer-Verlag.
- Printz, B., Lutts, S., Hausman, J. F., & Sergeant, K. (2016). Copper Trafficking in Plants and Its Implication on Cell Wall Dynamics. *Front Plant Sci*, 7, 601.

- Quinn, J. M., & Merchant, S. (1995). Two copper-responsive elements associated with the *Chlamydomonas* Cyc6 gene function as targets for transcriptional activators. *Plant Cell*, 7(5), 623-628.
- Ragauskas, A. J., & Yoo, C. G. (2018). Editorial: Advancements in Biomass Recalcitrance: The Use of Lignin for the Production of Fuels and Chemicals. *Frontiers in Energy Research*, 6.
- Rajani, S., & Sundaresan, V. (2001). The Arabidopsis myc/bHLH gene ALCATRAZ enables cell separation in fruit dehiscence. *Curr Biol*, 11(24), 1914-1922.
- Rodriguez, F. I., Esch, J. J., Hall, A. E., Binder, B. M., Schaller, G. E., & Bleeker, A. B. (1999). A copper cofactor for the ethylene receptor ETR1 from Arabidopsis. *Science*, 283(5404), 996-998.
- Roeder, A. H., & Yanofsky, M. F. (2006). Fruit development in Arabidopsis. *Arabidopsis Book*, 4, e0075.
- Rojas-Murcia, N., Hématy, K., Lee, Y., Emonet, A., Ursache, R., Fujita, S., De Bellis, D., & Geldner, N. (2020). High-order mutants reveal an essential requirement for peroxidases but not laccases in Casparian strip lignification. 2020.2006.2017.154617.
- Roppolo, D., De Rybel, B., Denervaud Tendon, V., Pfister, A., Alassimone, J., Vermeer, J. E., Yamazaki, M., Stierhof, Y. D., Beeckman, T., & Geldner, N. (2011). A novel protein family mediates Casparian strip formation in the endodermis. *Nature*, 473(7347), 380-383.
- Sato, Y., Demura, T., Yamawaki, K., Inoue, Y., Sato, S., Sugiyama, M., & Fukuda, H. (2006). Isolation and characterization of a novel peroxidase gene ZPO-C whose expression and function are closely associated with lignification during tracheary element differentiation. *Plant Cell Physiol*, 47(4), 493-503.
- Schindelin, J., Arganda-Carreras, I., Frise, E., Kaynig, V., Longair, M., Pietzsch, T., Preibisch, S., Rueden, C., Saalfeld, S., Schmid, B., Tinevez, J. Y., White, D. J., Hartenstein, V., Eliceiri, K., Tomancak, P., & Cardona, A. (2012). Fiji: an open-source platform for biological-image analysis. *Nat Methods*, 9(7), 676-682.
- Schneeberger, K. (2014). Using next-generation sequencing to isolate mutant genes from forward genetic screens. *Nat Rev Genet*, 15(10), 662-676.
- Schuetz, M., Benske, A., Smith, R. A., Watanabe, Y., Tobimatsu, Y., Ralph, J., Demura, T., Ellis, B., & Samuels, A. L. (2014). Laccases direct lignification in the discrete secondary cell wall domains of protoxylem. *Plant Physiol*, 166(2), 798-807.
- Schulten, A., Bytomski, L., Quintana, J., Bernal, M., & Kramer, U. (2019). Do Arabidopsis Squamosa promoter binding Protein-Like genes act together in plant acclimation to copper or zinc deficiency? *Plant Direct*, 3(7), e00150.
- Schulten, A., & Krämer, U. (2017). Interactions Between Copper Homeostasis and Metabolism in Plants. In F. M. Cánovas, U. Lüttge, & R. Matyssek (Eds.), *Progress in Botany Vol. 79* (pp. 111-146). Cham: Springer International Publishing.
- Shigeto, J., Itoh, Y., Hirao, S., Ohira, K., Fujita, K., & Tsutsumi, Y. (2015). Simultaneously disrupting AtPrx2, AtPrx25 and AtPrx71 alters lignin content and structure in Arabidopsis stem. *J Integr Plant Biol*, 57(4), 349-356.
- Shigeto, J., Kiyonaga, Y., Fujita, K., Kondo, R., & Tsutsumi, Y. (2013). Putative cationic cell-wall-bound peroxidase homologues in Arabidopsis, AtPrx2, AtPrx25, and AtPrx71, are involved in lignification. *J Agric Food Chem*, 61(16), 3781-3788.
- Skotheim, J. M., & Mahadevan, L. (2005). Physical limits and design principles for plant and fungal movements. *Science*, 308(5726), 1308-1310.

- Smith, R. A., Schuetz, M., Roach, M., Mansfield, S. D., Ellis, B., & Samuels, L. (2013). Neighboring parenchyma cells contribute to Arabidopsis xylem lignification, while lignification of interfascicular fibers is cell autonomous. *Plant Cell*, 25(10), 3988-3999.
- Sommer, F., Kropat, J., Malasarn, D., Grosseohme, N. E., Chen, X., Giedroc, D. P., & Merchant, S. S. (2010). The CRR1 nutritional copper sensor in Chlamydomonas contains two distinct metal-responsive domains. *Plant Cell*, 22(12), 4098-4113.
- Spence, J., Vercher, Y., Gates, P., & Harris, N. (1996). 'Pod shatter' in Arabidopsis thaliana, Brassica napus and B-juncaea. *Journal of Microscopy-Oxford*, 181, 195-203.
- Swetha, C., Basu, D., Pachamuthu, K., Tirumalai, V., Nair, A., Prasad, M., & Shivaprasad, P. V. (2018). Major Domestication-Related Phenotypes in Indica Rice Are Due to Loss of miRNA-Mediated Laccase Silencing. *Plant Cell*, 30(11), 2649-2662.
- The Gene Ontology, C. (2019). The Gene Ontology Resource: 20 years and still GOing strong. *Nucleic Acids Res*, 47(D1), D330-D338.
- Tobimatsu, Y., & Schuetz, M. (2019). Lignin polymerization: how do plants manage the chemistry so well? *Curr Opin Biotechnol*, 56, 75-81.
- Tognolli, M., Penel, C., Greppin, H., & Simon, P. (2002). Analysis and expression of the class III peroxidase large gene family in Arabidopsis thaliana. *Gene*, 288(1-2), 129-138.
- Tottey, S., Waldron, K. J., Firbank, S. J., Reale, B., Bessant, C., Sato, K., Cheek, T. R., Gray, J., Banfield, M. J., Dennison, C., & Robinson, N. J. (2008). Protein-folding location can regulate manganese-binding versus copper- or zinc-binding. *Nature*, 455(7216), 1138-1142.
- Ursache, R., Andersen, T. G., Marhavy, P., & Geldner, N. (2018). A protocol for combining fluorescent proteins with histological stains for diverse cell wall components. *Plant J*, 93(2), 399-412.
- Vlad, D., Kierzkowski, D., Rast, M. I., Vuolo, F., Dello Ioio, R., Galinha, C., Gan, X., Hajheidari, M., Hay, A., Smith, R. S., Huijser, P., Bailey, C. D., & Tsiantis, M. (2014). Leaf shape evolution through duplication, regulatory diversification, and loss of a homeobox gene. *Science*, 343(6172), 780-783.
- Wang, C. Y., Zhang, S., Yu, Y., Luo, Y. C., Liu, Q., Ju, C., Zhang, Y. C., Qu, L. H., Lucas, W. J., Wang, X., & Chen, Y. Q. (2014). MiR397b regulates both lignin content and seed number in Arabidopsis via modulating a laccase involved in lignin biosynthesis. *Plant Biotechnol J*, 12(8), 1132-1142.
- Wang, J., Feng, J., Jia, W., Chang, S., Li, S., & Li, Y. (2015). Lignin engineering through laccase modification: a promising field for energy plant improvement. *Biotechnol Biofuels*, 8, 145.
- Wang, J. W., Czech, B., & Weigel, D. (2009). miR156-regulated SPL transcription factors define an endogenous flowering pathway in Arabidopsis thaliana. *Cell*, 138(4), 738-749.
- Wang, Z. P., Xing, H. L., Dong, L., Zhang, H. Y., Han, C. Y., Wang, X. C., & Chen, Q. J. (2015). Egg cell-specific promoter-controlled CRISPR/Cas9 efficiently generates homozygous mutants for multiple target genes in Arabidopsis in a single generation. *Genome Biol*, 16, 144.
- Weigel, M., Varotto, C., Pesaresi, P., Finazzi, G., Rappaport, F., Salamini, F., & Leister, D. (2003). Plastocyanin is indispensable for photosynthetic electron flow in Arabidopsis thaliana. *J Biol Chem*, 278(33), 31286-31289.
- Welinder, K. G., Justesen, A. F., Kjaersgard, I. V., Jensen, R. B., Rasmussen, S. K., Jespersen, H. M., & Duroux, L. (2002). Structural diversity and transcription of class III peroxidases from Arabidopsis thaliana. *Eur J Biochem*, 269(24), 6063-6081.

- Weng, J. K., & Chapple, C. (2010). The origin and evolution of lignin biosynthesis. *New Phytol*, *187*(2), 273-285.
- Willis, C. G., Hall, J. C., Rubio de Casas, R., Wang, T. Y., & Donohue, K. (2014). Diversification and the evolution of dispersal ability in the tribe Brassiceae (Brassicaceae). *Ann Bot*, *114*(8), 1675-1686.
- Wu, G., Park, M. Y., Conway, S. R., Wang, J. W., Weigel, D., & Poethig, R. S. (2009). The sequential action of miR156 and miR172 regulates developmental timing in Arabidopsis. *Cell*, *138*(4), 750-759.
- Xing, S., Salinas, M., Hohmann, S., Berndtgen, R., & Huijser, P. (2010). miR156-targeted and nontargeted SBP-box transcription factors act in concert to secure male fertility in Arabidopsis. *Plant Cell*, *22*(12), 3935-3950.
- Yamasaki, H., Abdel-Ghany, S. E., Cohu, C. M., Kobayashi, Y., Shikanai, T., & Pilon, M. (2007). Regulation of copper homeostasis by micro-RNA in Arabidopsis. *J Biol Chem*, *282*(22), 16369-16378.
- Yamasaki, H., Hayashi, M., Fukazawa, M., Kobayashi, Y., & Shikanai, T. (2009). SQUAMOSA Promoter Binding Protein-Like7 Is a Central Regulator for Copper Homeostasis in Arabidopsis. *Plant Cell*, *21*(1), 347-361.
- Yamasaki, K., Kigawa, T., Inoue, M., Tateno, M., Yamasaki, T., Yabuki, T., Aoki, M., Seki, E., Matsuda, T., Nunokawa, E., Ishizuka, Y., Terada, T., Shirouzu, M., Osanai, T., Tanaka, A., Seki, M., Shinozaki, K., & Yokoyama, S. (2004). A novel zinc-binding motif revealed by solution structures of DNA-binding domains of Arabidopsis SBP-family transcription factors. *J Mol Biol*, *337*(1), 49-63.
- Yang, G. D., Yan, K., Wu, B. J., Wang, Y. H., Gao, Y. X., & Zheng, C. C. (2012). Genomewide analysis of intronic microRNAs in rice and Arabidopsis. *J Genet*, *91*(3), 313-324.
- Yi Chou, E., Schuetz, M., Hoffmann, N., Watanabe, Y., Sibout, R., & Samuels, A. L. (2018). Distribution, mobility, and anchoring of lignin-related oxidative enzymes in Arabidopsis secondary cell walls. *J Exp Bot*, *69*(8), 1849-1859.
- Yruela, I. (2013). Transition metals in plant photosynthesis. *Metallomics*, *5*(9), 1090-1109.
- Zhang, H., Zhao, X., Li, J., Cai, H., Deng, X. W., & Li, L. (2014). MicroRNA408 is critical for the HY5-SPL7 gene network that mediates the coordinated response to light and copper. *Plant Cell*, *26*(12), 4933-4953.
- Zhang, S. D., Ling, L. Z., & Yi, T. S. (2015). Evolution and divergence of SBP-box genes in land plants. *BMC Genomics*, *16*, 787.
- Zhao, Q., & Dixon, R. A. (2011). Transcriptional networks for lignin biosynthesis: more complex than we thought? *Trends Plant Sci*, *16*(4), 227-233.
- Zhao, Q., Nakashima, J., Chen, F., Yin, Y., Fu, C., Yun, J., Shao, H., Wang, X., Wang, Z. Y., & Dixon, R. A. (2013). Laccase is necessary and nonredundant with peroxidase for lignin polymerization during vascular development in Arabidopsis. *Plant Cell*, *25*(10), 3976-3987.
- Zoghalmi, A., & Paes, G. (2019). Lignocellulosic Biomass: Understanding Recalcitrance and Predicting Hydrolysis. *Frontiers in Chemistry*, *7*.

Supplementary figures

Dataset: 10 developmental stages from data selection: AT_AFFY_ATH1-0
Showing 1 measure(s) of 1 gene(s) on selection: AT-0

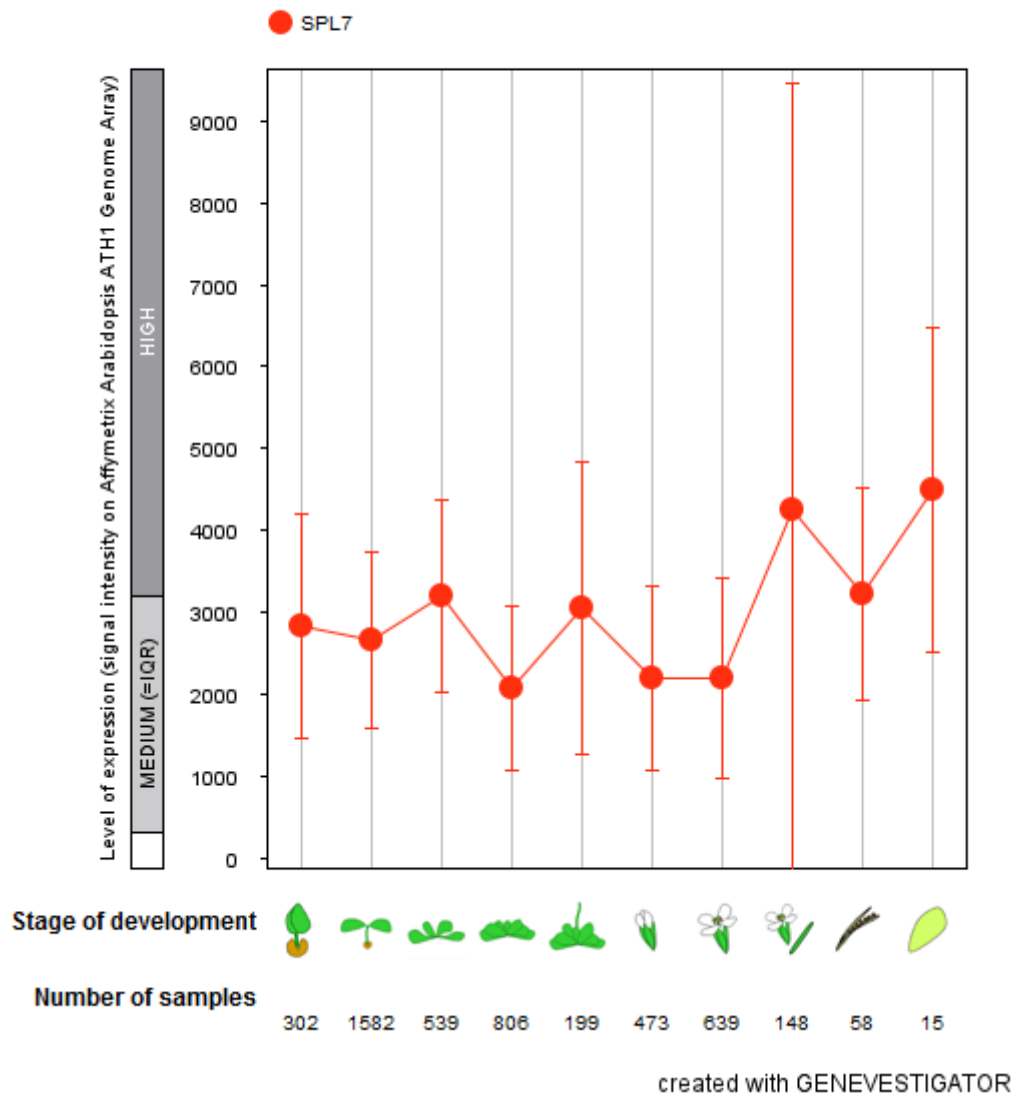


Figure S1: *SPL7* expression across developmental stages in *A. thaliana*. Gene expression screened by Genevestigator with data from genome array (Hruz *et al.*, 2008). The expression value indicated for a given stage of development is the average of expression of all samples annotated as such developmental stage. Only wild-type genotypes were considered.

List of abbreviations

<i>A. thaliana</i>	Arabidopsis thaliana
bp	base pair
<i>C. hirsuta</i>	Cardamine hirsuta
CDS	Coding sequence
CLSM	Confocal laser scanning microscopy
cM	centi Morgan
Col-0	Columbia 0 strain
dCAPS	Derived Cleaved Amplified Polymorphic Sequences
EMS	ethyl methane sulphonate
FPKM	Fragments per kilobase per million mapped fragments
MS	Murashige & Skoog
<i>lig1, lig2</i>	<i>less lignin 1, 2</i>
Ox	Oxford strain
PAM	Protospacer adjacent motif
PCR	Polymerase chain reaction
SBP	SQUAMOSA PROMOTER BINDING PROTEIN
sgRNA	Single guide RNA
<i>SPL</i>	<i>SQUAMOSA-PROMOTER BINDING PROTEIN-LIKE</i> gene Family
SNP	Single-Nucleotide Polymorphism
T1, T2, T3	Generation of transformed seeds

Acknowledgements

First, I want to thank Dr. Angela Hay for her great guidance and support during my PhD. Thank you for sharing your knowledge and for being always positive with my work.

I would like to thank my thesis committee members Prof. Dr. Ute Höcker, Prof. Dr. Siegfried Roth and specially Dr. Peter Huijser for all the help and discussions about *SPL7*, microscopy, etc. I want to thank also Dr. Stephan Wagner for all his support as PhD coordinator.

I want to thank Prof. Dr. Miltos Tsiantis for leading a very scientifically stimulating department, Dr. Sabine Metzger for the ICP-MS measurements and Dr. Xiangchao Gan for the bioinformatic help. Also, I want to thank Dr. Hugo Hofhuis and Dr. Penny Sarchet who first examined the *lig1* mutant. I also want to use this opportunity to thank Aristeidis for his help, the greenhouse team, media staff and the workers who are essential for the institute.

It has been great to work in the Hay group. I would like to thank past and present members of the group for all their help, discussions, cake meetings, berry harvestings and lunch times (Anahit, Wolfram, Léa...). It has been a great experience to work together with several students during my PhD: thanks a lot to Ilsa Schneider and Patrizia Kroll for their great work and contribution to the project. Also, to Jenna Krumbach and Bianca Bohmeier.

I would like to thank also the people in the Tsiantis department and specially Chidi, Shanda, Aleksandra, Lukas (gracias por la traducción), Cristina and Francesco. A very very special thanks to Luke for his mentoring spirit and all the guidance.

I want to thank the people from EHKurdigungs, garden, Spaniards, basketball, bouldering... for making the time here very nice and fun! You are many! También a los que están más lejos, Fran, Héctor, Víctor, Sergio, Irene, Álex, Carmen...

Muchas gracias a mi madre y a mi padre por hacer de mi educación una prioridad, por apoyarme en mis ilusiones y por recordarme siempre las cosas que de verdad importan. Gracias a mis hermanas por ser las mejores del mundo. Por leerme la lección mientras estaba dormido, por las aventuras en Salamanca, Alemania, Granada... Gracias a Angelita por iniciarme en los experimentos explosivos. Muchas gracias a toda la familia!

Quiero dar las gracias a Paloma por su ayuda y por todo el tiempo que estamos compartiendo. ¡Sí que ha merecido la pena venir!

Contribution acknowledgements

Penny Sarchet identified the *lig1* mutant in an EMS mutagenesis screen and performed the first phenotype examinations. Hugo Hofhuis generated the mapping cross of *lig1* with the Nz accession and phenotyped a F₂ segregating population that I later genotyped for fine mapping the causal mutation. H. Hofhuis extracted DNA from the segregating population and prepared the libraries for DNaseq. Xiangchao Gan run the bioinformatics pipeline to analyse the DNaseq data and generated a table of SNPs with linkage values. H. hofhuis extracted the RNA from *lig1* and wild type and prepared the cDNA libraries for the RNA-seq experiment. Xiangchao Gan run the bioinformatics pipeline to analyse the RNAseq output and generated a table of differentially expressed genes. I interpreted and further analyse data from this RNAseq. Sabine Metzger (UoC) run the Cu measurements samples in the ICP-MS platform at the UoC and provided the Cu measurements as concentration values. Patrizia Kroll contributed to establish the aeroponics system. P. Kroll performed the sample preparations for Cu measurements of the plants grown in the aeroponics system and for the *SPL7* transgenic plants carrying different numbers of *SPL7* copies. P. Kroll performed the *SPL7* expression analysis by qRT-PCR for the *SPL7* transgenic plants carrying different *SPL7* copies. Patrizia Kroll performed these experiments as part of the MSc thesis.

Erklärung

"Ich versichere, dass ich die von mir vorgelegte Dissertation selbständig angefertigt, die benutzten Quellen und Hilfsmittel vollständig angegeben und die Stellen der Arbeit – einschließlich Tabellen, Karten und Abbildungen –, die anderen Werken im Wortlaut oder dem Sinn nach entnommen sind, in jedem Einzelfall als Entlehnung kenntlich gemacht habe; dass diese Dissertation noch keiner anderen Fakultät oder Universität zur Prüfung vorgelegen hat; dass sie – abgesehen von unten angegebenen Teilpublikationen – noch nicht veröffentlicht worden ist, sowie, dass ich eine solche Veröffentlichung vor Abschluss des Promotionsverfahrens nicht vornehmen werde. Die Bestimmungen der Promotionsordnung sind mir bekannt. Die von mir vorgelegte Dissertation ist von Dr. Angela Hay betreut worden."

Köln, 21.09.2020

Curriculum vitae

Persönliche Daten

Name Miguel Pérez Antón
Email perez@mpipz.mpg.de
Anschrift Venloer Straße 628, 50827, Köln
Geboren am 28.04.1990 in Burgos
Staatsangehörigkeit Spanische

Akademische Ausbildung

Seit 2016.10 **Promotionsstudent** am Max-Planck-Institut für Pflanzenzüchtungsforschung, Köln, (Deutschland), in der Arbeitsgruppe von Dr. Angela Hay. Thema: "Mechanism of localized lignin deposition in explosive fruit."
2013-2014 **Masterarbeit** an der Universidad de Granada, Granada (Spanien), in der Arbeitsgruppe von Prof. Dr. Roberto de la Herrán Moreno. Thema: "Analysis of molecular markers in the genus *Muscari*."
2013 **ERASMUS Praktikum** am Zoologisches Forschungsmuseum Alexander Koenig, Bonn (Deutschland) in der Arbeitsgruppe von Dr. Dennis Rödder. Thema: "Analysis of *Tarentola* specimens for phylogenetic analysis."
2008-2013 **Studium der Biologie** an der Universidad de Salamanca, Salamanca (Spanien).

Schulische Ausbildung

2002 – 2008 Gymnasium Pintor Luis Sáez, Burgos (Spanien)